ISSN 2663-0419 (Online)
ISSN 2218-8754 (Print)

AZERBAIJAN NATIONAL ACADEMY OF SCIENCES

ANAS TRANSACTIONS

EARTH SCIENCES



www.journalesgia.com

2023
№2

We are Crossref Member

ELSEVIER Scopus

Crossref
This journal is included and indexed in the GeoRef database

REDAKSİYA HEYƏTI

Əlizadə Ak.A. – baş redaktor (Azərbaycan), Qədirov F.Ə. – baş redaktorun müavini (Azərbaycan), Süleymanov B.Ə. – baş redaktorun müavini (Azərbaycan), Quliyev İ.S. – baş redaktorun müavini (Azərbaycan), Babayev Q.R. – baş redaktorun müavini) (Azərbaycan), Babazadə V.M. (Azərbaycan), Calalov Q.İ. (Azərbaycan), Əliyeva E.H. (Azərbaycan), Əfəndiyev Q.M. (Azərbaycan), Feyzulayev Ə.Ə. (Azərbaycan), Kəngərli T.N. (Azərbaycan), Məmmədov P.Z. (Azərbaycan), Muxtarov A.Ş. (Azərbaycan), Salmanov A.M. (Azərbaycan), Yetirmişli Q.C. (Azərbaycan).

Allen Mark (Böyük Britaniya), Aydın Ali (Türkiyə), Çelidze T. L. (Gürcüstan), Eppelbaum L.V. (İsrail), İsmail-zadə Ə.T. (Almaniya), Kalafat Doğan (Turkiyə), Kərimov V.Y. (Rusiya), Qliko A.O. (Rusiya), Lavruşin V.Y (Rusiya), Reilinger R. (ABŞ), Takeşi Sagiya (Yaponiya), Talebian M. (İran), Tibaldi Alessandro (İtaliya), Zavyalov A.D. (Rusiya).

EDITORIAL BOARD

Alizadeh Ak.A. – Editor-in-Chief (Azerbaijan), Kadirov F.A. – Deputy Editor-in-Chief (Azerbaijan), Suleimanov B.A. – Deputy Editor-in-Chief (Azerbaijan), Guliyev I.S. – Deputy Editor-in-Chief (Azerbaijan), Babayev G.R. – Deputy Editor-in-Chief (Azerbaijan), Afandiyev G.M. (Azerbaijan), Aliyeva E.H. (Azerbaijan), Babazade V.M. (Azerbaijan), Feyzullayev A.A. (Azerbaijan), Jalalov G.I. (Azerbaijan), Kangarli T.N. (Azerbaijan), Mammadov P.Z. (Azerbaijan), Mukhtarov A.Sh. (Azerbaijan), Salmanov A.M. (Azerbaijan), Yetirmishli G.J. (Azerbaijan).

Allen Mark **(**United Kingdom), Aydın Ali (Türkiye), Chelidze T.L. (Georgia), Eppelbaum Lev V. (Israil), Gliko A.O. (Russia), Ismail-zadeh A.T. (Germany), Kalafat Doğan (Türkiye), Kerimov V.Y. (Russia), Lavrushin V.Y. (Russia), Reilinger R. (USA), Takeshi Sagiya (Japan), Talebian M. (Iran), Tibaldi Alessandro (Italy), Zavyalov A.D. (Russia).

РЕДАКЦИОННАЯ КОЛЛЕГИЯ

Ализаде Ак.А. – главный редактор (Азербайджан), Кадиров Ф.А. – зам.главного редактора (Азербайджан), Сулейманов Б.А. – зам.главного редактора (Азербайджан), Гулиев И.С. – зам.главного редактора (Азербайджан), Бабаев Г.Р. – зам.главного редактора (Азербайджан), Алиева Э.Г. (Азербайджан), Бабазаде В.М. (Азербайджан), Джалалов Г.И. (Азербайджан), Етирмишли Г.Дж. (Азербайджан), Кенгерли Т.Н. (Азербайджан), Мамедов П.З. (Азербайджан), Мухтаров А.Ш. (Азербайджан), Салманов А.М. (Азербайджан), Фейзуллаев А.А. (Азербайджан), Эфендиев Г.М. (Азербайджан).

Айдын Али (Турция), Аллен Марк (Великобритания), Глико А.О. (Россия), Завьялов А.Д. (Россия), Исмаил-заде А.Т. (Германия), Калафат Доган (Турция), Керимов В.Ю. (Россия), Лаврушин В.Ю. (Россия), Рейлингер Р. (США), Такеши Сагия (Япония), Талебиан М. (Иран), Тибальди Алессандро (Италия), Челидзе Т.Л. (Грузия), Эппельбаум Л.В. (Израиль).

Buraxılışına məsul: **Hafiz Abıyev**

Dizayn/Qrafika: **Kərim Nəbiyev**
Xəlil Nəbiyev

Veb-redaktor: **Tofiq Rəşidov**

Jurnal Azərbaycan MEA Geologiya və Geofizika İnstitutunda yığılmış və səhifələnmişdir

* * *

Responsible for the issue: **Hafiz Abiyev**

Design/Graphycs: **Karim Nabiyev**
Khalil Nabiyev

Web-editor: **Tofig Rashidov**

This journal has been prepead at the Geology and Geophysics Institute of Azerbaijan National Academy of Sciences

* * *

Ответственный за выпуск: **Хафиз Абиев**

Дизайн/графика: **Керим Набиев**
Халил Набиев

Веб-редактор: **Тофиг Рашидов**

Журнал набран и сверстан в Институте геологии и геофизики НАН Азербайджана

* * *

Ünvan: AZ1001, Bakı şəhəri, İstiqlaliyyət küçəsi 30, "ANAS Transactions, Earth Sciences"

Address: "ANAS Transactions, Earth Sciences" 30, Istiglaliyyat str., Baku, Azerbaijan, AZ1001

Адрес: AZ1001, г. Баку, Истиглалият, 30. Редакция "ANAS Transactions, Earth Sciences"

* * *

İcraçı redaktorlar: **A.A.İsrafilova, C.S.Qurbanova**
Executive Editors: **A.A.Israfilova, J.S.Gurbanova**
Исполнителные редакторы: **А.А.Исрафилова**
Дж.С.Курбанова

ELM NƏŞRİYYATI

Formatı: 60x84$^{1/8}$. Həcmi: 12,75 ç.v.
Tirajı: 300 nüsxə

© "Elm" nəşriyyatı, 2023

ANAS Transactions **Earth Sciences** **2 / 2023**

http://www.journalesgia.com

NATURAL AND TECHNOGENIC CATASTROPHIC BLOWOUTS AND GAS EXPLOSIONS IN THE ARCTIC AND OTHER REGIONS (ONSHORE AND OFFSHORE)

Bogoyavlensky V.I., Bogoyavlensky I.V., Nikonov R.A.

Oil and Gas Research Institute of the Russian Academy of Sciences (OGRI RAS)

3, Gubkina, Moscow, Russia, 119333: geo.ecology17@gmail.com

Keywords: *Earth degassing, gas blowouts and explosions, mud volcanoes, gas seeps, remote sensing, unmanned aerial vehicles*

Summary. The authors created the geoinformation system "The Arctic and World Ocean" (GIS "AWO") with a huge amount of constantly updated geospatial data, allowing a comprehensive analysis of various natural and man-made phenomenon directly or indirectly related to the degassing of the Earth. In the Arctic, a large amount of expeditionary work has been carried out with a wide range of geological and geophysical methods, which is analyzed in conjunction with remote sensing data from space and using unmanned aerial vehicles. This made it possible to obtain fundamentally new information about the gas-dynamic mechanisms of dangerous processes in the permafrost, including catastrophic gas blowouts and explosions with the formation of giant craters, and large mud volcanic structures. In total in the north of Western Siberia about 18.5 thousand potentially dangerous objects were identified, including 4.5 thousand intensive gas blowout zones on the bottoms of thermokarst lakes, as a result of which underwater craters-pockmarks are formed. This gave possibility to identify the most dangerous gas-explosive zones in the north of Western Siberia, mainly located in the eastern part of the Yamal peninsula. Taking into account previously discovered mud volcanoes on the land of Alaska, Greenland and Iceland, as well as on the bottom of the Beaufort, Kara and Norwegian seas, it can be argued that there is a Circum-Arctic mud volcanic province.

© 2023 Earth Science Division, Azerbaijan National Academy of Sciences. All rights reserved.

Introduction

In recent decades due to the global warming attention has significantly increased to the study of various processes of greenhouse gas emissions into the atmosphere and changes in their concentration in the atmosphere (Jackson et al., 2020; Report…, 2022; State…, 2023). The concentration of greenhouse gases grow rapidly, which causes the intensification of greenhouse effect, melting of glaciers and rising of the World Ocean level up to 4.6 mm per year in last decade (State…, 2023).

Among the causes of natural and anthropogenic emissions of greenhouse gases, where methane is one of the most dangerous, deep and near-surface processes, only a part of which appears on the Earth surface, including the bottom of the World Ocean, as widespread seeps of underground fluids, mostly mixtures of hydrocarbon gases, are of particular importance (Hovland et al., 1984; Judd, Hovland, 2007; Bogoyavlensky, 2012; Etiope, 2015; Guliyev et al., 2018; Bogoyavlensky et al., 2020b; Kerimov, Abdullayeva, 2022). Over the half-century history of studying submarine gas emission from the bottom of various parts of the World Ocean, hundreds of papers have been published (Hovland et al., 1984; Judd, Hovland, 2007; Sergienko et al., 2012; Etiope, 2015; Paul et al., 2015; Andreassen et al., 2017; Guliyev et al., 2018; Mironyuk et al., 2019; Bogoyavlensky et al., 2021d; Bogoyavlensky et al., 2022a; Kerimov, Abdullayeva, 2022;Bogoyavlensky et al., 2022c; Kishankov et al., 2022; Bogoyavlensky, Kishankov, 2023; Sokolov et al., 2023).

Massive gas blowouts causing the formation of large and giant craters (tens or even hundreds of meters in diameter) are widely spread both onshore and offshore (Hovland et al., 1984; Judd, Hovland, 2007; Andreassen et al, 2017; Bogoyavlensky, 2020; Bogoyavlensky et al., 2020b; Bogoyavlensky, 2021; Bogoyavlensky et al., 2021a; Bogoyavlensky et al., 2021b; Bogoyavlensky et al., 2022a).

Moreover some of the papers are dedicated to the study of active degassing from the bottoms of the Arctic thermokarst lakes with continuous or sporadic taliks (Kruglikov, Kuzin, 1973; Walter et al., 2006; Badu, 2018; Bogoyavlensky et al., 2018; Bogoyavlensky et al., 2020a; Bogoyavlensky, 2021; Bogo-

yavlensky et al., 2021c; Bogoyavlensky et al., 2021b). Many of these lakes have bubbles of frozen gas in their ice cover and numerous craters (pockmarks) on the bottom.

One of the most dangerous processes of the Earth degassing is the formation of mud volcanoes (MVs) (Kopf, 2002; Aliyev et al., 2015; Bogoyavlensky, Bogoyavlensky, 2022; Yusubov, Guliyev, 2022). The global research of Azerbaijani scientists (Aliyev et al., 2015) gives the information about 2505 MVs, the most of which (1401 or 55.9%) were discovered on the bottom of the World Ocean. The presence of MVs is one of the prospecting indicators for oil and gas, wherein they give significant information of sedimentary cover lithology. The gas erupted from MVs frequently explodes and self-ignites. The height of burning flares above MVs can reach hundreds of meters, the measured height is up to 500 m (Aliyev et al., 2015; Yusubov, Guliyev, 2022). In 1940 the height on the mud volcanic island Khare-Zirya (Bulla) was even 1200 m (Yusubov, Guliyev, 2022, p. 18).

In the Circum-Arctic region MVs were found onshore, in Alaska, Greenland and Iceland, and offshore, in the Beaufort, Kara, Norwegian and Barents seas (Haakon Mosby and Borealis) (Paull et al., 2015; Serov et al., 2015; Mironyuk et al., 2019; Bogoyavlensky, Bogoyavlensky, 2022).

Oil and Gas Research Institute of the Russian Academy of Sciences (OGRI RAS) studies the processes of the Earth degassing in their various geological forms and appearances for more than 30 years, the results were reported on many conferences, including (Earth degassing …, 2002). The studies of the authors are not limited geographically by the north latitudes of the Arctic regions with cryolithogenesis, but expand to other parts of the World related to different forms of natural and technogenic degassing, including mud volcanism, gas hydrate dissociation and behind-the-casing flows (Bogoyavlensky et al., 2018; Bogoyavlensky, 2020; Bogoyavlensky et al., 2020a; Bogoyavlensky et al., 2020b; Bogoyavlensky, 2021; Bogoyavlensky et al., 2021b; Bogoyavlensky et al., 2021c; Bogoyavlensky, Bogoyavlensky, 2022; Bogoyavlensky et al., 2022a; Bogoyavlensky et al., 2022b).

The main goal of this work is to comprehensively analyze the insufficiently studied dangerous endogenous processes of generation, accumulation and migration of gaseous hydrocarbons up to their discharges on the Earth surface and the bottom of the World Ocean in the form of permanent, pulsating and/or periodic powerful impulse (explosive) degassing of the subsoil, often leading to catastrophic changes in terrain, including the formation of giant craters and landslides.

Methods

Over the past decade, the authors have annually carried out expeditionary work in the Arctic to study a new dangerous phenomenon associated with the processes of powerful emissions, self-ignition and explosions of gas on land, as well as from the bottoms of thermokarst lakes, rivers and coastal zones of the Kara Sea (Bogoyavlensky et al., 2018; Bogoyavlensky, 2020; Bogoyavlensky et al., 2020a; Bogoyavlensky et al., 2020b; Bogoyavlensky, 2021; Bogoyavlensky et al., 2021b; Bogoyavlensky et al., 2021c; Bogoyavlensky et al., 2021d; Bogoyavlensky, Bogoyavlensky, 2022; Bogoyavlensky et al., 2022a). Also expeditions have been carried out in the Azov and Black seas, Tatarstan, Tula, Nizhniy Novgorod and Saratov regions. Field studies in the Arctic involves a wide set of geological and geophysical methods including seismic prospecting (2D-4D), ground penetrating radar studies, echo sounding, shallow drilling, gas, water and ground sampling for geochemical analysis.

In all of the studied regions the unmanned aerial vehicles (UAV) are used with great efficiency. They give possibility to receive fundamentally new data on unique objects. The photogrammetric processing of data from UAV Mavic Pro and Mavic Mini (DJI, China) in Agisoft Metashape («Geoscan», Russia) and ArcGIS (ESRI, USA) software allows building 3D-4D models of the investigated objects available for additional study in virtual reality (Bogoyavlensky, 2021; Bogoyavlensky et al., 2021b; Bogoyavlensky et al., 2021c). The scaled layouts of digital models using additive techno logy are also made on a 3D printer.

Particular information is Earth remote sensing (RS) data from space, which in many cases provide an opportunity for a retrospective analysis of the features of potentially dangerous objects formation, as well as catastrophic events that have occurred since the first large-scale satellite imagery started in the early 1960s. The ArcticDEM digital elevation models are widely used allowing monitoring the changes of terrain, especially in places of catastrophic gas blowouts and explosions (Bogoyavlensky, 2021; Bogoyavlensky et al., 2021b; Bogoyavlensky et al., 2021c).

In the study of methane concentration in the atmosphere we use the TROPOMI spectrometer data from Sentinel-5P satellite of the European Space Agency Copernicus program, held for the “Global monitoring for Environment and Security of Earth and its atmosphere” (GMES) (Bogoyavlensky et al., 2020b; Bogoyavlensky et al., 2022b).

The Arctic and World Ocean (AWO) GIS was created based on ArcGIS software in 2008 (Bogoyavlensky et al., 2018; Bogoyavlensky, 2020; Bo-

goyavlensky et al., 2020a; Bogoyavlensky et al., 2020b; Bogoyavlensky, 2021; Bogoyavlensky et al., 2021b; Bogoyavlensky et al., 2021c; Bogoyavlensky, Bogoyavlensky, 2022; Bogoyavlensky et al., 2022a). The geospatial data including the authors' and other scientists' information is uploading in it to form continuously developing and systematized data arrays (Big Data), available for complex analysis. In particular, the "AWO" GIS contains data on natural hazards like earthquakes, stratovolcanoes, MVs, meteorite craters, craters of gas blowouts, oil and gas seeps, gas hydrates, pingos and perennial heaving mounds (PHMs), thermokarst lakes with gas blowouts craters (TLGBCs) on the bottoms, sea ice, catastrophes while drilling and transportation of oil and gas, and others (Fig. 1). An integrated approach to the study of various geospatial data makes it possible to reveal hidden trigger relationships that have direct or indirect impact on the degassing of the Earth and other processes.

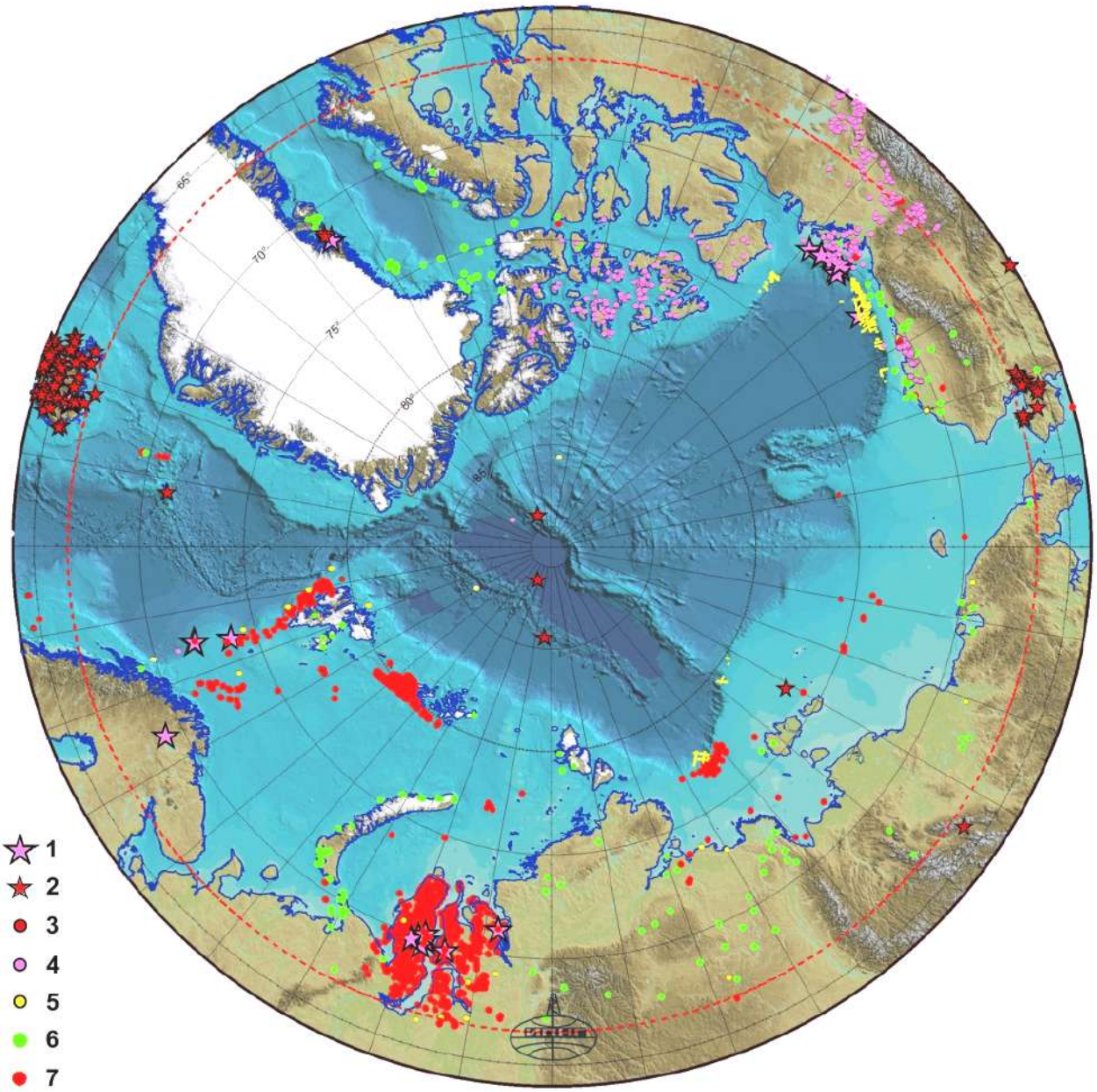


Fig. 1. The cartographic scheme of oil and gas shows onshore and offshore Arctic region (version-23, 2023). Legend: 1– MVs; 2 – stratovolcanoes; 3 – gas hydrates (proven); 4 – gas hydrates based on log data; 5 – gas hydrates based on BSR; 6 – gas seeps; 7 – oil seeps

Results and discussion

1. Explosive degassing in the Arctic

Since 2014 the authors study regions and objects of massive (explosive) gas blowouts with formation of craters. In "AWO" GIS there are about 20 of them analyzed in different degrees of detail (Fig. 2). Some of them (C1, C2, C9, C17 and others, as mentioned in "AWO" GIS) formed near the infrastructure of the Bovanenkovo oil and gas condensate field on the Yamal Peninsula. In all three eyewitness cases (C3, C11 and C12) there was self-ignition and explosion of gas (Bogoyavlensky et al., 2018; Bogoyavlensky, 2020; Bogoyavlensky et al., 2020a; Bogoyavlensky et al., 2020b; Bogoyavlensky, 2021; Bogoyavlensky et al., 2021b; Bogoyavlensky et al., 2021c; Bogoyavlensky, Bogoyavlensky, 2022; Bogoyavlensky et al., 2022b). In our opinion, confirmed by a number of facts, these self-ignition and explosion have happened due to electrostatic discharges (Bogoyavlensky, 2020; Bogoyavlensky, 2021). We think that these processes are the main triggers of gas self-ignition during the MVs eruptions in the Azov and Black seas region and in other places (Bogoyavlensky, Bogoyavlensky, 2022).

The results of the Bovanenkovo C17 object studies, on which in May-June 2020 a powerful gas blowout occurred with the formation of a giant crater are Of particular interest (see Fig. 2 - C). As a result of photogrammetric processing of pictures taken during the expedition from the DJI Mavic Pro UAV at two height levels (including the photos from inside the crater), a digital 3D model was built in Agisoft Metashape software. Based on this model, a high-precision 3D plastic model on a scale of 1:800 was created using additive technology on a 3D printer (Fig. 3). The use of new technologies of "Industry 4.0" made it possible for the first time to create a high-precision digital twin of the underground cavity and gas blowout crater of the unique Bovanenkovo C17 object, which allows surveying the underground space in virtual reality.

As a result of the gas blowout and explosion study authors have no doubts that explosions in the Arctic were preceded by the formation of giant gas-saturated cavities in the ground ice (real thermokarst), the upper parts of which, under the action of a gas-dynamic mechanism, formed PHMs on the Earth surface (Bogoyavlensky, 2020; Bogoyavlensky, 2021). At abnormal gas pressures in the cavities, which significantly exceed the lithostatic pressure and the elastic-strength characteristics of frozen rocks, explosive destruction of the tops of the PHMs occurs with the formation of giant craters. In particular, during the formation of the C1 crater the pressure of gas exceeds the lithostatic more than 9 times (assuming the density of frozen rocks in the upper part of the section as 1.7 g/cm^3) (Bogoyavlensky, Garagash, 2015; Bogoyavlensky, 2020; Bogoyavlensky, 2021).



Fig. 2. Giant cavities in ground ice after the blowouts and explosions of gas on the Yamal Peninsula. A - C1, B - C12, C - C17 (photos by V.I.Bogoyavlensky, 2014, 2015 and 2020)

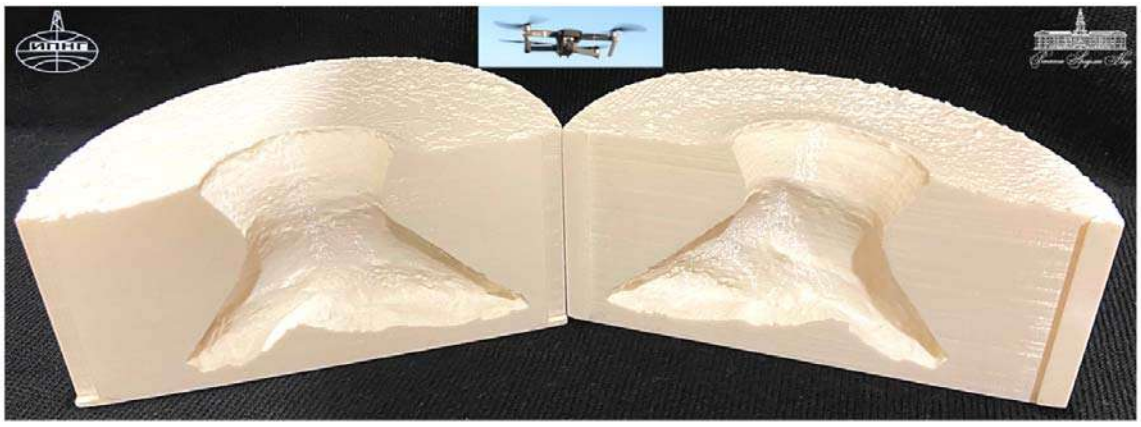


Fig. 3. Physical 3D-model of the underground cavity and gas blowout crater on the Bovanenkovo C17 object

With the use of RS data, including winter satellite images and ArcticDEM, more than 14000 PHMs were detected in the north of Western Siberia. In a comprehensive analysis of the detected objects of powerful gas blowouts, it was found that the greatest danger is presented by PHMs, located not in khasyreys, like classic frost mounds - bulgunnyakhs (closed systems), but by PHMs with an open inflow of underground gas-saturated fluids (gas in free and/or dissolved states), usually located on the hills and slopes of sea terraces, as well as in the channels and floodplains of rivers (Bogoyavlensky, 2020; Bogoyavlensky, 2021). Such PHMs are formed by the gas-dynamic mechanism.

2. Degassing from the bottoms of thermokarst lakes

More than half a century ago, in the north of Western Siberia, near the Urengoy oil and gas condensate field, thermokarst lakes with gas blowout craters (TLGBC) at the bottoms were discovered for the first time, while geochemical studies of methane in them showed its deep genesis (Kruglikov, Kuzin, 1973). The authors continued the search and study of TLGBCs in the last decade using RS data from space and during numerous helicopter flights over the Yamal Peninsula (Bogoyavlensky et al., 2020a; Bogoyavlensky et al., 2020b; Bogoyavlensky et al., 2021b; Bogoyavlensky et al., 2021c; Bogoyavlensky et al., 2022b).

Figure 4-A shows the WorldView-2 satellite image (July 20, 2022, ultra-high resolution 30-50 cm) of the previously unnamed TLGBC discovered in the central part of Yamal 60 m north of Lake Tobato and named by us Tobato-Severnoye (70.697° N, 71.0234° E). This lake has dimensions of 320x500 m, and the diameters of the largest craters at its bottom reach 19 m (not counting the sizes of the merged craters). Such objects have also been found on a number of neighboring lakes, including Tobato. It should be noted that the number of pockmark craters at the bottom of some of the lakes is many hundreds, and possibly even thousands. The visible by the resolution of WorldView-2 satellite image number of craters on the bottom of Tobato-Severnoye lake (Fig. 4-A) is about 350.

It should be noted that at the bottoms of the TLGBCs, small accumulative uplifts (parapets) are observed around the recently formed craters, which are made of bottom sediments ejected by gas (for example, see Fig. 4-A). Different-temporal satellite images show that over the course of several years, loose accumulative deposits of parapets are washed out and slide inward, while the diameters of the craters increase, and the depths decrease.

As a result of the studies in the north of Western Siberia (the Yamal, Gydansky and Tazovsky peninsulas), according to RS data from space, more than 4.4 thousands of degassing zones from TLGBCs, as well as rivers and coastal zones of the Kara Sea, were discovered and shown on Fig. 4-B. Based on a comprehensive analysis of the TROPOMI spectrometer data (Sentinel-5P satellite), an unambiguous regional relationship between the identified degassing zones and areas of increased methane concentration in the atmosphere was established (Bogoyavlensky et al., 2020b).

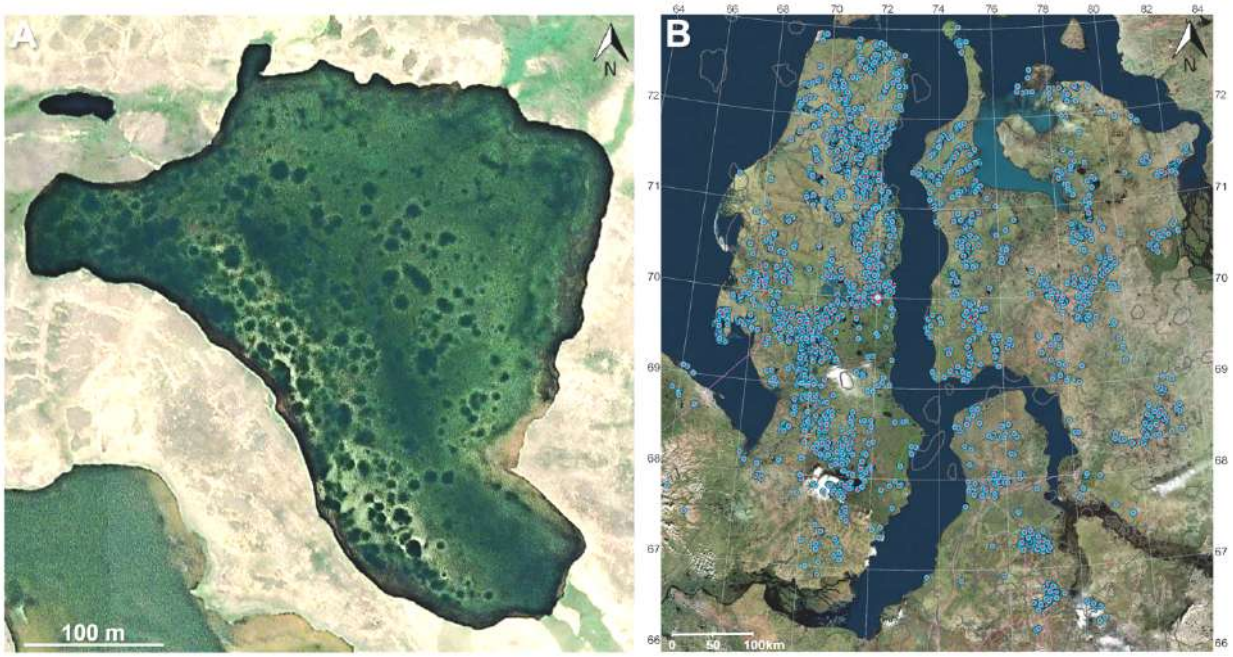


Fig. 4. WorldView-2 satellite image of the Tobato-Severnoye lake with gas blowout craters on the bottom (A) and cartographic scheme of TLGBC distribution in the north of Western Siberia (B)

3. Mud volcanism

On a number of discovered objects of intensive degassing on the Yamal Peninsula, the authors substantiate the mud volcanic mechanism of eruptions. According to GOST R 57123-2016 (GOST…, 2016), an MV is "a geological formation that constantly or periodically erupts mud and gases", usually confined to faults.

Periodical eruptions of underground fluids were detected and explored on TLGBC Otkrytiye (Fig. 5-A) with size of 440x750 m, situated in the central part of the Yamal Peninsula (70.006° N, 72.01° E). In 2019 there was a powerful gas blowout (pneumatic explosion) on a crater C (see Fig. 5-A), which broke the ice of 1.5 m thickness and spread the ice boulders on more than 50 m distance (Bogoyavlensky et al., 2020a). The analysis of satellite images from Sentinel-2 and Landsat-8 during the melting of ice (May-June) proved that the blowouts had occurred from the same crater C during winters of 2016-2019. But in 2020-2023 there were no witnesses of significant gas blowouts.

According to RS data and on the basis of expeditionary work at the TLGBC Otkrytiye, four neighboring large craters (diameter from 30 to 40 m) were found, located along the predicted deep submeridional fault (azimuth 345°), as well as several craters of smaller diameter up to 4-6 m (Fig.5-B). Conducting expeditionary studies using echo sounding and ground penetrating radar made it possible to detect landslide bodies on the walls of the craters and the bottom of the lake, formed by presumably loamy rock erupted from vents. In connection with the foregoing, four underwater objects with large craters on Lake Otkrytiye can be classified as MVs with a high probability according to GOST R 57123-2016 (GOST…, 2016).

RS data also showed several thermokarst lakes on Yamal, at the bottom of which, with clear water, cone-shaped volcano-like uplifts are observed (Bogoyavlensky, 2023). Fig. 6-A shows the WorldView-2 summer satellite image, from 13th of July, 2018 with ultra-high spatial resolution, of a large (1.6x2.1 km) thermokarst lake Labvarto, located in the central part of the Yamal Peninsula (69.985° N, 71.9356° E), situated in 3.7 km to the south-west from Lake Otkrytiye., Three zones of pockmark existence (P1, P2 and P3) and two objects (V1 and V2), which we identified as mud volcanic structures, were found at its bottom. This is confirmed by their specific conical shape and the presence of rounded/elliptical calderas with vents, which are especially visible on the V1 volcano, together with the sinter forms on its surface (see Fig. 6-B1).

Taking into account the fact that the thickness of lake ice can reach 1.5-2.0 m in these latitudes, we believe that the depth of the top of the V1 volcano is not less than these values. The top of the V1 object has dimensions of 75x80 m, and its visible base is 150x185 m. Due to new eruptions of mud breccia, the top of the volcano can rise above the water level, but its formation is limited by erosion and annual shearing by melting ice moving downwind.

According to RS data in 1985-2022 (Landsat and Sentinel) direct signs of winter gas eruptions from V1 and V2 tops were found in the form of annual early (May-June) thaws in ice above them, as well as trails of distribution of gas jets and/or reservoir fluids with dissolved gas in the water during the summer ice-free period (Fig. 6-B2).

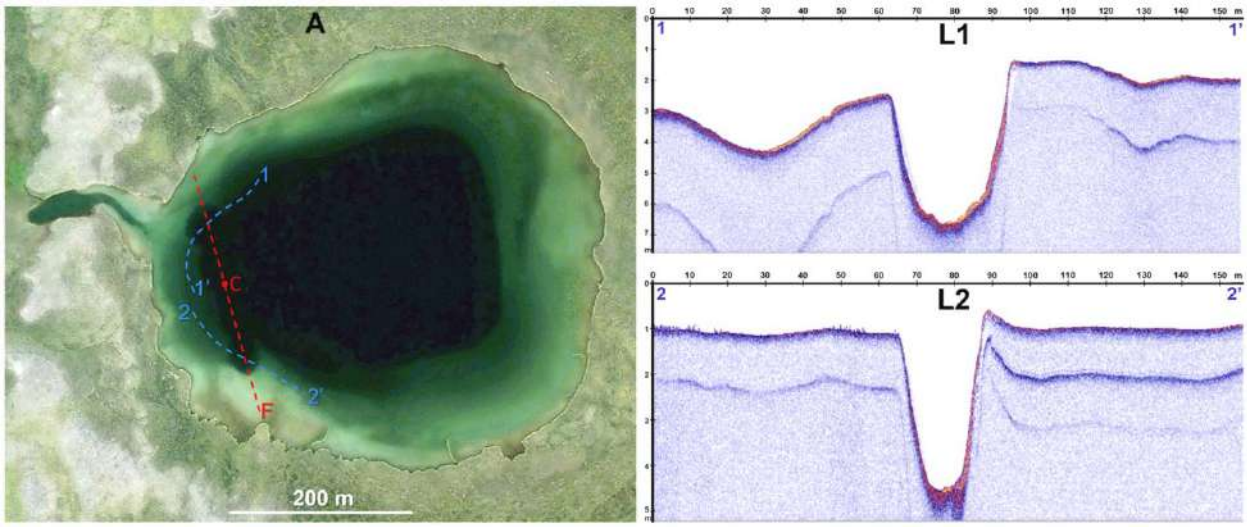


Fig. 5. WV-2 satellite image (13 of July, 2018) of Otkrytiye thermokast lake (A) and two echo sounding data records (L1 and L2) from profiles 1-1' and 2-2' through the underwater craters. Legend for Fig. 5-A: 1-1' and 2-2' – the L1 and L2 profiles location; F – predicted fault strike position; C – crater of gas blowout

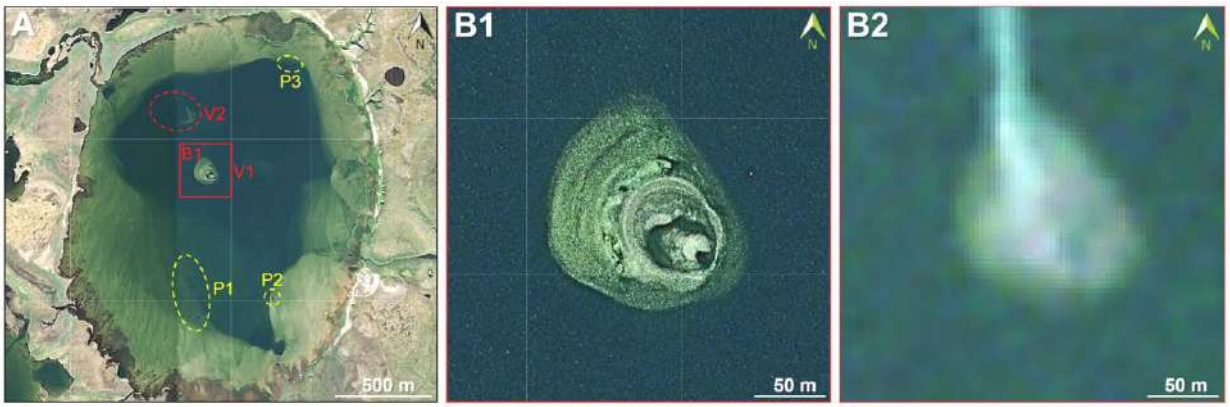


Fig. 6. Thermokarst lake on the Yamal Peninsula with degassing zones: P1, P2 and P3 – pockmarks; V1 and V2 – mud volcanoes

4. Technogenic eruptions of hydrocarbon mixtures

The authors analyzed the consequences of catastrophic blowouts (fountains) of mixtures of gas and oil with the formation of giant craters near the heads of emergency exploration wells drilled in the Arctic, in the southern regions of Russia and in the Caspian region, as well as in a number of oil and gas producing countries of the world (USA, Mexico, Canada, Indonesia, etc.) (Bogoyavlensky et al., 2017a; Bogoyavlensky, Bogoyavlensky, 2019). Thus, important information was obtained on the basis of RS data from space. Despite the liquidation of the fountains many decades ago, it has been proven that active emission of hydrocarbons continues at the present time at some of the studied objects.

As one of the examples, let us cite one of the biggest disasters in the Arctic happened on November, 1980 during the postcompletional flow test of the Kumzhinskaya-9 well located near the mouth of the Pechora River, on the left bank of the Maliy Gusinets channel in the north of the Kumzhinskoye gas condensate field, discovered in 1973 (Bogoyavlensky et al., 2017b). Due to the technogenic pool, formed in the upper part of the section with the area of around 30 km^2 (gas blowouts were detected in the 3 km radius), the gas escaped in the atmosphere in a number of points, including wells 9, 5, 10 and 134. It led to the formation of 3 giant craters from 70 to 130 m in diameter near the heads of destructed wells, flooded by river water, on the emergency site with the size of 260x600 m (Fig. 7A). The hard fight with catastrophic gushing continued for about 6.5 years (2362 days). The fire on the gushing fountain was put out only on the 18th of May in 1987. The lake, closed with the dams, was created on the emergency site in the channel of the Pechora River (Bogoyavlensky, 2020; Bogoyavlensky et al., 2017b).

On the WorldView-2 satellite image (taken from ESRI database) the pronounced thaws and holes in the ice are seen, polluted with liquid hydrocarbons even 36 years after the catastrophe (Fig. 7-B). Such ice cover breaches are visible every year from 2016 to 2023 on the different satellite images, including Sentinel-2 and Landsat-8. In 2023 the emission of HCs was seen on images from Sentinel-2 on May 3, 17, 20, 22, 23 and 25 (the traces of fluids were detected also on of March 18 and 24).

Conclusion

The authors performed a large amount of expeditionary work with a wide range of geological and geophysical methods in the Arctic, which, together with RS data from space, made it possible to obtain fundamentally new information about the gas-dynamic mechanisms of dangerous processes in the permafrost, including catastrophic gas blowouts and explosions with the formation of giant craters. There is no doubt that the studied craters were formed at the sites of existence of underground gas-saturated cavities (thermokarst) formed under the action of endogenous mechanisms, and the explosions occurred due to a gas-dynamic mechanism with superlithostatic gas pressure in the cavity.

There is a widely spread Earth degassing happening in the Western Siberia. About 4.5 thousand of intensive gas blowout zones were detected from the bottoms of thermokarst lakes. On the basis of statistical data on the distribution of perennial heaving mounds and thermokarst lakes with gas blowouts craters the most dangerous areas were identified in the north of the Western Siberia.

On Yamal at the bottoms of thermokarst lakes with through and/or non-through taliks, a number of mud volcanic degassing objects, including large mud volcanic structures were discovered for the first time. Taking into account a number of previously discovered MVs onshore Alaska, Greenland and Iceland, as well as on the bottom of the Beaufort, Kara and Norwegian seas, it can be argued that there is a Circum-Arctic mud volcanic province.

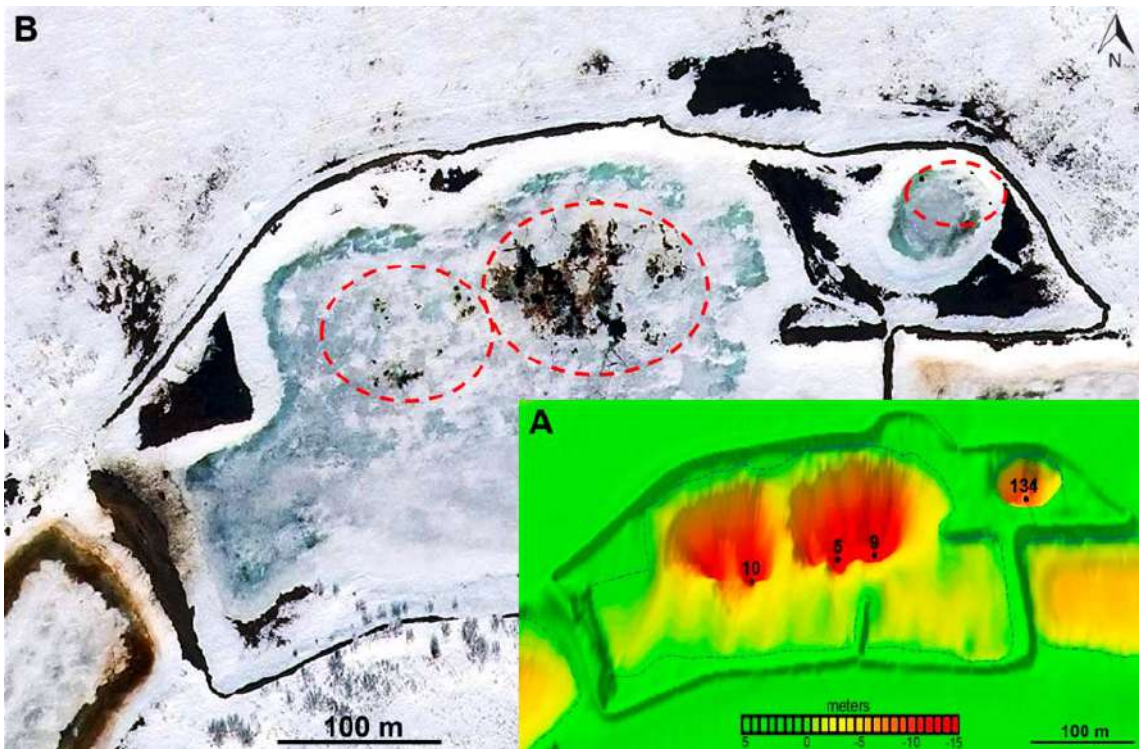


Fig. 7. Kumzhinskoye field disaster: 3D digital elevation model of technogenic lake bottom with craters and surrounding land (A) and WorldView-2 satellite image from the 2nd of May 2016 (B)

The authors are grateful to the Government of the Yamalo-Nenets Autonomous District, Gazprom PJSC, NOVATEK PJSC and the Russian Center for Arctic Development for the long-term support of expeditionary work on Yamal.

Funding

The research was carried out according to the state assignment of the Oil and Gas Research Institute of the Russian Academy of Sciences on the topic "Improving the efficiency and environmental safety of the oil and gas resources development in the Arctic and Subarctic zones of the Earth in a changing climate" (122022800264-9).

REFERENCES

Aliyev Ad. A., Guliyev I.S., Dadashev F.G., Rakhmanov R.R. The mud volcano atlas of the World. Nafta-Press. Baku, 2015, 323 p. (in Russian).

Andreassen K., Hubbard A., Winsborrow M. et al. Massive blow-out craters formed by hydrate-controlled methane expulsion from the Arctic seafloor. Science, Vol. 356, 2017, pp. 948-953, DOI: 10.1126/science.aal4500.

Badu Yu.B. Cryogenic strata of gas-bearing structures in Yamal. On the influence of gas deposits on the formation and development of cryogenic strata. Nauchny mir. Moscow, 2018, 232 p. (in Russian).

Bogoyavlensky V.I. Fundamental aspects of the catastrophic gas blowout genesis and the formation of giant craters in the Arctic. Arctic: Ecology and Economy, Vol. 11, No. 1, 2021, pp. 51-66, DOI: 10.25283/2223-4594-2021-1-51-66 (in Russian).

Bogoyavlensky V.I. Natural and technogenic threats in fossil fuels production in the Earth cryolithosphere. Russian Mining Industry, No. 1(149), 2020, pp. 97-118, DOI 10.30686/1609-9192-2020-1-97-118 (in Russian).

Bogoyavlensky V.I. New data on mud volcanism in the Arctic on the Yamal Peninsula. Doklady Earth Sciences, Vol. 512, No. 1, 2023, pp. 92-99, DOI: 10.1134/S1028334X23601116 (in Russian).

Bogoyavlensky V.I. Prospects and problems of the Arctic shelf

ЛИТЕРАТУРА

Andreassen K., Hubbard A., Winsborrow M. et al. Massive blow-out craters formed by hydrate-controlled methane expulsion from the Arctic seafloor. Science, Vol. 356, 2017, pp. 948-953, DOI: 10.1126/science.aal4500.

Bogoyavlensky V., Bogoyavlensky I., Nikonov R., Kargina T., Chuvilin E., Bukhanov B., Umnikov A. New Catastrophic Gas Blowout and Giant Crater on the Yamal Peninsula in 2020: Results of the Expedition and Data Processing. Geosciences, Vol. 11, No. 71, 2021a, 20 p., DOI: 10.3390/geosciences11020071.

Bogoyavlensky V., Bogoyavlensky I., Nikonov R., Yakushev V., Sevastyanov V. Permanent gas emission from the Seyakha Crater of gas blowout, Yamal Peninsula, Russian Arctic. Energies, Vol. 14, No. 17, 5345, 2021b, DOI: 10.3390/en14175345.

Bogoyavlensky V.I., Kishankov A., Kazanin A., Kazanin G. Distribution of permafrost and gas hydrates in relation to intensive gas emission in the central part of the Laptev Sea (Russian Arctic). Marine and Petroleum Geology, Vol. 138, 2022, 105527, pp. 1-15, DOI: 10.1016/j.marpetgeo.2022.105527.

Etiope G. Natural Gas Seepage. The Earth's Hydrocarbon Degassing. Springer. Switzerland, 2015, 203 p. DOI: 10.1007/978-3-319-14601-0.

Hovland M., Judd A., King L. Characteristic features of pockmarks on the North Sea Floor and Scotian Shelf. Sedimen-

oil and gas fields development. Oil and drilling, No. 11, 2012, pp. 4-9 (in Russian).

Bogoyavlensky V.I., Bogoyavlensky I.V. Accidental and catastrophic gas blowouts during hydrocarbon resources development in the Arctic zones of the USA and Canada. Oil and drilling, No. 12, 2019, pp. 3-8 (in Russian).

Bogoyavlensky V.I., Bogoyavlensky I.V. Specificity of mud volcanic degassing of the Earth with catastrophic consequences. Labor safety in the industry, No. 12, 2022, pp. 20-28, DOI: 10.24000/0409-2961-2022-12-20-28 (in Russian).

Bogoyavlensky V.I., Garagash I.A. Justification of the formation process of gas blowout craters in the Arctic by mathematical modeling. Arctic: Ecology and Economy, No. 3, 2015, pp. 12-17 (in Russian).

Bogoyavlensky V.I., Kishankov A.V. Dangerous gas-saturated objects in the World Ocean: the Beaufort Sea, Alaska North Slope shelf. Arctic: Ecology and Economy, Vol. 13, No. 2, 2023, pp. 201-210, DOI: 10.25283/2223-4594-2023-2-201-210 (in Russian).

Bogoyavlensky V.I., Bogoyavlensky I.V., Kargina T.N. Catastrophic mud volcano eruption in Indonesia. Oil and drilling, No. 11, 2017a, pp. 2-11 (in Russian).

Bogoyavlensky V.I., Bogoyavlensky I.V., Kargina T.N. Catastrophic gas blowout in 2020 on the Yamal Peninsula in the Arctic. Results of comprehensive analysis of aerospace RS data. Arctic: Ecology and Economy, Vol. 11, No. 3, 2021c, pp. 362-374, DOI: 10.25283/2223-4594-2021-3-362-374 (in Russian).

Bogoyavlensky V., Bogoyavlensky I., Nikonov R., Kargina T., Chuvilin E., Bukhanov B., Umnikov A. New catastrophic gas blowout and giant crater on the Yamal Peninsula in 2020: Results of the expedition and data processing. Geosciences, Vol. 11, No. 71, 2021a, 20 p., DOI: 10.3390/geosciences11020071.

Bogoyavlensky V., Bogoyavlensky I., Nikonov R., Yakushev V., Sevastyanov V. Permanent Gas Emission from the Seyakha Crater of Gas Blowout, Yamal Peninsula, Russian Arctic. Energies, Vol. 14, No. 17, 5345, 2021b, DOI: 10.3390/en14175345.

Bogoyavlensky V.I., Erokhin G.N., Nikonov R.A., Bogoyavlensky I.V., Bryksin V.M. Study of catastrophic gas blowout zones in the Arctic based on passive microseismic monitoring (on the example of Lake Otkrytiye). Arctic: Ecology and Economy, No. 1, 2020a, pp. 53-64, DOI: 10.25283/2223-4594-2020-1-53-64 (in Russian).

Bogoyavlensky V.I., Kazanin A.G., Kishankov A.V., Kazanin G.A. Earth degassing in the Arctic: comprehensive analysis of factors of powerful gas emission in the Laptev Sea. Arctic: Ecology and Economy, Vol. 11, No. 2, 2021d, pp. 178-194, DOI: 10.25283/2223-4594-2021-2-178-194 (in Russian).

Bogoyavlensky V.I., Kishankov A., Kazanin A., Kazanin G. Distribution of permafrost and gas hydrates in relation to intensive gas emission in the central part of the Laptev Sea (Russian Arctic). Marine and Petroleum Geology, Vol. 138, 2022, 105527, pp. 1-15, DOI: 10.1016/j.marpetgeo.2022.105527.

Bogoyavlensky V.I., Kishankov A.V., Kazanin A.G., Kazanin G.A. Dangerous gas-saturated objects in the World Ocean: the East Siberian Sea. Arctic: Ecology and Economy, Vol. 12, No. 2, 2022a, pp. 157-171, DOI: 10.25283/2223-4594-2022-2-158-171 (in Russian)

Bogoyavlensky V.I., Perekalin S.O., Boichuk V.M., Bogoyavlensky I.V., Kargina T.N. Kumzhinskoye gas condensate field disaster: reasons, results and ways of eliminating the consequences. Arctic: Ecology and Economy, No. 1, 2017b, pp. 32-46, DOI: 10.25283/2223-4594-2017-1-32-46 (in Russian).

Bogoyavlensky V.I., Sizov O.S., Bogoyavlensky I.V., Nikonov R.A. Technologies for remote detection and monitoring of the Earth degassing in the Arctic: Yamal peninsula, Neito lake. Arctic: tology, Vol. 31, No. 4, 1984, pp. 471-480, DOI: 10.1111/j.1365-3091.1984.tb01813.

Jackson R. B., Saunois M., Bousquet P. et al. Increasing anthropogenic methane emissions arise equally from agricultural and fossil fuel sources. Environmental Research Letters, Vol. 15, No. 7, 2020, p. 071002, DOI: 10.1088/1748-9326/ab9ed2.

Judd A., Hovland M. Seabed fluid flow – impact on geology, biology and the marine environment. Cambridge University Press. Cambridge, 2007, 400 p., DOI: 10.1017/CBO9780511535918.

Kopf A.J. Significance of mud volcanism. Reviews of Geophysics, Vol. 40, No. 02, 2002, pp. 2-1–2-52, DOI: 10.1029/2000RG000093.

Paull C.K., Dallimore S.R., Caress D.W. et al. Active mud volcanoes on the continental slope of the Canadian Beaufort Sea. Geochemistry, Geophysics, Geosystems, Vol.. 16, No. 9, 2015, pp. 3160-3181, DOI:10.1002/2015GC005928.

Serov P., Portnov A., Mienert J. et al. Methane release from pingo-like features across the South Kara Sea shelf, an area of thawing offshore permafrost. Journal of Geophysical Research: Earth Surface, Vol. 120, No. 8, 2015, pp. 1515-1529, DOI: 10.1002/ 2015JF003467.

State of the Global Climate 2022. World Meteorological Organization. WMO-No.1316, 2023, 55 p.

Walter K.M., Zimov S., Chanton J.P., Verbyla D., Chapin III F.S. Methane bubbling from Siberian thaw lakes as a positive feedback to climate warming. Nature, Vol. 443, 2006, pp. 71-75, DOI: 10.1038/nature05040.

Алиев Ад.А., Гулиев И.С., Дадашев Ф.Г., Рахманов Р.Р. Атлас грязевых вулканов мира. Nafta-Press. Баку, 2015, 323 с.

Баду Ю.Б. Криогенная толща газоносных структур Ямала. О влиянии газовых залежей на формирование и развитие криогенной толщи. Научный мир. Москва, 2018, 232 с.

Богоявленский В.И. Новые данные о грязевом вулканизме в Арктике на полуострове Ямал. Доклады РАН, Науки о Земле, Вулканология, Т. 512, № 1, 2023, с. 92-99, DOI: 10.31857/S2686739723601084.

Богоявленский В.И. Перспективы и проблемы освоения месторождений нефти и газа шельфа Арктики. Бурение и нефть, № 11, 2012, с. 4-9.

Богоявленский В.И. Природные и техногенные угрозы при освоении месторождений горючих ископаемых в криолитосфере Земли. Горная промышленность, № 1(149), 2020, с. 97-118, DOI 10.30686/1609-9192-2020-1-97-118.

Богоявленский В.И. Фундаментальные аспекты генезиса катастрофических выбросов газа и образования гигантских кратеров в Арктике. Арктика: экология и экономика, Т. 11, № 1, 2021, с. 51-66, DOI: 10.25283/2223-4594-2021-1-51-66.

Богоявленский В.И., Богоявленский И.В. Аварийные и катастрофические выбросы газа при освоении ресурсов углеводородов в арктических зонах США и Канады. Бурение и нефть, № 12, 2019, с. 3-8.

Богоявленский В.И., Богоявленский И.В. Специфика грязевулканической дегазации Земли с катастрофическими последствиями. Безопасность труда в промышленности, № 12, 2022, с. 20-28, DOI: 10.24000/0409-2961-2022-12-20-28.

Богоявленский В.И., Гарагаш И.А. Математическое моделирование процесса образования кратеров газового выброса в Арктике. Арктика: экология, экономика, № 3, 2015, с. 12-17.

Богоявленский В.И., Кишанков А.В. Опасные газонасыщенные объекты на акваториях Мирового океана: море Бофорта, шельф Северного склона Аляски. Арктика: экология и экономика, Т. 13, № 2, 2023, с. 201-210, DOI: 10.25283/2223-4594-2023-2-201-210.

Богоявленский В.И., Богоявленский И.В., Каргина Т.Н. Катастрофический выброс газа в 2020 г. на полуострове

Ecology and Economy, No. 2(30), 2018, pp. 83-93, DOI: 10.25283/2223-4594-2018-2-83-93 (in Russian).

Bogoyavlensky V.I., Sizov O.S., Nikonov R.A., Bogoyavlensky I.V. Monitoring of the methane concentration changes in the Arctic atmosphere in 2019-2021 according to the TROPOMI spectrometer data. Arctic: Ecology and Economy, Vol. 12, No. 3, 2022b, pp. 304-319, DOI: 10.25283/2223-4594-2022-3-304-319 (in Russian).

Bogoyavlensky V.I., Sizov O.S., Nikonov R.A., Bogoyavlensky I.V., Kargina T.N. Earth degassing in the Arctic: the genesis of natural and anthropogenic methane emissions. Arctic: Ecology and Economics, No. 3 (39), 2020b, pp. 6-22, DOI: 10.25283/2223-4594-2020-3-6-22 (in Russian).

Earth degassing: geodynamics, fluids, oil and gas. Proceedings of international conference in memory of P.N.Kropotkin. GEOS. Moscow, 2002, 472 p. (in Russian).

Etiope G. Natural gas seepage. The Earth's hydrocarbon degassing. Springer. Switzerland, 2015, 203 p., DOI: 10.1007/978-3-319-14601-0.

GOST R 57123-2016 (ISO 19901-2:2004). Petroleum and natural gas industries – specific requirements for offshore structures. Part 2: Seismic design procedures and criteria. Standartinform. Moscow, 2016, 32 p. (in Russian).

Guliyev I.S., Mustayev R.N., Kerimov V.Yu., Yudin M.N. Earth degassing: scale and consequences. Mining Journal, No. 11, 2018, pp. 38-42 DOI: 10.17580/gzh.2018.11.06 (in Russian).

Hovland M., Judd A., King L. Characteristic features of pockmarks on the North Sea Floor and Scotian Shelf. Sedimentology, Vol. 31, No. 4, 1984, pp. 471-480, DOI: 10.1111/j.1365-3091.1984.tb01813.

Jackson R. B., Saunois M., Bousquet P. et al. Increasing anthropogenic methane emissions arise equally from agricultural and fossil fuel sources. Environmental Research Letters, Vol. 15, No. 7, 2020, p. 071002, DOI: 10.1088/1748-9326/ab9ed2.

Judd A., Hovland M. Seabed fluid flow – impact on geology, biology and the marine environment. Cambridge University Press. Cambridge, 2007, 400 p., DOI: 10.1017/CBO9780511535918.

Kerimov V.Yu., Abdullayeva V.K. Geography and scale of greenhouse gas degassing in Azerbaijan. ANAS Transactions, Earth Sciences, No. 1, 2022, pp. 51-67, DOI: 10.33677/ggianas20220100072 (in Russian).

Kopf A.J. Significance of mud volcanism. Reviews of Geophysics, Vol. 40, No. 02, 2002, pp. 2-1–2-52, DOI: 10.1029/2000RG000093

Kruglikov N.M., Kuzin I.L. Emissions of deep gas on the Urengoy field. Structural geomorphology and neotectonics of Western Siberia in connection with oil and gas bearing. Proceedings of ZapSibNIGNI, No. 37, 1973, pp. 96-106 (in Russian).

Mironyuk S.G., Ivanova A.A., Khlebnikova O.A. Landforms generated under fluid influence (fluidogenic) as an indicator of shelf interior oil-and-gas content. Proceedings of international conference "MARESEDU-2018" Vol. II (IV). JSC «PolyPRESS». Tver, 2019, pp. 120-125 (in Russian).

Paull C.K., Dallimore S.R., Caress D.W. et al. Active mud volcanoes on the continental slope of the Canadian Beaufort Sea. Geochemistry, Geophysics, Geosystems, Vol. 16, No. 9, 2015, pp. 3160-3181, DOI: 10.1002/2015GC005928.

Report on climate features in the Russian Federation for 2021. Rosgidromet. Moscow, 2022, 110 p. (in Russian).

Sergienko V.I., Lobkovsky L.I., Semiletov I.P. et al. The degradation of submarine permafrost and the destruction of hydrates on the shelf of East Arctic seas as a potential cause of the methane catastrophe: Some results of integrated studies in 2011. Doklady Earth Science, Vol. 446, No. 3, 2012, pp. 1132-1137, DOI: 10.1134/S1028334X12080144 (in Russian).

Serov P., Portnov A., Mienert J. et al. Methane release from pingo-like features across the South Kara Sea shelf, an area of thawing offshore permafrost. Journal of Geophysical Re-

Ямал в Арктике. Результаты комплексного анализа данных аэрокосмического зондирования. Арктика: экология и экономика, Т. 11, № 3, 2021c, с. 362-374, DOI: 10.25283/2223-4594-2021-3-362-374.

Богоявленский В.И., Богоявленский И.В., Каргина Т.Н. Грязевулканическая катастрофа в Индонезии. Бурение и нефть № 11, 2017a, с. 2-11.

Богоявленский В.И., Ерохин Г.Н., Никонов Р.А., Богоявленский И.В., Брыксин В.М. Изучение зон катастрофических выбросов газа в Арктике на основе пассивного микросейсмического мониторинга (на примере озера Открытие). Арктика: экология и экономика. № 1(37), 2020a, с. 93-104, DOI: 10.25283/2223-4594-2020-1-93-104.

Богоявленский В.И., Казанин А.Г., Кишанков А.В., Казанин Г.А. Дегазация Земли в Арктике: комплексный анализ факторов мощной эмиссии газа в море Лаптевых. Арктика: экология и экономика, Т. 11, № 2, 2021d, с.178-194, DOI: 10.25283/2223-4594-2021-2-178-194.

Богоявленский В.И., Кишанков А.В., Казанин А.Г., Казанин Г.А. Опасные газонасыщенные объекты на акваториях Мирового океана: Восточно-Сибирское море. Арктика: экология и экономика, Т. 12, № 2, 2022a, с. 158-171, DOI: 10.25283/2223-4594-2022-2-158-171.

Богоявленский В.И., Перекалин С.О., Бойчук В.М., Богоявленский В.И., Каргина Т.Н. Катастрофа на Кумжинском газоконденсатном месторождении: причины, результаты, пути устранения последствий. Арктика: экология и экономика, № 1, 2017b, с. 32-46, DOI: 10.25283/2223-4594-2017-1-32-46.

Богоявленский В.И., Сизов О.С., Богоявленский И.В., Никонов Р.А. Технологии дистанционного выявления и мониторинга дегазации Земли в Арктике: полуостров Ямал, озеро Нейто. Арктика: экология и экономика, № 2(30), 2018, с. 83-93, DOI: 10.25283/2223-4594-2018-2-83-93.

Богоявленский В.И., Сизов О.С., Никонов Р.А., Богоявленский И.В. Мониторинг изменений концентрации метана в атмосфере Арктики в 2019-2021 гг. по данным спектрометра TROPOMI. Арктика: экология и экономика, Т. 12, No. 3, 2022b, с. 304-319, DOI: 10.25283/2223-4594-2022-3-304-319.

Богоявленский В.И., Сизов О.С., Никонов Р.А., Богоявленский И.В., Каргина Т.Н. Дегазация Земли в Арктике: генезис природной и антропогенной эмиссии метана. Арктика: экология и экономика, № 3(39), 2020b, с. 6-22, DOI: 10.25283/2223-4594-2020-3-6-22.

ГОСТ Р 57123-2016 (ИСО 19901-2:2004). Нефтяная и газовая промышленность. Сооружения нефтегазопромысловые морские. Проектирование с учетом сейсмических условий. Стандартинформ. Москва, 2016, 32 с.

Гулиев И.С., Мустаев Р.Н., Керимов В.Ю., Юдин М.Н. Дегазация Земли: масштабы и последствия. Горный журнал, № 11, 2018, с. 38-42, DOI: 10.17580/gzh.2018.11.06.

Дегазация Земли: геодинамика, геофлюиды, нефть и газ. Материалы Международной конференции памяти академика П.Н. Кропоткина, 20-24 мая 2002 года, г. Москва. ГЕОС. Москва, 2002, 472 с.

Доклад об особенностях климата на территории Российской Федерации за 2021 год. Росгидромет. Москва, 2022, 110 с.

Керимов В.Ю., Абдуллаева В.К. География и масштабы дегазации парниковых газов в Азербайджане. ANAS Transactions, Earth Sciences, № 1, 2022, с. 51-67, DOI: 10.33677/ggianas20220100072.

Кругликов Н.М., Кузин И.Л. Выходы глубинного газа на Уренгойском месторождении. Труды ЗапСибНИГНИ, № 37, 1973, с. 96-106.

Миронюк С.Г., Иванова А.А., Хлебникова О.А. Флюидогенные формы рельефа как индикаторы нефтегазоносности недр шельфа. Труды VII Международной научно-

search: Earth Surface, Vol. 120, No. 8, 2015, pp. 1515-1529, DOI: 10.1002/ 2015JF003467.

Sokolov S.Yu., Moroz E.A., Zarayskaya Yu.A., Abramova A.S., Ananiev R.A., Sukhikh E.A. Mapping of dangerous geological objects and processes at the Northern and Central parts of the Barents Sea shelf according to the hydroacoustic data from RV "Akademik Nikolai Strakhov". Arctic: Ecology and Economy, Vol. 13, No. 2, 2023, pp. 164-179, DOI: 10.25283/2223-4594-2023-2-164-179 (in Russian).

State of the Global Climate 2022. World Meteorological Organization. WMO-No.1316, 2023, 55 p.

Walter K.M., Zimov S., Chanton J.P., Verbyla D., Chapin III F.S. Methane bubbling from Siberian thaw lakes as a positive feedback to climate warming. Nature, Vol. 443, 2006, pp. 71-75, DOI: 10.1038/nature05040.

Yusubov N.P., Guliyev I.S. Mud volcanism and hydrocarbon systems of South-Caspian Depression (according to the newest geophysical and geochemical data). Elm. Baku, 2022, 168 p. (in Russian).

практической конференции «Морские исследования и образование (MARESEDU-2018)», Том II (IV). ООО «ПолиПРЕСС». Тверь, 2019, с. 120-125.

Сергиенко В.И., Лобковский Л.И., Семилетов И.П. и др. Деградация подводной мерзлоты и разрушение гидратов шельфа морей Восточной Арктики как возможная причина «метановой катастрофы»: некоторые результаты комплексных исследований 2011 года. Докл. Акад. Наук, Т. 446, № 3, 2012, с. 330-335.

Соколов С.Ю., Мороз Е.А., Зарайская Ю.А. и др. Картирование опасных геологических объектов и процессов северной и центральной частей шельфа Баренцева моря по данным гидроакустического комплекса НИС «Академик Николай Страхов». Арктика: экология и экономика, Т. 13, № 2, 2023, с. 164-179, DOI: 10.25283/2223-4594-2023-2-164-179.

Юсубов Н.П., Гулиев И.С. Грязевой вулканизм и углеводородные системы Южно-Каспийской впадины (по новейшим данным геофизических и геохимических исследований). Элм. Баку, 2022, 168 с.

ПРИРОДНЫЕ И ТЕХНОГЕННЫЕ КАТАСТРОФИЧЕСКИЕ ВЫБРОСЫ И ВЗРЫВЫ ГАЗА В АРКТИКЕ И ДРУГИХ РЕГИОНАХ МИРА (СУША И АКВАТОРИЯ)

Богоявленский В.И., Богоявленский И.В., Никонов Р.А.
Институт проблем нефти и газа Российской академии наук (ИПНГ РАН), Россия
119333, Москва, ул.Губкина, 3: geo.ecology17@gmail.com

Резюме. Авторы статьи создали геоинформационную систему «Арктика и Мировой океан» с огромным объемом постоянно дополняемых геопространственных данных, позволяющих проводить комплексный анализ различных природных и техногенных явлений, прямо или косвенно связанных с дегазацией Земли. В Арктике выполнен большой объем экспедиционных работ с широким комплексом геолого-геофизических методов, которые проанализированы в комплексе с данными дистанционного зондирования Земли (ДЗЗ) из космоса и с применением беспилотных летательных аппаратов. Это позволило получить принципиально новую информацию о газодинамических механизмах опасных процессов в криолитозоне, включая катастрофические выбросы и взрывы газа с образованием гигантских кратеров и крупных грязевулканических построек. Всего на севере Западной Сибири выявлено около 18.5 тысяч потенциально опасных объектов, включая 4.5 тысяч зон интенсивных выбросов газа со дна термокрастовых озер, в результате которых образуются подводные кратеры-покмарки. Это позволило выделить наиболее газовзрывоопасные зоны на севере Западной Сибири, преимущественно расположенные в восточной части полуострова Ямал. С учетом ранее открытых грязевых вулканов на суше Аляски, Гренландии и Исландии, а также на дне морей Бофорта, Карском и Норвежском, можно утверждать о существовании Циркумарктической грязевулканической провинции. В Арктике, Каспийском и других регионах с помощью ДЗЗ исследованы причины и последствия техногенной дегазации недр на ряде аварийных скважин.

Ключевые слова: *дегазация Земли, выбросы и взрывы газа, грязевые вулканы, сипы газа, дистанционное зондирование Земли, беспилотные летательные аппараты*

ARKTİKADA VƏ DÜNYANIN DİGƏR REGİONLARINDA (QURU VƏ AKVATORİYALARDA) TƏBİİ VƏ TEXNOGEN FƏLAKƏTLİ TULLANTILAR VƏ QAZ PARTLAYIŞLARI

Boqoyavlenskiy V.İ., Boqoyavlenskiy İ.V., Nikonov R.A.
Rusiya Elmlər Akademiyasının Neft və Qaz problemləri İnstitutu, Rusiya
119333,Moskva, Gubkin küç., 3: geo.ecology17@gmail.com

Xülasə. Yerin deqazasiya proseslərinin öyrənilməsi Rusiya Elmlər Akademiyasının Neft və Qaz problemləri İnstitutu tədqiqatlarının əsas istiqamətlərindən biridir. Müəlliflər, geoməkani məlumatlarla daim zənginləşdirən nəhəng həcmə malik "Arktika və Dünya okeanı" (QİS "AMO") geoinformasiya sistemi yaratmışlar ki, o Yerin deqazasiyası ilə birbaşa və ya dolayı əlaqədə olan müxtəlif təbii və texnogen hadisələrin kompleks təhlilinə imkan verir. Arktikada geoloji-geofiziki metodların geniş kompleksi ilə böyük həcmli ekspedisiya işləri yerinə yetirilmiş, onlar pilotsuz uçuş aparatları tətbiq etməklə, kosmosdan Yerin distansion zondlaşdırma məlumatları (YDZ) kompleksilə birlikdə təhlil olunmuşlar. Bu, nəhəng kraterlərin və iri palçıq vulkanı qurumlarının əmələ gəlməklə fəlakətli tullantılar və qaz partlayışları daxil olmaqla, kriolitozonada təhlükəli proseslərin qaz-dinamik mexanizmləri haqqında prinsipial olaraq yeni informasiya almağa imkan verdi. Təkcə Qərbi Sibirin şimalında onların sayəsində sualtı krater-pokmarkaların yarandığı termokarstlı göllərin dibindən 4.5 qazların intensiv atılma zonaları daxil olmaqla,18.5 min potensial təhlükəli obyektlər aşkar edilmişdir. Bu Qərbi Sibirin şimalında, əksəriyyəti Yamal yarımadasının şərq hissəsində yerləşmiş ən təhlükəli qaz partlayışı zonalarını ayırmağa imkan verdi. Alyaska, Qrenlandiya və İslandiya zonalarında, həmçinin Bofort, Karsk və Norveç dənizlərinin dibində əvvəllər aşkar edilmiş palçıq vulkanlarını nəzərə alaraq, Sirkumartik palçıq vulkanı əyalətinin mövcudluğunu irəli sürmək olar. Yerin distansion zondlaşdırılmasını (YDZ) tətbiq etməklə Arktika, Xəzər və dünyanın digər regionlarında bir sıra qəzalı neft-qaz axtarış və kəşfiyyat quyularında yer təkinin texnogen deqazasiyasının səbəbləri və fəlakətli nəticələri tədqiq olunmuşdur.

Açar sözlər: *Yerin deqazasiyası, qazın atılma və partlayışları, palçıq vulkanları, qaz uğultusu, Yerin distansion zondlaşdırılması (YDZ), pilotsuz uçuş aparatları (PUA)*

ANAS Transactions **Earth Sciences** **2 / 2023**

http://www.journalesgia.com

THE IMPACT OF COULOMB STRESS CHANGES OF THE 2018 M_w7.5 PALU EARTHQUAKE, INDONESIA

Ahadov B.[1,2], Jin Sh.[3,4]

[1]Ministry of Science and Education of the Republic of Azerbaijan,
Institute of Geology and Geophysics, Azerbaijan
119 H. Javid ave., Baku, AZ1143: ahadovshao@gmail.com
[2]Ministry of Science and Education of the Republic of Azerbaijan,
Institute of Oil and Gas, Azerbaijan
9, F.Amirov ave., Baku, AZ 1000
[3]Shanghai Astronomical Observatory, Chinese Academy of Sciences
80 Nandan Road, Shanghai 200030, China
[4]School of Surveying and Land Information Engineering,
Henan Polytechnic University, Jiaozuo 454000, China

Keywords: *Coulomb stress, stress inversion, deformation, earthquake, Palu, Indonesia*

Summary. This paper studied the effects of Coulomb stress in understanding the proximity to failure on the Palu-Koro fault system. An earthquake occurred on a large strike-slip fault in the northern part of Sulawesi Island, Indonesia, on September 28, 2018. Coulomb stress increased by approximately 1 bar, corresponding closely to the locations of aftershocks and areas where stress dropped by more than 10 bars. Based on the focal mechanisms of the aftershocks and source models of the main shock, the Coulomb failure stress changes on both of the focal mechanism nodal planes are calculated. Additionally, we calculated the changes in Coulomb stress on the focal sources of each aftershock. Our stress model indicates a positive correlation within the areas of the extended Coulomb stress caused by the combination of seismic activities. We investigated the Coulomb stress as a possible origin for the aftershocks, which are most likely to slip optimally oriented for failure due to the local stress field generated by the mainshock. The Palu 7.5 earthquake led to the distribution of surface displacements. Moreover, calculated horizontal displacement increased in the NW-SW direction, ranging from 1 to 1.3 meters. The stress maps included in this paper are crucial in predicting the expected locations of future aftershocks and mitigating the potential for earthquakes.

© 2023 Earth Science Division, Azerbaijan National Academy of Sciences. All rights reserved.

Introduction

Shallow earthquakes frequently exert destructive effects on nearby communities. Historically, this region has witnessed numerous large earthquakes with a magnitude of 6 and above, and extensive ruptures spanning over 250 km throughout the past century. Notably, the largest earthquake took place on January 1996, ~ 100 km north of the earthquake that occurred on September 28, 2018. This 1996 earthquake transpired in the regional subduction zone at a shallow depth causing fatalities, substantial property damage, and numerous injuries in the surrounding area (Source: USGS). It's essential to acknowledge that central Sulawesi has been recording earthquakes since the 18th century. Many of these seismic events were catastrophic and were followed by tsunamis. Historically, Palu Bay witnessed a significant seismic event in 1927 that released a huge tsunami with a height of 15 m. In a similar event nearly seven decades later, Donggala was struck in 1996 by a tsunami with wave heights ranging between 1-3 m.

On September 28, 2018, a moment magnitude 7.5 earthquake struck the northern region of Palu, Sulawesi (Fig. 1). The mainshock occurred at a shallow depth on the Palu-Koro fault located within the interior of the Molucca microplate on the Sunda tectonic plate. The earthquake's focal mechanism solution indicates that it was caused by a strike-slip on

faults trending both north-south and west-east. This seismic event took place on the Palu-Koro fault with an approximate rupture length of 150 km. The earthquake resulted in significant damage to buildings and infrastructure leading to thousands of fatalities and even more injuries. The aftermath of this event included ground shaking, landslides, and a tsunami, all contributing to the catastrophic impact.

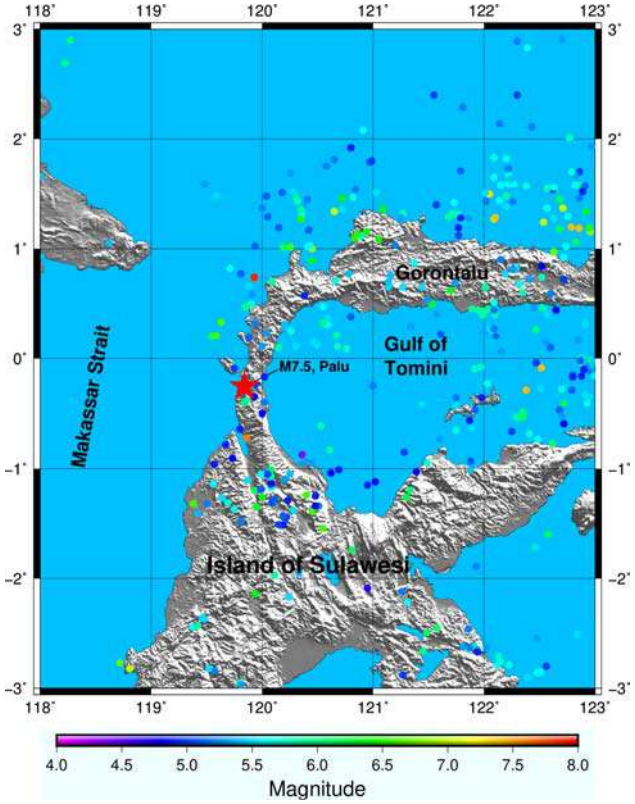


Fig. 1. Simplified topographic map of the study area. Highlighted dots are earthquakes $M_w \geq 4$ seismicity from ISC (1976-2018)

The concept of static Coulomb stress changes, induced by a primary earthquake, can potentially trigger subsequent earthquakes along neighbouring faults. Therefore, changes in earthquake stress can be employed in the evaluation of potential seismic hazards (King et al., 1994; Ahadov, Jin, 2019). The stress change and its effects associated with the Loma Prieta, California shock have been the subject of numerous studies (Lin, Stein, 2004; Reasenberg and Simpson, 1992). Hardebeck et al., (1998) applied the Coulomb stress transfer model to examine the impacts of the Landers and Northridge earthquakes. However, comparing co-seismic stress changes with earthquakes represents a significant oversimplification of the complex natural processes involved in earthquake triggering. Coulomb stress changes induced by the main shock are evaluated by calculating the stress variations across both optimally oriented and specific fault planes. The results from these calculations suggest that there is no clear evidence that the Coulomb stress changes created by the main shock facilitated the occurrence of the aftershocks.

We analyzed the correlation between components of the comprehensive Coulomb failure stress to understand the process of earthquake triggering accurately. We utilized stress interaction methods to determine how the earthquake affected the potential for failure along the Palu-Koro fault. These findings are applied to assess the acceleration or delay of future earthquakes in Palu, Sulawesi.

Tectonic Setting

Sulawesi Island is located among the Philippine, Australian, and Sunda plates and surrounds the continental convergence sections of the Sunda margin. The triple junction in Southeast Asia is highly seismically active and is characterized by active rotations of small blocks reported by both geological and kinematic studies (Kreemer et al., 2000; Silver, Moore, 1978; Simons et al., 2000; Stevens et al., 1999; Walpersdorf et al., 1998) (Fig. 2). The main active structures in Sulawesi are the Palu-Koro fault and its south-eastern extension to Matano. The Palu-Koro fault divides the islands into two blocks: the North Sula Block to the northeast and the Makassar Block to the southwest (Fig. 2). GPS and block modelling data suggest a slip rate of 42 mm/year in the area of the Palu-Koro fault (Socquet et al., 2006). A significant active structure on land in the west of Central Sulawesi is the NW-SE trending Palu-Koro strike-slip fault, which forms the boundary between the Makassar and North Sula blocks (Kreemer et al., 2000). The slip velocity on this fault is estimated to be within the range of 30-40 mm per year (Bellier et al., 2001). Certain parallel fault strands determine the margins of a pull-apart basin in Palu.

The Australian and Philippine plates are subducting beneath the Sunda plate at rates between 75-90 mm/year (Socquet et al., 2006). The W-E trending plate boundary zone extending from the New Guinea Trench to East Indonesia, establishes the relative motion between the Pacific and Australian plates via block rotations and transgression faulting (Tregoning et al., 2000; Wallace et al., 2004). The subduction of the Australian plate beneath the Sunda plate occurs at the Sunda-Banda Arc. The Java Trench extends from the collision in Australia to approximately 600 km south of Sulawesi. Specifically, the southwestern part of Sulawesi rotates counter-clockwise in relation to the Sunda Plate, while the North Sula Block and the northeastern Manado Block rotate clockwise towards the NNW.

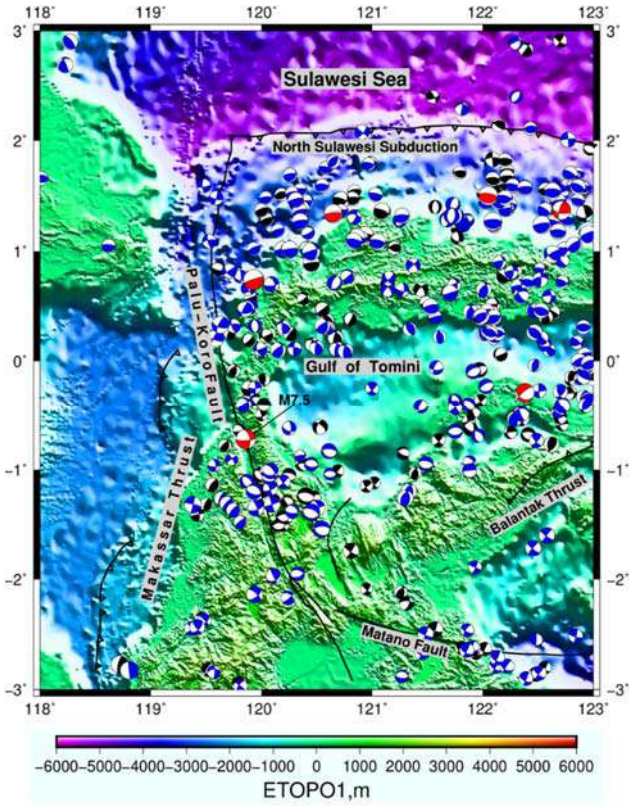


Fig. 2. Simplified topographic/bathymetric and tectonic setting map of the study area. Major active tectonic structures and faults are shown. The focal mechanism solutions are from the Global Centroid Moment Tensor (GCMT, black) and International Seismological Centre (ISC, blue) catalogs. Red balls are $M_w \geq 7$, 1976-2019.

Method

Coulomb Failure

While statistical seismology often provides probabilities for aftershock locations and timings, accurate prospective earthquake predictions demand a physical understanding of earthquake distribution. Comprehending how static stress accumulates over time through tectonic plate movement or co-seismic and post-seismic slip may serve as a foundation for determining earthquake probabilities over timeframes that extend beyond typical aftershock duration periods (Strader, 2014).

Variations in the Coulomb failure stress due to the mainshock are resolved onto the fault plane of the affected earthquake using strike, dip, and rake angles in the stress calculations. Future failure areas have been identified by the increased effects of the Coulomb stress.

$$\Delta\sigma_f = \Delta\tau - \mu'\Delta\sigma_n \qquad (1)$$

where $\Delta\tau$ and $\Delta\sigma_n$ are the change in normal and shear stresses on likely future fault planes. The effective coefficient of friction denoted as μ takes into account the effects of changes in pore pressure and typically ranges from 0 to 0.8 (Roeloffs, 1988). The confining stress can be related to fluid pore pressure by Skempton's coefficient, B, which quantifies the ratio of the change in pore pressure in a cavity to the change in applied stress. The Coulomb stress is contingent on the accuracy of the initial earthquake parameters. Minor variations in fault geometry and slip distribution can lead to significant alterations in Coulomb failure stress.

We used Coulomb 3.4 software (Lin and Stein, 2004; Toda et al., 2005) to compute the co-seismic static stress changes resulting from the magnitude 7.5 Palu earthquake on optimally oriented faults. In our model, the Earth was presumed to be a homogenous elastic half-space, and faults were treated as rectangular dislocations. To accommodate these assumptions, we considered values for Young's modulus, shear modulus, and Poisson's ratio were considered as $8x10^5$ bar, $3.2x10^5$ bar, and 0.25, respectively. We utilized an empirically value of 0.4 and 0.6 for the effective friction coefficient (μ'). To estimate the average slip for an earthquake, we applied empirical relationships from Wells and Coppersmith (1994) which correlate event rupture length, width, magnitude, and surface displacement.

Stress Inversion

The stress variations have been projected onto the optimally oriented mainshock strike-slip, thrust, and normal faults using the regional stress field defined in this study. The stress inversion method developed by Michael (1984) provided definitions for normal and shear stresses on a fault σ_n and:

$$\sigma_n = T_i n_i = \tau_{ij} n_i n_j \qquad (2)$$

$$\tau N_i = T_i - \sigma_n n_i = \tau_{ij} n_j - \tau_{jk} n_j n_k n_i = \\ = \tau_{kj} n_j \left(\delta_{jk} - n_i n_k\right) \qquad (3)$$

where δ_{ik} is the Kronecker delta, T is the traction along the fault, n is the fault normal and N is the unit direction vector of shear stress along the fault. Afterwards, equation (3) is revised as follows:

$$\tau_{kj} n_j (\delta_{ik} - n_i n_k) = \tau N_i \, . \qquad (4)$$

Michael (1984) employed the Wallace-Bott theory and defined the shear stress direction denoted as N with the slip direction s of shear movement along the fault. He further proposed that the shear stress τ on active faults maintains a consistent ratio across all studied earthquakes. Subsequently, equation (4) is represented in matrix form:

$$At = s \qquad (5)$$

where t represents the vector of stress components.

$$t = [\tau_{11}\tau_{12}\tau_{13}\tau_{22}\tau_{23}]^T \quad (6)$$

A is the 3 × 5 matrix calculated from fault normal n,

$$\begin{bmatrix} n_1(n_2^2+2n_3^2) & n_2(-n_1^2+n_3^2) & n_3(-2n_1^2-n_2^2) \\ n_2(1-2n_1^2) & n_1(1-2n_2^2) & -2n_1n_2n_3 \\ n_3(1-2n_1^2) & -2n_1n_2n_3 & n_1(1-2n_3^2) \\ n_1(-n_2^2+n_3^2) & n_2(n_1^2+2n_3^2) & n_3(-n_1^2-2n_2^2) \\ -2n_1n_2n_3 & n_3(1-2n_1^2) & n_2(1-2n_3^2) \end{bmatrix}^{\mathbf{T}} \quad (7)$$

The degree of correlation hinges on several factors: the precision of source/receiver hypocentre locations and focal mechanism parameters, as well as physical source characteristics. Michael's algorithm employs both nodal planes to try to identify the exact fault planes while determining the optimal stress tensor. A key feature of the algorithm is the calculation of the confidence limits of the principal stress axes directions, which is performed through a statistical method known as bootstrap resampling. The algorithm seeks to minimize the discrepancy between the slip direction and the projected tangential traction while maintaining a consistent and significant magnitude of tangential traction across various fault planes. Although it is somewhat conjectural, the use of a simple fracture criterion suggests keeping the tangential traction similar from one fault plane to another. This fracture criterion further implies that the isotropic component of the stress tensor dominated the normal traction on the fault planes.

Results and Discussion

Local stress inversion

Over the past 30 years, it has been widely accepted that the location and timing of recurring earthquakes (aftershocks) are largely influenced by stress changes resulting from displacement due to the main shock. Interest in the issue of the effect of stress changes on subsequent seismic activity was triggered following minor events 17 years before the 1992 earthquake near Landers, California (USA) with M 7.4 led to a stress increase at the epicentre and along the majority of the future rupture line (Stein et al., 1992). Furthermore, the majority of aftershocks occurred in the area where an increase in stress was observed. Multiple studies have since discovered a quantitative correlation between static voltage changes and the location of subsequent major shocks and aftershocks (Harris, 1998; Steacy et al., 2005; King, 2007; Hardebeck, Okada, 2018).

Alterations in Coulomb stress are derived from displacements associated with corresponding earthquakes. These displacements induce perturbations in the stress tensor within the fault, potentially leading to both shear and normal components. An increase in shear stress, contemporary with the displacement direction, and a decrease in normal stress collectively enhance the probability of future failure.

Numerous methods have been proposed to determine tectonic stress from earthquake focal mechanism solutions. The most commonly used methods were developed by Michael (1984) and Gephart and Forsyth (1984). These methods typically assume that tectonic stress is homogeneous within the region, that earthquakes occur on pre-existing faults with varying orientations, and that the slip vector aligns with the shear stress direction on the fault. In this study, we have used Focal Mechanism Solutions (FMS) from Harvard CMT (Ekström et al., 2012) and International Seismological Centre (ISC, http://www.isc.ac.uk) for our region of interest (Fig. 2).

Michael (1984) proposed determining the stress that minimizes the discrepancy between the resolved shear stress and the slip direction for each dataset. These algorithms outline the directions of the three principal stress axes, as well as the relative magnitudes of these stress axes. In this context, $\sigma1$, $\sigma2$, and $\sigma3$ indicate the maximum, intermediate, and minimum principal compressive stresses, respectively.

The defining feature of the stress field is its utility in outlining deformation zones and active tectonic structures at local and regional levels. We created two distinct datasets of focal mechanisms, one from GCMT and another from ISC to assess the capability of stress ratio R under varying stress conditions. We performed stress inversion on these fault planes using the same process developed by Vavryčuk (2014). The R-values for all zones fall within the range of 0.3 to 0.7 indicating that the magnitude of the intermediate principal stress ($\sigma2$) is relatively close to midway between the magnitudes of the $\sigma1$ and $\sigma3$ axes (when $R = 0.5$). The inversion results demonstrate that the maximum principal stress ($\sigma1$) is oriented in the NW-SE direction while the minimum stress axis ($\sigma3$) strikes in the NE-SW direction and is sub-vertical. The intermediate principal stress ($\sigma2$) is trending sub-horizontal for the Palu region (refer to Table, Fig. 3).

Comparison of stress tensor inversion results for the region

Region	σ_1(tr)	σ_1(pl)	σ_2(tr)	σ_2(pl)	σ_3(tr)	σ_3(pl)	Phi (R)
Palu	293.6	35.5	114.6	54.4	24	0.5	0.51±0.03

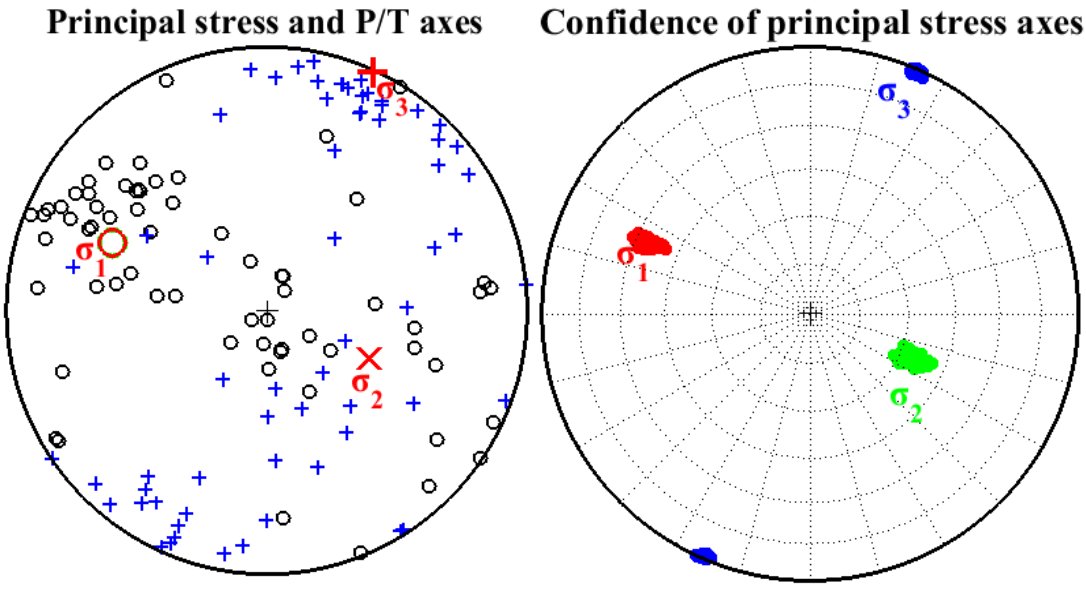


Fig. 3. The map represents the P and T axes of the focal mechanisms and dots delineate the distribution of the stress axis within the 95% confidence range. Azimuth (Az) and plunge (Pl)

Coulomb stress

We studied the Coulomb stress hypothesis for the 2018 Palu earthquake in Indonesia using focal mechanism solutions as receiver faults in the Coulomb stress pattern. The correlation between the Coulomb stress and seismic activity generated by the Palu event and preceding incidents suggests regions at risk for significant future events. The main shock was preceded by foreshocks starting about three hours earlier with an event located south of the epicenter. The Coulomb stress patterns were calculated at a depth of 10 km due to the main shock.

The stress model depicts four distinct lobes of increased Coulomb stress and four lobes of Coulomb stress reduction (Fig.4). The extended lobes are located at the end of the fault, while the regions of decreased Coulomb stress host the other lobes. The distribution of aftershocks aligns with these patterns. A Coulomb stress change of less than 1 bar is sufficient to trigger events, while the same amount can effectively suppress them (King et al., 1994). The largest lobe of the decreased Coulomb stress is centered on the epicenter of the rupture plane, where stresses dropped by approximately 11 bars. The stresses generated by earthquake slip can cause fracturing, and the resulting stress increases can lead to further earthquakes. Most of the aftershocks have occurred in areas where the Coulomb failure stress has increased by ≥ 1 bar, and a significant number of aftershocks are located where the stress has decreased in the E-S direction (Fig. 4).

Coulomb stress models are calculated on an optimally oriented fault plane using local stress results. The calculation results of the optimum orientations and Coulomb stress changes are presented in Figure 4 (b, c, and d). Negative Coulomb stress changes dominate within the rupture area, while positive stress changes are observed in the northwest and southeast parts of the rupture. In the case of normal faulting orientation (Fig. 4d), most of the aftershocks concentrate in the area of positive stress change, except for a few earthquakes in the rupture zone where negative stress changes were observed. The lobed models of stress variation using local stress adjustments encompass large areas of negative change that dominate towards landward and offshore of the main rupture with positive stress changes occurring in the SW-NE direction inland and offshore in the case of an optimum thrust faulting (Fig. 4c).

The vertical cross-section confirms that the fault plane is associated with the mainshock (Fig.5). The aftershocks occur in regions of negative stress changes and some are located in areas of positive stress changes. The vertical cross-sections provide extended data on the stress distribution in strike-slip faulting situations as seen in Figure 5. The study of the stress produced on a cross-section reveals that the Coulomb stress increase occurs in the areas where aftershocks were located at different depths. It can be seen that the region towards C-C' is more likely to have aftershocks due to increased stress accumulation. There are possibilities that the aftershocks might have propagated towards the south, and the most probable direction is towards the southeast.

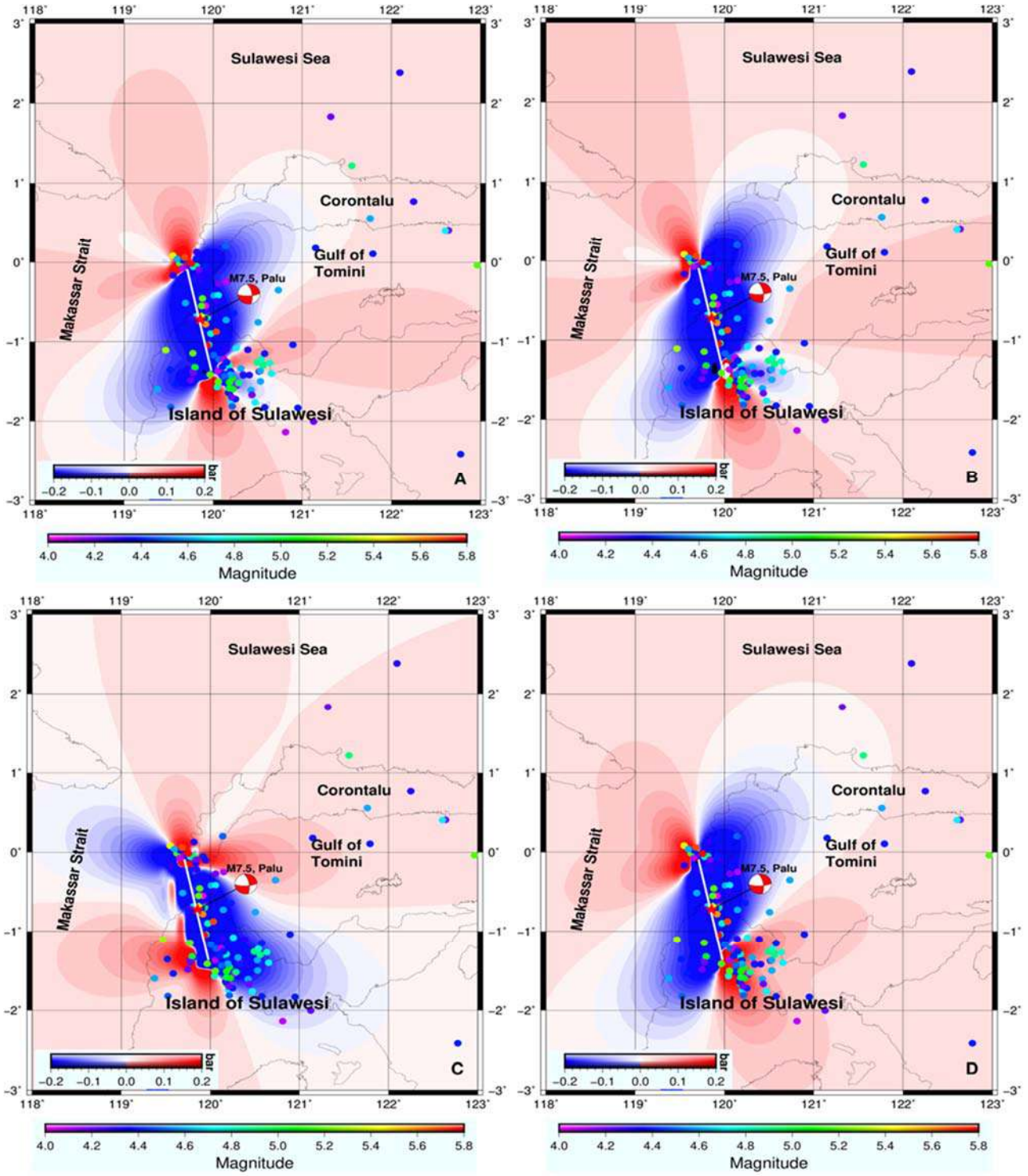


Fig. 4. Map shows Coulomb stress changes caused by the 2018 Palu earthquake calculated over the optimally oriented (a) strike 348^0; dip 57^0; rake -15^0 (gCMT) (b) strike-slip faulting (c) thrust faulting and (d) normal faulting. The highlighted dots denote the epicenters of the $M \geq 4$ aftershocks (USGS)

The assumed value for effective friction contributes to the calculated Coulomb stress changes, and thus the correspondence of Coulomb stress changes to aftershock distributions. Typically, studies aim to identify the effective coefficient of friction that leads to the best fit of aftershocks using this technique to infer frictional strength. King et al. (1994) found that adjustments to friction only had noticeable effects on aftershock correlations and thus preferred to use the value of 0.4. Moreover, Coulomb stress changes are calculated at different depths and friction values from a finite fault modelling result (USGS, us1000h3p4). The occurrence of several aftershocks in an area of the calculated Coulomb stress decrease may be due to the oversimplification of the fault slip, heterogeneities of crustal characteristics, or orientations of the fault.

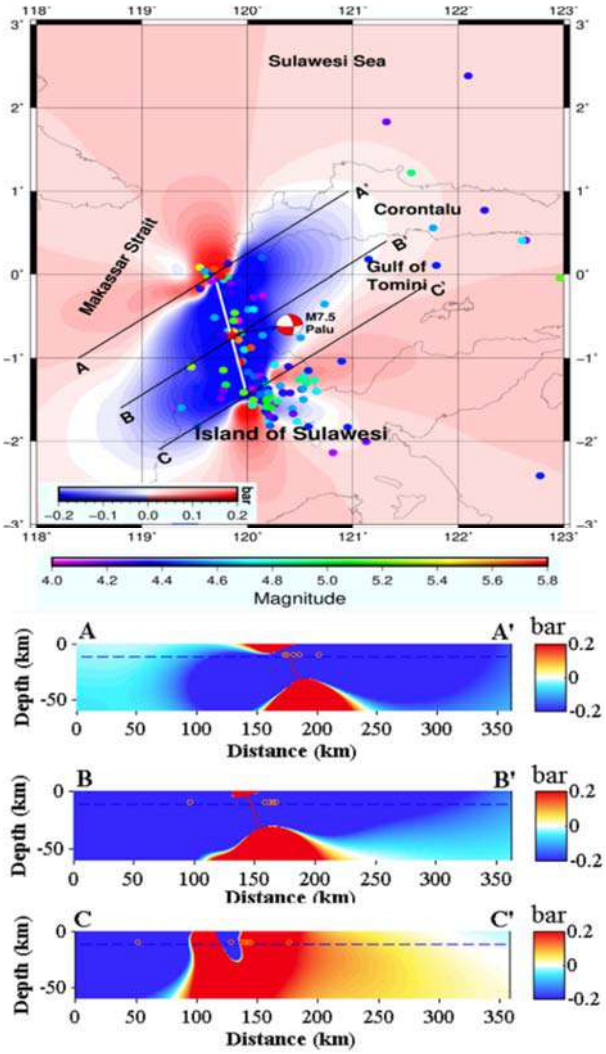


Fig. 5. Vertical cross-sections oriented perpendicular to the strike of the fault modelling during the 2018 Palu earthquake along lines P1 (A-A'), P2 (B-B') and P3 (C-C')

Figure 6 illustrates the effects of static stress when the friction coefficients are at typical values of 0.4 and 0.6. For different values a distinct level of difference is observed in the number of triggered aftershocks when the coefficient is 0.6 at a depth of 15 km, and 30% of the aftershocks occur in the areas of increased stress. The static Coulomb stress triggering effect does not improve significantly with variations in the friction coefficient value. Coseismic Coulomb stress change calculations have effectively described aftershock distributions following the 1995 Kobe, Japan earthquake (Toda et al., 1998), and the 1989 M = 7.1 Loma Prieta earthquake (Reasenberg, Simpson, 1992). The presence of several aftershocks in areas of the decreased Coulomb stress may result from oversimplifications of modeled fault slip or the existence of faults with different orientations. The application of Coulomb stress changes to explain aftershock distributions challenges the long-standing theory that earthquakes occur randomly.

Displacement and Strain rate

Therefore, considering all of the above mentioned, we calculated the average slip distribution from empirical relationships between average slip and magnitude. The earthquake struck the island of Sulawesi, approximately 78 km north of Palu. The earthquake triggered a tsunami that was 4 to 7 m high, which affected the coastal areas of western Sulawesi, including Donggala and the city of Palu. We created a displacement map that reveals vertical and horizontal surface movement across the entire fault. Figure 7 presents the results of calculations of the seismic displacement of the Earth caused by the earthquake. The fault extends to the southeast, and the most substantial horizontal displacement mainly occurs in the NNW and SW parts of the fault. Horizontal displacement in the north-south direction is larger than the displacement in the southwestern direction. The red color indicates positive displacement (elevation), while blue represents negative displacement. This map aids in understanding the type of faulting associated with an earthquake. Figure 8 demonstrates that the rupture from the Palu earthquake has the vertical displacements are approximately 2 m offshore in the NW direction.

The release of strain between events is what triggers earthquakes. In this study, we tried to understand the distribution of strain caused by the Palu earthquake. The strain tensor is calculated concerning six components: three normal and three shear strain components. The normal components of strain are oriented towards the *x, y,* and *z* directions. Figure 8 shows that aftershocks predominantly accumulate negative strain in various directions. However, not only negative strain significant for a future shock, but positive strain changes can also induce future events. A positive change in Coulomb stress in the future could be substantial enough to alter the level of strain on the regional fault, potentially causing rupture. Our analysis determined that the strain maps of the earthquake demonstrate a response that is roughly similar to that of the Coulomb stress indicating the accumulation of strain along the SE direction.

Conclusion

Assessing the Coulomb stress associated with earthquake slip has been confirmed to be an essential means of understanding diverse seismic phenomena. Such calculations have successfully illustrated aftershock distributions, the locations of triggered earthquakes, stress increases at the edges of a ruptured fault, and off-fault lobes of stress increase. Areas of Coulomb stress decrease have also been identified to align with regions of minimal aftershock activity.

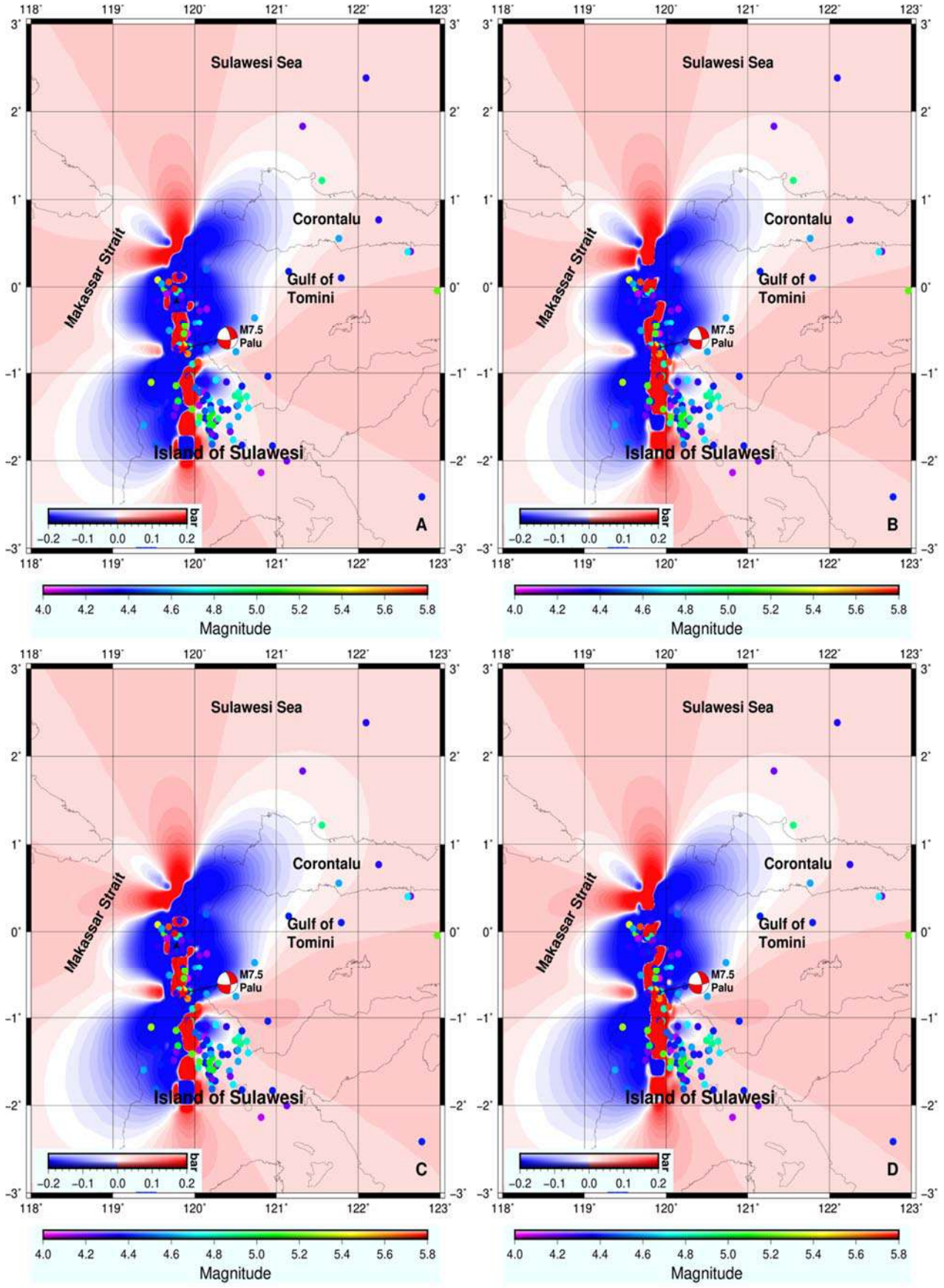


Fig. 6. Illustration of Coulomb stress changes based on Gavin Hayes's finite fault model (USGS/NEIC). (a) Depth: 10 km; μ 0.4, (b) Depth: 15 km; μ 0.4, (c) Depth: 10 km; μ 0.6, (d) Depth: 15 km; μ 0.6

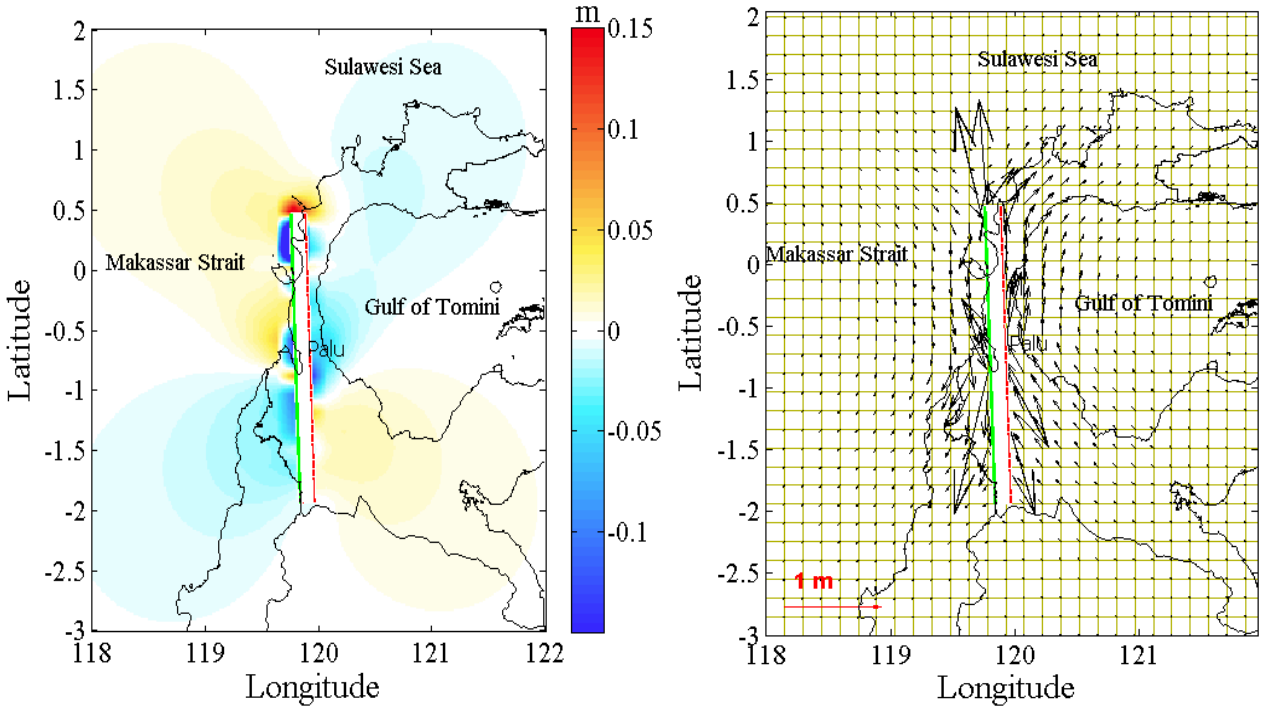


Fig. 7. Horizontal displacement map of the region enclosing the epicenter of the earthquake immediately after the mainshocks (**right**). Vertical cross-sectional view of the displacement of the crust (**left)**

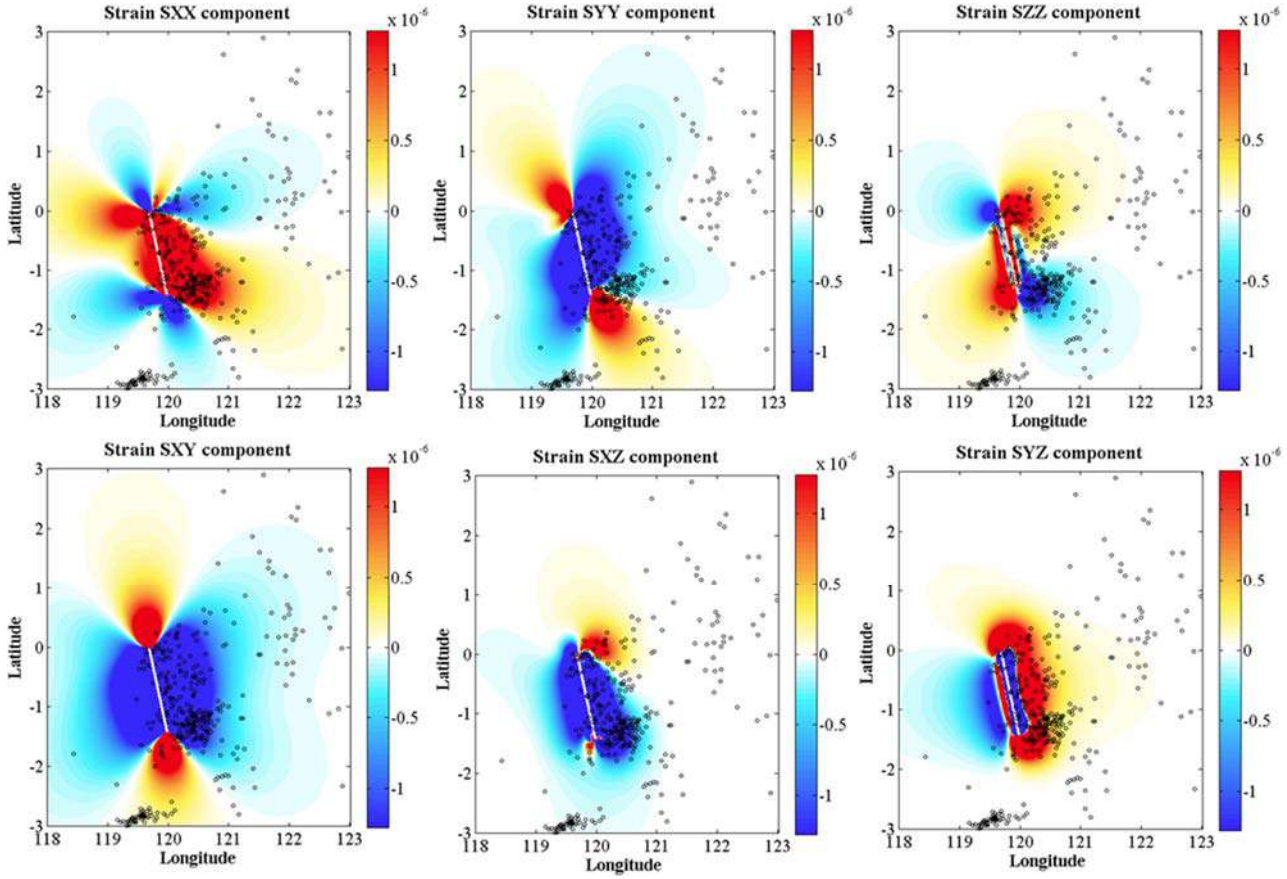


Fig. 8. Normal strain along the x-direction, y-direction, z-direction, and the shear strain in the XY, XZ, and YZ planes of the 2018 Palu earthquake

In this research, we focused exclusively on static stress changes transmitted from the co-seismic fault slips of the main shock. We examined Coulomb stress changes associated with the 2018 Mw7.5 Palu earthquake. The stress model maps demonstrated a correspondence between the main shocks and the observed spatial distribution of aftershocks. These aftershocks were found to be influenced by their relative locations to the rupture plane and source mechanisms, and their dense distribution areas expanded towards the southeast. The stresses transmitted by the Palu earthquake to the adjacent segment of the Palu-Koro fault loaded 1-2 bars of stress at the end of the rupture plane. Stress modelling confirms that minor increases (a few bars) may promote the occurrence of earthquakes. Coulomb stress modelling can serve as a powerful tool for seismic hazard mitigation and aftershock activity prediction. Stress reductions from the earthquake and triggering times are small relative to the recurrence time of the earthquakes.

Acknowledgement

All the maps are drawn using Generic Mapping Tools (GMT) (Wessel et al., 2013).

REFERENCES

Ahadov B., Jin S. Effects of Coulomb stress change on Mw> 6 earthquakes in the Caucasus region. Physics of the Earth and Planetary Interiors, Vol. 297, 106326, 2019, https//doi.org/ 10.1016/ j.pepi.2019.106326.

Bellier O., Sébrier M., Beaudouin T., Villeneuve M., Braucher R., Bourles D., Siame L., Putranto E., Pratomo I. High slip rate for a low seismicity along the Palu-Koro active fault in central Sulawesi (Indonesia). Terra Nova, Vol. 13, No. 4, 2001, pp. 463-470, DOI:10.1046/j.1365-3121.2001.00382.

Ekström G., Nettles M., Dziewoński A. The global CMT project 2004-2010: Centroid-moment tensors for 13,017 earthquakes. Physics of the Earth and Planetary Interiors, Vol. 200-201, 2012, pp. 1-9, DOI: 10.1016/J.pepi.2012.04.002.

Gephart J.W., Forsyth D.W. An improved method for determining the regional stress tensor using earthquake focal mechanism data: application to the San Fernando earthquake sequence. Journal of Geophysical Research: Solid Earth, Vol. 89, 1984, pp. 9305-9320, https://doi.org/10.1029/JB089iB11p09305.

Hardebeck J.L., Nazareth J.J., Hauksson E. The static stress change triggering model: Constraints from two southern California aftershock sequences. Journal of Geophysical Research: Solid Earth, Vol. 103, No. B10, 1998, pp. 24427-24437.

Hardebeck J.L., Okada T. Temporal stress changes caused by earthquakes: A review. Journal of Geophysical Research: Solid Earth, Vol. 123, No. 3-4, 2018, pp. 1350-1365, DOI:10.1002/2017jBO 14617.

Harris R.A. Introduction to special section: Stress triggers, stress shadows, and implications for seismic hazard. J. Geophys. Research., Vol. 103, No. B10, 1998, pp. 24347-24358.

King G.C., Stein R.S., Lin J. Static stress changes and the triggering of earthquakes. Bulletin of the Seismological Society of America, Vol. 84, No. 3, 1994, pp. 935-953.

King G.C.P. Fault interaction, earthquake stress changes, and the evolution of seismicity. Treatise on Geophysics, Vol. 4, 2007, pp. 225-255, DOI:10.1016/B978-044452748-6.00069-9.

Kreemer C., Holt W.E, Goes S., Govers R. Active deformation in eastern Indonesia and the Philippines from GPS and seismicity data. Journal of Geophysical Research: Solid Earth, Vol. 105**,** No. B1, 2000, pp. 663-680.

Lin J., Stein R.S. Stress triggering in thrust and subduction earthquakes and stress interaction between the southern San Andreas and nearby thrust and strike-slip faults. Journal of Geophysical Research: Solid Earth, Vol. 109, No. B2, 2004, 19 p., DOI:org/10.1029/2003JB002607

Michael A.J. Determination of stress from slip data: faults and folds. Journal of Geophysical Research: Solid Earth, Vol. 89, No. B13, 1984, pp. 11517-11526, DOI:10.1029/JBO89i13p11517.

Reasenberg P.A., Simpson R.W. Response of regional seismicity to the static stress change produced by the Loma

ЛИТЕРАТУРА

Ahadov B., Jin S. Effects of Coulomb stress change on Mw> 6 earthquakes in the Caucasus region. Physics of the Earth and Planetary Interiors, Vol. 297, 106326, 2019, https//doi.org/ 10.1016/ j.pepi.2019.106326.

Bellier O., Sébrier M., Beaudouin T., Villeneuve M., Braucher R., Bourles D., Siame L., Putranto E., Pratomo I. High slip rate for a low seismicity along the Palu-Koro active fault in central Sulawesi (Indonesia). Terra Nova, Vol. 13, No. 4, 2001, pp. 463-470, DOI:10.1046/j.1365-3121.2001.00382.

Ekström G., Nettles M., Dziewoński A. The global CMT project 2004-2010: Centroid-moment tensors for 13,017 earthquakes. Physics of the Earth and Planetary Interiors, Vol. 200-201, 2012, pp. 1-9, DOI: 10.1016/J.pepi.2012.04.002.

Gephart J.W., Forsyth D.W. An improved method for determining the regional stress tensor using earthquake focal mechanism data: application to the San Fernando earthquake sequence. Journal of Geophysical Research: Solid Earth, Vol. 89, 1984, pp. 9305-9320, https://doi.org/10.1029/JB089iB11p09305.

Hardebeck J.L., Nazareth J.J., Hauksson E. The static stress change triggering model: Constraints from two southern California aftershock sequences. Journal of Geophysical Research: Solid Earth, Vol. 103, No. B10, 1998, pp. 24427-24437.

Hardebeck J.L., Okada T. Temporal stress changes caused by earthquakes: A review. Journal of Geophysical Research: Solid Earth, Vol. 123, No. 3-4, 2018, pp. 1350-1365, DOI:10.1002/2017jBO 14617.

Harris R.A. Introduction to special section: Stress triggers, stress shadows, and implications for seismic hazard. J. Geophys. Research., Vol. 103, No. B10, 1998, pp. 24347-24358.

King G.C., Stein R.S., Lin J. Static stress changes and the triggering of earthquakes. Bulletin of the Seismological Society of America, Vol. 84, No. 3, 1994, pp. 935-953.

King G.C.P. Fault interaction, earthquake stress changes, and the evolution of seismicity. Treatise on Geophysics, Vol. 4, 2007, pp. 225-255, DOI:10.1016/B978-044452748-6.00069-9.

Kreemer C., Holt W.E, Goes S., Govers R. Active deformation in eastern Indonesia and the Philippines from GPS and seismicity data. Journal of Geophysical Research: Solid Earth, Vol. 105**,** No. B1, 2000, pp. 663-680.

Lin J., Stein R.S. Stress triggering in thrust and subduction earthquakes and stress interaction between the southern San Andreas and nearby thrust and strike-slip faults. Journal of Geophysical Research: Solid Earth, Vol. 109, No. B2, 2004, 19 p., DOI:org/10.1029/2003JB002607

Michael A.J. Determination of stress from slip data: faults and folds. Journal of Geophysical Research: Solid Earth, Vol. 89, No. B13, 1984, pp. 11517-11526, DOI:10.1029/JBO89i13p11517.

Reasenberg P.A., Simpson R.W. Response of regional seismicity to the static stress change produced by the Loma

Prieta earthquake. Science, Vol. 255, No. 5052, 1992, pp. 1687-1690, DOI:10.1126/science 255.5052.1687.

Roeloffs E.A. Hydrologic precursors to earthquakes: A review. Pure and applied geophysics, Vol. 126, 1988, pp. 177-209.

Silver E.A., Moore J.C. The Molucca sea collision zone, Indonesia. Journal of Geophysical Research: Solid Earth, Vol. 83, 1978, pp. 1681-1691.

Simons W., van Loon D., Waspersdorf A., Ambrosius B., Kahar J., Abidin H., Sarsito D., Vigny C., Abu S.H., Morgan P. Geodynamics of SE Asia: First results of the Sulawesi 1998 GPS campaign. In: Geodesy Beyond 2000, Springer. 2000, pp. 271-277.

Socquet A., Simons W., Vigny C., McCaffrey R., Subarya C., Sarsito D., Ambrosius B., Spakman W. Microblock rotations and fault coupling in SE Asia triple junction (Sulawesi, Indonesia) from GPS and earthquake slip vector data. Journal of Geophysical Research: Solid Earth,Vol. 111, No. B8, 2006, DOI: org/10.1029JBOO3963.

Stevens C., McCaffrey R., Bock Y., Genrich J., Subarya C., Puntodewo S. and Vigny C. Rapid rotations about a vertical axis in a collisional setting revealed by the Palu fault, Sulawesi, Indonesia. Geophysical Research Letters, Vol. 26, No. 17, 1999, pp. 2677-2680, DOI:org/10.1029/1999GE008344.

Strader A.E. The effects of Coulomb stress change on Southern California earthquake forecasting. UCLA. ProQuest ID: Strader_ucla_0031D_12803. Merritt ID: ark:/13030/m58d22pj, 2014,166 , DOI:10.13140/RG.22.36576.48647.

Steacy S., Nalbant S.S., McCloskey J., Nostro C., Scotti O., Baumont D. Onto what planes should Coulomb stress perturbations be resolved? J. Geophys. Res., Vol. 110, No. B5, 2005, B05S15, DOI: 10.1029/2004JBOO3356.

Stein R.S., King G.C.P., Lin J. Change in failure stress on the southern San Andreas fault system caused by the 1992 Magnitude = 7.4 Landers earthquake. Science, Vol. 258, 1992, pp. 1328-1332, DOI:10/1126science.258.5086.1328.

Toda S., Stein R.S., Reasenberg P.A., Dieterich J.H., Yoshida A. Stress transferred by the 1995 Mw= 6.9 Kobe, Japan, shock: Effect on aftershocks and future earthquake probabilities. Journal of Geophysical Research: Solid Earth, Vol. 103, No. 10, 1998, pp. 24543-24565, DOI:org/10.1029/98J600765.

Toda S., Stein R.S., Richards-Dinger K., Bozkurt S.B. Forecasting the evolution of seismicity in southern California: Animations built on earthquake stress transfer. Journal of Geophysical Research: Solid Earth, Vol. 110, No. 5, 2005, 17 p., DOI: 10.1029/2004JBOO3415.

Tregoning P., McQueen H., Lambeck K., Jackson R., Little R., Saunders S., Rosa R., Present-day crustal motion in Papua New Guinea. Earth, planets and space, Vol. 52, No. 10, 2000, pp. 727-730.

Vavryčuk V. Iterative joint inversion for stress and fault orientations from focal mechanisms. Geophysical Journal International, Vol. 199, No. 1, 2014, pp. 69-77, DOI: org/1093/gji/ggu224.

Wallace L.M., Stevens C., Silver E., McCaffrey R., Loratung W., Hasiata S., Stanaway R., Curley R., Rosa R., Taugaloidi J. GPS and seismological constraints on active tectonics and arc-continent collision in Papua New Guinea: Implications for mechanics of microplate rotations in a plate boundary zone. Journal of Geophysical Research: Solid Earth, Vol. 109, No. 5, 2004, DOI: 10.1029/2003JBOO2481

Wells D.L., Coppersmith K.J. New empirical relationships among magnitude, rupture length, rupture width, rupture area, and surface displacement. Bulletin of the seismological Society of America, Vol. 84, 1994, pp. 974-1002, DOI:org/10.1785/BSSA0840040974.

Wessel P., Smith W.H., Scharroo R., Luis J., Wobbe F. The generic mapping tools: improved version released. EOS, Transactions American Geophysical Union, Vol. 94, No. 45, 2013, pp. 409-410, DOI: 10.1002/2013EO450001.

Prieta earthquake. Science, Vol. 255, No. 5052, 1992, pp. 1687-1690, DOI:10.1126/science 255.5052.1687.

Roeloffs E.A. Hydrologic precursors to earthquakes: A review. Pure and applied geophysics, Vol. 126, 1988, pp. 177-209.

Silver E.A., Moore J.C. The Molucca sea collision zone, Indonesia. Journal of Geophysical Research: Solid Earth, Vol. 83, 1978, pp. 1681-1691.

Simons W., van Loon D., Waspersdorf A., Ambrosius B., Kahar J., Abidin H., Sarsito D., Vigny C., Abu S.H., Morgan P. Geodynamics of SE Asia: First results of the Sulawesi 1998 GPS campaign. In: Geodesy Beyond 2000, Springer. 2000, pp. 271-277.

Socquet A., Simons W., Vigny C., McCaffrey R., Subarya C., Sarsito D., Ambrosius B., Spakman W. Microblock rotations and fault coupling in SE Asia triple junction (Sulawesi, Indonesia) from GPS and earthquake slip vector data. Journal of Geophysical Research: Solid Earth,Vol. 111, No. B8, 2006, DOI: org/10.1029JBOO3963.

Stevens C., McCaffrey R., Bock Y., Genrich J., Subarya C., Puntodewo S. and Vigny C. Rapid rotations about a vertical axis in a collisional setting revealed by the Palu fault, Sulawesi, Indonesia. Geophysical Research Letters, Vol. 26, No. 17, 1999, pp. 2677-2680, DOI:org/10.1029/1999GE008344.

Strader A.E. The effects of Coulomb stress change on Southern California earthquake forecasting. UCLA. ProQuest ID: Strader_ucla_0031D_12803. Merritt ID: ark:/13030/m58d22pj, 2014,166 , DOI:10.13140/RG.22.36576.48647.

Steacy S., Nalbant S.S., McCloskey J., Nostro C., Scotti O., Baumont D. Onto what planes should Coulomb stress perturbations be resolved? J. Geophys. Res., Vol. 110, No. B5, 2005, B05S15, DOI: 10.1029/2004JBOO3356.

Stein R.S., King G.C.P., Lin J. Change in failure stress on the southern San Andreas fault system caused by the 1992 Magnitude = 7.4 Landers earthquake. Science, Vol. 258, 1992, pp. 1328-1332, DOI:10/1126science.258.5086.1328.

Toda S., Stein R.S., Reasenberg P.A., Dieterich J.H., Yoshida A. Stress transferred by the 1995 Mw= 6.9 Kobe, Japan, shock: Effect on aftershocks and future earthquake probabilities. Journal of Geophysical Research: Solid Earth, Vol. 103, No. 10, 1998, pp. 24543-24565, DOI:org/10.1029/98J600765.

Toda S., Stein R.S., Richards-Dinger K., Bozkurt S.B. Forecasting the evolution of seismicity in southern California: Animations built on earthquake stress transfer. Journal of Geophysical Research: Solid Earth, Vol. 110, No. 5, 2005, 17 p., DOI: 10.1029/2004JBOO3415.

Tregoning P., McQueen H., Lambeck K., Jackson R., Little R., Saunders S., Rosa R., Present-day crustal motion in Papua New Guinea. Earth, planets and space, Vol. 52, No. 10, 2000, pp. 727-730.

Vavryčuk V. Iterative joint inversion for stress and fault orientations from focal mechanisms. Geophysical Journal International, Vol. 199, No. 1, 2014, pp. 69-77, DOI: org/1093/gji/ggu224.

Wallace L.M., Stevens C., Silver E., McCaffrey R., Loratung W., Hasiata S., Stanaway R., Curley R., Rosa R., Taugaloidi J. GPS and seismological constraints on active tectonics and arc-continent collision in Papua New Guinea: Implications for mechanics of microplate rotations in a plate boundary zone. Journal of Geophysical Research: Solid Earth, Vol. 109, No. 5, 2004, DOI: 10.1029/2003JBOO2481

Wells D.L., Coppersmith K.J. New empirical relationships among magnitude, rupture length, rupture width, rupture area, and surface displacement. Bulletin of the seismological Society of America, Vol. 84, 1994, pp. 974-1002, DOI:org/10.1785/BSSA0840040974.

Wessel P., Smith W.H., Scharroo R., Luis J., Wobbe F. The generic mapping tools: improved version released. EOS, Transactions American Geophysical Union, Vol. 94, No. 45, 2013, pp. 409-410, DOI: 10.1002/2013EO450001.

Walpersdorf A., Rangin C., Vigny C. GPS compared to long-term geologic motion of the north arm of Sulawesi. Earth and Planetary Science Letters, Vol. 159, 1998, pp. 47-55.

Walpersdorf A., Rangin C., Vigny C. GPS compared to long-term geologic motion of the north arm of Sulawesi. Earth and Planetary Science Letters, Vol. 159, 1998, pp. 47-55.

ВЛИЯНИЕ ИЗМЕНЕНИЙ КУЛОНОВСКОГО НАПРЯЖЕНИЯ ПРИ ЗЕМЛЕТРЯСЕНИИ СИЛОЙ M_W =7.5 В ПАЛУ, ИНДОНЕЗИЯ В 2018 г.

Ахадов Б.[1,2], Чин Ш.[3,4]

[1]Министерство науки и образования Азербайджанской Республики, Институт геологии и геофизики
AZ1143, Баку, просп. Г.Джавида, 119: (ahadovshao@gmail.com)
[2]Министерство науки и образования Азербайджанской Республики, Институт нефти и газа, Азербайджан
AZ1000, Баку, ул. Ф.Амирова, 9
[3]Шанхайская астрономическая обсерватория, Китайская академия наук,
80 Нандан роуд, Шанхай 200030, Китай
[4]Школа геодезии и земельной информатики, Хэнаньский политехнический университет,
Цзяоцзо 454000, Китай

Резюме. В данной статье представлены результаты изучения влияния кулоновского напряжения для выяснения процесса разрушения системы разломов Палу-Коро. 28 сентября 2018 г. на крупном сдвиговом разломе в северной части острова Сулавеси, Индонезия, произошло землетрясение. В результате кулоновское напряжение увеличилось примерно на 1 бар в областях афтершоков и областях, где напряжение уменьшилось более чем на 10 бар. На основе фокальных механизмов афтершоков и моделей очагов главного толчка рассчитаны изменения кулоновского напряжения разрушения на обеих узловых плоскостях фокального механизма. Дополнительно были рассчитаны изменения кулоновского напряжения в очагах каждого афтершока. Представленная нами модель напряжений указывает на положительную корреляцию между расширенными кулоновскими полями напряжений, возникающими в результате сочетания сейсмической активности. Нами было исследовано кулоновское напряжение как возможный источник афтершоков, которые имеют тенденцию оптимально смещаться ввиду разрушения из-за локального поля напряжений, созданного основным толчком. Землетрясение силой 7.5 баллов, происшедшее в Палу, привело к распределению смещений поверхности. Кроме того, расчетное горизонтальное смещение варьрует от 1 до 1.3 метра в направлении СЗ-ЮЗ. Карты напряжений, включенные в эту статью, имеют большое значение для прогнозирования ожидаемых мест будущих толчков и снижения последствий землетрясений. Было подтверждено, что оценка кулоновского напряжения, связанного со смещением землетрясения, является важным средством понимания различных сейсмических явлений.

Ключевые слова*: кулоновское напряжение, инверсия напряжений, деформация, землетрясение, Палу, Индонезия*

2018 M_W = 7.5 PALU, İNDONEZİYA, ZƏLZƏLƏSİNİN COULOMB STRESS DƏYİŞİKLİKLƏRİNİN TƏSİRİ

Əhədov B.[1,2], Çin Ş.[3,4]

[1]Azərbaycan Respublikası Elm və Təhsil Nazirliyi, Geologiya və Geofizika Institutu
AZ1143, Bakı, G.Cavid prospekti, 119: ahadovshao@gmail.com
[2]Azərbaycan Respublikası Elm və Təhsil Nazirliyi, Neft və Qaz İnstitutu, Azərbaycan
AZ 1000, Bakı şəh., F. Əmirov küç., 9
[3]Şanxay Astronomiya Rəsədxanası, Çin Elmlər Akademiyası, Çin
80 Nandan Road, Şanxay 200030, Çin
[4]Henan Politexnik Universiteti, Geodeziya və Torpaq İnformasiya Mühəndisliyi Məktəbi
Jiaozuo 454000, Çin

Xülasə. Bu məqalədə Palu-Koro qırılma sistemində qırılma prosesini anlamaq üçün Coulomb gərginliyinin təsirləri araşdırılmışdır. 2018-ci il sentyabrın 28-də İndoneziyanın şimalındakı Sulavesi adasında böyük qırılıb-sürüşmə mexanizmli zəlzələ baş vermişdir. Nəticədə Coulomb (Kulon) gərginliyi təxminən 1 bar artmış və bu afterşokların paylandığı ərazilər ilə eyni zamanda gərginliyin 10 bardan çox aşağı düşdüyü ərazilərə aid olmuşdur. Məqalədə hər bir afterşok təkanların fokal mexanizmlərinə və əsas təkan mexanizm modellərinə əsasən, hər bir fokal mexanizmin hər iki nodal müstəvilərində Coulomb gərginliyinin dəyişməsi hesablanmışdır. Bundan əlavə afterşokların fokal mənbələrində Coulomb gərginlik dəyişiklikləri də hesablanmışdır. Əsas təkanın yaratdığı lokal gərginlik sahəsinə görə qırılma üçün optimal yerdəyişməyə meyilli olan afterşok təkanlarının mümkün mənbəyi kimi Coulomb gərginliyi araşdırılmışdır. Bizim gərginlik modelimiz seysmik aktivliyin təsirindən yaranan genişləndirilmiş Coulomb gərginlik bölgələri ilə müsbət korrelyasiya olduğunu göstərir. Palu 7.5 zəlzələsi yer səthində yerdəyişmələrə səbəb olmuşdur. Bundan başqa, hesablamalar üfüqi yerdəyişmənin Şimal-Qərb və Cənub-Qərb istiqamətində olduğunu və 1-1.3 metr arasında dəyişdiyini döstərmişdir. Palu zəlzələsinin Palu-Koro qırılmasının bitişik seqmentinə ötürdüyü gərginlik gərginliyi 1-2 bara çatma istiqamətində yükləyirdi. Gərginliyin modelləşdirilməsi təsdiq edir ki, kiçik artım (bir neçə bar) zəlzələlərin yaranmasına təkan verə bilər. Bu məqalədə göstərilən gərginlik xəritələri, gələcəkdəki afterşokların gözlənilən yerlərini proqnozlaşdırmaq və zəlzələ riskini azaltmaq üçün əhəmiyyətlidir.

Açar sözlər*: Coulomb stres, stres inversiyası, deformasiya, zəlzələ, Palu, Indoneziya*

ANAS Transactions Earth Sciences 2 / 2023

http://www.journalesgia.com

AQUIFER ACTIVITY MODEL IN HYDROCARBON FIELDS (SOUTH CASPIAN BASIN AS A CASE STUDY)

Salmanov A.M.[1], Garagozov E.Sh.[2], Ahmadov E.H.[3]

[1]SOCAR, Oil Gas Scientific Research Project Institute, Azerbaijan
88A, Zardabi ave., Baku, AZ1012
[2]SOCAR, Azneft PU, Azerbaijan
73, Neftchilar ave., Baku, AZ1000
[3]SOCAR Head office, Azerbaijan
121, Haydar Aliyev ave., Baku, AZ1021

Keywords: *aquifer, field, formation, field modeling, hydrodynamics, formation pressure, fluid*

Summary. The SCB (South Caspian Basin) is considered one of the world's unique in terms of hydrocarbon reserves. At present, the hydrocarbon potential of the basin has attracted foreign companies to conduct large-scale research here. As a result of these surveys, 120 structures were discovered in the Azerbaijani part of the SCB, of which 21 structures were identified as oil and gas and 17 fields are being developed.

The main purpose of the study is to analize the hydrodynamic activity characteristics of the basin, to improve field models, to develop efficient development scenarios, to more accurately forecast the reserves and resources of the field and, as a result, to develop a modeling of the aquifer basin of the South Caspian Basin. The hydrodynamic activity model of the basin is especially important in the modeling of oil and gas and gascondensate fields. While modeling the hydrocarbon-water contact and the movement mechanism (Fetkovich, Carter Tracy, inactive), for the improvment an effective field development plan, it is necessary to clarify pressure, direction of movement, etc., which is possible only as a result of the compilation and analysis of the basin activity model. The advantage of the study is that the used data from oil and gas fields related to the surrounding basins, and the volumes of gas produced from the basin were calculated in reservoir conditions. In this regard, the research is of great theoretical and practical importance.

© 2023 Earth Science Division, Azerbaijan National Academy of Sciences. All rights reserved.

Introduction

In general, the South Caspian Basin is divided into three parts according to its geological, structural-tectonic, lithological-stratigraphic and orohydrographic features, which are the Absheron, the Baku archipelagos and the Deep Caspian.12 of the developed fields are located in the Absheron and 5 in the Baku archipelagos. The depth of the sea in the basin is up to 1000 m. The main object of exploitation in the basin is the Productive Seria (PS) sediments, the thickness of which varies between 2800-4000 m. Most of the developed fields operate in active water flooding, gas cap and dissolved gas regimes. At the same time, in some fields (the Neft Dashlari, shallow water Guneshli, the Azeri-Chirag-Guneshli, etc.) development was carried out by injection. At present, the oil recovery factor in the SCB has reached 0.23 and the gas recovery factor has reached 0.22 (Abasov et al., 1997; Salmanov et al., 2021; Нариманов, 1998; Велиева, 1997).

Investigative methods

As a result of large-scale seismic and exploration drilling in the basin, the structural and tectonic form of the area was studied and three-dimensional structural models were created (Fig.1). The three-dimensional model also shows that the depth in the Absheron archipelago is shallower than in other areas due to the top and bottom of the PS (1500-3000 m according to Pereriv series - PrS). The south-western part of the Baku archipelago is also more hypsometrically shallower (2000-3000 m according to PrS). It should be noted that this factor has made it relevant to conduct large-scale exploration work in these areas. The deeper areas of the PS are the central parts of the SCB (5000-7000 m according to the PrS).

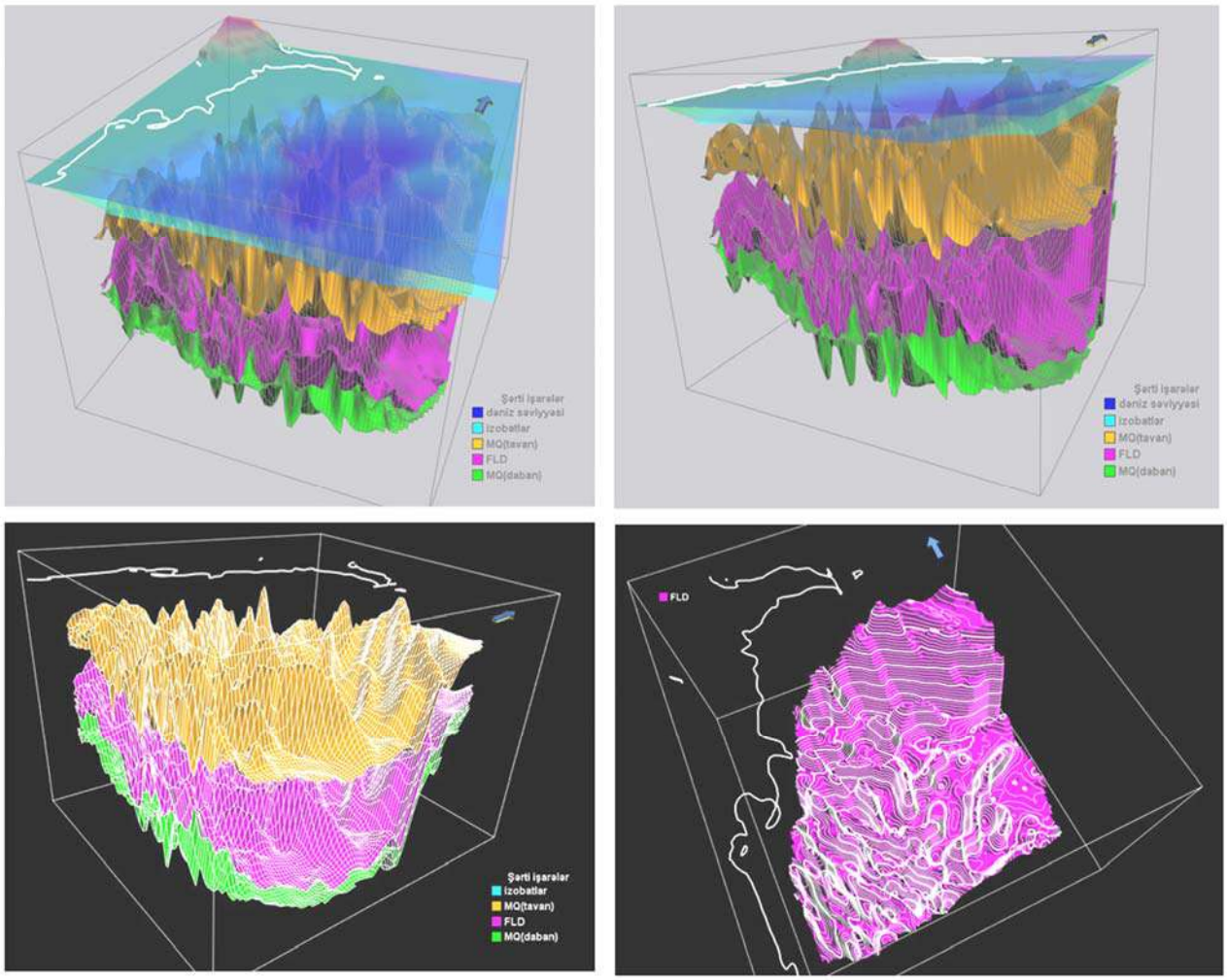


Fig. 1. 3D structural-tectonic models of the SCB

Due to the characteristics of the individual structures in the SCB, the main complex structures are located in the Absheron archipelago. The Absheron uplift zone is more geologically complex. In the north-western part of uplift zone, the top of the PS is almost eroded. The thickness of the PS towards the center of the SCB is also increasing. It requires deeper exploration and drilling in the area.

The developed three-dimensional structural-tectonic model of the South Caspian Basin made it possible to study these tectonic features in more detail. The model fully reflects the structural and tectonic structure of the top and bottom of PS sediments. The uplifts and structures located in the Azerbaijani sector of the Caspian Sea were analyzed in the general case, and then analyzed on regions (the Absheron Archipelago, the Baku Archipelago and the deep Caspian region). These models are very important in the classification of structures, basin modeling, and the compilation of regional tectonic maps (Salmanov et al., 2021; Салманов и др., 2019; Rahimov et al., 2019; Ahmadov, Veliyev, 2019; Шыхова, 2018; Искендеров и др., 2017). From this point of view it would be correct to consider the model currently compiled as a single three-dimensional structural-tectonic model for the South Caspian Depression. It is necessary to collect, systematize and analyze the following geological data to develop a basin activity model:

– Seismic exploration and prospecting drilling work on stratigraphic units (main horizons);

– Lithofacial features of the basin;

– Accumulated fluid volumes on deposits and horizons – regional drainage maps;

– Formation pressure on the field (initial and current).

The hydrodynamic activity model of the basin was compiled on the basis of the mentioned geological data with the following sequence of processes (Fig. 2).

The following calculation method was used to calculate the produced geological and field data brought to the stratum conditions and produced fluids (oil, water, gas) in the reservoir conditions:

$$Q_{total} = (Q_{osc} / \rho_o + Q_{water} + V_{girc}) - V_{iw}$$

where, Q_{total} – volume of the accumulated total fluid, m^3;

Q_{osc} – quantity of oil is measured under standart conditions, ton;

ρ_o – density of oil and condensate, kg/m^3;

Q_{water} – volume of the produced water, m^3;

V_{girc} – volume of gas produced in reservoir conditions, m^3;

V_{iw} – volume of the injected water into the formation, m^3.

The initial formation pressure in the unexplored areas of the basin was predicted on the basis of depth dependence graphs (Fig. 3).

Based on these graphs, the first formation pressure in the unexplored areas of the basin at the corresponding horizons were calculated and maps of the field distribution of the first averaged pressures derived by interpolation were compiled (Fig. 4). It can be seen from all the maps that the main hydrodynamic impact on the developed deposits of the basin is associated with deep areas of the southern Caspian. The forces of motion created by such high pressure make it possible to predict the source and direction of activity. But the main mechanisms of movement of the water basin, its velocity, directions can be determined as a result of other studies (Ворошилов, 2001; Ahmadov, 2013).

In Fig. 5 regional drainage maps of the basin on the horizons were compiled. As noted, to increase the accuracy level of drainage maps, the accumulated fluid volumes were calculated in reservoir conditions (Fig. 5).

The research work shows that the main movement of the water basin is directed towards the areas that are drained. An analytical approach has been applied to calculate the current formation pressure depending on the fluid volumes produced to investigate the dynamics of water flow. To determine the dependence of the volume of fluid extracted in the basin on the current formation pressure, first of all, the condition was accepted that the water basin is inactive, and the corresponding drop in reservoir pressure per volume of extracted fluid in 1 million m^3 was calculated (Fig. 6).

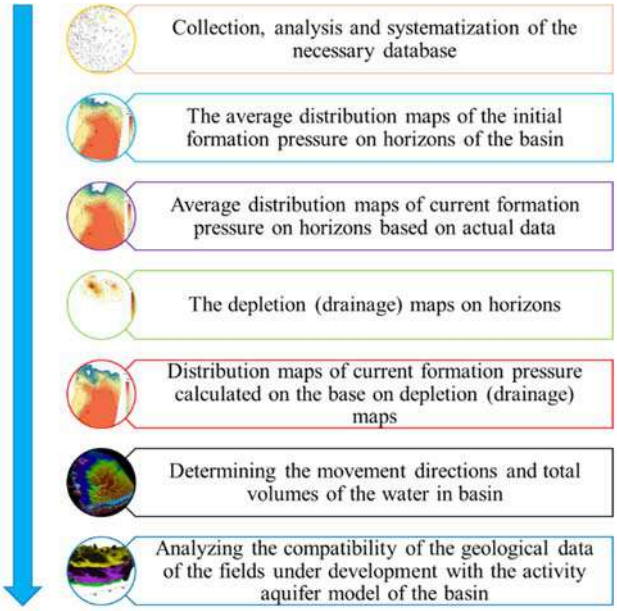


Fig. 2. Scheme of the creation model of hydrodynamic activity of the basin

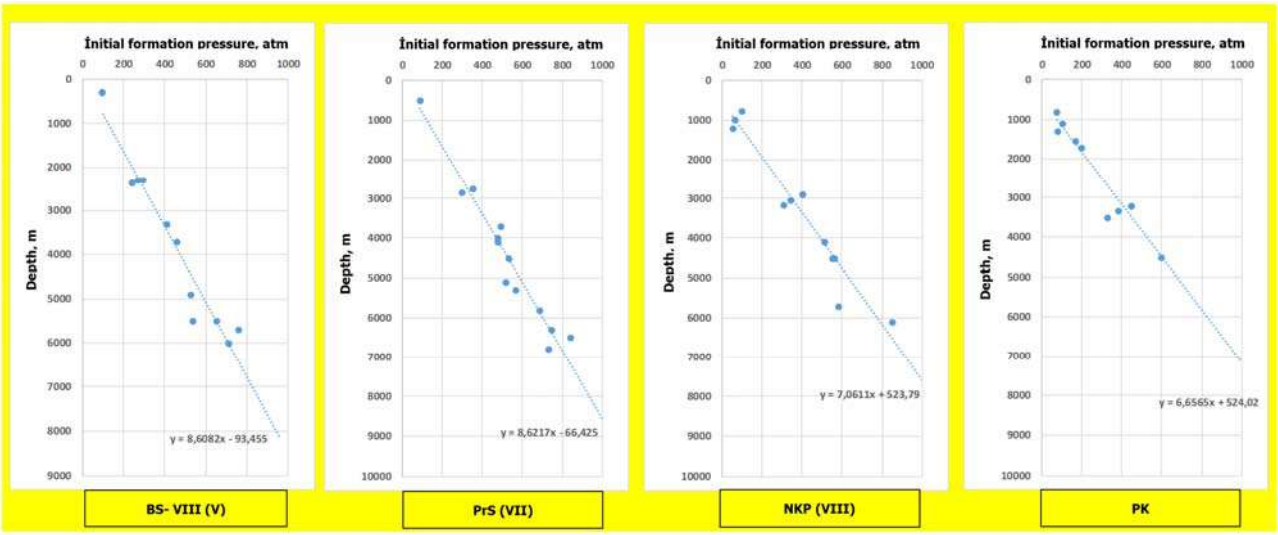


Fig. 3. Graphs of depth dependence of the initial formation pressure

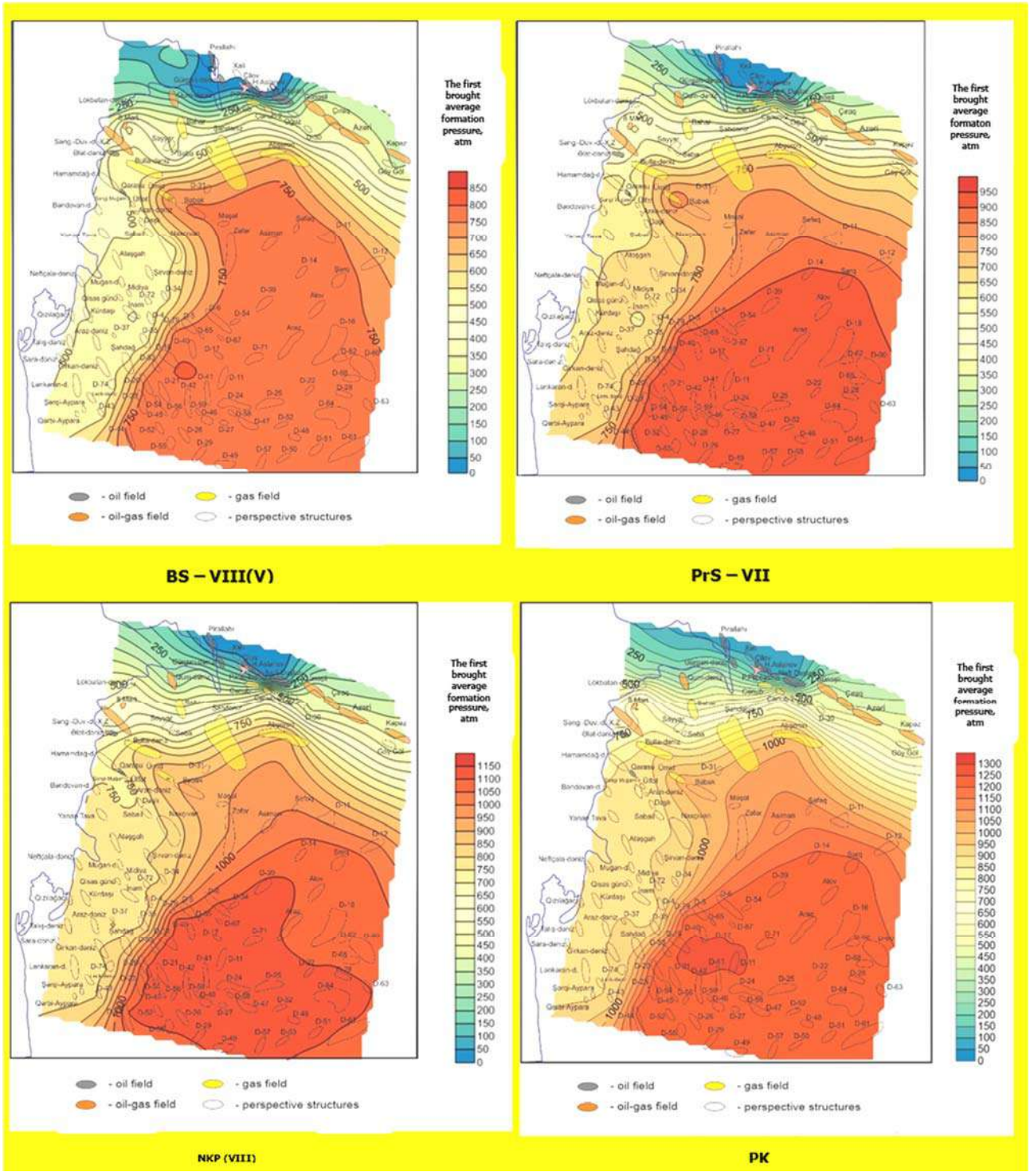


Fig. 4. Maps of the pressure distribution of the initial formation along the horizons

As we know, in accordance with the volume of fluid produced in the deposits, the pressure of the formation should also fall. This pressure drop should change according to a straight-line graph defined in the dependency graphs. But the scatter charts show that in most fields the decline formation pressure, which depends on the volume of produced fluid, is very low. The reason for this can only be due to the movement of the water basin and partial retention of reservoir pressure due to natural forces. For the case of inactivity of the basin the current formation pressure in the fields was calculated by the method:

$$k = (P_{initial}-P_{current}) / Q_{total}$$

where, k – is the pressure drop coefficient of the layer corresponding to the volume of the produced fluid in 1 mln m^3;

$P_{initial}$ – is the initial formation pressure, atm

$P_{current}$ – is the current formation pressure, atm

Q_{total} – is the volume of total fluid extracted from that field.

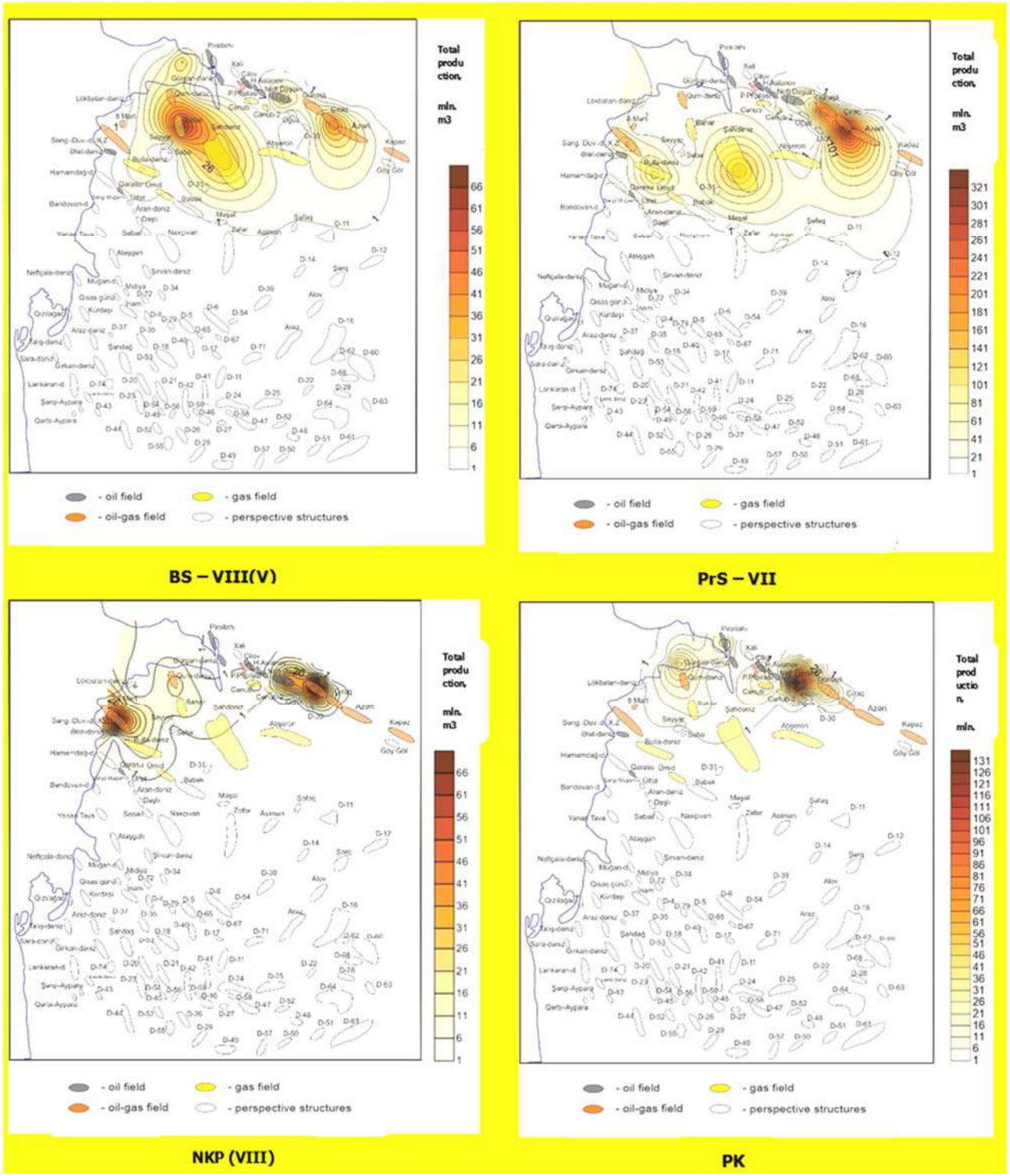


Fig. 5. Total fluid maps collected on horizons (regional drainage maps)

If we calculate the current layer pressure ("how much should it be") using the corresponding formation pressure drop trend to the output fluid volume of 1 million m^3, then we get the following mathematical expression:

$$P_{curr.calc} = P_{initial} - k_{trend} \cdot Q_{total}$$

where, $P_{curr.calc}$ – is the calculated current formation pressure, atm;

$P_{initial}$ – is the initial formation pressure, atm;

k_{trend} – is the coefficient calculated by the method of the trend of the formation pressure drop corresponding to the volume of the produced fluid in 1 million m^3;

Q_{total} – is the volume of total fluid extracted from that field.

Thus, the distribution maps of the calculated current pressure of the formation are compiled (Fig.7).

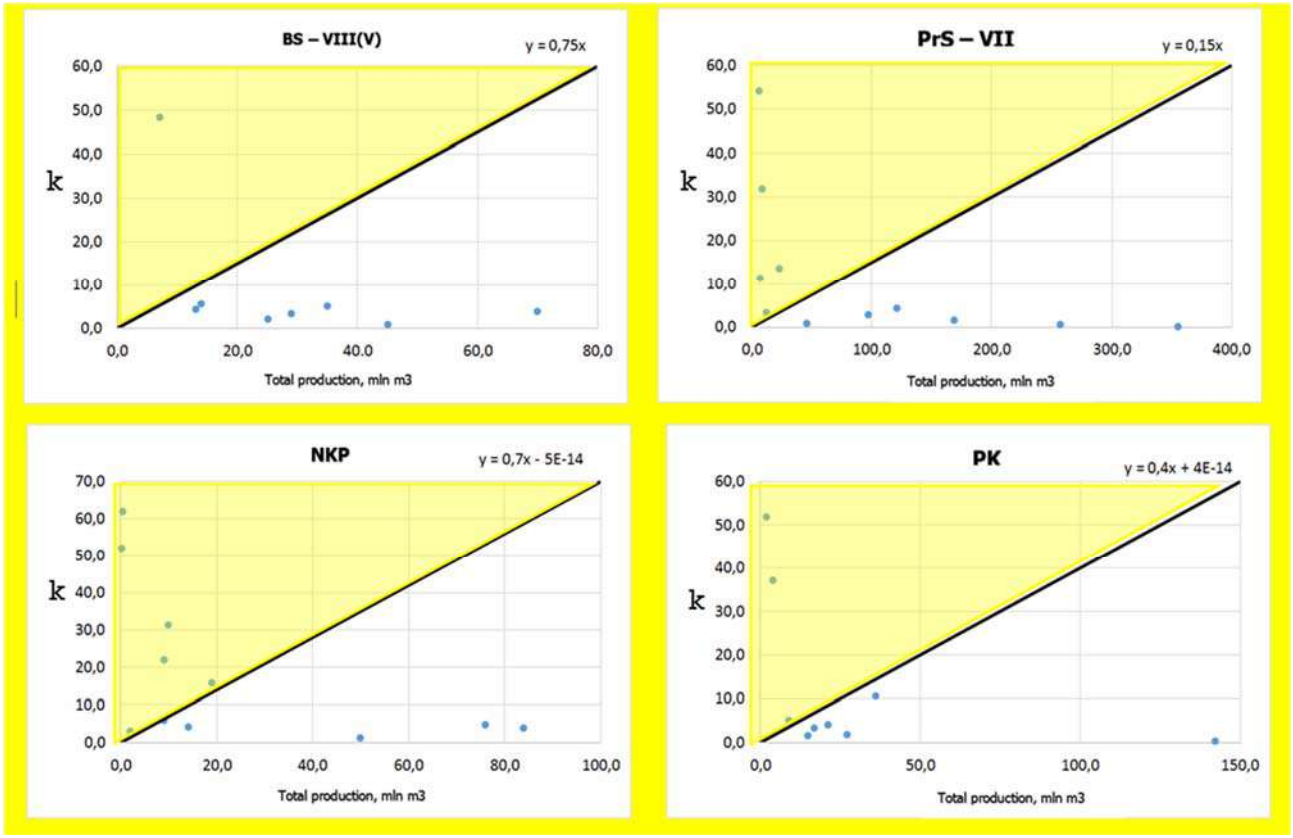


Fig. 6. Graphs of the corresponding drop in formation pressure to the volume of the extracted fluid of 1 million m^3 on the horizons

Determination of the hydrodynamic activity of the water basin (direction of movement, velocity, mechanism, etc.) for the study, a joint analysis of the current pressure maps of the layer (Fig. 8) was carried out compiled on the basis of actual measured data, cumulative maps of the remote fluid (regional drainage maps) and corresponding calculated maps of the current pressure of the remote fluid layer.

Thus, in the VIII horizon of the Balakhani formation (BS) in the direction of the Bahar, Gum-Deniz, Neft Dashlari, Azeri-Chirag-Guneshli deposits, the current formation pressure should have been less than 50 atm. But the formation pressure was partially maintained (200-250 atm in the ACG field). The analysis of regional drainage and average distribution maps of actual current formation pressure shows that the main direction of the water basin on the VIII horizon of the Balakhani reservoir moved in the direction of the Neft Dashlari, Azeri-Chirag-Guneshli, Bahar and Gum-Deniz deposits, and about 110-170 million m^3 of water moved in these directions.

This movement (dynamics) on the PrS is higher. Thus, about 500-570 million m^3 of water were put into motion in the direction of the Neft Dashlari, Azeri-Chirag-Guneshli, Bahar, Shah Deniz and dry fields located on the Absheron.

The results are characterized more differently in the lower part of the PS. The water basin of the Upper Kirmaki sandstone (NKP) and Lower Kirmaki (PK) formation is more passive than the upper part of the PS. Thus, the water basin of the NKP reservoir moved mainly in the direction of the Neft Dashlari, shallow water fields of the Guneshli, Gum Deniz and Sangachal-Duvanny-Khara-Zira, and about 110-150 million m^3 of water moved in these directions. According to the PK layer, the water basin moved in the direction of the Palchig Pilpilesi, Neft Dashlari and shallow water Guneshli fields, and about 150-180 million m^3 of water moved in these directions.

Results and Discussion

In order to determine the reliability of the results of large-scale research work, the obtained results were subjected to comparative analysis with field-geological and operational indicators of hydrocarbon deposits under development in the basin. Thus, the oil and water boundaries at the Guneshli field are actively irrigated mainly from the southern wing. In the upper part of the PS at the AChG fields (VIII, IX, X horizons of the Balakhani layer and PrS), although active irrigation was carried out from the northern wing, but the southern wing was irrigated faster, and the water-oil boundaries moved more actively. The main development horizons of the southern wing at the Sangachal-Duvanny-Khara-Zira, Alat-Deniz, Bulla-Deniz and Umid fields are water-saturated. In addition, the eastern periclinal of the Bulla-Sea field is irrigated faster.

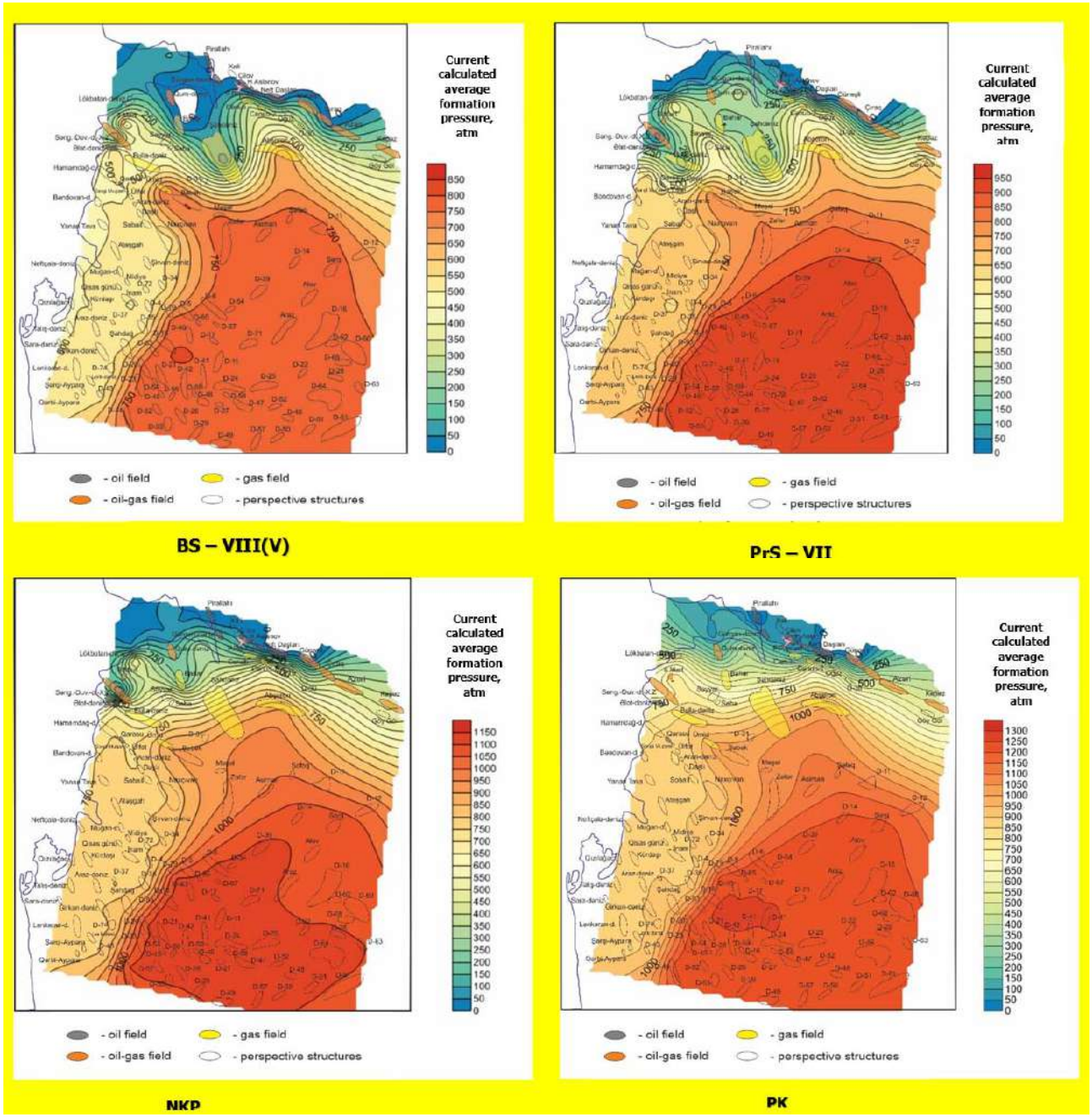


Fig. 7. Maps of current average formation pressure calculated on horizons

At the Absheron field, based on the analysis of attribute maps compiled along the VIII horizon and the PrS of the Balakhani layer, there is a shift of hydrocarbon boundaries to the north and a saturation of hydrocarbons in the southern wing of the field. The analysis of hydrodynamic conditions at the marked fields also confirms the results of the research work, that is, the hydrodynamic activity of the water basin in the SCB from the northeast to the northwest.

Conclusions and Recomendations

Based on the conducted large-scale research work and comparative analysis of the compiled two-dimensional model of hydrodynamic activity of the SCB water basin, the following results were obtained and useful suggestions were given:

– Actual historical indicators of field development and analysis of the aquafer show that in the upper horizons of the PS and PrS, the aquafer is more active than in the southern one, about 700-900 million m^3 of water moved along these horizons in this direction.

– In the lower horizons of the PT (except the Gala layers), it is less active than in the upper horizons. This is due to the fact that the lower horizons of the PS are involved in development on small areas. About 300-400 million m^3 of water moved from south to north along the lower horizons of the PS.

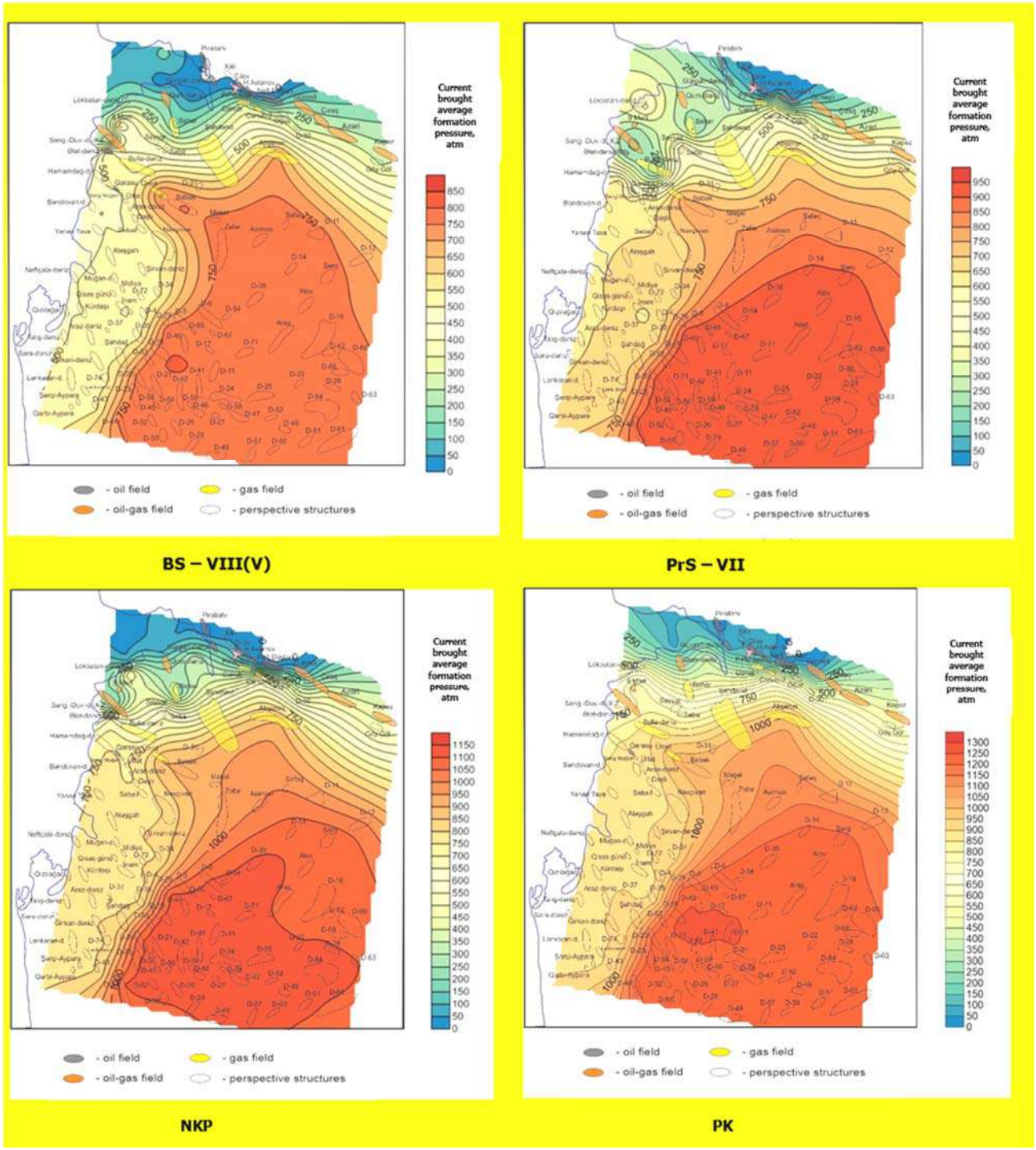


Fig. 8. Maps of actual current average formation pressure on horizons

– The basin activity model provides serious assistance in ensuring the efficiency of field development, deployment of a network of wells, design and proper conduct of water treatment, accurate compilation of a hydrodynamic model of deposits, forecasting resources, forecasting pressure in the basin.

– Research should be expanded, in particular, the lithophase model should be developed more precisely.

– An adequate reservoir model of the hydrodynamic activity should also be compiled for the Kura basin.

– The results obtained should be transferred from the 2D model to the 3D model, which will ensure the work of the current and historical model of the movement of the reservoir.

REFERENCES

Abasov M., Azimov E., Aliyarov R. A. et. al. Theory and practice of geological – geophysical studies and development of marine oil and gas fields: on the example of South-Caspian depression. Azerneshr. Baku, 1997, 203 p.

Ahmadov E.H. Study of water injection efficiency through modern geological-mathematical models in Guneshly field. Journal of Environmental Science and Engineering B, Vol. 2, No. 10, New York, 2013, pp. 574-577.

Ahmadov E.H., Veliyev R.V. Methods of minimization of uncertainties and geological risks based on Umid gas-condensate field. Georesursy, Vol. 21, No. 1, 2019, pp. 92-98.

Iskenderov M.M., Abuzarova A.G., Kazimov R.R., Samedzade A.A. Some results of lithological and facies analysis of terrigenous deposits of the productive stratum in the zone of the Sangachal-Duvanny-Khara-Zira adasy uplifts. Azerbaijan Oil Industry, No. 9, 2017, pp. 3-11 (in Russian).

Narimanov A.A. Regional oil-bearing complex of the South Caspian Depression. Conference Materials "Structure and Oil and Gas Content of Inland Sea Depressions". Moscow, 1998, pp. 81-89 (in Russian).

Rahimov F.V., Ahmadov E.H., Khasayev A.G. Studying the influence of estimation parameters on oil reserves by taking into account geological risks. III International conference on geology of the Caspian Sea and adjacent reas, Baku, 2019, pp. 1-6.

Salmanov A., Karagozov E., Ahmadov E. New classification model based on complication extents of structures. SOCAR Proceedings, No. 1, 2021, pp. 14-20, http://dx.doi.org/10.5510/OGP20210100475.

Salmanov A.M., Ahmadov E.H., Rahimov F.V. Geological assessment of reservoir factors of the Umid-Babek area**.** SOCAR Proceedings, No. 3, 2019, pp. 8-14, http://dx.doi.org/10.5510/OGP20190300392 (in Russian).

Shikhova L.F. Regularities in the distribution of reservoir properties of productive series rocks of the Absheron Archipelago fields. Geologist of Azerbaijan, No. 22, 2018, c. 90-101 (in Russian).

Veliyeva E.B. Simulation of Azerbaijani oil deposits in connection with their production. Azerbaijan Oil Industry, No. 1, 1997, pp. 13-16 (in Russian).

Voroshilov V.G. Mathematical modeling in geology. Publishing House TPU.Tomsk, 2001, 124 p. (in Russian).

ЛИТЕРАТУРА

Abasov M., Azimov E., Aliyarov R.A. et. al. Theory and practice of geological – geophysical studies and development of marine oil and gas fields: on the example of South-Caspian depression. Azerneshr. Baku, 1997, 203 p.

Ahmadov E.H. Study of water injection efficiency through modern geological-mathematical models in Guneshly field. Journal of Environmental Science and Engineering B, Vol. 2, No. 10, New York, 2013, pp. 574-577.

Ahmadov E.H., Veliyev R.V. Methods of minimization of uncertainties and geological risks based on Umid gas-condensate field. Georesursy, Vol. 21, No. 1, 2019, pp. 92-98.

Rahimov F.V., Ahmadov E.H., Khasayev A.G. Studying the influence of estimation parameters on oil reserves by taking into account geological risks. III International conference on geology of the Caspian Sea and adjacent reas, Baku, 2019, pp. 1-6.

Salmanov A., Karagozov E., Ahmadov E. New classification model based on complication extents of structures. SOCAR Proceedings, No. 1, 2021, pp. 14-20, http://dx.doi.org/10.5510/OGP20210100475.

Велиева Э.Б. Моделирование нефтяных залежей Азербайджана в связи с их выработкой. Азербайджанское Нефтяное Хозяйство, No. 1, 1997, с. 13-16.

Ворошилов В.Г. Математическое моделирование в геологии. Изд. ТПУ.Томск, 2001, 124 с.

Искендеров М.М., Абузарова А.Г., Кязимов Р.Р., Самедзаде А.А. Некоторые результаты литолого-фациального анализа терригенных отложений продуктивной толщи в зоне поднятий Сангачал-Дуванны-Хара-Зира адасы. Азербайджанское Нефтяное Хозяйство, No. 9, 2017, с. 3-11.

Нариманов А.А. Регионально нефтеносный комплекс Южно-Каспийской впадины. Материалы конференции «Структура и нефтегазоносность впадин внутренних морей». Москва, 1998, с. 81-89.

Салманов А., Ахмедов Э., Рагимов Ф. Геологическая оценка пластовых параметров площади Умид-Бабек. SOCAR Proceedings, No. 3, 2019, с. 8-14, http://dx.doi.org/10.5510/OGP20190300392.

Шыхова Л.Ф. Закономерности распределения коллекторских свойств пород Продуктивной толщи месторождений Абшеронского архипелага. Геолог Азербайджана, No. 22, 2018, с. 90-101.

МОДЕЛИРОВАНИЕ ГИДРОДИНАМИЧЕСКОЙ АКТИВНОСТИ БАССЕЙНА НА УГЛЕВОДОРОДНЫХ МЕСТОРОЖДЕНИЯХ (НА ПРИМЕРЕ ЮЖНО-КАСПИЙСКОЙ ВПАДИНЫ)

Салманов А.М.[1], Гарагезов Э.Ш.[2], Ахмедов Э.Г.[3]

[1]Научно-исследовательский проектный институт нефти и газа ГНКАР, Баку, Азербайджан
AZ1012, Баку, просп. Зардаби, 88А
[2]ПО "Азнефть" ГНКАР, Азербайджан
AZ1000, Баку, просп.Нефтчиляр, 73
[3]ГНКАР, Азербайджан
AZ1021, Баку, просп. Г.Алиева, 121

Резюме. Исследование проводилось на примере одного из крупнейших бассейнов по запасам углеводородов в Азербайджане – Южно-Каспийского бассейна.

Южно-Каспийский бассейн считается одним из уникальных бассейнов мира по запасам углеводородов. В этом бассейне проведены масштабные геолого-геофизические исследования и геологоразведочные работы. В настоящее время углеводородный потенциал бассейна привлек иностранные компании для проведения здесь масштабных исследований. В результате этих изысканий в Азербайджанской части Южно-Каспийского бассейна обнаружено 120 структур, из них 21 структура определена как нефтегазовая и 17 месторождений разрабатываются.

Основная цель исследования – проанализировать характеристики гидродинамической активности бассейна, усовершенствовать модели месторождения, разработать эффективные сценарии разработки, более точно прогнозировать запасы и ресурсы месторождения и, как следствие, разработать рабочую гидродинамическую модель аквифера. Модель гидродинамической активности бассейна особенно важна при моделировании нефтяных и газоконденсатных месторождений. При моде-

лировании водо-углеводородных контактов и механизма движения (Феткович, Картер Трейси, неактивный) для уточнения эффективного плана разработки месторождения учитываются давление, скорость, направление движения и т.д. аквифера. Следует пояснить, что это возможно только в результате разработки и анализа гидродинамической модели активности бассейна. Преимущество исследования заключается в том, что здесь использовались данные о нефтяных и газовых месторождениях, относящихся к окружающим бассейнам, а объемы добытого газа рассчитывались в условиях пласта. С этой точки зрения данная исследовательская работа имеет важное теоретическое и практическое значение.

Ключевые слова: *аквифер, месторождение, свита, моделирование месторождений, гидродинамика, пластовое давление*

KARBOHİDROGEN YATAQLARINDA SU HÖVZƏSİNİN HİDRODİNAMİK AKTİVLİK MODELİ (CƏNUBİ XƏZƏR ÇÖKƏKLİYİNİN TİMSALINDA)

Salmanov A.M.[1], Qaragözov E.Ş.[2], Əhmədov E.H.[3]
[1] SOCAR-ın Neft və Qaz Layihə Institutu, Bakı, Azərbaycan
AZ1012, Bakı, Zərdabi prospekti, 88A
[2] SOCAR-ın «Azneft» Istehsalat Birliyi, Azərbaycan
AZ1000, Bakı,Neftçilər prospekti, 73
[3]SOCAR, Azərbaycan
AZ1021, Bakı, Q.Əliyev prospekti, 121

Xülasə. Tədqiqat işi karbohidrogen ehtiyatlarının həcminə görə Azərbaycanın ən böyük neftli-qazlı hövzəsinin – Cənubi Xəzər Çökəkliyinin timsalında yerinə yetirilmişdir. Cənubi Xəzər Çökəkliyi dünyada karbohidrogen ehtiyatlarının həcminə görə unikal hövzələrdən biri hesab edilir. Bu hövzədə irimiqyaslı geoloji-geofiziki tədqiqatlar, axtarış-kəşfiyyat işləri aparılmışdır. Hazırda hövzənin karbohidrogen potensialı xarici şirkətləri burada böyük həcmdə tədqiqat işləri aparmaq üçün cəlb etmişdir. Bu tədqiqatlar nəticəsində Cənubi Xəzər Çökəkliyinin Azərbaycan hissəsində 120 struktur aşkar edilmişdir ki, bunlardan da 21 strukturun neft-qazlılığı müəyyənləşdirilmiş və 17 yataq işlənməyə cəlb edilmişdir. Tədqiqatın əsas məqsədi hövzənin hidrodinamik aktivlik xüsusiyyətlərinin tədqiqi, yataqların modellərinin təkmilləşdirilməsi, səmərəli işlənmə ssenarilərinin tərtibi, sahənin ehtiyat və resurslarının daha dəqiq proqnozlaşdırılması və nəticədə Cənubi Xəzər Çökəkliyinin su hövzəsinin işlək aktivlik modelinin tərtib olunmasıdır. Hövzənin hidrodinamik aktivlik modeli xüsusilə, neft-qaz və qaz-kondensat yataqlarının modelləşdirilməsində mühüm əhəmiyyət kəsb edir. Yataqların səmərəli işlənmə planının tərtibi üçün karbohidrogen-su hüdudları və hərəkət mexanizimi (Fetkoviç, Karter Treysi, non-aktiv) modelləşdirilərkən su hövzəsinin təzyiqi, hərəkət sürəti, hərəkət istiqamətləri və s. dəqiqləşdirilməlidir ki, bu da yalnız hövzənin aktivlik modelinin tərtibi və təhlili nəticəsində mümkün olur. Tədqiqatın üstünlüyü ondan ibarətdir ki, burada ətraf hövzələrə aid olan neft və qaz yataqlarının məlumatlarından istifadə edilmiş və hövzədən çıxarılan qaz həcmləri lay şəraitində hesablanmışdır. Bu baxımdan qeyd olunan tədqiqat işinin mühüm nəzəri-təcrübi əhəmiyyəti vardır.

Açar sözlər: *su hövzəsi, yataq, lay, yataqların modelləşdirilməsi, hidrodinamika, lay təzyiqi, fluid*

ANAS Transactions **Earth Sciences** **2 / 2023**

http://www.journalesgia.com

THERMAL TOMOGRAPHY APPLICATION FOR PROSPECTING IN THE SEDIMENTARY BASINS

Khutorskoy M.D.
RAS Geological Institute, Moscow, Russia
7, Pyzhevsky lane, Moscow, 119017: mdkh1@yandex.ru

Keywords: *temperature, heat flow, sedimentary basin, salt-dome, modeling*

Summary. A thermal tomography technology has been developed, which is recommended to be included in the prospecting and exploration work complex in hydrocarbon fields. The practical value of the thermotomographic technique is to find temperature boundaries that control a particular process of generating or transforming a substance. It has been established that the oil and gas fields localization is controlled by the temperature rise in the sedimentary layer, which are associated with "thermal domes". Heat flow refraction occurs at the boundaries of the domes with country rocks due to the contrast in thermal conductivity of evaporites and terrigenous rocks between the domal zones. This is the main cause of heat flow variation in the lateral and vertical directions in the sedimentary basins. Close correlation between zones of elevated temperature in the sedimentary rocks and petroleum occurrences is confirmed by the results of 2D and 3D geothermal field modeling. 3D temperature models distribution in the Western Arctic area, in the Precaspian, Pripyat and North German depressions are presented. The previously noted relations of oil and gas fields to the deep faults in the studied basins create prerequisites for consideration of the geothermal field as a genetic factor controlling the tectonic features and petroleum resources of the sedimentary and salt-dome basins.

© 2023 Earth Science Division, Azerbaijan National Academy of Sciences. All rights reserved.

High capital costs at the regional exploration and evaluation stages can be significantly reduced through the use of high-tech geological and geophysical technologies for processing and interpreting existing materials for measuring potential geophysical fields, the results of two- and three-dimensional seismic exploration, the results of basin and thermotomographic modeling, studying the physical and rheological properties of core material.

In this enumeration, a relatively new and unconventional method is "thermotomographic modeling" based on the calculation of deep temperatures and heat flux density in the modern section and in the geological past, including when the catagenesis of organic matter occurred in the Paleozoic basin.

The thermotomographic modeling technology developed at the GIN RAS based on temperatures and heat flow distribution in the modern lithosphere and the sedimentary rocks thermophysical properties as well as on the results of reconstruction of sedimentation. The basis for the project implementation is our own original geothermal data obtained by temperature measurements in deep wells of sedimentary basins, determination of the thermal conductivity of core from well sections, as well as calculations of radiogenic heat generation during spontaneous decay of long-lived isotopes.

The application of theoretical and methodological geothermal aspects in geological exploration practice in oil and gas fields is now becoming ubiquitous. Suffice is to recall that no software product implementing basin modeling technology can do without setting the reduced heat flow as a boundary condition, and thermophysical properties (temperature and thermal conductivity, heat capacity) as model parameters. It follows from this that the accuracy and, consequently, reliability in predicting oil and gas potential using basin modeling depend on the correctness of setting the reduced heat flow as a condition at the lower boundary of the modeling domain.

By reduced heat flow, we mean the heat flow that flows to the sole of the active radiogenic heat generation (RTG) layer. The thickness of this layer depends on the concentration of long-lived isotopes ^{238}U, ^{232}Th, ^{40}K in the Earth's crust, and in platform structures it usually varies from 7 to 20 km. Such a noticeable depth variation makes it necessary to analyze in more detail the share of radiogenic heat in the total heat balance and empirically investigate the reduction, i.e., the decrease in heat flow with depth as the concentration of the listed long-lived isotopes decreases.

Technique of geothermal modeling

The use of three-dimensional geothermal modeling, which we identified as a thermal tomography method (Khutorskoy et al., 2003), is based on volumetric interpolation of the geothermal field. The application of this method opened up opportunities to detect anomalies of temperature and heat flow, which did not appear at all while analyzing the one- or two-dimensional distribution of these parameters.

Especially vividly, the greater informative value of 3D geothermal models compared to 1D and 2D models is manifested in isometric structures, which in most cases are depressions of sedimentary basins.

The practical significance of the thermotomographic technique is to find temperature boundaries that control a particular process of generation or transformation of a substance.

Deep subsurface temperatures along the seismic lines are calculated using the THERMOGRAPHY software (Хуторской, 1996). The calculations are based on the thermal properties of crustal layers in compliance with the established refractor velocities.

Temperature distribution in the sequence is deduced using the finite element method with a quadratic approximation of the temperature function between the junctures of a rectangular grid. The program provides for a grid of 41×41 junctures which solves a two-dimensional problem: what linear dimensions along the *X* and *Z*- axes can be changed by the operator. Lateral flow is assumed to be absent at the lateral boundaries of the modeling domain, that is, $\partial T/\partial x = 0$. We assumed the temperature at the seafloor–water interface known from meteorological data (~1°C) to be the upper end value and heat flow to be the lower end value. Inside the modeling domain, contrasting media configurations and their thermal properties, including thermal diffusivity a (m^2/s), thermal conductivity k (W/(m· K)), and normalized thermal source density ($Fi=A/(c.\rho)$) (K/s), were preset. Within the TERM program, which is responsible for calculations, the linear dimensions (Lx and Lz, km) of the modeling domains were preset to determine the linear dimensions of the junctures (Lx/41 and Lz/41) as well as the solution discretization interval (Ma). The time step of the iteration process was selected automatically by the program and calculated as $\tau = 10^{-7} \cdot (Z^2/4a)$, where Z is the thickness of the modeling domain.

As a result of the digital solution of the thermal conductivity equation, temperate and heat flow distribution $q(z)$ and $q(x)$ for the preset thermal medium at the final moment of the discretization phase were obtained. The file of results renamed as the file of initial temperatures, and calculations in the next phase begin with the final moment of the previous step. Solution discretization is convenient when it is necessary to introduce changes into the thermal medium in response to structural and material changes in geologic sequence, to preset the distribution of new thermal sources and discharge zones, and to revise the estimated paleothermal field parameters. If heat and mass transfer should be included in the model, it can be imitated by presetting end temperature values and/or adiabatic gradients in the depth interval covered by convection.

For each profile, the end temperature value was taken at the upper boundary and heat flow at the lower boundary (q_{bd}) in compliance with the value measured in the nearest well (q_{obs}) minus heat flow generated in the crustal layer above the lower boundary of the modeling domain as a result of the spontaneous decay of long-lived radioactive isotopes (q_{est}), that is, $q_{bd} = q_{obs} - q_{est}$.

The reduced heat flow varied within 30-40 mW/m^2.

A specific feature of three-dimensional modeling is the estimation of temperatures and consequently all other geothermal parameters in the latitude–longitude–depth geometry for the whole region. Using the volumetric interpolation of the TECPLOT program, we obtained a three-dimensional temperature distribution pattern over the whole study interval (down to 35 km) and for the whole region. A similar procedure was applied to obtain a three-dimensional heat flow distribution pattern. The program enables the depth slices of temperature and heat flow values and isothermal surfaces to be plotted for any interval.

Geothermal studies in the Barents Sea

The intense exploration for oil and gas fields in shelf basins that commenced in the 1980s included offshore and deep drilling on islands accompanied by thermal logging. In addition, the first measurements of the heat flow in wells were performed at that time in the southern Kara Sea. In the 1980s-1990s the measurements of heat flow by submersible sounds were performed in the central and southeastern Barents Sea (Verzhbitsky, 2002; Левашкевич, 2005) and the empirical data were subsequently processed with allowance for seasonal bottom-temperature fluctuations (Суетнов, Никульшина, 1988). The processing of thermal measurements made it possible to estimate thermal gradients, while thermophysical studies of drill cores resulted in measurement of the heat conductivity of rocks. These works provided the first conditional values of heat flow in the region under consideration. However, the geothermal measurements in wells were sparse and insufficient for adequate mapping of the temperature and heat flow distribution in such a vast-territory, especially for calculation of deep temperatures in the lithosphere.

Nevertheless, the analysis of available data obtained by measurements in wells and thermal sounding revealed a tendency for an increase in heat flow in the northeastern and northwestern directions. For example, in the zone of conjugation of the Kola microplate and the Baltic Shield, the heat flow averages 54 mW/m^2 and amounts to 70 mW/m^2 in the North Barents Basin and Central Barents Uplift. To a first approximation, such a trend in heat flow variations can be explained by approaching the North Atlantic spreading center, where the thermal activity of the asthenosphere increases. At the same time, our data indicate that the crust of the Barents Plate is subjected to secondary processes, which become younger in the northern direction.

On the basis of interpretation of geothermal data, it was suggested that the secondary thermal processes are related to rifting (Khutorskoy et al., 2003). Modeling of the nonstationary thermal field in order to calculate deep temperatures and heat flows was performed along each of the profiles shown in Fig. 1.

The geotraverses extend via the wells, where the conditional heat flow measurements were conducted. Such measurements made it possible to correctly set the Neumann (second-type) boundary conditions at the lower margin of each profile.

Initial conditions for temperature calculation were set for 60 Ma ago. As follows from paleotectonic reconstructions for the Barents Sea (Верба, Шаров, 1988; Устрицкий, Храмов, 1984), the present-day structure of the crust was already formed by that time. Therefore, the evolution of the thermal field, if it occurred, was related to relaxation of initial thermal heterogeneities rather than to the reorganization of structural and thermophysical elements. Under such boundary and initial conditions, the temperature within the modeling region is rapidly coming to a steady state, which was a priori accepted as a criterion of calculation correctness. The duration of time steps was 10 Ma. Thus, six control stages were taken over the time interval of 60 Ma to verify the stationary state. The modeling has shown that, since the third step, i.e., 30 Ma after the onset of calculation, all the profiles are characterized by a steady-state thermal field.

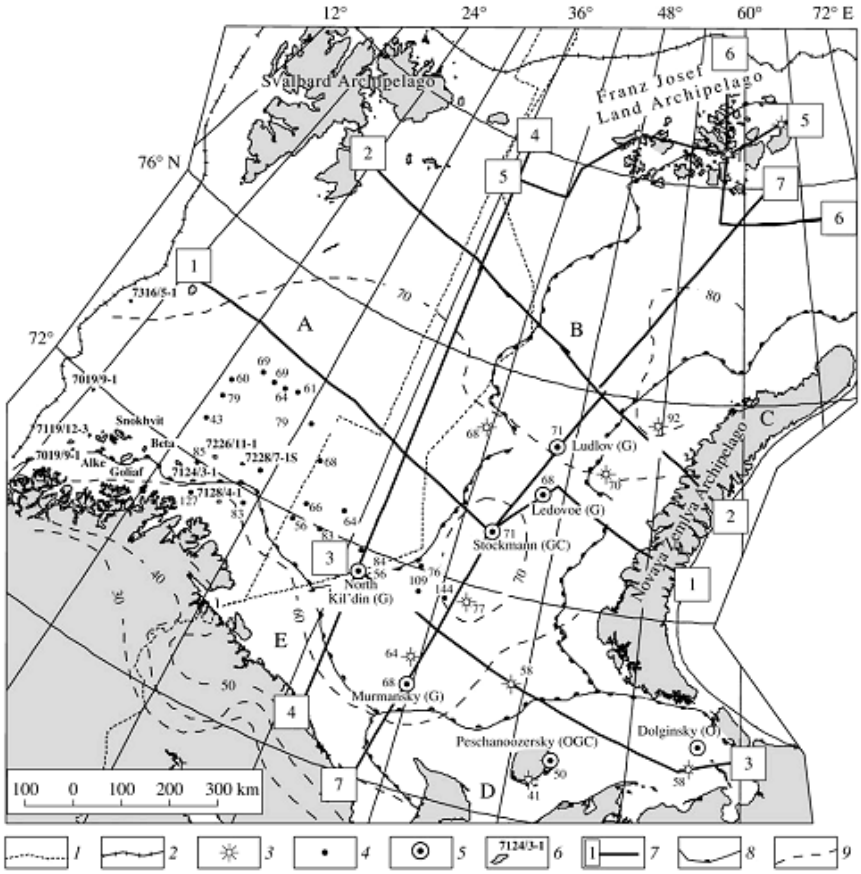


Fig. 1. Map of the heat flow density in the Barents Sea region and adjacent areas. (1) Border of Russia and median line (according to the proposal of Norway of 1970); (2) shelf edge; (3) deep well; (4) station of heat-flow measurements and its value, mW/m^2; (5) petroleum fields in the Russian sector; (6) the same in the Norwegian sector; (7) line of seismic and geological profile and its number; (8) boundaries of regional tectonic elements; (9) contour line of heat flow, mW/m^2. Tectonic elements (letters in figure): (A) Svalbard Plate, (B) East Barents Megatrough, (C) Pai-Khoi–Novaya Zemlya Fold System, (D) Pechora Plate, (E) Kola Homocline. Fluid type: (G) gas, (GC) gas condensate, (OGC) oil–gas condensate, (O) oil

The technique of computing 3D models was described above. Here, we note only that the procedure consists of two stages.

At the first stage, the temperature sections along geotraverses are placed into a three-dimensional plot according to coordinates of their onset, end, and bend points, if there are any. In addition, the modeling accuracy is estimated at this stage by comparison of calculated and measured temperatures at intersections of profiles. The least square method, which was applied to estimate the modeling accuracy, shows that discrepancy between depths of the same isotherms is ~100 m, i.e., 0.7% of the total modeling depth, which equals to 15 km. We consider this uncertainty as admissible.

At the second stage, with the use of 2D temperature ranges as boundary conditions, the 3D volumetric interpolation is carried out. If the distance between profiles is less, the accuracy of the interpolation procedure will be higher. We used as many as 123 geotraverses characterized by CMP and DSS profiling data for the Barents-Kara region in our previous 3D models.

However, the modeling technique used in this work differs from the previous one by the detailed analysis of the geological situation based on drilling results. Therefore, we developed the model using only the seven above-mentioned geotraverses. It is particularly noteworthy to compare models of the first and second generations and to ascertain the factors responsible for their differences, if any exists.

The results obtained at the first stage of 3D modeling – allocation of temperature ranges in the 3D plot – are shown in Fig. 2. A special original computer program that takes into account the depth and position of each profile and transforms initial data of 2D modeling into the TECPLOT format was used to implement this procedure.

Volumetric interpolation resulted in obtainment of the model of the temperature field, which makes it possible to determine a temperature in any point of 3D space (Fig. 3). A special blanking in this figure shows temperature domes beneath the South Barents Syneclise and the Pechora–Barents Zone of buried uplifts. The dome extends to the South Kara Basin, where it looks autonomously because of the temperature screen beneath Novaya Zemlya (New Land). In fact, the formation of both domes has the same cause, namely, the occurrence of thick and low-conductivity sediments and the respective increase in the geothermal gradient within this zone. Northward, this effect is enhanced by the local increase in the terrestrial heat flow in the Stockmann–Lunin area and the North Barents Basin. The latter factor determines the appearance of another temperature dome in the western part of the region at the edge of the Norwegian shelf, where the sedimentary cover is relatively thin, but the heat flow is slightly higher in comparison with the background level established for the Barents Plate.

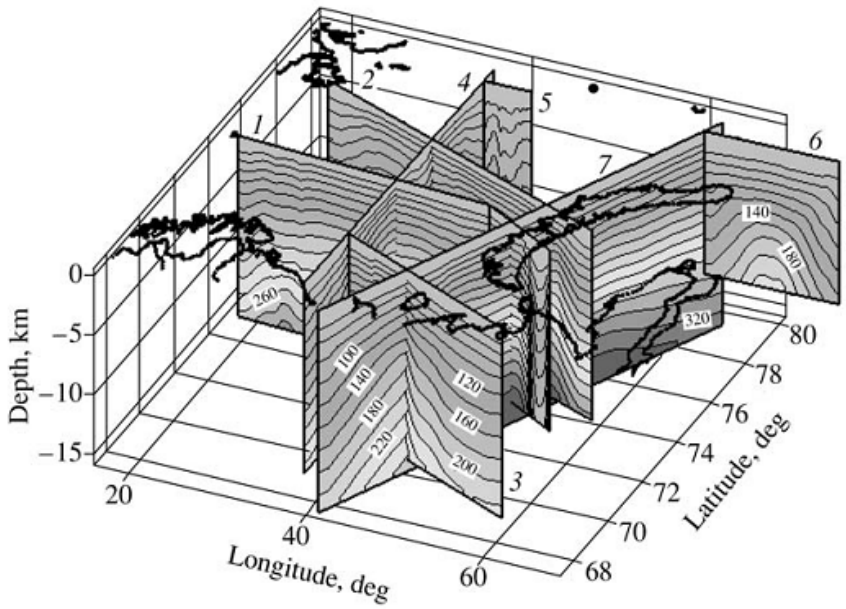


Fig. 2. Temperature sections placed on a 3D plot. See text for explanations. Numerals correspond to numbers of profiles

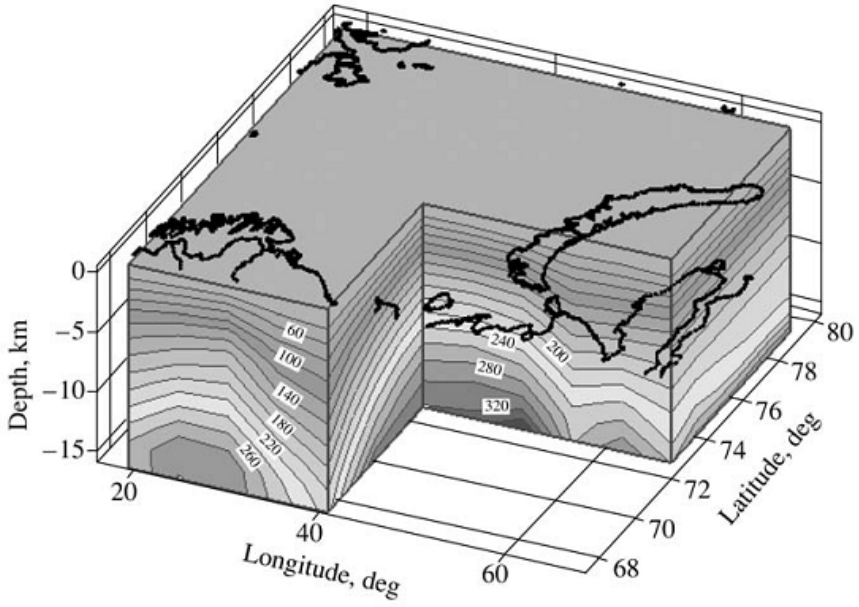


Fig. 3. A 3D model of the temperature field. Isotherms, °C

Gas and gas-condensate fields discovered in the southeastern part of the Barents Sea and South Kara Basin are localized above the temperature dome. Previously, we pointed out that the Stockmann, Ludlov, Ledovy, North Murmansk, Rusanov, and Leningrad fields are confined to the apical part of the temperature dome. This character of localization can probably be used as an additional criterion to forecast the petroleum resource potential.

The North-Caspian Basin

The North Caspian Basin is traditionally recognized within the boundaries of the salt-dome region. Its north-western limit is traced along the pre-Kungurian tectonic and sedimentary scarp, as high as 1500 m, which extends in the submeridional direction from Kotelnikovo in the south via Volgograd to Saratov in the north and turns abruptly to the east extending at the latitude of Uralsk toward Orenburg. The basin is limited by the Ural Foldbelt in the east, the South Emba Paleozoic tectonic rise in the southeast, and the Donbass-Tuarkyr system of inversion highs in the southwest (Volozh et al., 1998).

The Caspian Basin had taken its shape within these boundaries as a closed structure only by the end of the Early Permian, when the Ural orogenic belt was formed at its eastern boundary and an inversion-type uplift existed on the spot of the present-day Donbass-Tuarkyr rift system. Before that time various parts of this system were related to different sedimentary basins. The western half of the basin was a part of the sedimentary basin that had been continuously evolving since the Late Riphean, and its eastern part was a fragment of a large orogenic region until the Early Devonian. In the Devonian and Early Carboniferous the entire territory of the basin was a vast area of sedimentation covering the shelf of a deep-water marginal basin in paleogeographic terms. This basin was localized in front of the subduction zone that separated the East European continent from the Ural paleoocean.

The Kungurian (Permian) evaporites, which occur as domes and stocks due to their tectonic and gravitational instability are a specific feature of the North Caspian Basin. They mainly consist of rock salt with scarce sulfate segregations and variably thick interbeds of sulfate–terrigenous rocks including mudstone, sandstone, and anhydrite. The dip angles of these rocks vary from a few degrees to 75° because of the ductile flow of salt from the intermediate zones to the cores of the salt massifs. The domes partly or entirely intrude into Upper Permian sedimentary rocks. In some cases, where the domes ceased to grow in the Paleozoic, the overlying Mesozoic rocks lie horizontally; while in other places, where the domes continued to grow further, these rocks are tilted at various angles controlled by the time and rate of the salt rise. In plan the domes are round, elliptical, elongated, or star-shaped. The round domes are characteristic of the central part of the basin while the elongated ones are characteristic of its margins.

The rock salt has a high thermal conductivity ranging from 5.5 to 6.5 W/(m · K) and significantly exceeds the heat conductivity of the terrigenous rocks of 1.6-2.0 W/(m · K). This high conductivity contrast and the steep rock contacts are responsible for the marked redistribution of the terrestrial heat flow. Like other potential fields, the heat flow propagates along the paths of least resistance, being concentrated in the

salt domes and discharging in the zones between them. Thus, heat flow refraction is the main cause of the heterogeneous heat flow in the North Caspian Basin. Analyzing the empirical data, it is possible to see that the positive heat flow anomalies above the salt domes are produced mainly by structural and geological heterogeneities as well as by the presence of rock salt layers as heat conductors.

As the structural and thermal heterogeneities in the North Caspian Basin produce lateral and vertical variations in the geothermal gradient and heat flow density, an estimation of their background values by simple averaging encounters difficulties and requires the detailed study of temperature distribution practically in each hole.

The mosaic tectonic pattern of the basin, especially of its larger central part, known as the Central North Caspian Depression should also be taken into account. Here the salt domes are round, and a two-dimensional approximation of the thermal field introduces obvious error. The 2D approximation of the heat flow is possible only in the marginal parts of the basin where the salt swells and ridges are dominant structures. In this connection, we used 3D modeling and representation of the geothermal field for the entire territory of the North Caspian Basin.

The 3D temperature and other geothermal parameter distributions were made on the basis of temperature logging of wells and on some special-purpose measurements.

We began our study with a tie-in of the wells, the estimation of well standing after drilling operations; a digitizing of the temperature logs; and the compilation of a database with the appropriate graphic materials. As a result of this work we collected data on temperature in 115 wells drilled in the region, including 16 deep wells drilled to a depth of more than 4 km (Fig. 4).

To plot the isotherms in 3D geometry, we used the holes with the most reliable data on the deep temperature distribution; the locations of these holes are shown in Fig. 5.

Figure 6a demonstrates the obvious temperature rise at depth from NE to SW. For example, in the eastern part of the basin near the boundary with the Mugodzhary Mountains, the temperatures at depths of 2 and 3 km are 40-45 and 60-65°C respectively, whereas in the South Emba and Mangyshlak areas the temperatures are 55-60 and 70-75°C at the same depth. At a first approximation, these data are consistent with the heat flow decrease in the eastern part of the North Caspian Basin owing to the nonstationary screening of the terrestrial heat flow in the southern Ural and Mugodzhary Mountains (Хуторской, 1996).

A similar pattern is observed in the geothermal gradient distribution within a depth interval of 0-5 km (Fig. 6b), where its values increase southwestward from 15 to 40-45 mK/m. It appears that the gradient is stabilized at 20-35 mK/m level at a depth of 3-4 km. In the eastern part of the basin, the temperature is 40-45 and 60-65°C at depths of 2 and 3 km, respectively, whereas in the South Emba district and Mangyshlak Peninsula the temperature is 55-60 and 70-75°C at the same depths. It indicates that heat flow diminishes in the east due to screening of the deep heat flow in the southern Urals and Mugodzhary Mountains in the geological past.

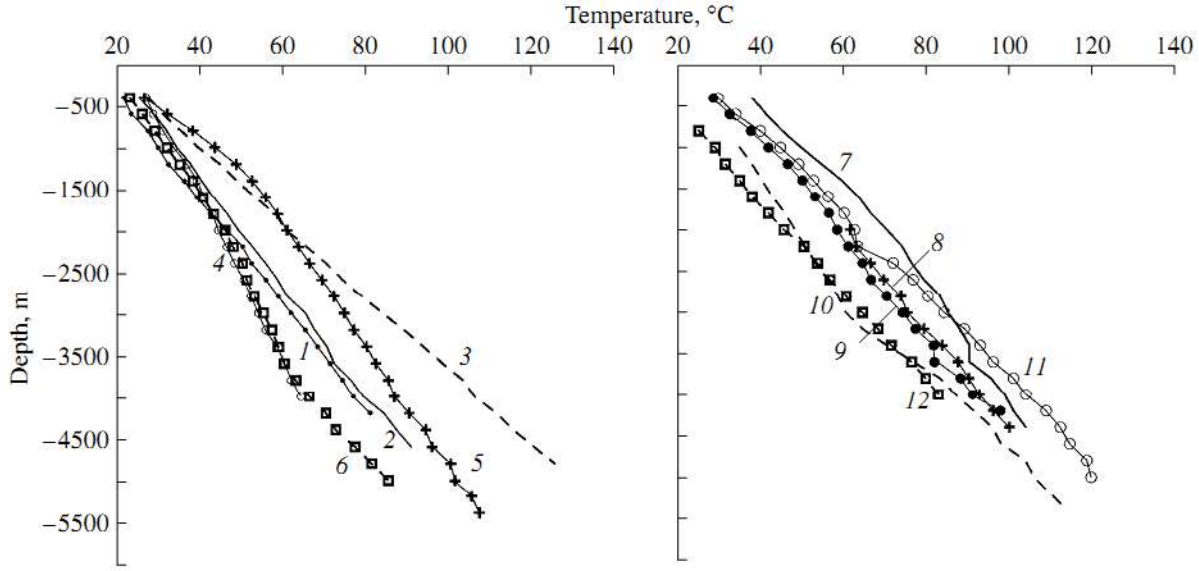


Fig. 4. Thermograms of some deep wells in the North Caspian Basin.
Wells: (1) Blaksai-89p, (2) Karatyube-34, (3) Karatyube-35, (4) Kumsai-2, (5) Biikzhal-SG2, (6) Kursai-4, (7) Teresken-1p, (8) Teplovskaya-1p, (9) West Teplovskaya-2p, (10) Tashlinskaya-25p, (11) Aralsorskaya-SG1, (12) Khobdinskaya-1

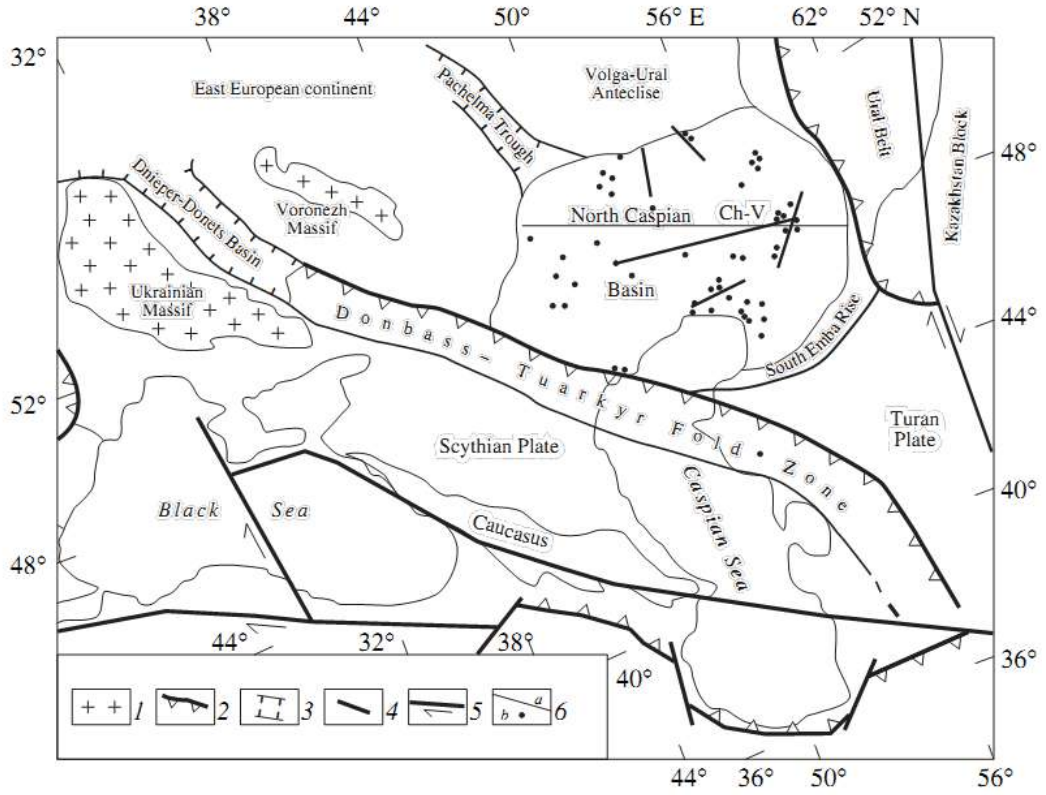


Fig. 5. Tectonic setting of the North Caspian Basin. (1) Continental basement rise, (2) suture, (3) rift system boundary, (4) fault, (5) transcontinental shear zone, (6) profile line: (a) Chelkar-Volgograd (Ch–V) DSS profile, (b) well bearing temperature data

Ascending westward from the longitude of the Mugodzhary Mountains, the isotherms form several domes, the apices of which are localized in the areas of South Emba, Mertvy Kultuk Sor, the North Mangyshlak Peninsula, as well as in the Astrakhan and Buzuluk arches (Khutorskoy et al., 2010). Thus, the spatial association of thermal domes and zones with economic petroleum resources occurs in the Pericaspian region as elsewhere.

The Pripyat basin

The Pripyat Basin is localized in the trough bearing the same name and situated between the Belarussian and Voronezh anteclises and the Zhlobin Saddle in the north and the Ukrainian Shield in the south, which divide them. The basin extends for 280 km in the W–E direction and reaches 150 km in width, being an element of the planetary fault belt called the Sarmatian-Turan Lineament that strikes in the northwestern direction from the spurs of the Hissar Range in the east, extends south of the Pericaspian Basin to the Podlyassy-Brest Trough in the west. This lineament effectively connects the East and West European evaporite provinces.

The Pripyat Trough is bounded in the north and south by mantle rooted faults. A number of W–E trending faults are traced within the trough, and some of them are of mantle origin, as well. (Айзберг и др., 2007).

The trough is filled with sedimentary rocks in the stratigraphic range from the Middle Devonian to the Middle Triassic and was formed in the Late Paleozoic. The maximum thickness of the platform cover is 5.5-6.0 km. The upper and lower Upper Devonian salt-bearing sequences are separated by a carbonate-clayey intrasalt sequence. The upper salt-bearing sequence is predominant. Its maximum thickness of 3 km is established near the northern wall of the trough (Айзберг и др., 2007), whereas in the central and southern parts the thickness is 0.6-2.5 km and 0.7-2.0 km respectively.

The thickness of the lower salt-bearing sequence is several times less than that of the upper one. In contrast to the lower sequence, the upper sequence is characterized by more pronounced salt tectonics with well-developed salt domes, plugs and swells. The evaporite sequences were deposited in a transgressing deepwater marine basin. The sedimentation was accompanied by active faulting and volcanic activity in the northeastern part of the trough and the adjacent territory. Sedimentary-volcanic sequences and alkali basalts are coeval with evaporite sequences (Геология Беларуси, 2001).

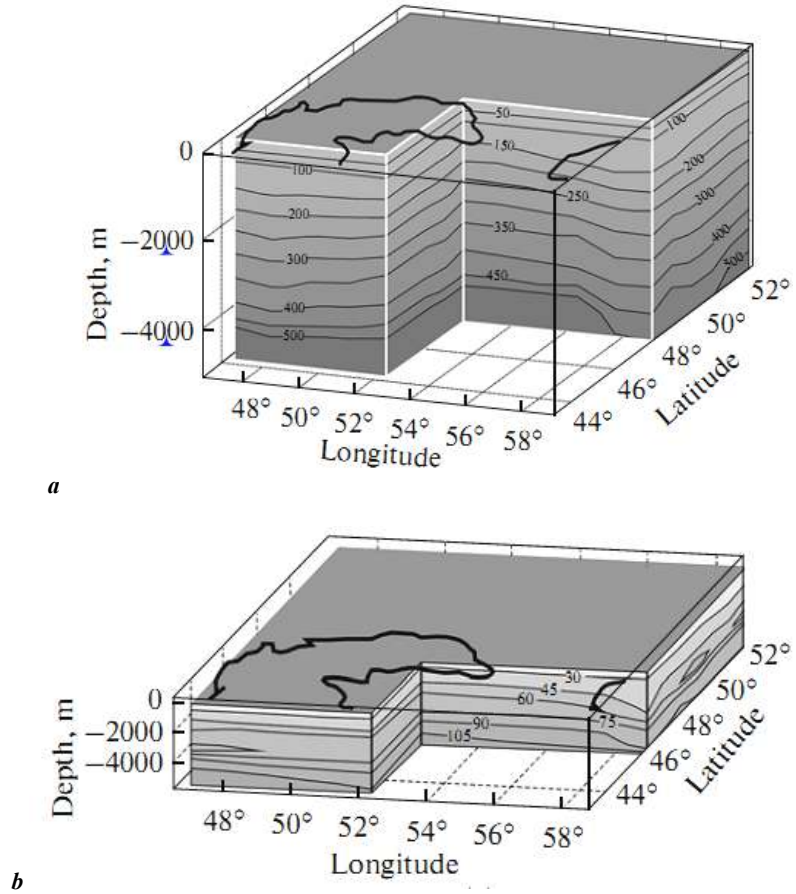


Fig. 6. 3D models of deep temperature distribution in Pericaspian Basin:
(a) temperature distribution within interval of drilling (0-50 km); (b) the same in Earth's crust (0-5 km)

The geothermal characterization of the trough is based on temperature measurements in more than 200 wells. Most wells are located in the northern zone of the trough. Its southern part is less studied. The heat flow has been calculated in most wells (Пархомов, 1985; Tsybulya, Levashkevich, 1990). The thermograms measured in the northern, central, and southern zone are shown in Fig. 7.

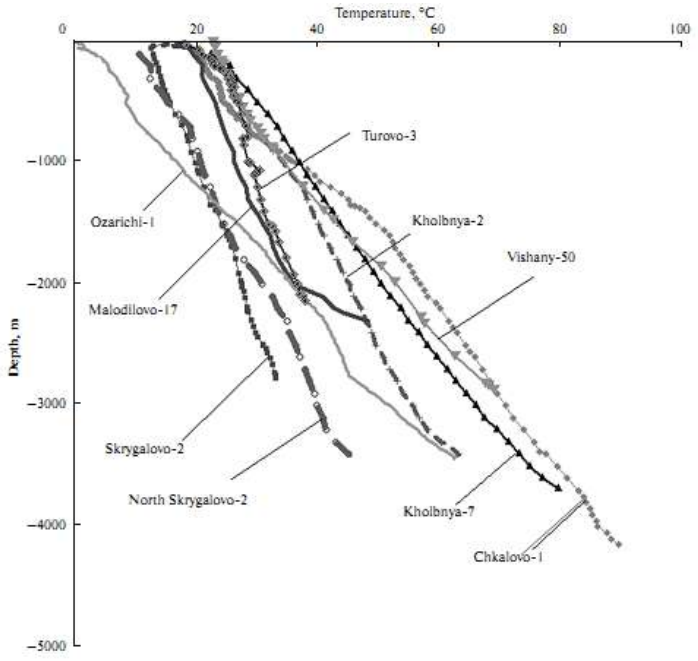


Fig. 7. Thermograms of deep wells in the Pripyat Basin

The configuration of the thermograms in the northern zone (Vishany, Chkalovo, Ozarichi wells) differs from those in other two zones indicating a special geothermal setting. This difference is reflected in the heat flow density, which is 45-50 mW/m^2 in the marginal southern and 60-75 mW/m^2 in the northern zones.

The causes of different background heat flow values in the northern and southern parts of the trough were discussed in (Tsybulya, Levashkevich, 1990). The authors of this publication attach great importance to the refraction of the heat flow related to structural and thermophysical inhomogeneities and consider this factor to be crucial for interpretation of the lateral variation within the same zone. For example, above the apical parts and margins of the Rechitsa and Pervomaisky salt domes, the heat flow attains 124 and 106 mW/m^2, respectively, whereas the background heat flow in the zone as a whole is 75 mW/m^2. At the same time, a different contribution of radiogenic heat generation and variable permeability of deep faults for the fluids provides an additional influx of heat in the zones under comparison. The calculated contribution of radiogenic heat in the northern part of the trough is 29 mW/m^2 compared to 13 mW/m^2 in the southern zone. The appreciable difference in the radiogenic component of the heat flow is explained firstly by different values of specific heat generation (0.5-1.0 μW/m^3) in the southern zone and 1.5-2.0 μW/m^3 in the northern zone) and secondly by thickening of the granitic-metamorphic crustal layer, which provides the main contribution to radiogenic heat generation in the northern zone. The remainder of the background heat flow is generated by its supply from the mantle and the lower crust along permeable deep faults, which are more numerous in the northern zone than in the southern one. According to geophysical data, these deep faults drain the mantle.

It is noteworthy that the oil fields are confined to the W–E-trending deep faults and are concentrated mainly in the positive anomalies of heat flow in the northern zone. Attention to the relationship between the petroleum resource potential of the sedimentary cover and temperature was first paid in (Garetsky et al., 1990). It was pointed out that the temperature in the Northern Fault Zone is higher than in the marginal Southern Fault Zone. As it follows from temperature measurements in wells, the difference is 20-25°C at similar levels. The temperature increases from the west eastward in the Northernmost Fault Zone.

Quantitative estimation of the temperature field in the Pripyat Basin was carried out on the basis of its 3D-modeling using the above mentioned technology. The initial data were data on the temperature in wells and on the thermal conductivity of the rocks in the section. The thermophysical structure was set on the basis of seismic CDP profiling and deep seismic sounding (DSS) along a series of N–S-trending lines (Thibo et al., 2003).

Detailed knowledge of the heat flow and its radiogenic component made it possible to specify the reduced heat flow at the lower edge of the modeling region (a depth of 6 km) in particular lithotectonic zones and the distribution of radiogenic heat sources within this region. At the upper edge coinciding with the neutral layer, the mean annual temperature (8°C) is established from measurements in wells.

The 3D temperature model of the upper crust in the Pripyat Basin is shown in Fig. 8 together with the location of deep faults and oil fields. A northward increase in temperature is clearly seen. At a depth of 4 km, the temperature in the southern part of the trough is 45-50°C and increases to 65-70°C in its northern part. At a depth of 6 km, the corresponding values are 65-70°C and 85-90°C. It can be shown that the temperature conditions of catagenesis of oil (T =120°C) is attained in the northern part of the basin at a depth of 8.5-9.0 km while extrapolating the temperature to a depth.

Thus, we reveal the same tendency of temperature distribution in the Earth's crust as it has been described in the Pericaspian Basin. The oil fields are confined to the temperature cupola, or the zone of rising isotherms in the sedimentary cover (Fig. 8). In the Pripyat Basin, the temperature cupola is related to the deep faults that provide additional mass and heat transfer. It implies that a possible cause of the thermal anomalies is the supply of deep, hydrocarbon- bearing fluids along the permeable fault zones. Such a process ensures a higher background heat flow in the northern part of the Pripyat Basin in comparison with the Pericaspian Basin, where no indications of advective heat and mass transfer are established to date.

The North German basin

The North German Basin occupies the middle part of the Central European petroleum province (CEPP) and is filled with Phanerozoic sedimentary rocks up to 12-14 km in total thickness. The Devonian terrigenous and carbonate rocks occur at the base of the section, upsection, they give way to Lower Carboniferous carbonate rocks. The Upper Carboniferous and Lower Permian (Rotliegende) rocks are composed of terrigenous coarse–clastic rocks; often these are red beds. The Upper Permian rocks (Zechstein) consist of terrigenous and carbonate rocks in the lower part of the section, which are replaced upward with anhydrite and dolomite and further with rock salt and anhydrite. Rock salt is the most abundant in the Strassfurt Formation (van Wees et al., 2000).

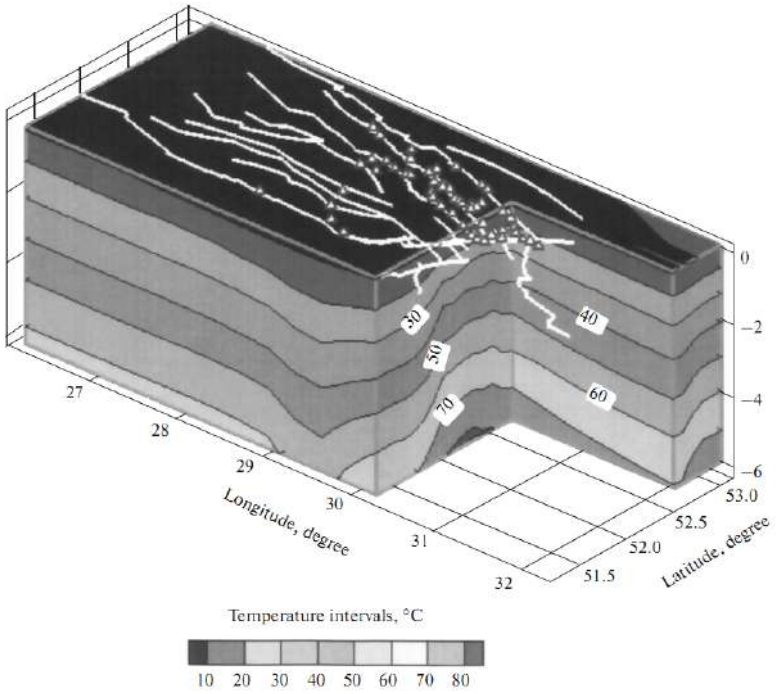


Fig. 8. 3D temperature model of the Earth's crust in the Pripyat Basin. The white lines are deep faults; the white triangles are oil fields

The North German Basin adjoins the North Sea Syneclise. Before the Cenozoic, the basin consisted of a number of troughs expressed in the Mesozoic sedimentary cover. The large Lower Saxonian Trough, extending in the latitudinal direction occupies the western part of the basin; the small Hannover and Gifhorn troughs striking in the meridional and southwestern directions are situated eastward. The SW-trending West and East Holstein troughs are outlined in the northwest of the North German Basin.

The basin as a whole is characterized by the development of salt tectonics that involves the Upper Permian (Zechstein) salt. Extended and exposed linear salt ridges are typical (Bayer et al., 1999).

The North German Basin is distinguished by a complex structure dominated by the intersection of the Rhenish and Hercynian dislocations different in age and orientation, which are accompanied by variations in the thickness of the Cretaceous, Jurassic, and Triassic sequences and sharp unconformities. The basin is asymmetric in cross section. The thickness of the Paleozoic rocks attains 5 km and the Mesozoic rocks are as thick as 8 km. The Triassic sequence contains members of rock salt up to 100 m thick (Clausen, Pedersen, 1999).

Hydrocarbon occurrences are noted within a wide stratigraphic interval. Hydrocarbons have been found in the Paleogene, Cretaceous, Jurassic, Triassic, Permian, and Carboniferous rocks. The gas reservoirs are hosted mainly in the Permian, Triassic, and to a lesser extent, Carboniferous sedimentary rocks, determining the spatial zoning in the localization of oil and gas pools.

Within the state borders of Germany, a few tens of mainly small oil and gas fields are known. The oil fields are located in the northern part of the North German Basin (Reikenhagen, Grimmen, Lüttow), in its northeastern (Gubben, Lüben, Staakow), and in the southwestern parts (Fallstein); the gas fields are concentrated in the southeastern part of the basin (Буштар, Львов, 1979).

The largest buried Lower Saxonian Trough is situated in the south of the North German Basin. The trough is expressed in the stratigraphic range from the Upper Triassic to the Lower Cretaceous and especially pronounced in the Upper Jurassic rocks. In the west, the Lower Saxonian Trough is closed at the northeastern plunging of the Central Netherland Rise (Emsland Slope), where the thickness of the Jurassic and Cretaceous rocks is markedly reduced (Mazur, Scheck-Wenderoth, 2005).

The lowland portion of the North German Basin is located in eastern Germany, in the middle part of the CEPP. Carboniferous, Devonian, and Ordovician rocks are penetrated in this part of the basin.

The structure of the Polish part of the basin is controlled by conjugation of the Precambrian platform (Baltic Syneclise) in the northeast with the epi-Hercynian platform (North German Basin) in the south-east. The junction zone is expressed in a buried foredeep that adjoins the Baltic Syneclise in the northeast and the Mid-Polish Swell exposed in the

Swiétokrzyskie Mountains. This part of the basin is filled largely with Mesozoic (up to 8 km) and Paleozoic (more than 12 km) sequences. The Paleozoic section is characterized by a thick (2500 m) Permian salt-bearing sequence. Most of the hydrocarbon fields are localized in the Foresudeten Homocline, where 25 gas fields (Otyn, Senkowice, Cheklin, etc.) and six oil and oil-gas fields (Rybaki, Polenzko, Nova-Söl, etc.) were discovered after 1960.

As in the above mentioned basins, the hydrocarbon fields are attracted to thermal anomalies. At the same time, the heat flow in the CEPP is higher than in the Pripyat and Pericaspian basins. According to (Majorowicz et al., 2003), the background heat flow is 80-85 mW/m^2 here, i.e., corresponding to the anomalous values in other basins.

A 3D temperature model was plotted for the quantitative characterization of the deep temperature regime in the North German Basin (Fig.9). This model is based on temperature in wells and the thermal conductivity of rocks in section, as well as on the data concerning the structural and geological setting along the DDS lines (Majorowicz et al., 2003; Thibo et al., 2003).

Comparison of deep temperatures in the Pericaspian, Pripyat, and North German basins

Depth, km	Temperature, °C			
	Pericaspian	Pripyat	North German (eastern part)	North German (western part)
0–5	42 8–104	37 8–74	87 9–242	86 9–165
5–10	105 46–159	–	215 106–397	214 93–306
10–20	192 95–274	–	366 194–612	343 168–477

Note: numerator is the average temperature; denominator is the temperature range.

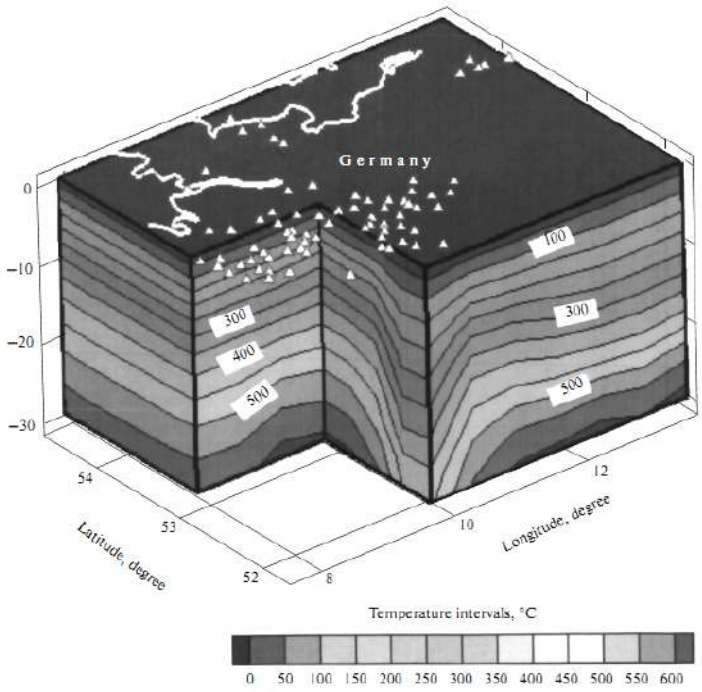


Fig. 9. 3D temperature model of the western part of the North German Basin (Saxsonian sector). White triangles are oil fields

The model heat flow and temperature that extends in Poland show a notable increase in heat flow (up to 100 mW/m^2 against the background value of 65 mW/m^2) and the appearance of thermal cupolas in the temperature section. These anomalies are confined to the eastern (Silesian) part of the North German Basin enriched in salt domes and related hydrocarbon fields. A decrease in heat flow down to background level is noted at the longitude 20°E (Fig. 10), where salt domes disappear. According to (Bayer et al., 1999), this is precisely the place where the crystallinicum of the East European Platform borders on the eastern margin of the CEPP.

The catagenetic temperature interval of organic matter transformation, which is favorable to the formation of hydrocarbon concentrations occurs in the zone of the section at a depth of 3.0-4.5 km (Table).

We cannot rule out the occurrence of hydrocarbons in the northeastern segment of the section beyond the salt dome zone, but the catagenetic interval is located here at a depth of 6.0-6.5 km. The 3D model of deep temperature in the eastern part of the North German Basin (Fig. 10) shows a pronounced temperature cupola related to faults and salt domes, i.e., to the area of oil fields. A temperature cupola in the 3D temperature model (Fig. 9) is spatially correlated with oil fields in the western part of the North German Basin.

Conclusions

(1) The geothermal field of such isometric regions as the Barents Sea Basin can be reliably depicted only in 3D geometry. This technique offers an opportunity to estimate both lateral and vertical variations of the thermal field. (2) Temperature and heat-flow anomalies are formed as a result of nonstationary distribution of heat sources and structural and thermophysical heterogeneities determined by lithological and tectonic factors. (3) The thermotomographic analysis of petroliferous basins has shown that economic accumulations of hydrocarbons are localized above zones of rising isotherms or thermal domes that were outlined for the first time by 3D modeling of the geothermal field in the eastern Barents Sea and the southern Kara Sea.

Of three considered salt dome basins in northern Eurasia, the Pericaspian and North German basins may be referred to the exogonal type, whereas the Pripyat Basin – to the intracontinental type. All of the basins underwent deep and persistent sagging in the Late Paleozoic with accumulation of evaporites (rock salt and anhydrite) intercalated by terrigenous rocks.

Under the effect of gravity and tangential compression, the salt-bearing sequences were transformed into salt domes, plugs, and swells, which cut through or deform the overlying rocks. Halogenic rocks have anomalously high thermal conductivity in comparison with terrigenous rocks. The contrast in thermal conductivity and the sharp structural boundaries between the salt domes and sedimentary rocks of the interdomal zones create conditions for perturbation of the terrestrial heat flow, which is concentrated in the salt bodies and brings about distinct anomalies of heat flow above the apexes of the salt domes and their marginal parts. These anomalies exceed the background values by 50-60% and should be considered one of the main features of the geothermal field in the salt dome basins.

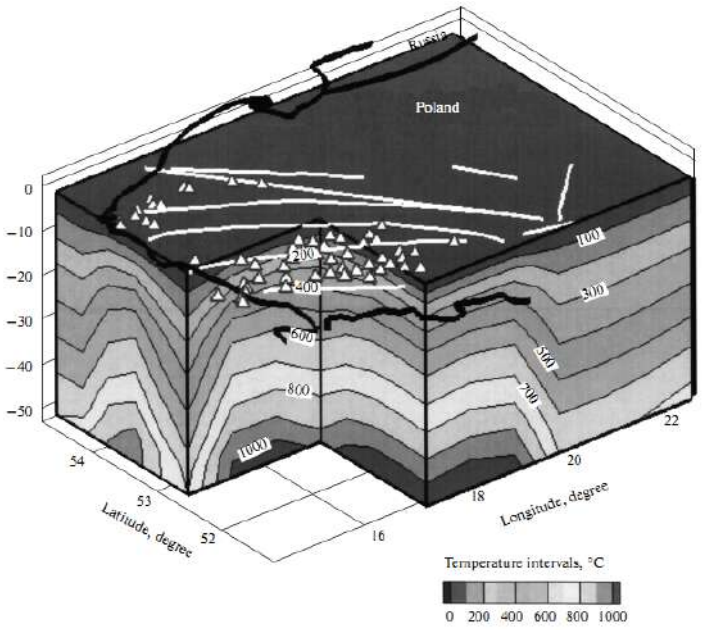


Fig. 10. 3D temperature model of the eastern part of the North German Basin (Silesian sector). White lines are deep faults; white triangles are oil fields

The spatial distribution of the salt domes and variation of their shapes show their close relations to faults. As a rule, the salt domes are localized along the fault zones and elongated along their strikes. The salt domes with isometric or star-shaped contours in plan view are confined to the central, most subsided parts of the Pericaspian and North German basins.

The considered salt dome basins are distinguished by high petroleum resource potential. Oil pools are penetrated at different depth levels and in various structural relationships with the evaporites. The general tendency links the oil fields to fault zones and zones of elevated temperature in the sedimentary cover.

The term thermal cupola (Khutorskoy et al., 2003) is introduced into the geological and geophysical terminology to denote the zones of elevated isotherms clearly expressed in the temperature sections of 2D and 3D models and spatially coinciding with hydrocarbon fields. Thermal cupolas reveal close spatial relationships to the above localized hydrocarbon fields in all of the studied shelf or evaporite basins. It is evident that in the areas of thermal cupolas the temperature interval of catagenesis of organic matter is located nearer to the Earth's surface. The three salt dome basins considered here are not exceptions in this respect. These basins demonstrate spatial combinations of fault zones, oil fields, areas of higher heat flow, and thermal cupolas in the field of deep temperature.

According to 3D modeling, the temperature range at a depth of 1000-2000 m is 30-36°C in the Barents Basin, 28-46°C in the Pericaspian Basin, 28-40°C in the Pripyat Basin, and 38-88°C in the North German Basin, so that the North-German Basin is the most heated.

Calculation of depths where the catagenetic temperature is suitable for transformation of organic matter yields 6-7 km for Barents Basin, 7.0-8.5 km for the Pericaspian Basin, 8.5-9.5 km for the Pripyat Basin, and 3-7 km for the North German Basin.

Acknowledgments

This study was supported by the Russian Science Foundation, project nos. 23-17-00019.

REFERENCES

Aizberg R.E., Garetsky R.G., Karabanov A.K. et al. Faults of the earth's crust on the territory of Belarus. Krasiko-Print. Minsk, 2007, c. 294-348 (in Russian).

Bayer U., Scheck M., Rabbel W. et al. An intergrated study of the NE German Basin. Tectonophysics, Vol. 314, No. 1-3, 1999, pp. 285-307.

Bushtar M.S., Lyvov M.S. Petroleum and gas geography and geology of the USSR and foreign countries. Nedra. Moscow, 1979, 368 p. (in Russian).

Clausen O.R. and Pedersen P.K. Late Triassic structural evolution of the southern margin of the Ringkobing Fyn High, Denmark. Mar. and Petrol. Geol., Vol. 16, No. 7, 1999, pp. 653-665.

Garetsky R.G., Pechernikov V.V., Aizberg R.E. and S. V. Klushin. Reflection of deep structure of the Pripyat Paleorift in thermobaric indexes of platform cover. Sov. Geol., No. 3, 1990, pp. 93-98.

Geology of Belarus. Institute of Geological Sciences of the National Academy of Sciences of Belarus. Minsk, 2001, 815 p. (in Russian).

Khutorskoi M.D. Geothermometry of the Central Asian Foldbelt. Peoples' Friendship University of Russia. Moscow, 1996, 285 p. (in Russian).

Khutorskoi M.D., Podgornykh L.V., Gramberg I.S., Leonov Yu.G. Thermal tomography of the West Arctic Basin. Geotectonics, Vol. 37, No. 3, 2003, pp. 245-261.

Khutorskoi M.D., Teveleva E.A., Tsybulya L.A., Urban G.I. Heat flow in salt_dome basins of Eurasia: A comparative study. Geotectonics, Vol. 44, No. 4, 2010, pp. 289-304.

Levashkevich V.G. Patterns of distribution of the geothermal field of the outskirts of the East European Platform (Barents Sea and Belarus-Baltic regions). Doctoral Dissertation in Geology and Mineralogy. Moscow State University, Moscow, 2005, 332 p.

Majorowicz J.A., Cermak V., Šafanda J. et al. Heat flow models across the Trans-European Suture Zone in the area of the POLONAISE-97 seismic experiment. Phys. Chem. Earth, Vol. 28, No. 9-11, 2003, pp. 375-391.

Mazur S., Scheck-Wenderoth M. Constraints on the tectonic evolution of the Central European Basin system revealed

ЛИТЕРАТУРА

Айзберг Р.Э., Гарецкий З.Г., Карабанов А.К. и др. Разломы земной коры на территории Белоруссии. Красико-принт. Минск, 2007, с. 294-348.

Буштар М.С., Львов М.С. География и геология нефти и газа СССР и зарубежных стран. Недра. Москва, 1979, 368 с.

Верба М.Л., Шаров Н.В. Современное состояние и основные проблемы глубинного строения Баренцева моря. В: Апатиты. Т. 1. Геол. инст., Кольский науч. центр, Российская акад. Наук, 1988, с. 1-41.

Геология Беларуси. Институт геологических наук НАН Беларуси. Минск, 2001, 815 с.

Левашкевич В.Г. Закономерности распределения геотермического поля окраин Восточно-Европейской Платформы (Баренцевоморский и Белорусско-Прибалтийский регионы). МГУ, Москва, 2005, 332 с.

Пархомов М.Д. Тепловой режим Припятского прогиба. Сейсмологические и геотермические исследования в Белоруссии. Наука и техника. Минск, 1985, с.124-130.

Суетнов В.В., Никульшина Е.А. Результаты изучения параметров нейтрального слоя в донных отложениях Южного Баренцева моря. Геотермальные исследования морского дна. Наука. Москва, 1988, с. 128-134.

Устрицкий В.И., Храмов А.Н. Геологическая история Арктики с позиций тектоники литосферных плит. В: Моря Советской Арктики. Недра. Ленинград, 1984, с. 253-265.

Хуторской М.Д. Геотермия Центрально-Азиатского складчатого пояса. РУДН. Москва, 1996, 285 с.

Bayer U., Scheck M., Rabbel W. et al. An intergrated study of the NE German Basin. Tectonophysics, Vol. 314, No. 1-3, 1999, pp. 285-307.

Clausen O.R. and Pedersen P.K. Late Triassic structural evolution of the southern margin of the Ringkobing Fyn High, Denmark. Mar. and Petrol. Geol., Vol. 16, No. 7, 1999, pp. 653-665.

Garetsky R.G., Pechernikov V.V., Aizberg R.E. and S. V. Klushin. Reflection of deep structure of the Pripyat Paleorift in thermobaric indexes of platform cover. Sov. Geol., No. 3, 1990, pp. 93-98.

by seismic reflection profiles from Northern Germany. Netherlands J. Geosci. (Geol. Mijnb.), Vol. 84, No. 4, 2005, pp. 389-401.

Parkhomov M.D. Thermal regime of the Pripyat trough seismic and geothermal research in Belorussia. Nauka i Tekhnika. Minsk, 1985, pp. 124-130 (in Russian).

Suetnov V.V. and Nikul'shina E.A. Results of studying the parameters of a neutral layer in bottom sediments of the Southern Barents Sea. Geothermal studies on Seafloor. Nauka. Moscow, 1988, pp. 128-134 (in Russian).

Thibo H., Janik T., Omelchenko V.D. et al. Upper lithospheric seismic velocity structure across the Pripyat Trough and the Ukrainian Shield along the EUROBRIDGE'97 Profile. Tectonophysics. Vol. 371, No. 1, 2003, pp. 41-79.

Tsybulya L.A., Levashkevich V.G. Heat flow in the Pripyat Trough and caused of its heterogeneity. Journal of Geology, No. 4, 1990, pp. 20-38.

Ustritsky V.I., Khramov A.N. Geological history of the arctic in terms of plate tectonics. In: Seas of the Soviet Arctic. Nedra. Leningrad, 1984, pp. 253-265 (in Russian).

van Wees J.D., Stephenson R.A., Ziegler P.A. et al. On the origin of the Southern Permian Basin, Central Europe. Mar. and Petrol Geol., Vol. 17, 2000, pp. 43-59.

Verba M.L., Sharov N.V. The State of the art and main problems of the deep structure of the Barents Sea Region. Apatity. Vol. 1. Geol. Inst., Kola Sci. Center, Russian Acad. Sci., 1988, pp. 1-41 (in Russian).

Verzhbitsky E.V. Geothermal regime, seafloor tectonics, and hydrocarbon generation temperatures in the eastern part of the Barents Sea. Geotectonics, Vol. 36, No. 1, 2002, pp. 76-85.

Volozh Yu.A., Antipov M.P., Khortov A.V., Yurov Yu.G. Structure and tectonic setting of the pre jurassic complexes of sedimentary cover in Caspian Sector of the Northern Peritethys. Proceed. of the Society of Exploration Geophysicists (SEG). Moscow, 1998.

Khutorskoi M.D., Podgornykh L.V., Gramberg I.S., Leonov Yu.G. Thermal tomography of the West Arctic Basin. Geotectonics, Vol. 37, No. 3, 2003, pp. 245-261.

Khutorskoi M.D., Teveleva E.A., Tsybulya L.A., Urban G.I. Heat flow in saltdome basins of Eurasia: A comparative study. Geotectonics, Vol. 44, No. 4, 2010, pp. 289-304.

Majorowicz J.A., Cermak V., Šafanda J. et al. Heat flow models across the Trans-European Suture Zone in the area of the POLONAISE-97 seismic experiment. Phys. Chem. Earth, Vol. 28, No. 9-11, 2003, pp. 375-391.

Mazur S., Scheck-Wenderoth M. Constraints on the tectonic evolution of the Central European Basin system revealed by seismic reflection profiles from Northern Germany. Netherlands J. Geosci. (Geol. Mijnb.), Vol. 84, No. 4, 2005, pp. 389-401.

Thibo H., Janik T., Omelchenko V.D. et al. Upper lithospheric seismic velocity structure across the Pripyat Trough and the Ukrainian Shield along the EUROBRIDGE'97 Profile. Tectonophysics. Vol. 371, No. 1, 2003, pp. 41-79.

Tsybulya L.A., Levashkevich V.G. Heat flow in the Pripyat Trough and caused of its heterogeneity. Journal of Geology, No. 4, 1990, pp. 20-38.

van Wees J.D., Stephenson R.A., Ziegler P.A. et al. On the origin of the Southern Permian Basin, Central Europe. Mar. and Petrol Geol., Vol. 17, 2000, pp. 43-59.

Verzhbitsky E.V. Geothermal regime, seafloor tectonics, and hydrocarbon generation temperatures in the eastern part of the Barents Sea. Geotectonics, Vol. 36, No. 1, 2002, pp. 76-85.

Volozh Yu.A., Antipov M.P., Khortov A.V., Yurov Yu.G. Structure and tectonic setting of the pre jurassic complexes of sedimentary cover in Caspian Sector of the Northern Peritethys. Proceed. of the Society of Exploration Geophysicists (SEG), Moscow, 1998.

ПРИМЕНЕНИЕ ТЕРМИЧЕСКОЙ ТОМОГРАФИИ ДЛЯ РАЗВЕДКИ В ОСАДОЧНЫХ БАССЕЙНАХ

Хуторской М.Д.

Геологический институт РАН, Россия

119017, Москва, Пыжевский переулок, 7: mdkh1@yandex.ru

Резюме. Разработана технология термической томографии, которую рекомендуется включить в комплекс поисково-разведочных работ на месторождениях углеводородов. Практическое значение термотомографической методики заключается в нахождении температурных границ, контролирующих тот или иной процесс генерации или трансформации вещества, расчете глубины гидротермальных изменений рудного вещества, глубины зон фаций метаморфизма, положения изотермы Кюри. Для прогнозирования нефтегазоносности оценивается глубина температурного интервала, в котором происходят катагенетические изменения органического вещества. Численный расчет глубинных температур производился на основе решения двухмерного уравнения теплопроводности с неограниченным числом контрастных комплексов и с учетом радиогенной теплогенерации в масштабах модельной области. На нижней границе области моделирования задавался тепловой поток при условии отсутствия радиогенной теплогенерации (редуцированный тепловой поток). Установлено, что локализация месторождений нефти и газа определяется повышением температуры в осадочном слое, которое связано с «термическими куполами». Рефракция теплового потока происходит на границах куполов с вмещающими породами из-за контраста теплопроводности эвапоритов и терригенных пород между купольными зонами. Это является основной причиной изменения теплового потока в латеральном и вертикальном направлениях в осадочных бассейнах. Тесная корреляция между зонами повышенных температур в осадочных породах и нефтегазопроявлениями подтверждается результатами 2D и 3D моделирования геотермического поля. Представлены результаты измерения теплового потока и трехмерные модели распределения температуры в Западной Арктике, в Прикаспийской, Припятской и Северо-Германской впадинах. Рассчитана глубина расположения температурных условий катагенеза органического вещества, что в первом приближении позволяет прогнозировать глубину нефтематеринского комплекса. Отмеченная ранее связь месторождений нефти и газа с глубинными разломами в изученных бассейнах создает предпосылки для рассмотрения теплового поля как генетического фактора, контролирующего тектонические особенности и нефтегазовые ресурсы осадочных и солянокупольных бассейнов.

Ключевые слова: *температура, тепловой поток, осадочный бассейн, соляной купол, моделирование*

ÇÖKMƏ HÖVZƏLƏRİN KƏŞFİYYATINDA TERMİK TOMOQRAFİYANIN TƏTBİQİ

Xutorskoy M.D.
REA-nın Geologiya institutu, Rusiya
119017, Moskva, Pıjevskiy döngəsi, 7: mdkh1@yandex.ru

Xülasə. Karbohidrogen yataqlarında axtarış-kəşfiyyat işləri kompleksinə daxil edilməsi tövsiyə olunan termiki tomoqrafiyanın texnologiyası işlənilmişdir. Termotomoqrafik metodikanın tətbiqi əhəmiyyəti, maddənin bu və ya digər generasiya və yaxud transformasiya prosesini nəzarətləndirən, temperatur sərhədlərinin tapılmasından ibarətdir. Neft-qazlılığın proqnozlaşdırılması üçün üzvi maddənin katagenenik dəyişməsinin baş verdiyi temperatur intervalının dərinliyi qiymətləndirilir. Həmin metodika vasitəsilə hidrotermal dəyişmənin, metamorfizmin fasiya zonalarının dərinliyi, Küri izotermlərinin mövqeyi hesablanır. Dərinlik temperaturlarının ədədi qiyməti kontrast komplekslərin məhdudsuz sayına malik, istilikkeçirmənin iki ölçülü tənliyinin həlli əsasında və model sahəsi miqyasında radiogen istilik generasiyası nəzərə alınmaqla yerinə yetirilirdi. Modelləşdirmə sahənin alt sərhədində radiogen istilik generasiyasının (reduksiya olunmuş istilik axını) olmadığı şəraitdə istilik axını verilirdi. Təyin edilmişdir ki, neft və qaz yataqlarının lokallaşması "termik gümbəz"lərlə əlaqədar olan çökmə qatda temperaturun yüksəlməsi ilə müəyyən edilir. İstilik axının refraksiyası, evaporitlərin istilikkeçiriciliyinin və terrigen süxurların gümbəz zonaları arasında kontrastlığı səbəbindən, gümbəzlərin yerləşdirici süxurlarla sərhədində baş verir. Bu, çökmə hövzələrdə lateral və şaquli istiqamətlərdə istilik axınının dəyişməsinin əsas səbəbidir. Çökmə süxurlarda yüksəlmiş temperatur zonaları və neft-qaz təzahürləri arasındakı sıx korrelyasiya geotermik sahənin 2D və 3D modelləşdirmə nəticələri ilə təsdiq olunur. Qərbi Arktikada, Xəzəryanı, Pripyat və Şimali Almaniya əyilmələrində istilik axınları ölçmələrinin nəticələri təqdim edilmişdir. Üzvi maddənin katagenetik temperatur şəraitinin yerləşmə dərinlikləri hesablanmışdır ki, o ilk yanaşmadan neft mənbəyi kompleksinin dərinliyini proqnozlaşdırmağa imkan verir. Öyrənilmiş hövzələrdə, əvvəl qeyd edilmiş neft və qaz yataqlarının dərinlik qırılmaları ilə əlaqəsi, çökmə və duz gümbəzli hövzələrin tektonik xüsusiyyətlərini və neft-qaz ehtiyatlarını nəzarətləndirən istilik sahəsini genetik amil kimi qəbul etməyə zəmin yaradır.

Açar sözlər: *temperatur, istilik axını, çökmə hövzə, duz gümbəzi, modelləşdirmə*

ANAS Transactions Earth Sciences 2 / 2023

http://www.journalesgia.com

SEISMIC ANALYSIS OF THE SHAMKIR RESERVOIR AREA THROUGH INSIGHTS INTO THE DYNAMICS OF THE EARTHQUAKE CHARACTERISTICS

Babayev T.H., Aliyev Y.N., Muradi I.B., Aliyev M.M.

Ministry of Science and Education of the Republic of Azerbaijan,
Institute of Geology and Geophysics, Azerbaijan
119, H.Javid Ave., Baku, AZ1143

Keywords: *the Shamkir water reservoir, the Middle Kur depression, b-value, Gutenberg-Richter law, intensity, ground motion, seismotectonic model*

Summary. This paper is dedicated to analyze the Shamkir reservoir area applying different tools using earthquake catalogs as a source to build up a long-term seismicity rate. The study area surrounds the western part of the Middle Kur depression and the north-eastern part of the Lesser Caucasus. The area covering 4300 km^2, is squeezed under seismic impact of mountainous zones such as the Greater Caucasus slope from the north and the northeastern part of the Lesser Caucasus from the south. The analysis was done estimating b-value, describing the relative distribution size of earthquake. Two catalogs of earthquakes were used to proceed the research: until 2015 with historical period (№1) and instrumental period between 1966-2018 (№2). b-value was estimated for each catalog defining M_c – magnitude of completeness, M_{max} – maximum magnitude and bins – magnitude steps on the Gutenberg-Richter linear relationship. For the catalogs №1 and №2, b-value was found 0.64 and 0.52, respectively. Furthermore, this study investigates the intensity distribution on the characteristic of earthquake faults computed by means of empirical relationship between maximum magnitude the source (faults) can generate and the length of the source (faults). The intensity that could be used to describe earthquake shaking in the northern part of the site of interest was observed as VII (MSK-64) and in the southern part as VIII.

© 2023 Earth Science Division, Azerbaijan National Academy of Sciences. All rights reserved.

Introduction

The study area is the Shamkir water reservoir region (Fig. 1) situated between the southern slope of the Greater Caucasus and the northern part of the Lesser Caucasus within the Eurasian plate and focusing on the area with location from (45.83 E, 41.14 N) to (46.61 E, 40.85 N) as a northern boundary and from (45.53 E, 40.67 N) to (46.30 E, 40.38 N) as the southern boundary and with the area of 4298.8 km^2 ~ 4300 km^2 (Babayev, Babayev, 2023). The core part of the structure is directed to the east in the form of a linear anticline, separates the Agjakend and Kepaz synclines and is interrupted by a transverse fault slide in the Tartar River bed (Alizadeh et al., 2016; Fig. 2).

The boundaries and the area of study zone is defined using ArcGIS 10.7 (ESRI, 2018) software. The purpose in this paper is to conduct the research of the seismicity applying empirical tools from the values in the appropriate earthquake catalogues, compute and estimate intensity shaking based on the faulting characteristics. We analyzed the seismicity regarding the assessment of the b-value of Gutenberg-Richter law and distribution of intensity through the study area generated by empirical ways.

Tectonics of the area

In the tectonic aspect, the region is categorized in two parts: the northern part of the site is a plain region being a part of the Middle Kur depression with the Pleistocene and Holocene sediments; the southern semi-zone of the site is a mountainous region containing mostly Middle Jurassic sediments. The northern region is included to Jeyranchol zone within Middle Kur mega-zone. The Middle Kur separates the southern slope of the Greater Caucasus and the northern part of the Lesser Caucasus (Bochud, 2011). The southern region of the research area is in the Lok-Karabakh zone within the Lesser Caucasus mountain-fold zone which is relatively seismically active (Alizadeh et al., 2016). In terms of stress orientation, the area is characterized by a dominant NNE-SSW-oriented compressional stress field which controls the overall occurrence of earthquakes and that most seismic events are represented by reverse faulting or strike-slip faulting (Tibaldi et.al., 2020; Babayev et.al., 2020a).

The Jeyranchol zone is located in the west of the Middle Kur depression (Alizadeh et al., 2016). It is bordered by the Lesser Caucasus zone in the south

along the Kur uplift. Three anticlines occur in the structure of the zone, the arch parts of them are disturbed by fault-overlaps (Alizadeh et al., 2016). It is divided into three belts: the Mammadtepe-Koyrukkeylan northern belt, the Ortagash-Quyrugenchi central belt and the Kur southern belt (Alizadeh et al., 2016). The Mammadtepe-Koyrukkeylan belt consists of Oglutepe, Mammadtepe, Saloglu, Garatepe, Gurzundag, Koyrukkeylan, South and North Jeyranchol and Tersdeller anticlines (Alizadeh et al., 2016). The Ortagash-Quyrugenchi belt covers Buyukkesik, Gushguna, western, central and eastern Ortagash, Quyrugenchi, Bayramli and Yenikend anticlines. The Kur belt contains Garayazi, Soyugbulag, Poylu, Zayam and Khuluf anticlines (Alizadeh et al., 2016).

The southern area of the research including the Lok-Karabakh zone is called Shamkir semi-zone which is the oldest and most complex structural element of the Lok-Karabakh zone that has passed the long tectonic development stage (Alizadeh et al., 2016). It consists of the Shamkir and Goygol uplifts in the west and east respectively. The Shamkir uplift is a huge heterogeneous and folded-block structure and is bounded by the Tovuzchay and Ganjachay transversal faults from the west and east respectively (Alizadeh et al., 2016). In its internal structure, the Central Shamkir and Lazılar-Arigdam uplifted blocks, which are secondary structures of the subregion and pan-Caucasus direction, and the Badakand and Gadabey downlifts, which border them from the north and south, respectively, are distinguished. The Goygol uplift is a south-westerly displacement continuation of the Shamkir uplift along the Ganjachay fault-slip. The core part of the structure is directed to the east in the form of a linear anticline, separates the Agjakend and Kepaz synclines and is interrupted by a transverse fault slide in the Tartar River bed (Alizadeh et al., 2016; Fig. 2). The geology of the study area changes from Mesozoic to Cenozoic according to the geological basemap we used in this research (Fig. 1). The southern zone mainly consists of Middle part of the Middle Jurassic (J_2^2). We also observe few amounts of rocks of the Lower Jurassic (J_1), intrusive rocks of the Middle and Upper Jurassic and Lower Cretaceous, and the rocks of the Upper part of the Middle Jurassic (Callovian) and Upper Jurassic (J_2^3-J_3), The Upper part of the Lower Cretaceous – Lower Paleocene (K_1^2-P_1^1) and very little section of the Pleistocene (Q_1^2-Q3) rocks laying from older to younger (Babayev, Babayev, 2023). According to Alizade et.al. (2016), these Jurassic sediments mainly contain volcanic, slightly less volcanic-sedimentary and sedimentary rocks. Alizade et.al. (2016) also proposes that in some places of Jurassic granites, granodiorites, diorites intrusions are spread. The northern zone consists of Pleistocene (Q_1^2-Q^3) rocks being more contemporary. Little sections of the Upper part of the Middle Jurassic (Callovian) and Upper Jurassic (J_2^3-J_3), the Upper part of the Lower Cretaceous – Lower Paleocene (K_1^2-P_1^1), Paleocene and Lower Eocene (P_1^2-P_2^1), Oligocene and Lower Miocene (P_3-N_1^1) are also spread over in this zone (Fig.1). Shamkir water reservoir is laid on the Holocene (Q_4) deposits. In this part of the area sediments are the “Agcagil” (N_2^2a) and continental layers and “Agcagil” (N_2^2a) sediments lie transgressively and under an angular unconformity on older rocks (Гадиров, 2012). The bottom of these sediments is represented by basal conglomerates. They do not appear on the surface. They consist of clays interspersed with sand and sandstone beds.

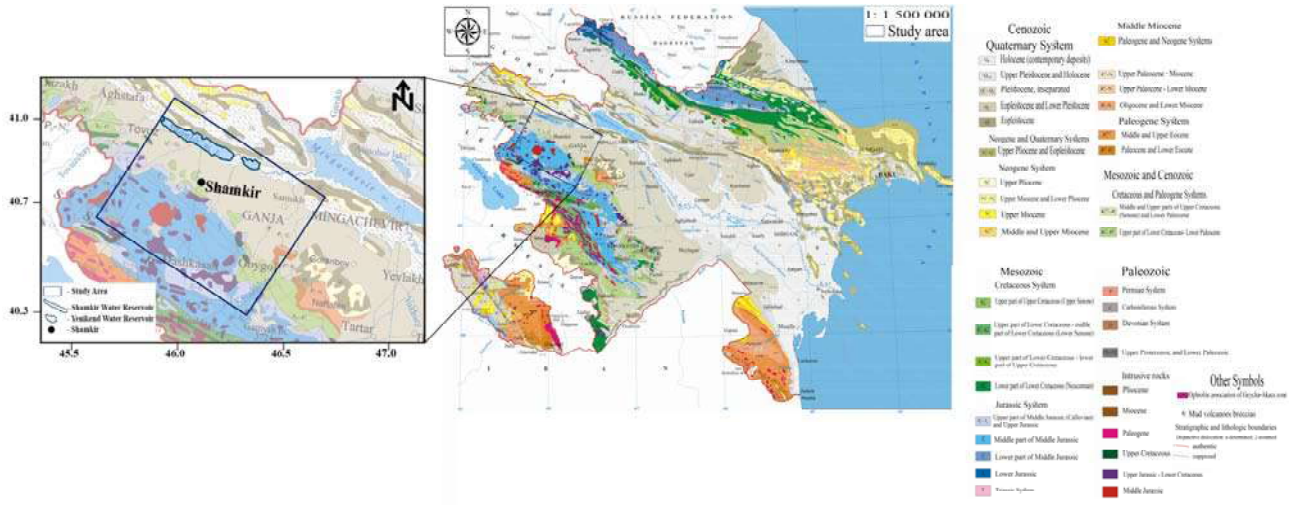


Fig. 1. The study area on geological map of Azerbaijan

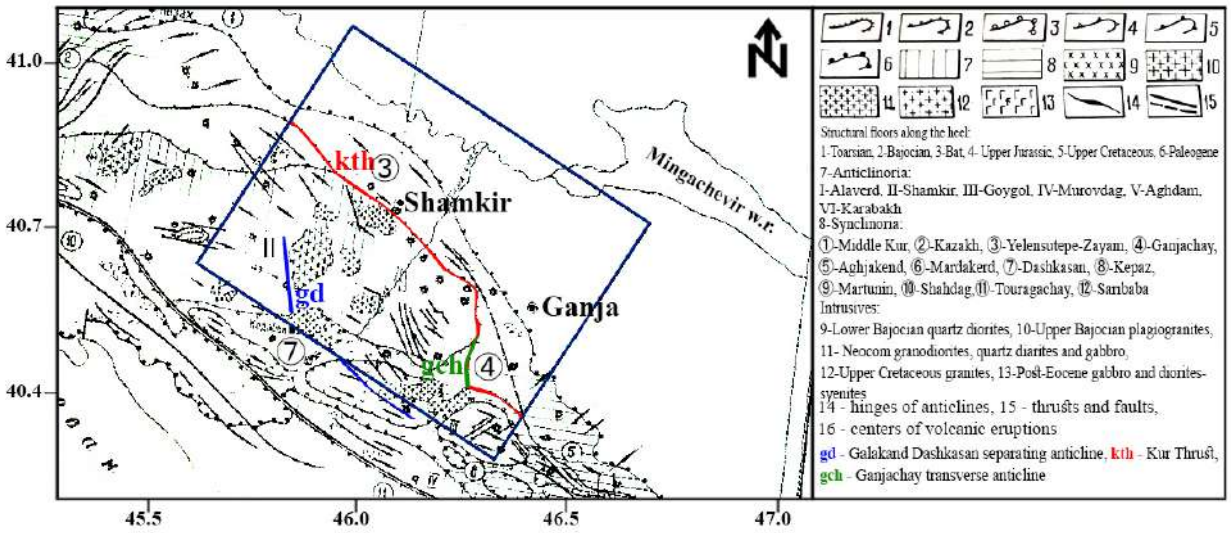


Fig. 2. Tectonics of the research area (Babayev, Babayev, 2023; Aliyev, 1961)

Methodology

Data selection criteria. To analyze the seismicity of the study area we have addressed two catalogs of seismicity (Table 1). The first is the earthquake catalog of Azerbaijan which involves the events registered between the years 427 and 2016. The next catalog is the earthquake catalog of Mingachevir region which is a region with high seismicity adjacent to the study area. It involves 1074 events registered between 1894 and 2018 years. We have filtered both catalogs with the criteria of compatibility to the study area. The procedure to filter the catalogs starts with use of ArcGIS 10.7 (ESRI, 2018) software. The events of the catalogs were illustrated on the map (Fig.7) according to their spatial distribution inside and outside the study area.

Thus, we worked with 1343 events in the first and 101 events in the second catalog. Tables 2 and 3 show selection from the catalogs.

As introduced in Table 1, we will name the catalog "EQ Catalogue_Azerbaijan 427-2016" as №1 and catalog "erqs Catalogue_Mingachevir 1894-2018" as №2.

Table 1

Used catalogs for the study area

Numeration of catalogs	Name of Catalogs	Number of events after filtration	Time range after filtration
№1	EQ Catalogue_Azerbaijan 427-2016	1343	427-2015
№2	erqs Catalogue_Mingachevir 1894-2018	101	1966-2018

Table 2

A fragment from "EQ Catalogue_Azerbaijan 427-2016"

Year	Day	Lat	Lon	H (km)	Mlh	K
427		40.5	46.5	12	6.7	15.7
1235		40.6	46.2	10	5.72	14.3
1826	25	40.7	46.2	15	4.3	11.7
1867	23	40.6	46.3	15	5.8	14.4
1900	18	40.6	46.4	12	4.4	11.9
1902	24	40.5	46.0	15	4.2	11.6
1903	18	40.7	46.4	12	4.6	12.1
1908	14	41.1	46.1	36	4.0	11.2
1910	18	40.7	46.3	18	4.5	12.1
1910	10	40.8	46.0	9	4.2	11.6
1929	11	40.4	46.2	15	3.9	11.0

Year	Day	Lat	Lon	H (km)	Mlh	K
1929	9	40.4	46.3	8	3.2	0
1931	8	40.7	46.3	20	4.3	11.7
1931	12	40.6	46.3	10	3.6	0
1939	4	40.8	46.7	22	3.6	0
1949	17	41.1	46.1	17	4.0	11.2
1962	12	41.0	45.9	5	4.2	11.6
1964	26	40.4	46.2	0	1.7	7.0
1964	1	40.6	45.9	0	2.2	8.0
1964	3	40.7	46.1	0	2.22	8.0
1964	8	40.9	46.0	0	2.5	8.5
1964	15	40.9	45.9	0	3.33	10.0
1964	27	40.8	46.1	0	2.78	9.0
1964	16	40.8	46.0	0	2.78	9.0

Mlh – magnitude of the earthquake; K – energy class of the earthquake

Table 3

A fragment from "erqs Catalogue_Mingachevir 1894-2018"

Year	mon	day	hours	second	Lat	Lon	H	Ml
1966	3	6	12	48	40.9	46.5	0	2.4
1976	8	10	10	21	40.8	46.6	0	2.4
1977	8	25	15	12	40.9	46.5	0	1.9
1978	7	16	21	48	40.9	46.6	0	1.9
1979	5	17	15	6	40.9	46.5	0	2.7
1980	11	21	15	31	40.9	46.4	0	1.3
1981	5	20	12	50	41.0	46.3	0	3.0
1981	10	6	14	58	40.9	46.5	0	2.4
1983	8	13	2	11	40.9	46.6	0	3.5
1985	5	24	6	8	40.8	46.6	10	2.0
1985	12	30	17	17	40.9	46.6	0	2.3
1986	2	6	0	20	40.87	46.4	0	1.9
1989	9	19	14	32	41.0	46.34	21	2.7
1990	4	13	3	57	40.91	46.55	32	2.7
1991	8	18	5	50	40.93	46.39	21	2.6
1992	6	2	18	54	41.0	46.25	0	2.5
1992	8	27	22	8	40.93	46.43	10	1.1
1994	9	20	6	34	40.9	46.5	0	2.5
2000	9	13	23	26	40.9	46.5	0	1.8
2001	2	28	23	3	40.9	46.35	0	2.6
2002	12	5	10	40	40.94	46.28	31	2.8
2003	2	5	1	0	40.85	46.51	14	2.3
2004	3	15	20	3	40.97	46.33	0	2.3
2005	1	29	11	40	40.98	46.39	23	2.2
2007	1	5	16	50	40.85	46.58	36	2.6

It is seen from the tables that depth for some events is set at 0. This case is mostly related to the low value of magnitude. It can be observed that for M=1.0 depth could be H=0.5-0.8 km, for M=3.0, H=1 km and for M=3.5, H=2 km (Цхакая, 1962; Varazanashvili, 1999). It concludes that those quakes occurred near- and sub-surface. Fig.3 illustrates the spatial distribution of magnitudes of earthquakes from the catalogs №1 (3a) and №2 (3b).

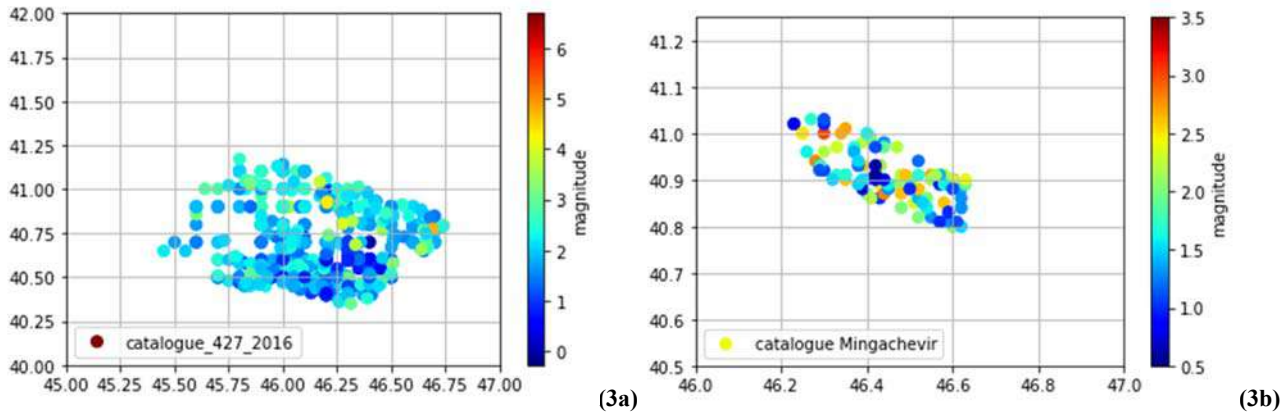


Fig. 3. Spatial distribution of magnitudes of earthquakes. (3a) catalog Nº1, (3b) catalog Nº2

Gutenberg-Richter Law. Richter (1935) proved that earthquakes are not uniformly distributed in time, space and magnitude. Earthquakes are distributed with respect to invariable scale of magnitudes being self-similar and obeying a power law or fractal scaling (Kulhanek, 2005). The distribution of earthquakes with respect to the magnitude is assessed by Gutenberg and Richter (1942) relation (GR law, briefly) – also known as Ishimoto and Iida (1939) – with the following empirical formula:

$$log\ N = a - bM \ \text{ or } \ N = \ 10^{a-bM}, \qquad (1)$$

where N is the number of earthquakes greater than and equal to M, the magnitude of the earthquakes, a and b are the real constants.

b-value estimation. "b" is the slope of the GR law equation. It is a parameter describing the relative size distribution of earthquakes. b-value is estimated by the following main techniques (El-Isa, Eaton, 2014):

- Linear least-square fit
- Maximum-likelihood estimation (Utsu, 1965):

$$b = log\ log\ \frac{e}{M_{av}-M_{min}} = \frac{0.43}{M_{av}-M_{min}}, \qquad (2)$$

where M_{av} is the mean of the observed magnitudes and M_{min} is the minimum magnitude – threshold magnitude in the events catalog. The relation above is defined for continuous distribution (Kulhanek, 2005).

In theory we expect similar results from these techniques, but empirically these methods do not necessarily yield the same b-values for the same seismicity data (El-Isa, Easton, 2014). For instance, El-Isa (2013) reports average differences in b-value about 0.1-0.2 between two methods based on analysis of global catalogs. Felzer (2007) points out: "In general, the least-square regression method may be disproportionately influenced by the largest earthquake magnitudes, whereas the maximum-likelihood method weights each earthquake equally". Some researchers such as Milojevic (2010), have mentioned that the least-square fitting to logarithmically binned data could be more preferable than the maximum likelihood method due to its instructivity (El-Isa, Eaton, 2014). In this research we decided to apply linear least-square fitting during estimation of b-value. The very first step in applying Gutenberg-Richter law (Gutenberg and Richter, 1942) for a catalog is to plot cumulative number of earthquakes in logarithmic scale respect to the magnitudes with N ≥ M where N – cumulative number of earthquakes and M – magnitudes (Fig. 4) to illustrate relation between the frequency of earthquakes and their magnitude. In the plot we apply linear regression method in order to find the slope of linearity and the intersection with the y-axis which are b- and a-values respectively due to the formula (1).

To apply the linear regression method, we have to correctly define M_c – magnitude of completeness, M_{max} – maximum magnitude till which the linear fit goes on (Godano et al., 2014; Godano et al., 2021), magnitude bin – simply the step for the magnitudes. For the catalog Nº1, M_c=3, M_{max}=4.8, bins=0.1 M_c, M_{max}, bins were defined as 3.0, 4.8, 0.1 respectively and for Nº2 as 1.0, 2.6, 0.1 respectively.

Intensity analysis. The analysis of earthquakes intensity based on the faulting characteristics, using empirical relationship between magnitude generation, allows determining the state of intensity; therefore, in this study we used equations (3) and (4) (Шебалин, 1961; Kuliyev, 1980), which allow determining the best-fit regional intensity scattering. Equation (3) generates the expected maximum magnitude due to the fault length (Fig. 5). Equation (4) generates the intensity for the area due to the expected maximum magnitude and depth of quake.

$$M = 2 * log\ (\mathrm{L}) + 2, \qquad (3)$$

$$I_0 = 1.5 * M - 3.3 * log\ (\mathrm{H}) + 2.7, \qquad (4)$$

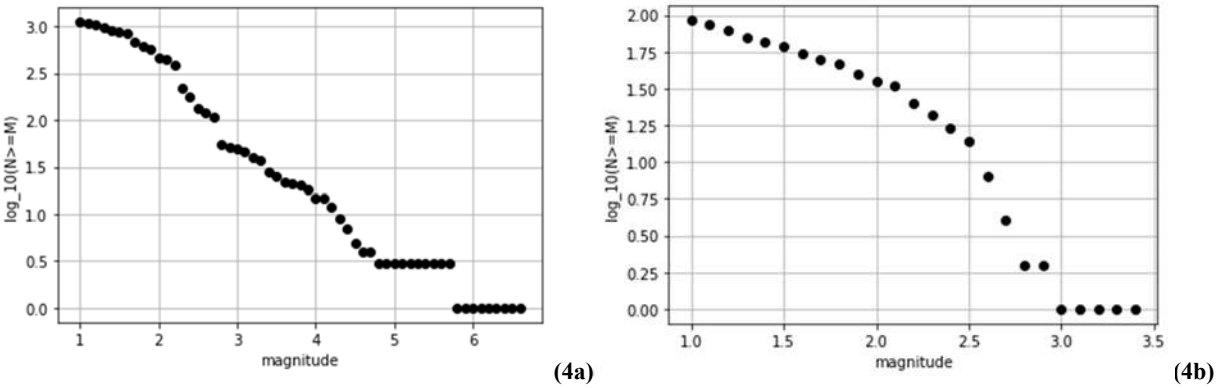


Fig. 4. Cumulative number of earthquakes in logarithmic scale against the magnitudes with N ≥ M with N – cumulative number of earthquakes and M – magnitudes (Gutenberg and Richter, 1942). (4a) Nº1, (4b) Nº2

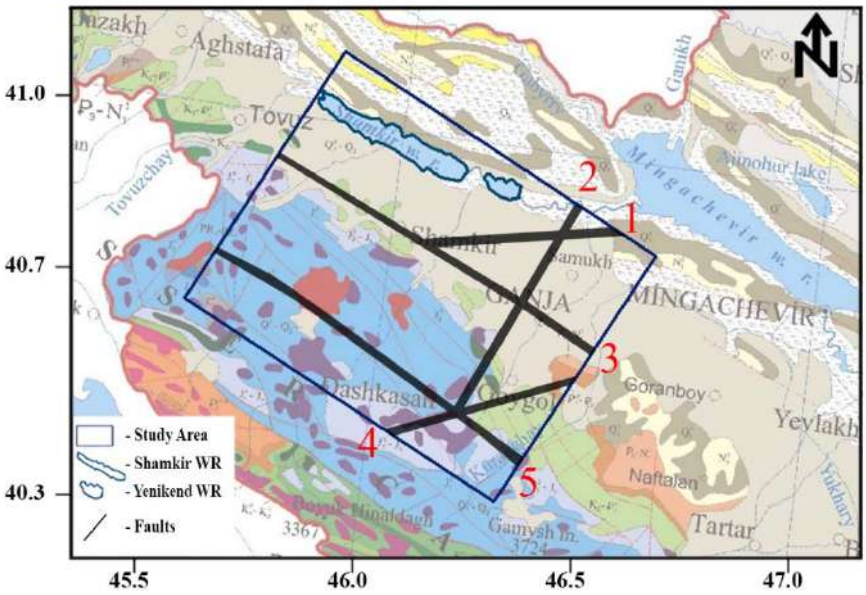


Fig. 5. Fault map of the study area
Note: Digits on the map refers to the enumeration of the faults, see Table 6

where M is maximum magnitude expected, L is the fault length and H is the depth of the earthquake with magnitude M.

Intensity shaking at the site of study in this research is determined from magnitude-fault relationship. This relationship is usually derived empirically from the motion database of past earthquakes. These relationships are simple functions of earthquake magnitude and source-site length with some additional source parameters-constants.

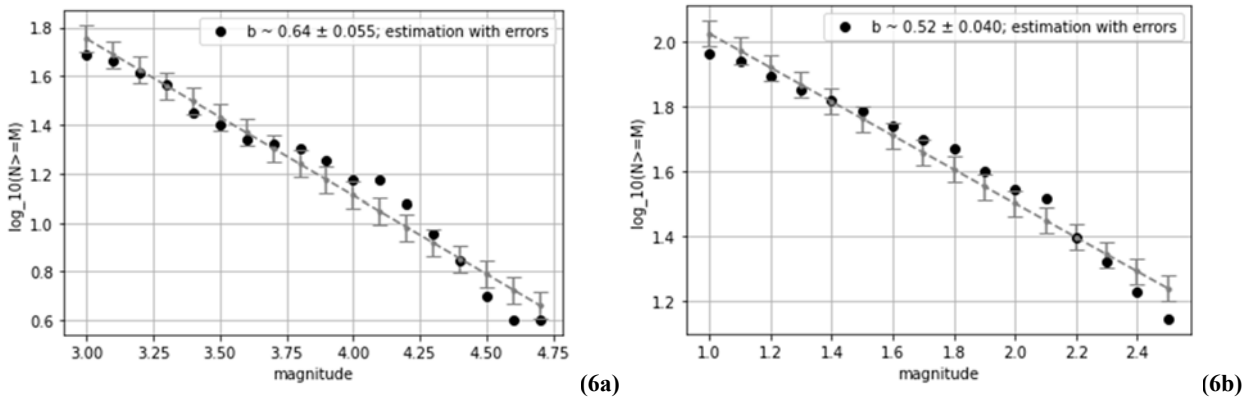
Results and Discussion

b-value estimation results. B- and a-values were obtained for each catalog applying linear least-square fitting (El-Isa, Eaton, 2014). B-value was at 0.64 and 0.52 and a-value was at 3.68 and 2.55 for the catalogs Nº1 and Nº2, respectively. The results of b-value are shown in Fig. 6 for both catalogs.

Seismicity analysis. Babayev et.al. (2020b) has shown that lower value of *b* represents higher activity of seismicity. Our results of b-value are more or less close to the b-values of the Shamakhi-Ismayilli and Zagatala regions presented by the mentioned study in which these zones were assessed relatively higher seismically active in the total area of the study due to the lower value of *b* (Babayev et al. 2020b; Babayev, Aliyev, 2019). Fig. 7 illustrates the spatial distribution of the earthquakes in both catalogs through the study area.

We observe relatively active seismicity in the northern and south-eastern parts of the study area. In the northern part, the activity is observed in the Shamkir and Yenikend water reservoirs which could be supposed that it is related to the seismicity of the Mingachevir water reservoir which is adjacent to the Shamkir and Yenikend water reservoirs by the Kur river (Telesca et.al., 2013), which are separately pre-

sented in Fig. 8b. Therefore, considering catalog Nº2 as a supporting argument (Fig. 8a), we could mention the triggering impact of the Mingachevir water reservoir (Telesca et.al., 2017) to the study area (Fig. 8b). Table 4 and 5 represent the extraction of earthquakes illustrated in Fig. 8b catalogs Nº1 and Nº2 respectively.



(6a) (6b)

Fig. 6. b-values for catalogs. (6a) Nº1, (6b) Nº2

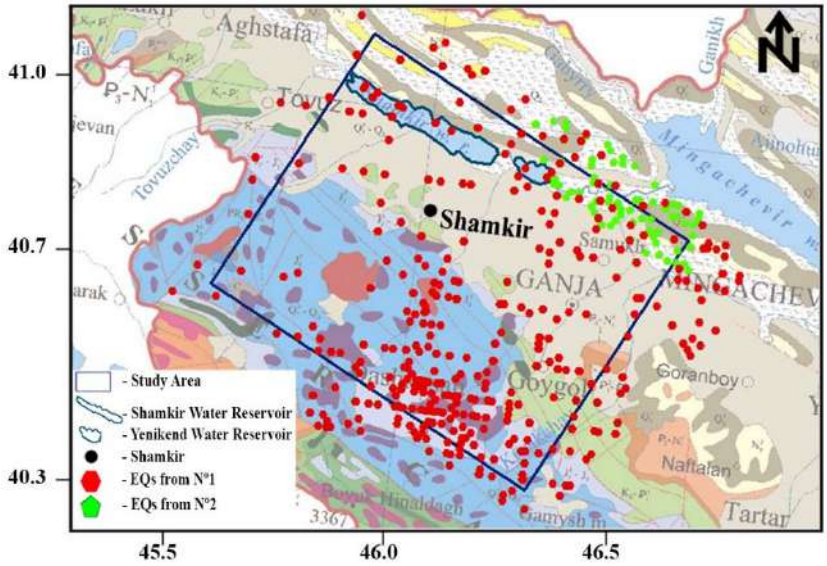
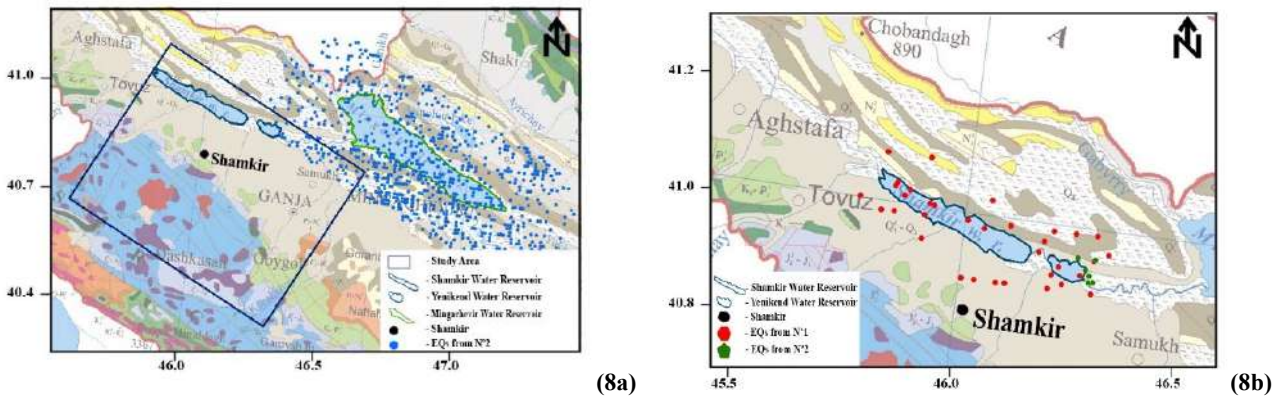


Fig. 7. Spatial distribution of the earthquakes through the study area. Dark blue frame borders the study area. Red hexagons represent earthquakes from catalog Nº1, green pentagons represent earthquakes from catalog Nº2



(8a) (8b)

Fig. 8. Earthquakes from catalogs occurred in the territory of the Shamkir and Yenikend water reservoirs or adjacent to them. (8a) All the events of Mingachevir catalog (Nº2) are distributed on the map

It is seen that the events are around the study frame that is considered as the impact of the Mingachevir water reservoir activity to the Shamkir water reservoir. Blue circles represent the earthquakes, (8b) red hexagons represent earthquakes from catalog Nº1, green pentagons represent earthquakes from catalog Nº2 that are in the study frame.

Table 4

Events from catalog Nº1 occurred in the territory of the Shamkir and Yenikend water reservoirs

Year	Lat	Lon	H (km)	Mlh	K
1962	41.0	45.9	5	4.20	11.6
1964	40.9	46.0	0	2.50	8.5
1964	40.9	46.0	0	2.50	8.5
1964	40.9	46.0	0	2.22	8.0
1964	41.0	46.1	0	1.67	7.0
1964	40.9	46.2	0	2.22	8.0
1965	41.0	45.8	0	2.78	9.0
1965	41.0	45.8	0	3.33	10
1966	41.0	46.1	0	2.78	9.0
1966	41.0	45.9	0	2.78	9.0
1968	41.0	45.8	0	2.78	9.0
1968	40.9	46.0	10	2.78	9.0
1968	41.1	45.9	0	2.78	9.0
1969	41.0	46.2	0	2.78	9.0
1971	40.9	46.2	0	2.78	9.0
1973	40.9	46.1	0	1.94	7.5
1973	40.9	46.2	0	2.50	8.5
1974	41.1	45.9	0	2.78	9.0
1974	41.1	45.9	0	2.78	9.0
1974	41.1	45.8	0	1.67	7.0
1976	40.9	46.0	0	1.67	7.0
1977	41.0	46.2	0	2.22	8.0
1977	41.1	45.9	0	3.33	10.0
1978	40.96	45.9	0	2.78	9.0
1979	41.1	45.8	25	3.33	10.0
1979	41.1	45.9	0	2.22	8.0
1979	41.1	45.8	0	1.67	7.0
1979	41.0	46.1	0	2.22	8.0
1980	40.9	46.3	0	2.78	9.0
1980	40.9	46.3	0	3.89	11.0
1980	40.9	46.3	0	1.67	7.0
1981	40.9	46.0	0	2.78	9.0
1981	41.0	46.3	0	2.78	9.0
1981	41.0	46.0	0	1.67	7.0
1981	41.0	46.2	20	2.78	9.0
1982	41.1	45.8	0	2.44	8.4
1982	41.0	46.0	0	2.22	8.0
1983	41.0	45.9	0	2.06	7.7
1983	41.0	45.9	0	2.00	7.6
1984	40.9	46.3	0	1.67	7.0
1984	41.0	45.8	0	1.67	7.0
1984	41.0	45.9	0	1.67	7.0
1985	40.9	46.0	0	2.33	8.2
1985	41.0	46.2	0	1.89	7.4
1985	40.9	46.2	0	2.78	9.0
1985	41.0	46.0	25	1.67	7.0
1985	41.1	45.9	0	2.56	8.6

Year	Lat	Lon	H (km)	Mlh	K
1985	40.9	46.1	0	2.33	8.2
1986	40.9	46.03	31	3.50	10.3
1986	41.1	45.8	0	1.67	7.0
1987	41.0	45.83	20	2.33	8.2
1987	40.91	46.23	30	2.50	8.5
1988	41.0	45.8	0	2.44	8.4
1988	40.9	46.0	0	1.89	7.4
1989	41.0	46.2	0	0.89	5.6
1989	41.1	45.8	0	2.06	7.7
1990	40.9	46.2	3	1.50	6.7
1990	41.0	46.0	0	1.89	7.4
1991	41.04	45.86	13	2.50	8.5
1991	40.9	46.08	1	1.44	6.6
1991	41.05	45.83	15	2.56	8.6
1991	40.94	46.22	0	1.78	7.2
1991	40.9	46.1	0	1.72	7.1
1992	41.0	45.8	0	2.22	8.0
1992	41.0	46.25	0	2.33	8.2
1993	40.99	46.04	22	2.39	8.3
1994	41.0	46.1	0	2.61	8.7
2000	40.9	46.1	0	2.22	8.0
2000	41.0	46.0	0	2.22	8.0
2000	40.93	46.27	22	3.06	9.5
2002	40.9	46.0	0	2.56	8.6
2002	40.96	46.17	11.7	2.11	7.8
2002	40.94	46.28	31	2.61	8.7
2004	41.04	46.05	24	2.06	2.8
2004	40.97	46.33	0	2.11	0
2007	40.98	46.18	0	1.56	0
2008	41.0	45.8	0	1.56	0
2013	41.02	45.91	13.63	2.35	0
2013	41.04	45.83	14.05	2.77	0
2014	40.96	46.3	11.1	2.15	0
2015	40.93	46.2	10.16	4.31	0
2015	41.02	45.92	10.0	2.58	0
2015	41.03	45.85	12	3.17	0
2015	41.02	45.75	14	2.11	0

Table 5

Events from catalog Nº2 occurred on the areas of the Shamkir and Yenikend water reservoirs

Year	Mon	Day	Hours	Second	Lat	Lon	H (km)	Ml
2002	12	5	10	40	40.94	46.28	31	2.80
2013	10	18	13	39	40.96	46.26	23	1.60
2014	12	16	18	18	40.96	46.30	11	2.20
2015	1	14	19	30	40.93	46.29	20	0.50
2015	3	5	0	44	40.92	46.30	13	1.10
2015	7	3	5	20	40.93	46.29	17	1.80
2018	8	3	21	26	40.92	46.29	11	1.13

As the b-value is a parameter describing seismicity analysis (Babayev et al., 2020b), we decided to estimate b-value in the three subdivisions of the study frame in order to verify our uncertainty about the variety of seismicity in the area. We divided the research zone into 3 parts roughly: the northern (Part I) – the part where the Shamkir and Yenikend water reservoirs are of main focus and the impact of Mingachevir zone is considered; the middle part (Part II) – where impact of the seismically active Ganja zone is

captured; and the southern part (Part III) – where seismicity of the Lesser Caucasus is examined (Fig. 9). During gridding the parts, the earthquakes were clustered respectively. As we clearly see that the events of Mingachevir catalog (Nº2) occur inside the Part I, we decided to merge those Mingachevir (Nº2) events to the events of Nº1 occurring in the same Part I. Thus, all the red and green quakes in Part I are clustered as the same group (Fig. 9).

After gridding of the area and clustering of the earthquakes, we re-estimated b-value. However, we changed M_c, M_{max}, bins for each part, necessarily, in order to get the best linear fitting. M_c, M_{max}, bins for the northern part are at 1.5, 4.5, 0.3, for the middle part – at 1.0, 5.0, 0.5 and for the southern part – at 3.0, 7.0, 1.0, respectively. b-values are at 0.72 for the northern, 0.59 for the middle and 0.32 for the southern parts accordingly. Fig. 10 illustrates the distribution map of b-values. Considering the result of Babayev et al. (2020b) which was a comparative analysis of seismicity with correlation of b-value, PGA (Peak Ground Acceleration) and Intensity (MSK-64), we adopt that seismicity relation between three divisions could be averaged and defined as follows: Part I < Part II < Part III.

Intensity analysis. Another goal of our study was to identify and to predict the intensity range of ground shaking that may occur from an earthquake at a particular magnitude along a fault. Consequently, an intensity (MSK-64) map for the study area was plotted (Fig. 11) applying equation (3) and (4). The faults capable of causing an event throughout the study area were listed in Table 6. Fig. 11 illustrates that intensity for the study area is estimated VII – VIII (MSK-64). Obviously, the area coinciding to the Lesser Caucasus zone has higher seismicity setting at VIII. However, intensity of VII that observed in the area of the Middle Kur depression also remarks a significant seismicity. This zone is under seismic impact of the seismically active territories such as Mingachevir from north-east, Ganja from south-east and Lesser Caucasus from the southern part.

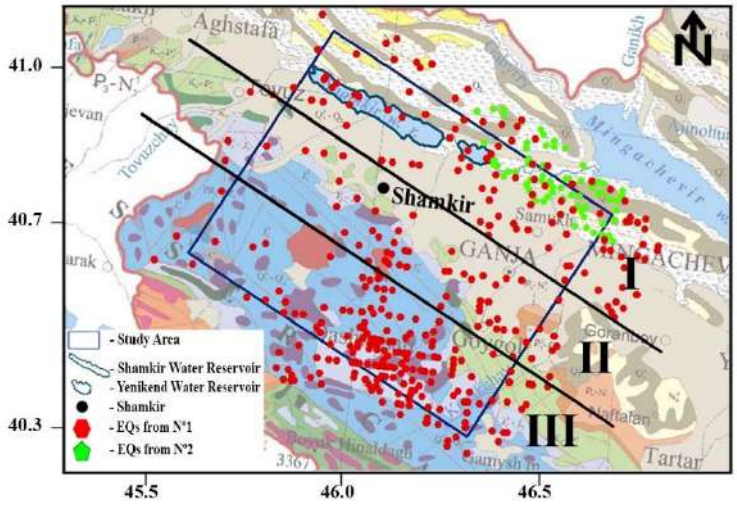


Fig. 9. The study area segmented into three parts in order to compute b-value spatial distribution

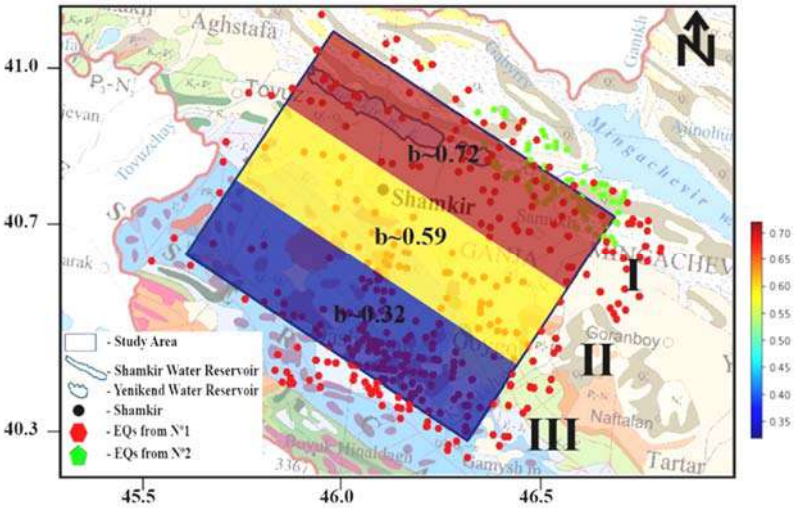


Fig. 10. Spatial distribution of b-value along the study area

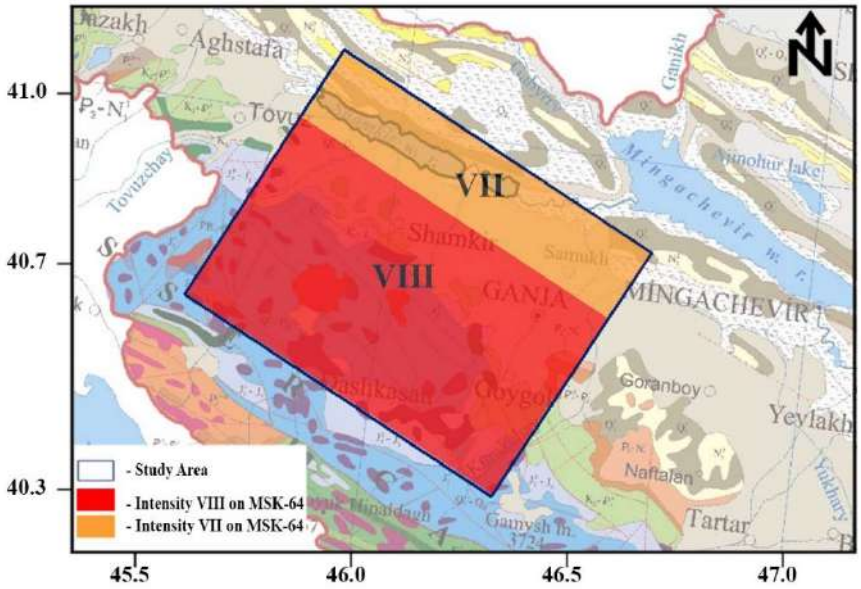


Fig. 11. Intensity (MSK-64) distribution map based on fault length along the study area

Table 6

Faults used to estimate intensity along the study area

N	L (km)	M	H (km)	I_0
1	39	5.2	10	7
2	48.8	5.4	10	7
3	73.7	5.7	10	8
4	36.4	5.1	10	7
5	74	5.7	10	8

Note: *Respective numeration of the faults (N) can be traced on the Fig. 5*

Conclusion

This study was dedicated to the seismicity analysis of the Shamkir water reservoir areas and adjacent territories using different tools. During the study, Gutenberg-Richter Law – b-value analysis and intensity estimation with faults of the region were applied. In terms of intensity analysis, the study zone was assessed of intensity VII-VIII (MSK-64) from north to south and in terms of b-value distribution, the study area is divided into three parts with b-values 0.72 for part I, 0.59 for part II and 0.32 for part III demonstrating seismically active character with the following regularity: part I < part II < part III. The intensity results indicate that, for engineering purposes this methodology can provide realistic ground-motion information in advance of an earthquake, including a model of what will actually happen.

Acknowledgments

The authors are thankful to the Republican Center of Seismic Survey at Azerbaijan National Academy of Sciences (ANAS) for providing earthquake catalogue. The study was performed at International Laboratory at Institute of Geology and Geophysics of the Ministry of Science and Education of the Republic of Azerbaijan and Institute of Methodologies for Environmental Analysis National Research Council (Italy) "Earthquake space-time analysis and hazard laboratory (ESTAHL)".

REFERENCES

Aliyev O.B. Stratigraphy and fauna of the cretaceous sediments of the north-eastern part of the Lesser Caucasus (between Qoshqarchay and Terterchay). AzSSR AN publishing house. Baku, 1961, 26 p. (in Russian).

Alizadeh A.A., Guliyev I.S., Kadirov F.A., Eppelbaum, L.V. Geosciences of Azerbaijan. Volume I: Geology, Cham: Springer. 2016, p. 340, https://doi.org/10.1007/978-3-319-27395-2.239.

Babayev G., Aliyev M. Seismic b-value study in southern slope of Greater Caucasus (Azerbaijan). Proceedings of the 2nd International Electronic Conference on Geosciences, 8-15 June 2019, MDPI: Basel, Switzerland, DOI: 10.3390/ IECG2019-06227.

Babayev G., Telesca L., Agayeva S., Ismail-zade T., Muradi I., Aliyev Y., Aliyev M. Seismic hazard analysis for southern

ЛИТЕРАТУРА

Alizadeh A.A., Guliyev I.S., Kadirov F.A., Eppelbaum L.V. Geosciences of Azerbaijan. Volume I: Geology, Cham: Springer. 2016, p. 340, https://doi.org/10.1007/978-3-319-27395-2.239.

Babayev G., Aliyev M. Seismic b-value study in southern slope of Greater Caucasus (Azerbaijan). Proceedings of the 2nd International Electronic Conference on Geosciences, 8-15 June 2019, MDPI: Basel, Switzerland, DOI: 10.3390/ IECG2019-06227.

Babayev G., Telesca L., Agayeva S., Ismail-zade T., Muradi I., Aliyev Y., Aliyev M. Seismic hazard analysis for southern slope of the Greater Caucasus (Azerbaijan). Pure and Applied Geophysics, Vol. 177 (8), 2020b, pp. 3747-3760, https://doi.org/10.1007/s00024-020-02478-0.

slope of the Greater Caucasus (Azerbaijan). Pure and Applied Geophysics, Vol. 177 (8), 2020b, pp. 3747-3760, https://doi.org/10.1007/s00024-020-02478-0.

Babayev G., Yetirmishli G., Kazimova S., Kadirov F., Telesca L. Stress field pattern in the northeastern part of Azerbaijan. Pure Appl. Geophys., Vol. 177(3), 2020a, pp. 2739-2751, Springer Nature Switzerland AS, https://doi.org/10.1007/s00024-019-02371-5.

Babayev T., Babayev G. Tectonic, geological, geomorphological and seismic analysis of Shamkir region and surroundings based on bibliographical review. Proceedings of Azerbaijan High Technical Educational Institutions (PAHTEI), Vol. 33(04), No. 10, 2023, pp. 73-81, DOI: 10.36962/PAHTEI33102023-73 (in Azerbaijani).

Bochud M. Tectonics of the Eastern Greater Caucasus in Azerbaijan. Thesis for: Phd n° 1733, Hauterive (Fribourg), Switzerland, 2011, 207 p.

El-Isa Z., Eaton D.W. Spatiotemporal variations in the b-value of earthquake magnitude–frequency distributions: Classification and causes. Tectonophysics, Vol. 615-616, 2014, pp. 1-11, http://dx.doi.org/10.1016/j.tecto.2013.12.001.

El-Isa Z.H. Continuous-cyclic variations in the b-value of the earthquake frequency-magnitude distribution. Earthquake Science, Vol. 26, 2013, pp. 301-320, https://doi.org/10.1007/s11589-013-0037-9.

ESRI. ArcGIS Desktop: Release 10.8. Environmental Systems Research Institute. Redlands: ESRI, 2018.

Felzer K. Calculating the Gutenberg-Richter b-value. USGS publication. 2007.

Godano C., Convertito V., Pino N.A. The signal to noise ratio and the completeness magnitude: the effect of the COVID-19 lockdown. Atmosphere, Vol. 12(5), 2021, 525, https://doi.org/10.3390/atmos12050525.

Godano C., Lippiello E., Arcangelis de L. Variability of the b value in the Gutenberg–Richter distribution, Geophysical Journal International, Vol. 199, No. 3, December 2014, pp. 1765-1771, https://doi.org/10.1093/gji/ggu359.

Gutenberg B., Richter C.F. Earthquake magnitude, intensity, energy and acceleration. Bulletin of the Seismological Society of America, Vol. 32, 1942, pp. 163-191.

Ishimoto M., Iida K. Observations sur les seismes enregistres parle microsismographe construit dernierement (1). Bulletin of the Earthquake Research Institute, Vol. 17, 1939, pp. 443-478.

Kadirov V.K. Gravity exploration in the study of geological structure and oil and gas content of Middle Kura depression of Azerbaijan. Journal of Geophysics (Geofizicheskiy jurnal), T. 34, No. 1, 2012, pp. 183-189 (in Russian).

Kulhanek O. Seminar on b-value. Prague Centre of Mathematical Geophysics, Meteorology and their Applications (MAGMA). Seminar paper, Department of Geophysics, Charles University. Prague, Czech, 2005.

Kuliev F.T. Macroseismic field equation of Azerbaijan. Seismological Bulletin of the Caucasus for 1977. Metsniereba.Tbilisi, 1980, pp.129-140 (in Russian).

Milojevic S. Power law distributions in information science: making the case for logarithmic binning. Journal of the American Society for Information Science and Technology, Vol. 61, 2010 No. 12, pp. 2417-2425, 10.1002/asi.21426.

Richter C.F. An instrumental earthquake magnitude scale. Bulletin of the Seismological Society of America, Vol. 25, No. 1, 1935, pp. 1-32.

Shebalin N.V. The intensity, magnitude and depth of the earthquake source. Earthquakes in the USSR, Nauka. Moscow, 1961, pp. 126-138 (in Russian).

Telesca L., Kadirov F., Yetirmishli G., Safarov F., Babayev G., Ismayilova S. Statistical analysis of the 2003-2016 seismicity of Azerbaijan and surrounding areas. Journal of Seismol-

Babayev G., Yetirmishli G., Kazimova S., Kadirov F., Telesca L. Stress field pattern in the northeastern part of Azerbaijan. Pure Appl. Geophys., Vol. 177(3), 2020a, pp. 2739-2751, Springer Nature Switzerland AS, https://doi.org/10.1007/s00024-019-02371-5.

Bochud M. Tectonics of the Eastern Greater Caucasus in Azerbaijan. Thesis for: Phd n° 1733, Hauterive (Fribourg), Switzerland, 2011, 207 p.

El-Isa Z., Eaton D.W. Spatiotemporal variations in the b-value of earthquake magnitude–frequency distributions: Classification and causes. Tectonophysics, Vol. 615-616, 2014, pp. 1-11, http://dx.doi.org/10.1016/j.tecto.2013.12.001.

El-Isa Z.H. Continuous-cyclic variations in the b-value of the earthquake frequency-magnitude distribution. Earthquake Science, Vol. 26, 2013, pp. 301-320, https://doi.org/10.1007/s11589-013-0037-9.

ESRI. ArcGIS Desktop: Release 10.8. Environmental Systems Research Institute. Redlands: ESRI, 2018.

Felzer K. Calculating the Gutenberg-Richter b-value. USGS publication. 2007.

Godano C., Convertito V., Pino N.A. The signal to noise ratio and the completeness magnitude: the effect of the COVID-19 lockdown. Atmosphere, Vol. 12(5), 2021, 525, https://doi.org/10.3390/atmos12050525.

Godano C., Lippiello E., Arcangelis de L. Variability of the b value in the Gutenberg–Richter distribution, Geophysical Journal International, Vol. 199, No. 3, December 2014, pp. 1765-1771, https://doi.org/10.1093/gji/ggu359.

Gutenberg B., Richter C.F. Earthquake magnitude, intensity, energy and acceleration. Bulletin of the Seismological Society of America, Vol. 32, 1942, pp. 163-191.

Ishimoto M., Iida K. Observations sur les seismes enregistres parle microsismographe construit dernierement (1). Bulletin of the Earthquake Research Institute, Vol. 17, 1939, pp. 443-478.

Kulhanek O. Seminar on b-value. Prague Centre of Mathematical Geophysics, Meteorology and their Applications (MAGMA). Seminar paper, Department of Geophysics, Charles University. Prague, Czech, 2005.

Milojevic S. Power law distributions in information science: making the case for logarithmic binning. Journal of the American Society for Information Science and Technology, Vol. 61, 2010, No. 12, pp. 2417-2425, 10.1002/asi.21426.

Richter C.F. An instrumental earthquake magnitude scale. Bulletin of the Seismological Society of America, Vol. 25, No. 1, 1935, pp. 1-32.

Telesca L., Kadirov F., Yetirmishli G., Safarov F., Babayev G., Ismayilova S. Statistical analysis of the 2003-2016 seismicity of Azerbaijan and surrounding areas. Journal of Seismology, Vol. 21, No. 6, 2017, pp. 1467-1485, https://doi.org/10.1007/s10950-017-9677-x.

Telesca L., Lovallo M., Babayev G., Kadirov F. Spectral and informational analysis of seismicity: An application to the 1996-2012 seismicity of Northern Caucasus–Azerbaijan part of Greater Caucasus–Kopet Dag Region. Physica A Statistical Mechanics and Its Applications, Vol. 392, No. 23, 2013, pp. 6064-6078, https://doi.org/10.1016/j.physa.2013.07.031.

Tibaldi A., Tsereteli N., Varazanashvili O., Babayev G., Barth,A., Mumladze T., Bonali F.L., Russo E., Kadirov F., Yetirmishli G., Kazimova S. Active stress field and fault kinematics of the Greater Caucasus. Journal of Asian Earth Sciences, Vol. 188, 2020, 104108, https://doi.org/10.1016/j.jseaes.2019.104108.

Utsu T. A method for determining the value of b in a formula log n = a – bM showing the magnitude–frequency relation for earthquakes. Geophys. Bull. Hokkaido Univ., Vol. 13, 1965, pp. 99-103.

ogy, Vol. 21, No. 6, 2017, pp. 1467-1485, https://doi.org/10.1007/s10950-017-9677-x.

Telesca L., Lovallo M., Babayev G., Kadirov F. Spectral and informational analysis of seismicity: An application to the 1996-2012 seismicity of Northern Caucasus–Azerbaijan part of Greater Caucasus–Kopet Dag Region. Physica A Statistical Mechanics and Its Applications, Vol. 392, No. 23, 2013, pp. 6064-6078, https://doi.org/10.1016/j.physa.2013.07.031.

Tibaldi A., Tsereteli N., Varazanashvili O., Babayev G., Barth,A., Mumladze T., Bonali F.L., Russo E., Kadirov F., Yetirmishli G., Kazimova S. Active stress field and fault kinematics of the Greater Caucasus. Journal of Asian Earth Sciences, Vol. 188, 2020, 104108, https://doi.org/10.1016/ j.jseaes.2019.104108.

Tskhakaya A.D. On depths of Caucasian earthquakes. Izv. Akad. Nauk SSSR, Ser. Geofiz., No. 5, 1962, pp. 577-584 (in Russian).

Utsu T. A method for determining the value of b in a formula log n = a – bM showing the magnitude–frequency relation for earthquakes. Geophys. Bull. Hokkaido Univ., Vol. 13, 1965, pp. 99-103.

Varazanashvili O.Sh. Seismic hazard assessment of Georgia by deterministic and probabilistic methods. Journal of Georgian Geophysical Society, Issue (A), Solid Earth, Vol. 4, 1999, pp. 35-45.

Varazanashvili O.Sh. Seismic hazard assessment of Georgia by deterministic and probabilistic methods. Journal of Georgian Geophysical Society, Issue (A), Solid Earth, Vol. 4, 1999, pp. 35-45.

Алиев О.Б. Стратиграфия и фауна меловых отложений северо-восточной части. Малого Кавказа. Автореф. диссерт. Изд-во АН АзССР. Баку, 1961, 26 с.

Гадиров В.Г. Гравиразведка при изучении геологического строения и нефтегазоносности площадей Среднекуринской впадины Азербайджана. Геофизический журнал, Т. 34, No. 1, 2012, с.183-189.

Кулиев Ф.Т. Уравнение макросейсмического поля Азербайджана. Сейсмологический бюллетень Кавказа за 1977 г. Мецниереба. Тбилиси, 1980, с. 129-140.

Цхакая А.Д. О глубинах кавказских землетрясений. Изв. Акад. Наук СССР, сер. Геофиз., No. 5, 1962, с. 577-584.

Шебалин Н.В. Балльность, магнитуда и глубина очага землетрясений. В кн.: Землетрясения в СССР. Наука. Москва, 1961, с. 126-138.

Babayev T., Babayev Q. Biblioqrafik icmal əsasında Şəmkir rayonu və ətrafının tektonik, geoloji, geomorfoloji və seysmik təhlili. Azərbaycan ali texniki məktəblərinin xəbərləri, cild 33 (04), No. 10, 2023, s. 73-81.

СЕЙСМИЧЕСКИЙ АНАЛИЗ ТЕРРИТОРИИ ШАМКИРСКОГО ВОДОХРАНИЛИЩА ПО ДАННЫМ ДИНАМИЧЕСКИХ ХАРАКТЕРИСТИК ЗЕМЛЕТРЯСЕНИЙ

Бабаев Т.Х., Алиев Я.Н., Муради И.Б., Алиев М.М.

Министерство науки и образования Азербайджанской Республики, Институт геологии и геофизики
AZ1143, Баку, просп. Г.Джавида, 119

Резюме. Данная статья посвящена анализу территории Шамкирского водохранилища с применением различных методов, используя каталоги землетрясений в качестве источника для долгосрочного анализа сейсмичности. Территория исследования охватывает западную часть Среднекуринской впадины и северо-восточную часть Малого Кавказа. Территория, занимающая 4300 км^2, находится под сейсмическим воздействием горных зон, таких как склон Большого Кавказа с севера и северо-восточная часть Малого Кавказа с юга. Анализ был проведен путем оценки значения b, характеризующий относительную величину распределения землетрясения. Для проведения исследований использовались два каталога землетрясений: с историческим периодом до 2015 года (№1) и инструментальным периодом с 1966 по 2018 годы (№2). Значение b было оценено путем определения M_c-уровня представительной магнитуды, M_{max} – максимальной магнитуды и пошаговой магнитуды по линейной зависимости Гутенберга-Рихтера. Для каталогов №1 и №2 было оценено значение b, равное 0.64 и 0.52 соответственно. Кроме того, в данной работе исследуется распределение интенсивности по активным разломам, генерирующим землетрясения, вычисленное с помощью эмпирической зависимости между максимальной магнитудой, которую может генерировать источник (разломы), и длиной источника (разломов). Интенсивность сотрясений в северной части территории доходит до отметки VII (MSK-64), а в южной части – до VIII баллов.

Ключевые слова: *Шамкирское водохранилище, Среднекуринская впадина, значение b, закон Гутенберга-Рихтера, интенсивность, движение грунта, сейсмотектоническая модель*

ZƏLZƏLƏLƏRİN DİNAMİK XÜSUSİYYƏTLƏRİNİN MƏLUMATLARINA ƏSASƏN ŞƏMKİR SU ANBARININ ƏRAZİSİNİN SEYSMİK TƏHLİLİ

Babayev T.H., Aliyev Y.N., Muradi I.B., Aliyev M.M.

Azərbaycan Respublikası Elm və Təhsil Nazirliyi, Geologiya və Geofizika Institutu
AZ1143, Bakı, G.Cavid prospekti, 119

Xülasə. Bu məqalə Şəmkir su anbarının ərazisinin uzunmüddətli seysmiklik səviyyəsinin təyin olunması üçün mənbə kimi zəlzələ kataloqlarından istifadə etməklə müxtəlif üsulların tətbiqi ilə təhlilinə həsr edilmişdir. Tədqiqat sahəsi Orta Kür çökəkliyinin qərb hissəsini və Kiçik Qafqazın şimal-şərq hissəsini əhatə edir. 4300 km^2 sahəni əhatə edən ərazi şimaldan Böyük Qafqaz yamacı və cənubdan Kiçik Qafqazın şimal-şərq hissəsi kimi dağlıq zonaların seysmik təsiri altında sıxılır. Təhlil zəlzələnin nisbi paylanma ölçüsünü təsvir edən b-qiymətinin hesablanması aparılmışdır. Tədqiqatın aparılması üçün iki zəlzələ kataloqundan istifadə edilmişdir: 2015-ci ilədək olan tarixi dövr (Nº1) və 1966-2018-ci illər arasında (Nº2) olan instrumental dövr. b-qiyməti hər bir kataloq üçün Qutenberq-Rixter xətti əlaqəsi üzrə Mc – maqnituda həddinin yekunlanma parametri, Mmax – maksimal maqnituda və interval – maqnituda intervallarını təyin edərək qiymətləndirilmişdir. Nº1 və Nº2 kataloqları üçün b-qiyməti müvafiq olaraq 0.64 və 0.52 hesablanıldı. Bundan əlavə, bu tədqiqat maksimal maqnituda və mənbənin (qırılmalar) uzunluğu arasındakı empirik əlaqə vasitəsilə hesablanmış, zəlzələləri əmələ gətirən qırılmaların xüsusiyyətlərinə əsasən intensivlik paylanmalarını araşdırır. Tədqiqat sahəsinin şimal hissəsində zəlzələnin intensivliyi VII (MSK-64), cənub hissəsində isə VIII ballıq müşahidə edilmişdir.

Açar sözlər: *Şəmkir su anbarı, Orta Kür çökəkliyi, b-qiyməti, Qutenberq-Rixter qanunu, intensivlik, yer hərəkəti, seysmotektonik model*

ANAS Transactions Earth Sciences 2 / 2023

http://www.journalesgia.com

OPTIMIZATION OF RESERVOIR WATERFLOODING WITH UNSTABLE DISPLACEMENT FRONT

Shakhverdiev A.Kh.[1], Shestopalov Y.V.[2], Mandrik I.E.[3], Arefyev S.V.[4]

[1]Russian State Geological Prospecting University, Russia
23, Miklukho-Maklay str., Moscow, 117997
[2]Academy of Technology and Environment, University of Gävle,
Gävle, SE-801 76 Sweden
[3]PJSC LUKOIL Russia
11, Sretensky Boulevard, Moscow, 101000
[4] LUKOIL-Western Siberia LLC, Russia

Keywords: *waterflooding, instability of displacement front, optimization, fingering, catastrophe theory, phase plane*

Summary. Non-stationary flooding of oil-saturated reservoirs has a long-standing and durable place as the main secondary method of oil production and maintenance of reservoir pressure in the development of most oil reservoirs. The water injection into the reservoir creates a delayed problem – the inevitable, often catastrophic flooding of oil production wells, provoked by a sudden and irreversible change in water saturation. The theory of two-phase flow filtration created by Buckley and Leverett does not take into account the loss of stability of the displacement front, which provokes an abrupt change and a triplicity of the water saturation value. Therefore, a mathematically simplified approach was proposed at one time, a repeatedly differentiable approximation to exclude a "jump" in water saturation. Such a simplified solution led to well-known negative consequences of the waterflooding practice, which experts call the "viscous instability of the displacement front", the "fingering displacement front". This work has presented a novel approach to formulation decisive rules for the first time allowing timely detection and prevention of the consequences of loss of stability of the displacement front and targeted control of the flooding system by stopping, forcing, limiting operating modes, assigning workover solutions of producing and injection wells. It is possible to quickly solve important short-term practical tasks passing traditional labor-intensive incorrect deterministic tasks and complex methods of solution mobilizing the injected water and controlling the fluid production rate, more precisely water and oil on the basis of the discriminant criterion.

© 2023 Earth Science Division, Azerbaijan National Academy of Sciences. All rights reserved.

1. Introduction

Conceptual foundations of the new paradigm. Several theoretical and applied problems remain outstanding in the field of scientific research on reservoir management with the dominance of a deterministic approach to research in recent years. Water flooding improvement under instability of the displacement front is most complex and important problems, and therefore, it has won the recognition of specialists as the main secondary method of oil recovery and enhanced oil recovery technology. Water flooding has become widespread primarily because of the manufacturability, availability, and inexpensiveness of water for injection into formations. However, this method does not provide the high-design planned indicators of the oil field development process.

The quality and quantity of studies related to the reservoir water flooding problems has increased significantly after the widespread use of geological and hydrodynamic mathematical modeling and its truncated modification including proxy models, sector and other simplified versions of model solutions but the shortcomings and imperfections inherent in the traditional approach remain.

The multidimensional geological and hydrodynamic models of multiphase flow solve the main long- and medium-term problems of oil and gas-saturated reservoir management including water flooding as a secondary method of increasing oil recovery. At the same time, important short-term operational flooding tasks cannot be solved using models, the main purpose of which is to calculate

options for rational reservoir development for the purposes of drafting project documentation.

There is also an unsolved scientific and methodological problem of the Buckley-Leverett theory, which is used to mathematical formulation the flooding process in all existing hydrodynamic simulation software, the presence of a "jump" in water saturation and the triplicity of its value when oil is displaced by water are not taken into account. Ignoring this fact significantly reduces the efficiency of the water flooding, results in disruption of the optimal reservoir pressure maintenance, premature flooding of production wells is provoked, stagnant and poorly drained oil saturated zones are formed (Brouwer, Jansen, 2002; Sharma et al., 2020).

There are more than enough reasons for concern about the negative consequences due to the jump and triplicity of the water saturation value obtained in the Buckley-Leverett theory, some authors in their critical assessments regard the results as "absurd", and the lack of an exhaustive solution to the problem is an "intellectual dead end" (Buckley, Leverett, 1942; Rodygin, 2012). Anyway, at this stage, it is not possible to achieve a full-fledged unification of the waterflooding technology, since the two-phase flow theory based on the Buckley-Leverett theory does not enable the influence of the displacement front instability and, most importantly, timely preventing its negative consequences, which provoke an abrupt change in water saturation, which is fraught with catastrophic water breakthroughs to production wells (Duan et al., 2015).

The further fate of this «jump» in water saturation caused serious collisions among specialists. As a means of overcoming problems, it was proposed to calculate phase permeability based on water saturation with mathematically smooth approximations. However, it turned out that the simplified mathematical approximation does not correspond to an adequate physical mechanism of stability loss by the displacement front formed under rough conditions of interaction of hydrodynamic, capillary, molecular, inertial and gravitational forces.

Recently, there have been numerous laboratory and field studies, numerical experiments aimed at solving theoretical and practical problems of optimizing the process of non-stationary waterflooding, in which the above problem is confirmed (Baryshnikov et al., 2017; Brouwer, Jansen, 2002; Dake, 2001; Klebanov et al., 1982; Nigmatulin et al., 2014; Шахвердиев, Шестопалов, 2019; Shakhverdiev et al., 2019, 2021; Шахвердиев, Арефьев, 2021).

In an experimental study (Rodygin, 2012) of the dynamics of water content in bulk oil-saturated samples using the method of filtration waves of pressure (FWP) in relation to the basic provisions of the Buckley-Leverett theory, the author concludes that "an increase in the amplitude of pressure waves leads to an increase in the water content rate of the sample", that is, an increase in water saturation.

A number of authors try to solve the problem of the "jump" and the triplicity of water saturation using the fractal geometry of the structure of the oil displacement front (Baryshnikov et al., 2017; Ding et al., 2020; Duan et al., 2015). An attempt is made to explain the mechanism of oil displacement according to the principle of harmony of the flow structure (Baryshnikov et al., 2017). Based on the Hele-Shaw model in the experimental work (Baryshnikov et al., 2017), the development of instability of the displacement front of a viscous fluid from a porous medium in the form of jets when displaced by a fluid having a lower viscosity was studied. A change in the proportion of the volume of the pore space involved in jets of the displacing fluid was shown under oil displacement. The phenomenon of an abrupt change in the proportion of the total volume of the displacing jet in the volume of the pore space of the array at the leading edge of the displacement front was discovered and described at the viscosity ratios of liquids much smaller than one (Baryshnikov et al., 2017).

The authors of the study (Udy et al., 2017) note under implementation of the reservoir waterflooding that the gained experience shows that traditional and generally accepted approaches to waterflooding do not work here.

Nevertheless, the experience of applying new modifications of waterflooding technologies, which are usually used as the main method of reservoir pressure maintenance, as well as a method of enhanced and improved oil recovery in the development of oil and gas fields with scientifically based application, contains hidden potential.

Craig F.F. states according to the Buckley-Leverett equations, the conclusion follows that the velocity should have been the same for two different saturations, i.e. such saturation should be at a given point in the reservoir at the same time. To show even greater absurdity of this assumption, it should be noted that if the initial saturation gradient arose ahead of the displacement front prior to water injection, then we will obtain three different saturation values in the reservoir area according to the calculated data. Buckley and Leverett realized the physical impossibility of such a situation. They noted that the real saturation curve undergoes a discontinuity. Due to the three-valued saturation distribution, some researchers hesitated to apply the frontal displacement equation (Craig, 1971).

Dake L.P. expressed the problem as follows: "According to literary sources, such a triple value of

saturation has been a certain intellectual problem for reservoir engineers for many years. Buckley and Leverett themselves claim that the triple value could have been avoided if they had been able to take capillary effects into account in their theory. Others suggested that this could be avoided by using a special method for solving differential equations known as the method of characteristic functions" (Dake, 2001).

Isaak Charnyi believed that "…starting from a certain point in time, the saturation distribution may turn out to be multi-valued, for example, similar to Riemann waves of finite amplitude, which are studied in the theory of shock waves. Obviously, the ambiguity of S_B (water saturation) is physically impossible" (Чарный, 1963).

Robert Nigmatulin actually confirms the same thesis and recommends looking for a solution in the field of the Riemannian compression wave in gas: "The function F_w' is nonmonotonic. During the evolution of the initial distribution of water saturation, when $\frac{d^2F}{dx^2} < 0$ occurs everywhere, the solution is obtained transferring along the characteristics (in a kinematic wave) of the initial distribution of water saturation. If there are zones where $\frac{d^2F}{dx^2} > 0$, then there is a "tipping" of the wave, similar to the tipping of the Riemann compression wave in gas, when large disturbances propagate at a higher velocity compared to weaker ones, which leads to the ambiguity of water saturation. The absurdity of such solutions led to the need to introduce surface or discontinuity (jump) of wave parameters (Klebanov et al., 1982; Nigmatulin et al., 2014).

Finally, there were attempts to find a numerical solution to the problem in hydrodynamic simulation of two-phase flow filtration in a porous medium. Aziz H., Settari E. came to the conclusion that: "Although both types of approximation (conductivity), as will be shown below, are second-order approximations, they lead to erroneous results. This is illustrated for the numerical solution of the Buckley-Leverett problem. With insignificant P_c (capillary pressure) in the *SS*-method equation, we obtain an almost hyperbolic problem with the correct solution, very close to the Buckley-Leverett solution. However, when grinding the mesh, the numerical results obtained by the "weighing" scheme differ from the real ones" (Aziz, Settari, 1986).

Similar opinions were expressed by many well-known scientists and specialists, and recommended looking for a solution to this complex problem in another field of mathematics (Шахвердиев, Шестопалов, 2019; Шахвердиев, 2004, 2017; Shakhverdiev et al., 2019, 2021; Шахвердиев, Арефьев, 2021; Wang et al., 2017).

It should be borne in mind that the engineering concepts that simplify and distort both the physical mechanism and the mathematical approximation of the water flooding parameters under conditions of instability of the displacement front lead to well-known theoretical solutions that differ greatly from the applied results. The well-known negative consequences of the waterflooding practice referred to experts as "viscous instability of the displacement front", "finger-shaped displacement front", "premature water breakthrough", "fractal geometry of the displacement front" indicate a low quality of flooding due to misunderstanding of the consequences of a simplified representation of the mechanism of the displacement process and ignoring adequate mathematical apparatus. Predicting and preventing the consequences of these catastrophic phenomena – surges in water saturation has become a very difficult task (Arnold et al., 2005; Skauge et al., 2009; Thompson, 1982). Therefore, it is extremely important to substantiate the physical mechanism of the formation and advancement of the displacement front and the early forecast of the growth or advancing rate of the water phase in the stream at certain sites and stages of the waterflooding (Мандрик и др., 2010; Мирзаджанзаде, Шахвердиев, 1997; Шахвердиев, Арефьев, 2021).

2. Problem statement

Let's consider the traditional joint isothermal flow of a two-phase liquid in a homogeneous porous medium as an argument in the absence of phase transitions by a system of differential continuity equations for each of the phases:

$$\left.\begin{aligned} \frac{\partial Q_w(x,t)}{\partial x} &= -m\frac{\partial \sigma_w}{\partial t} \\ \frac{\partial Q_o(x,t)}{\partial x} &= -m\frac{\partial \sigma_o}{\partial t} \end{aligned}\right\} \quad (1)$$

where Q_o, Q_w – are respectively accumulated oil and water extraction, σ_o, σ_w – are saturation of the medium with oil and water, m – is porosity.

In this case, from the ratio for the saturation $\sigma_o = 1 - \sigma_w$ we get

$$\left.\begin{aligned} \frac{\partial Q_w(x,t)}{\partial x} &= -m\frac{\partial \sigma_w}{\partial t} \\ \frac{\partial Q_o(x,t)}{\partial x} &= m\frac{\partial (1-\sigma_w)}{\partial t} \end{aligned}\right\} \quad (2)$$

Adding up the equations of system (2), we get:

$$\frac{\partial [Q_w(x,t)+Q_o(x,t)]}{\partial x} = 0$$

or

$$Q_w(x,t)+Q_o(x,t) \to Q_f(t). \quad (3)$$

The obtained result (3) shows that the volumetric flow rate $Q_f(t)$ does not depend on the spatial coordinate x, but depends only on time t. This does not mean that each individual phase also does not depend on the spatial coordinate. As a dynamic system, the dependence on time and on the spatial coordinate of the volume flow rate of each of the phases – oil and water – is of interest. Thus, the solution of system (2) does not allow estimating the dynamic behavior of each phase in the structure of a two-phase flow depending on the spatial coordinate x and the time t.

Having performed the known transformations of system (1) and solving the corresponding characteristic equation, we obtain (Abbasi et al., 2018; Чарный, 2006; Craig, 1971; Dake, 2001; Duan et al., 2015; Rose, Rose, 2004):

$$X_w = X_w(\sigma_w, 0) + \frac{V_w t}{m} f'(\sigma_w), \qquad (4)$$

where $X_w(\sigma_w, 0)$ is the initial distribution of water saturation at $t = 0$, m is porosity, V_w is the filtration rate of the aqueous phase, $f'(\sigma_w)$ is the derivative of the Buckley-Leverett function.

Fig. 1 shows the distribution of water saturation along the direction of the displacement front advance for different time points, obtained using the dependence (4). As can be seen from Fig. 1, there is a polysemy (triplicity) of the water saturation values at a certain point in time. Thus, attempts to obtain an acceptable result of solving the classical system of continuity equations and the filtration equation fail.

Fig. 1 shows the initial saturation field $s_0(x, 0)$ at $t = 0$ and the resulting $t > 0$ subsequent saturation field s_1; s_2; s_3. This is the simplest transformation of energy, consisting of merging and disappearance of the minimum and maximum under the action of a saturation jump forming one of the elementary catastrophes presented in Fig. 1, where the area is indicated in yellow and represents the zone of instability of the displacement front. According to the catastrophe theory, the resulting surface of the "fold" should be projected onto the plane of the control parameter, which divides this plane into an unstable one highlighted in yellow and the rest of the stable component as shown in Fig. 1. From a technological point of view, the instability predicted with a discriminant in water below zero combined with a discriminant in oil above zero is of interest, since this condition is a negative harbinger of a catastrophic breakthrough of water to producing wells.

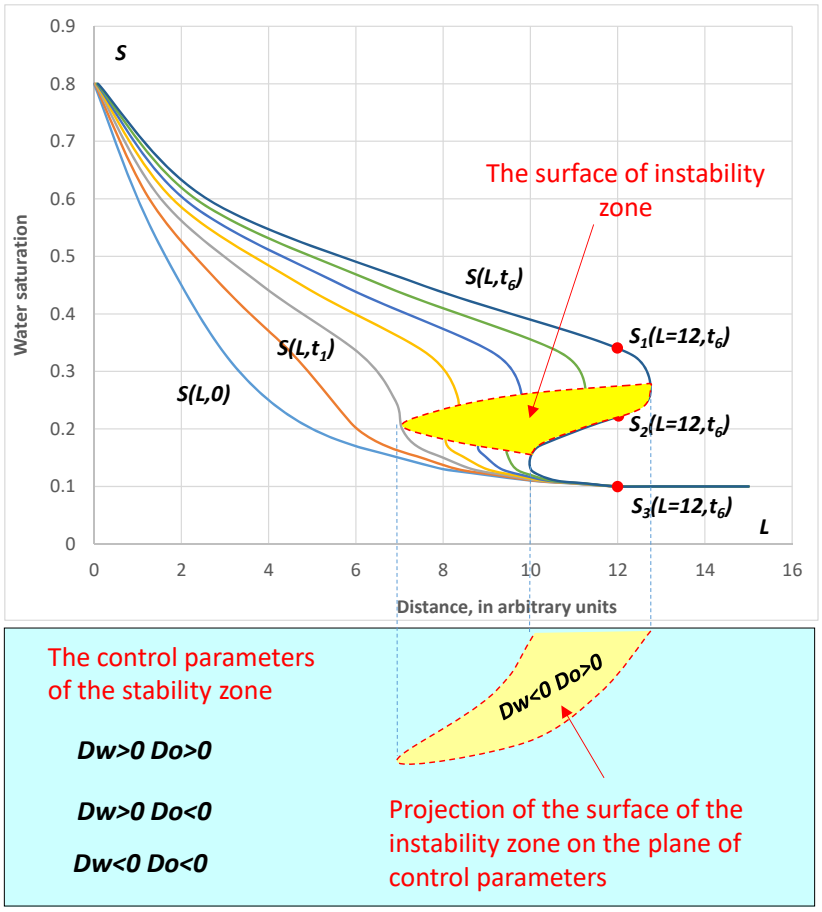


Fig. 1. The instability zone formed by the "jump" and the triplicity of water saturation

The above mentioned argument emphasizes the need to create a new scientific paradigm for the study of a dynamic multiphase filtration system designed to solve such operational tasks as an addition to the well-known geological and hydrodynamic models for the development of deposits of liquid and gaseous hydrocarbons.

It is fundamentally important to formulate and solve the problem of predicting the rate of change of the oil and water phases in the structure of the fluid flow leading to instability of the displacement front established on the basis of a control parameter developed in the theory of catastrophes calculated on the basis of the actual field data of wells operation obtained promptly. In this case, it is necessary to transform the actual data into certain new knowledge – unified control parameters that allow analyzing, monitoring and optimizing non-stationary flooding systems as provided for in the theory of catastrophes for discontinuous functions that change by leaps (Ermoliev et al., 2019).

It should be noted for the sake of objectivity that the mathematical apparatus known today as the "catastrophe theory" had not yet been developed at the time of the creation of the Buckley-Leverett theory, although the theory of Whitney singularities, the theory of Poincare bifurcations, and the basics of topology were well known to mathematicians (Gaiko, 2000). But the new mathematics was not popular in the engineering environment and this mathematical apparatus was not widely used in applied problems of technology.

The above mentioned theoretical prerequisites and argumentation indicate the need for an independent study of the dynamic behavior of the main indicators of the time development process.

3. Mathematical formulations

The qualitative theory of polynomial quadratic dynamical systems is the key to the formation of a discriminant criterion as a control parameter. The theory of catastrophes explores dynamical systems that make up a wide class of nonlinear systems including those described by quadratic polynomials.

The time series of the dynamics of current and accumulated oil and water withdrawals from the wells during the studied time period can also be described by a similar system of differential equations of growth models (Шахвердиев, Шестопалов, 2004, 2017; Shakhverdiev et al., 2019, 2021; Шахвердиев, Арефьев, 2021).

$$\begin{aligned} \frac{dQ_0}{dt} &= a_0 Q_0^2 + b_0 Q_0 + c_0 \\ \frac{dQ_w}{dt} &= a_w Q_w^2 + b_w Q_w + c_w \end{aligned} \tag{5}$$

where $a_o, b_o, c_o, a_w, b_w, c_w$ are constant coefficients characterizing the behavior of the phases, Q_o and Q_w is the accumulated selection of oil and water, respectively.

It is assumed that system (5) describes the evolution in time at a given interval $t \in (t_0, t_1)$ and at given constant values of the parameters of the problem $a_o, b_o, c_o, a_w, b_w, c_w$, the accumulated production of oil $Q_o(t)$ and water $Q_w(t)$. In practice, the accumulated and current well selections are known, which makes it possible to determine the coefficients of the polynomials of the system (5) in the first approximation as constant values for a given time interval. For this purposes, it is necessary to qualitatively investigate the behavior of the solutions of system (5) using the mathematical apparatus of polynomial quadratic dynamical systems (Шахвердиев, Шестопалов, 2019; Shakhverdiev, Mandrik, 2007). To this end, it is necessary to consider the properties of the general solution of each of the equations of the system on the phase plane Q_o of t, depending on the parameters of the problem. It is also necessary to consider the behavior and properties of solutions of the system on the phase plane Q_o, Q_w based on all parameters of the problem.

The creation of a qualitative theory that includes a description of all special and critical points of an autonomous symmetric polynomial dynamical system and the construction of the entire variety of its phase portraits is quite a difficult task. To do this, it is necessary to obtain general solutions and solutions to Cauchy problems in all possible classes defined by various types of factorizations, which as will be shown are determined by a combination of signs and absolute values of discriminants of polynomials, and to identify their most important properties.

It should be noted that, in general, polynomial dynamical systems are not integrable and the description of each of their new integrable families is an important independent contribution to the theory of dynamical systems. In particular, even two-dimensional systems which right-hand sides are polynomials of the second degree of two variables are not integrable, and the theory of such systems is far from complete (Barenblatt et al., 2003; Gaiko, 2000). Using the results and the integration technique (Шахвердиев, Шестопалов, 2019; Shakhverdiev et al., 2014; Shakhverdiev et al., 2022), we show that system (5) is integrable into elementary functions. This fact is important (a) both from a theoretical point of view, since a new class of integrable dynamical systems is fully described, and (b) from a practical one, since it makes it possible to build a complete qualitative theory and obtain –

without the use of numerical integration – all general and particular solutions of the system and the corresponding problems with initial conditions (Cauchy problem).

Carrying out a qualitative analysis of two-dimensional APDS in this paper, we provide a description and visualization of various scenarios of models of specific processes using the proven integrability (5) in elementary functions. The obtained results are generalized for the first time in a compact matrix and criterion form, which allows determining various types of all rest points of the system (5), as well as its stable and unstable solutions and their singular points depending on the signs of the discriminants of the polynomials. The latter is of decisive importance for practical applications of the results of the qualitative theory constructed in the work.

In order to conduct a complete qualitative study of the solutions of an autonomous system including the analysis of all its possible critical and singular points and solutions, we consider the behavior of the solutions of the autonomous system (5) and the corresponding equation on the phase plane (Q_o, Q_w) depending on the parameters of the problem.

We assume that the system (5) and the equations derived from it

$$\frac{dQ_W}{dQ_O} = \Phi(Q_O, Q_W), \quad \Phi(Q_O, Q_W) = \frac{f_W(Q_W)}{f_O(Q_O)}, \quad (6)$$

describe the dynamics of changes in Q_w depending on Q_0. This dynamics is obtained in the form of solutions of equation (6) under various "initial" conditions $Q_W(Q_O^0) = Q_W^0$ and corresponding curves $Q_W = Q_W(Q_O)$ on the phase plane (Q_O, Q_W).

In order to construct a qualitative theory of polynomial quadratic DS and introduce a discriminant criterion of qualitative theory, we concretize, following (Шахвердиев, Шестопалов, 2019), the definitions of classes D^{++}, D^{-+}, D^{+-} and D^{--} as sets $\{f_o, f_w\}$ of pairs of polynomials $f_o(Q_O) = a_o {Q_O}^2 + b_o Q_O + c_0$ and $f_w(Q_w) = a_w {Q_w}^2 + b_w Q_w + c_w$ such that

$$D^{++}: D_o = {b_o}^2 - 4a_o c_o > 0$$

and

$$D_w = {b_w}^2 - 4a_w c_w > 0;$$

$$D^{-+}: D_o < 0 \text{ и } D_w > 0;$$
$$D^{+-}: D_o > 0 \text{ и } D_w < 0;$$
$$D^{--}: D_o < 0 \text{ и } D_w < 0.$$

Using integration methods and formulas (Шахвердиев, Шестопалов, 2019; Shakhverdiev, 2019; Shakhverdiev, 2004; Шахвердиев, 2017), we will summarize in a table (Table) all explicit formulas for the general solution of equation (6) with respect to phase variables (Q_O, Q_W) for classes $D^{\pm}$ with nonzero discriminants, as well as for classes $D^{0\pm}, D^{\pm 0}$, when one of the discriminants turns to 0.

General solutions of the equation $\frac{dQ_w}{dQ_O} = \frac{a_w {Q_w}^2 + b_w Q_w + c_w}{a_o {Q_O}^2 + b_o Q_O + c_0}$ in classes $D^{\pm}$, $D^{0\pm}$, $D^{\pm 0}$

№№	Classes	Example of the equation	General solutions $\frac{dQ_w}{dQ_O} = \frac{a_w {Q_w}^2 + b_w Q_w + c_w}{a_o {Q_O}^2 + b_o Q_O + c_0}$, $Q_O^0 = \frac{b_O}{2a_O}$, $Q_W^0 = \frac{b_W}{2a_W}$
1	D^{++}	$\frac{dQ_w}{dQ_O} = \frac{Q_w(Q_w - 1)}{Q_O(Q_O - 1)}$	$Q_W(Q_O; C) == Q_W^1 - \frac{\sqrt{D_W}}{a_W\left(-1 + C\left\lvert\frac{Q_O - Q_O^2}{Q_O - Q_O^1}\right\rvert^{\rho}\right)}$, $\rho = \sqrt{\frac{D_W}{D_O}} > 0.$
2	D^{++}	$\frac{dQ_w}{dQ_O} = \frac{{Q_w}^2}{Q_O(Q_O - 1)}$	$Q_W(Q_O; C) = Q_W^0 + \frac{1}{\frac{a_w}{\sqrt{D_o}}\ln\left\lvert\frac{Q_O - Q_O^2}{Q_O - Q_O^1}\right\rvert + C}$
3	D^{++}	$\frac{dQ_w}{dQ_O} = \frac{Q_w(Q_w - 1)}{{Q_O}^2}$	$Q_W(Q_O; C) = Q_W^1 + \frac{\sqrt{D_w}}{a_w}\frac{1}{1 + Ce^{\frac{\sqrt{D_w}}{a_o(Q_O + Q_O^0)}}}$
4	D^{++}	$\frac{dQ_w}{dQ_O} = \frac{{Q_w}^2}{{Q_O}^2}$	$Q_W(Q_O; C) = Q_W^0 - \frac{1}{\frac{a_w}{a_o(Q_O^0 - Q_O)} + C}$

№№	Classes	Example of the equation	General solutions $\frac{dQ_w}{dQ_O}=\frac{a_w{Q_w}^2+b_wQ_w+c_w}{a_o{Q_O}^2+b_oQ_O+c_0}$, $Q_O^0=\frac{b_O}{2a_O}$, $Q_W^0=\frac{b_W}{2a_W}$
5	D^{++}	$\frac{dQ_w}{dQ_O}=\frac{{Q_w}^2+1}{Q_O(Q_O-1)}$	$Q_W(Q_O;C)=-Q_W^0+P\tan\left(\frac{\rho}{2}\ln\left\lvert\frac{Q_O-Q_O^1}{Q_O-Q_O^2}\right\rvert+C\right)$, $\rho=\sqrt{-\frac{D_w}{D_o}}>0, P=\frac{\sqrt{-D_w}}{2a_w}$
6	D^{++}	$\frac{dQ_w}{dQ_O}=\frac{Q_w(Q_w-1)}{{Q_O}^2+1}$	$Q_W(Q_O;C)=Q_W^1-\frac{\sqrt{D_w}}{P}\frac{1}{-1+Ce^{-2\rho\tan^{-1}\left(\frac{Q_O^0+Q_O}{P}\right)}}$, $\rho=\sqrt{-\frac{D_w}{D_o}}>0, P=\frac{\sqrt{-D_o}}{2a_o}$
7	D^{++}	$\frac{dQ_w}{dQ_O}=\frac{{Q_w}^2+1}{{Q_O}^2+1}$	$Q_W(Q_O;C)==-Q_W^0+P_2\tan\left(\rho\tan^{-1}\left(\frac{Q_O^0+Q_O}{P_1}\right)+C\right)$, $\rho=\sqrt{\frac{D_w}{D_o}}>0,\ P_1=\frac{\sqrt{-D_o}}{2a_o},\ P_2=\frac{\sqrt{-D_w}}{2a_w}$
8	D^{++}	$\frac{dQ_w}{dQ_O}=\frac{{Q_w}^2+1}{{Q_O}^2}$	$Q_W(Q_O;C)=Q_W^0+P\tan\left(\frac{\sqrt{-D_w}}{2}\left(\frac{1}{a_o(Q_O^0-Q_O)}+C\right)\right)\ P=\frac{\sqrt{-D_w}}{2a_w}$
9	D^{++}	$\frac{dQ_w}{dQ_O}=\frac{{Q_w}^2}{{Q_O}^2+1}$	$Q_W(Q_O;C)=Q_W^0-\frac{1}{\frac{2a_w}{\sqrt{-D_o}}\tan^{-1}\left(\frac{Q_O^0+Q_O}{P}\right)+C}$, $P=\frac{\sqrt{-D_o}}{2a_o}$

4. Solutions analysis and visualization of phase portraits

The main property of a Dynamic System (DS) is its stability, which is used to assess how the system reacts to external influences when it is assumed that its current state remains unchanged. If disturbances increase over time, this leads to a loss of stability accompanied by a sharp (catastrophic) transition to a qualitatively new state.

A systematic study of the properties of solutions of DS (5) or Equation (6) allows drawing the following conclusions: the formation of catastrophic changes in solutions within various scenarios of the development of disasters occurs when the sign of one of the discriminants of square trinomials changes, that is, while moving from one class $D^{\pm}$ to another. The latter corresponds to the transition of the system described by DS from one state to a qualitatively different one. At the same time, each class corresponds to a special structure of decision curves. A change in this structure including a catastrophic one accompanied by the appearance of new types of partial solutions that are absent in the "previous" class occurs when one parameter is varied – the discriminant D_o or D_w of one of the three terms. The D^{++} class plays a special role as the 'source' of such changes, since, as it was shown, solutions have the largest number of critical points (four).

Transitions $D^{++}\to D^{0+}$ or $D^{++}\to D^{+0}$ from class D^{++} to class D^{0+} or D^{+0} take place when the discriminants of the square trinomials of equation (5) $D_o={b_o}^2-4a_oc_o={a_o}^2(Q_o^1-Q_o^2)^2>0$ or $D_w={b_w}^2-4a_wc_w={a_w}^2(Q_w^1-Q_w^2)^2>0$ (for $a_o,a_w\neq 0$) in class D^{++} tends to 0, which is equivalent to the limit transition $Q_o^2-Q_o^1\to 0+(Q_o^2>Q_o^1)$ or $Q_w^2-Q_w^1\to 0+(Q_w^2>Q_w^1)$. The latter means that the distance between the Q_o or Q_w – coordinates of the critical points tends to 0, that is, the critical points converge and merge along one of the sides of the rectangle at the vertices of which they are located (in the D^{++} class).

Below are fragments of a series of phase portraits that characterize all the most important transitions between classes and scenarios for the development of disasters as a result of variation of one of the discriminants.

Transition from class D^{++} to class D^{+-} through classes D^{+0}, D^{00}, D^{0-}

A. Transition from class D^{++} to class D^{+0}

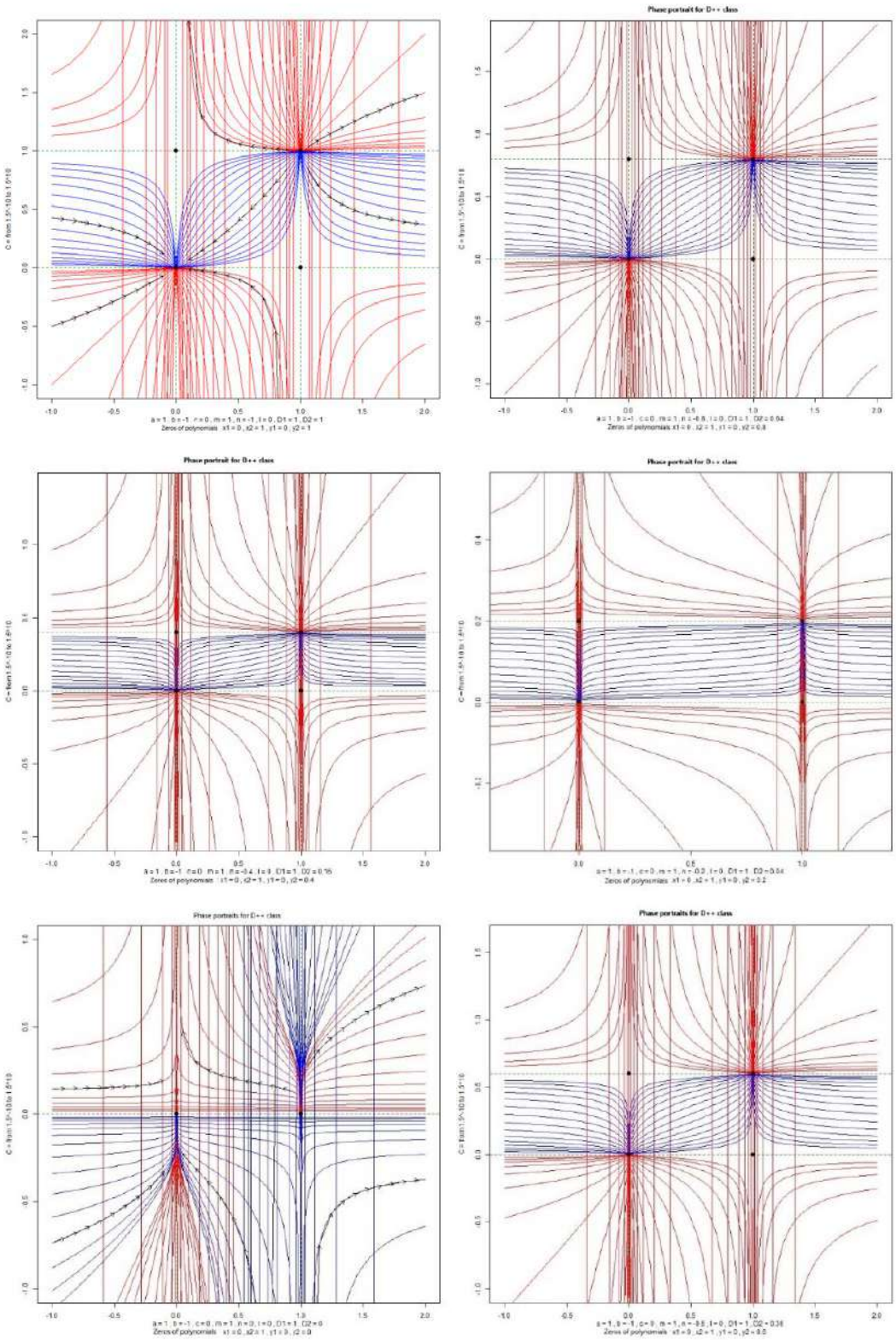


Fig. 2. Phase portraits during the transition from class D^{++} to class D^{+0}

The approach to the transition from class D^{++} to class D^{00} through D^{+0} class, that is, the convergence and merging of nodal and saddle singular points, which are located on the left and right sides of the rectangle in Fig. 2a-2d occurs with a decrease and a tendency to 0 of the discriminant D_w (D_w = 1, 0.64, 0.36, 0.16, 0.04 in Fig. 2a-2d, respectively), so,

that the distance between the Q_w coordinates of the singular points tends to 0. When the = 0, in D^{+0} class there is a merger (a) of two singular nodal and saddle points 1 and 3 (the left two in Fig. 2a-2d) as a result of which one point 1 is formed (in Fig. 2e) is a stable "one-sided" node, and (b) two nodal and saddle singular points 2 and 4 (the right two in Fig. 2a-2d), resulting in one point 2 – an unstable "one-sided" node (Fig. 2e). A gap is also formed at D_w =0 and a discontinuous "fold" characteristic of class D^{+0}.

5. Visualization and analysis of solutions curves to Cauchy problems

Solutions of the Cauchy problems are particular solutions, that is, solutions obtained from the general solution formula for a specific value of an arbitrary constant that corresponds to the initial conditions set. Such solutions pass through a given point (Q_o^0, Q_w^0) of the phase plane (Q_O, Q_w) and the local uniqueness theorem of the solution is fulfilled.

Class D^{+-} if $a_o = 1, b_o = 0, c_o = -0.25$, $D_0 = 1$; $a_w = 1$, $b_w = 2$, $c_w = 1.25$, $D_w = -1$ for each point of the plane (Q_o^0, Q_w^0) with $Q_o^0 \neq \pm 0.5$, $Q_O \neq \pm 0.5$ and

$$C = C_0 = C(Q_o^0, Q_w^0) = \tan^{-1}(2Q_w^0 + 2) - \\ -\frac{1}{2}\ln\left|\frac{Q_o^0+0.5}{Q_o^0-0.5}\right|, \quad Q_o^0 \neq \pm 0.5 \qquad (8)$$

Function

$$Q_w(Q_O, C_0) = -1 + \frac{1}{2}\tan\left(\frac{1}{2}\ln\left|\frac{Q_O+0.5}{Q_O-0.5}\right| + \right. \\ \left. +\tan^{-1}(2Q_w^0 + 2) - \frac{1}{2}\ln\left|\frac{Q_o^0+0.5}{Q_o^0-0.5}\right|\right) \qquad (9)$$

is a solution to the Cauchy problem

$$\frac{dQ_w}{dQ_O} = \frac{{Q_w}^2 + 2Q_w + 1.25}{{Q_O}^2 - 0.25}, \qquad Q_w(Q_o^0) = Q_w^0.$$

At least two scenarios of the behavior of solutions to the Cauchy problem are possible:

(a) at $-0.5 < Q_o^0 < 0.5$ and any Q_w^0 are monotonically increasing functions that lie in the band between two special stationary solutions

$$Q_O = -0.5, Q_O = 0.5;$$

(b) at $Q_o^0 > 0.5$ or $Q_o^0 < -0.5$ and any Q_w^0 are monotonically decreasing unbounded functions that lie outside the band between two stationary solutions. In this case, the entire phase plane is filled with solution curves (Fig. 3).

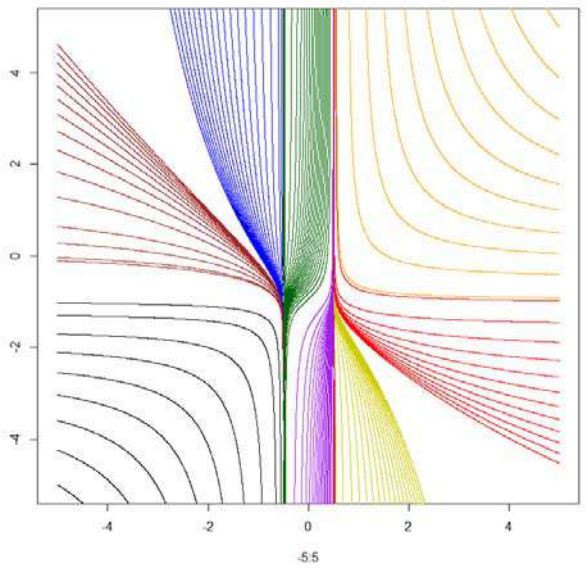


Fig. 3. Graph of curves of solutions of the Cauchy-function problem (9) for D^{+-}. Black and blue lines at *C*= from -1.4652 to -0.4388, brown lines at *C*=from 1.1611 to 1.5823, dark yellow and orange lines at *C*=from 0.0689 to 1.4652, red lines at *C*=from-1.43 to 0.05, purple lines at *C*= from 1.1866 to 1.97, green lines at *C*= from 0.129 to 1.026

For D^{-+} class function

$$Q_w(Q_O) = \frac{1}{1 + C_0 e^{\tan^{-1}Q_O}} = \\ = \frac{1}{1 + \left(1 - \frac{1}{Q_w^0}\right) e^{\tan^{-1}Q_O - \tan^{-1}Q_o^0}}$$

is for $Q_w^0 \neq 0$ the solution of the Cauchy problem

$$\frac{dQ_w}{dQ_O} = \frac{Q_w(Q_w-1)}{{Q_O}^2+1}, \; Q_w(Q_o^0) = Q_w^0.$$

Thus, $C_0 < 0$ is performed for $0 < Q_w^0 < 1$, and therefore, the curves of solutions to the Cauchy problems are, for any values of Q_o^0, graphs of bounded monotone functions that all lie in the band between two stationary solutions $Q_w = 0, Q_w = 1$. If $Q_w^0 > 1$, then the curves of solutions to the Cauchy problems are, for any values of Q_o^0, graphs of the unlimited monotone functions that lie outside the band between two stationary solutions as it is seen in Fig. 4 and 5. We can conclude about at least two possible scenarios of the behavior of the curves of solutions to the Cauchy problems:

(a) for $0 < Q_w^0 < 1$ and any Q_o^0: monotonically decreasing functions that lie in the band between two stationary solutions $Q_w = 0, Q_w = 1$;

(b) for $Q_w^0 > 1$ or $Q_w^0 < 0$ and any x_0: monotonically increasing unbounded functions that lie outside the band between the lines $Q_w = 0, Q_w = 1$.

In this case, the entire phase plane is filled with solution curves.

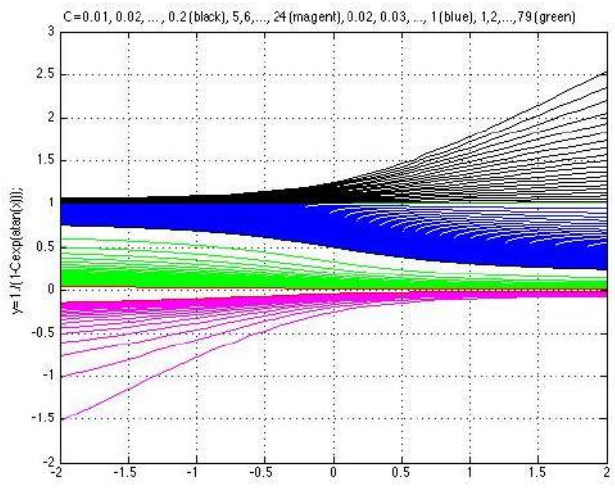


Fig. 4. General solution of D^{-+} class $Q_w(Q_O; C) = \frac{1}{1-Ce^{\tan^{-1}Q_O}}$, $C = -0.02, -0.04, \dots, -1$ (blue curves), $-2, -3, \dots, -79$ (green curves), $0.02, 0.04, \dots, 0.2$ (black curves), $5,6, \dots, 24$ (purple curves)

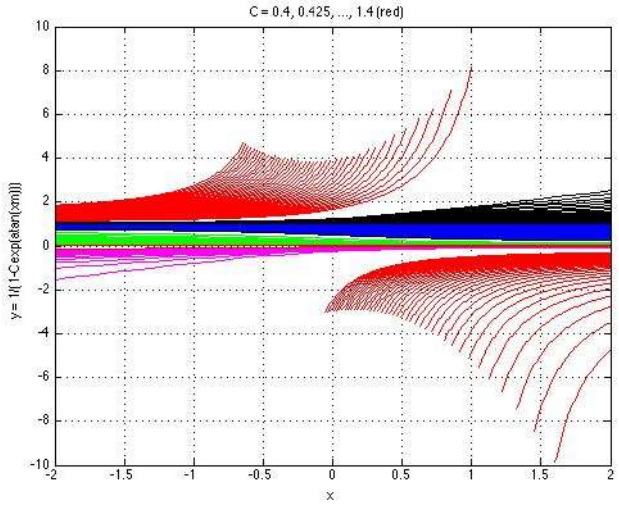


Fig. 5. General solution of D^{-+} class $Q_w(Q_O; C) = \frac{1}{1-Ce^{\tan^{-1}Q_O}}$, $C = -0.02, -0.04, \dots, -1$ (blue curves), $-2, -3, \dots, -79$ (green curves), $0.02, 0.04, \dots, 0.2$ (black curves), $5,6, \dots, 24$ (purple curves), $0.4, 0.425, \dots, 1.4$ (red curves of solutions with movable singular points)

The study of the properties of the general solutions of system (5) or equation (6) in all discriminant classes allows concluding about the exceptional richness of the qualitative diversity of these solutions. They include, in particular, all logistics-type scenarios (as a subset of D^{++} class solutions), as well as many other previously undescribed scenarios and types of transient disasters. This work is the first introductory study that provides the scientific community with a comprehensive study and application of this new class of integrable DS.

6. Application of results of qualitative analysis to solve the inverse problem

The practice of using a discriminant criterion to predict a water breakthrough is the following. It is necessary to determine the relationship between the rate of change of the measured values and these values themselves. The possibility of the above mentioned classification and qualitative analysis of solutions of equations in the time domain and autonomous equations is based on the known relationships between the rate of change of the measured quantities and these quantities themselves. These relations have the form of ordinary differential equations (6) and (7) resolved with respect to the derivative.

Using the Least Squares Method (LSM), it is possible to approximate by a quadratic polynomial the right part of the system (6) – the magnitude of the change in the measured value per unit of time (velocity) $v_{oi} = \frac{Q_{oi+1}-Q_{oi}}{t_{oi+1}-t_{oi}}$, $v_{wi} = \frac{Q_{wi+1}-Q_{wi}}{t_{wi+1}-t_{wi}}, v_{oi} \approx \frac{dQ_o}{dt}$, $v_{wi} \approx \frac{dQ_w}{dt}$, to get the ratio (6), more precisely, to solve the inverse problem – to determine the coefficients a_O, b_O, c_O, a_W, b_W, c_W using LSM, provided that the values of Q_{oi} and Q_{wi} i=1, 2 $i = 1,2, \dots n$ are known.

The above mentioned leads to the conclusion that the set of catastrophes of the growth equation is determined by the set of solutions obtained when the discriminants for oil and water are equal to zero. The resulting conclusion for the problem of hydrodynamic effect will take the following form:

$$D_O = {b_O}^2 - 4a_O c_O = 0$$
$$D_W = {b_W}^2 - 4a_W c_W = 0,$$

where the coefficients a_O, b_O, c_O, a_W, b_W, c_W for each oil or water phase are determined from equation (6) by the well-known least squares method (LSM), and the resulting system of algebraic equations is solved by the Gauss method.

The discriminant criterion and the corresponding strategies for choosing the operating mode of the well can be formulated as follows:

• when $D_O < 0$ and $D_W > 0$ (the family of solutions D^{-+} from Table), the selection of oil has a trend to increase, and water – to decrease, it is recommended to increase the selection of liquid from the well while studying the potential of pumping equipment;

• when $D_O > 0$ and $D_W < 0$ (the family of solutions D^{+-} from Table), the extraction of oil has a downward trend, and water – to increase, while a water breakthrough is possible, it is recommended to limit the extraction of liquid from the well or taking geological and technical operations on water shut-off;

• when $D_O < 0$ and $D_W < 0$ (the family of solutions D^{--} from Table), the oil and water withdrawals have an upward trend, it is recommended not to change the operating mode of the well and to perform geological and technical operations on water shut-off;

• when $D_O > 0$ and $D_W > 0$ (the D^{++} family of solutions in Table), oil and water withdrawals have a downward trend, it is recommended to carry out geological and technical operations on well stimulation.

An example of using a discriminant criterion for the development data of a specific object with the possibility of predicting the instability of the displacement front at a specific well is given below. According to the proposed methodology, the red line in Fig. 6(b) corresponds to the zero value of the discriminant, and this line determines the trend on the positive or negative side of the discriminant for water and oil, which occurs while the oil displacement front is unstable with water. Depending on the combination of the absolute value and the sign of the discriminant, the unstable state of the displacement front and the expected water breakthrough to the producing well are predicted in advance for three months, April 04.2019.

As it can be seen in Fig. 6, a water breakthrough has occurred since 04.2019 according to the discriminant criterion, this is confirmed by $D_o > 0$ $D_w < 0$ and is predicted three months before the water breakthrough while crossing the red line. At the same time, it is not possible to determine the instability of the displacement front and predict the water breakthrough in advance based on the dynamics of oil and water extraction in Fig. 6(a) on April 4, 2019. In this case, it is recommended to reduce the selection of fluid through the well, determine the cause of a possible water breakthrough, and take appropriate geological and technical measures, in particular, repair and insulation work to limit the growth of the water content of the well products. It is recommended to reduce the injection of water through the surrounding interacting injection wells for this period.

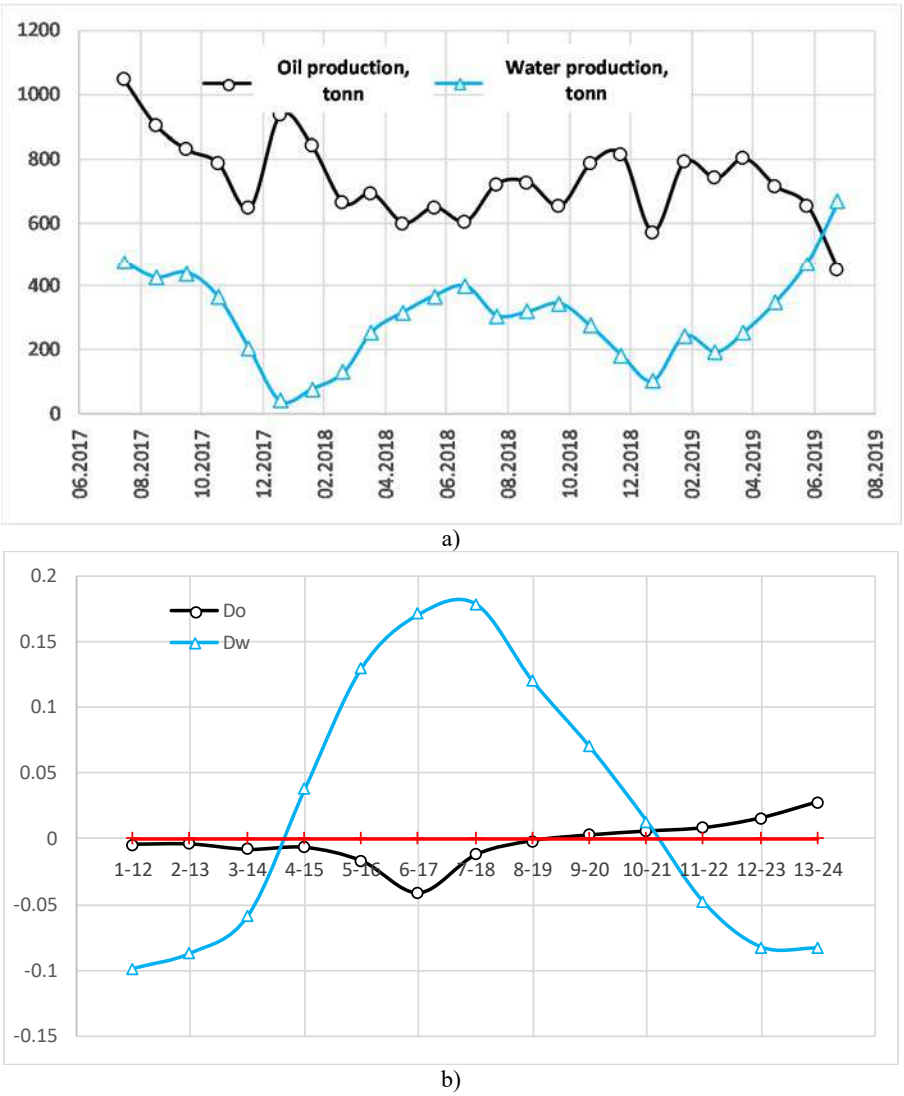


Fig. 6. Dynamics of oil and water production (a) and dynamics of discriminants (b) for well #3166G

It should be noted that the zone of instability of the displacement front on the discriminant plane corresponds to the state of instability in Fig. 6(b) starting from point 10-21, where D_w passes into the region of positive values (decrease), and D_w into the region of negative values (growth). As new data become available, further calculations are carried out in interactive mode according to the methodology for the subsequent specification of recommendations to optimize the operating modes of the wells.

7. Conclusions

The proposed new solutions to the direct and inverse problems of the catastrophe theory allow considering the consequences of instability of the displacement front in a timely manner and predicting the consequences of abrupt change and triplicity arising from the Buckley-Leverett theory.

A complete qualitative theory of such dynamical systems is constructed including an exhaustive analysis of all their singular points and features of solutions. The properties of solutions in the phase planes of parameters and in time are studied. It is shown that the discriminants of polynomials are the control parameters controlling the essential properties of solutions, a classification of solutions is proposed depending on the values and signs of the discriminants and belonging to a specific family D^{++}, D^{+-}, D^{-+} or D^{--}.

Decisive rules were formulated for the first time on the basis of the proposed criteria, allowing timely detection and prevention of the consequences of loss of stability of the displacement front and targeted regulation of the flooding system stopping, forcing, limiting operating modes, assigning well interventions to producing and injection wells. It is possible to quickly solve important short-term practical tasks passing traditional labor-intensive incorrect deterministic tasks and complex methods of solving them mobilizing the injected water and regulating the selection of liquid, more precisely water and oil, on the basis of the discriminant criterion.

It should be noted that the proposed methodology is sufficiently mobile and accurate for monitoring and controlling both the state of the flooding process and the well stock, and in general for the development of deposits in the "on-line" mode. There is a potential opportunity to replenish the database on a monthly basis based on the proposed criteria and decisive rules to make specific clarifications to the work program and geological and technical measures including while optimizing the reservoir pressure maintenance system by regulating the operating modes of producing and injection wells.

The proposed solutions are an integral part of the new concept of nonstationary flooding, which provides for an early forecast and taking measures in case of instability of the displacement front and, as a result, water breakthrough in producing wells.

The system optimization of flooding of oil fields is designed for a certain technological and economic effect of resource conservation and energy efficiency.

This opens up the possibility of system optimization of non-stationary flooding and the prospect of increased oil recovery and intensification of oil production, as well as effective mobilization of injected and extracted water and gas.

Declaration of competing interest

The authors declare that they have no known competing financial interests or personal relationships that could have appeared to influence the work reported in this paper.

REFERENCES

Abbasi J., Ghaedi M., Riazi M. A new numerical approach for investigation of the effects of dynamic capillary pressure in imbibition process. Journal of Petroleum Science and Engineering, Vol. 162, 2018, pp. 44-54, https://doi.org/10.1016/j.petrol.2017.12.035.

Arnold V.I., Davydov A.A., Vassiliev V.A., Zakalyukin V.M. Mathematical models and control of catastrophic processes. UNESCO Encyclopedia of Life Support Systems, Vol. II, EOLSS Publishers. Oxford, UK, 2005, pp. 3-46, http://www.eolss.net/SampleChapters/C02/E6-03A-07-05.pdf.

Aziz K., Settari A. Petroleum reservoir simulation. Elsevier Applied Science Publishers. London, 1986.

Barenblatt G.I., Patzek T.W., Silin D.B. The mathematical model of nonequilibrium effects in water-oil displacement. SPE Journal, Vol. 8(4), 2003, pp. 409-416, https://doi.org/10.2118/87329-PA.

Baryshnikov N.A., Belyakov G.V., Turuntaev S.B. Two-phase jet flows in porous media. Fluid Dynamics, Vol. 52, No. 1, 2017, pp. 128-137, https://doi.org/10.1134/S0015462817010124.

ЛИТЕРАТУРА

Abbasi J., Ghaedi M., Riazi M. A new numerical approach for investigation of the effects of dynamic capillary pressure in imbibition process. Journal of Petroleum Science and Engineering, Vol. 162, 2018, pp. 44-54, https://doi.org/10.1016/j.petrol.2017.12.035.

Arnold V.I., Davydov A.A., Vassiliev V.A., Zakalyukin V.M. Mathematical models and control of catastrophic processes. UNESCO Encyclopedia of Life Support Systems, Vol. II, EOLSS Publishers. Oxford, UK, 2005, pp. 3-46, http://www.eolss.net/SampleChapters/C02/E6-03A-07-05.pdf.

Aziz K., Settari A. Petroleum reservoir simulation. Elsevier Applied Science Publishers. London, 1986.

Barenblatt G.I., Patzek T.W., Silin D.B. The mathematical model of nonequilibrium effects in water-oil displacement. SPE Journal, Vol. 8(4), 2003, pp. 409-416, https://doi.org/10.2118/87329-PA.

Baryshnikov N.A., Belyakov G.V., Turuntaev S.B. Two-phase jet flows in porous media. Fluid Dynamics, Vol. 52, No. 1, 2017, pp. 128-137, https://doi.org/10.1134/S0015462817010124.

Brouwer D.R., Jansen J.D. Dynamic optimization of water flooding with smart wells using optimal control theory. Proceedings of the European Petroleum Conference, Aberdeen, United Kingdom, Paper Number: SPE-78278-MS, October 2002, https://doi.org/10.2118/78278-MS.

Buckley S.E., Leverett M.C. Mechanism of fluid displacement in sands. Transactions of the AIME, Vol. 146(01), 1942, pp. 107-116, https://doi.org/10.2118/942107-g.

Charnyi I.A. Underground fluid dynamics. Gostoptekhizdat. Moscow, 1963, 397 p. (in Russian).

Craig F.F.Jr. The reservoir engineering aspects of waterflooding. Society of Petroleum Engineers of AIME. New York, 1971, 142 p.

Dake L.P. The practice of reservoir engineering (Revised Edition). Elsevier. 2001, 572 p.

Ding L., Wu Q., Zhang L., Guérillot D. Application of fractional flow theory for analytical modeling of surfactant flooding, polymer flooding, and surfactant/polymer flooding for chemical enhanced oil recovery. Water, Vol. 12(8), 2020, p. 2195, https://doi.org/10.3390/W12082195.

Duan Y., Lu T., Wei M., Yu B., Zhang Z. Buckley-Leverett analysis for transient two-phase flow in fractal porous medium. Computer Modeling in Engineering and Sciences, Vol. 109, No. 6, 2015, pp. 481-504.

Ermoliev Y., Ermolieva T., Kahil T. et al. Stochastic optimization models for risk-based reservoir management. Cybernetics and System Analysis, Vol. 55, 2019, pp. 55-64, https://doi.org/10.1007/s10559-019-00112-z.

Gaiko V.A. On global bifurcations and Hilbert's sixteenth problem. Nonlinear Phenomena in Complex Systems, Vol. 1, 2000, pp. 11-27, https://doi.org/10.1.1.142.175.

Klebanov L.A., Kroshilin A.E., Nigmatulin B.I., Nigmatulin R.I. On the hyperbolicity, stability and correctness of the cauchy problem for the system of equations of two-speed motion of two-phase media. Journal of Applied Mathematics and Mechanics, Vol. 46, No. 1, 1982, pp. 66-74, https://doi.org/10.1016/0021-8928(82)90084-3.

Mandrik I.E., Panahov G.M., Shakhverdiev A.K. Scientific and methodological foundations for optimization of the process of enhanced oil recovery. Neftyanoe hozyajstvo. Moscow, 2010, 284 p. (in Russian).

Mirzajanzadeh A.K., Shakhverdiev A.Kh. Dynamic processes in oil and gas production. Nauka. Moscow, 1997 (in Russian).

Nigmatulin R.I., Lahey R.T., Taleyarkhan R.T., West C., Block R.C. On thermonuclear processes in cavitation bubbles. Physics Uspekhi, Vol. 57, No. 9, 2014, article id. 877-890, DOI:10.3367/UFNe.0184.201409b.0947.

Rodygin S.I. Dynamics of water content of an oil-saturated sample under pressure waves. Numerical simulation. Journal of Geo Resources, Vol. 1, No. 5, 2012, pp. 31-34.

Rose W., Rose D.M. "Revisiting" the enduring Buckley-Leverett ideas. Journal of Petroleum Science and Engineering, Vol. 45(3-4), 2004, pp. 263-290, https://doi.org/10.1016/J.PETROL.2004.08.001.

Shakhverdiev A.Kh. Optimization of oil field development process. Nedra. Moscow 2004, 452 p. (in Russian).

Shakhverdiev A.K. System optimization of non-stationary floods for the purpose of increasing oil recovery. Neftyanoe khozyaystvo - Oil Industry, No. 1, 2019, pp. 44-49, DOI:10.24887/0028-2448-2019-1-44-49.

Shakhverdiev A.Kh. Some conceptual aspects of systematic optimization of oil field development. Oil industry, No. 2, 2017, pp. 58-63 (in Russian).

Shakhverdiev A. Kh., Arefiev S.V. The concept of monitoring and optimization of oil reservoirs waterflooding under the conditions of displacement front instability. Neftyanoe khozyaystvo – Oil Industry, No. 11, 2021, pp.104-109, https://doi.org/10.24887/0028-2448-2021-11-104-109 (in Russian).

Brouwer D.R., Jansen J.D. Dynamic optimization of water flooding with smart wells using optimal control theory. Proceedings of the European Petroleum Conference, Aberdeen, United Kingdom, Paper Number: SPE-78278-MS, October 2002, https://doi.org/10.2118/78278-MS.

Buckley S.E., Leverett M.C. Mechanism of fluid displacement in sands. Transactions of the AIME, Vol. 146(01), 1942, pp. 107-116, https://doi.org/10.2118/942107-g.

Craig F.F.Jr. The reservoir engineering aspects of waterflooding. Society of Petroleum Engineers of AIME. New York, 1971, 142 p.

Dake L.P. The practice of reservoir engineering (Revised Edition). Elsevier. 2001, 572 p.

Ding L., Wu Q., Zhang L., Guérillot D. Application of fractional flow theory for analytical modeling of surfactant flooding, polymer flooding, and surfactant/polymer flooding for chemical enhanced oil recovery. Water, Vol. 12(8), 2020, p. 2195, https://doi.org/10.3390/W12082195.

Duan Y., Lu T., Wei M., Yu B., Zhang Z. Buckley-Leverett analysis for transient two-phase flow in fractal porous medium. Computer Modeling in Engineering and Sciences, Vol. 109, No. 6, 2015, pp. 481-504.

Ermoliev Y., Ermolieva T., Kahil T. et al. Stochastic optimization models for risk-based reservoir management. Cybernetics and System Analysis, Vol. 55, 2019, pp. 55-64, https://doi.org/10.1007/s10559-019-00112-z.

Gaiko V.A. On global bifurcations and Hilbert's sixteenth problem. Nonlinear Phenomena in Complex Systems, Vol. 1, 2000, pp. 11-27, https://doi.org/10.1.1.142.175.

Klebanov L.A., Kroshilin A.E., Nigmatulin B.I., Nigmatulin R.I. On the hyperbolicity, stability and correctness of the cauchy problem for the system of equations of two-speed motion of two-phase media. Journal of Applied Mathematics and Mechanics, Vol. 46, No. 1, 1982, pp. 66-74, https://doi.org/10.1016/0021-8928(82)90084-3.

Nigmatulin R.I., Lahey R.T., Taleyarkhan R.T., West C., Block R.C. On thermonuclear processes in cavitation bubbles. Physics Uspekhi, Vol. 57, No. 9, 2014, article id. 877-890, DOI:10.3367/UFNe.0184.201409b.0947.

Rodygin S.I. Dynamics of water content of an oil-saturated sample under pressure waves. Numerical simulation. Journal of Geo Resources, Vol. 1, No. 5, 2012, pp. 31-34.

Rose W., Rose D.M. "Revisiting" the enduring Buckley-Leverett ideas. Journal of Petroleum Science and Engineering, Vol. 45(3-4), 2004, pp. 263-290, https://doi.org/10.1016/J.PETROL.2004.08.001.

Shakhverdiev A.K. System optimization of non-stationary floods for the purpose of increasing oil recovery. Neftyanoe khozyaystvo – Oil Industry, No. 1, 2019, pp. 44-49, DOI:10.24887/0028-2448-2019-1-44-49.

Shakhverdiev A.H., Mandrik I.E. Influence of technological features of hardly recoverable hydrocarbons reserves output on an oil-recovery ratio. Neftyanoe khozyaystvo - Oil Industry, No. 5, 2007, pp. 76-79.

Shakhverdiev A.Kh., Arefyev S.V., Davydov A.V. Problems of transformation of hydrocarbon reserves into an unprofitable technogenic hard-to-recover reserves category. Neftyanoe khozyaystvo – Oil Industry, No. 4, 2022, pp. 3843, DOI:10.24887/0028-2448-2022-4-38-43.

Shakhverdiev A.Kh., Denisov A.V., Tumanova V.D. New optimization criteria of waterflood patterns preventing premature water breakthrough in the context of water-oil displacement front instability. 7th Scientific Exploration Conference, Tyumen 2021: Natural Resources Management as a Cross-Functional Process, Vol. 1, 2021, pp. 1-5, https://doi.org/10.3997/2214-4609.202150063.

Shakhverdiev A.Kh., Shestopalov Y.V., Mandrik I.E., Arefiev S.V. Alternative concept of monitoring and optimization

Shakhverdiev A.H., Mandrik I.E. Influence of technological features of hardly recoverable hydrocarbons reserves output on an oil-recovery ratio. Neftyanoe khozyaystvo - Oil Industry, No. 5, 2007, pp. 76-79.

Shakhverdiev Ah.K., Shestopalov Y.V. Qualitative analysis of quadratic polynomial dynamical systems associated with the modeling and monitoring of oil fields. Lobachevskii journal of mathematics, Vol. 40. No. 10, 2019, pp. 1695-1710, https://doi.org/10.1134/S1995080219100226 (in Russian).

Shakhverdiev A.Kh., Denisov A.V., Tumanova V.D. New optimization criteria of waterflood patterns preventing premature water breakthrough in the context of water-oil displacement front instability. 7th Scientific Exploration Conference, Tyumen 2021: Natural Resources Management as a Cross-Functional Process, Vol. 1, 2021, pp. 1-5, https://doi.org/10.3997/2214-4609.202150063.

Shakhverdiev A.Kh., Shestopalov Y.V., Mandrik I.E., Arefiev S.V. Alternative concept of monitoring and optimization water flooding of oil reservoirs in the conditions of instability of the displacement front. Neftyanoe Khozyaystvo - Oil Industry, No. 12, 2019, pp. 118-123, https://doi.org/10.24887/0028-2448-2019-12-118-123.

Shakhverdiev A.Kh., Panahov G.M., Abbasov E.M., Jiang R., Bakhtiyarov S. High efficiency EOR and IOR technology on in-situ CO2 generation. Neftyanoe khozyaystvo - Oil Industry, No. 5, 2014, pp. 90-95.

Shakhverdiev A.Kh., Arefyev S.V., Davydov A.V. Problems of transformation of hydrocarbon reserves into an unprofitable technogenic hard-to-recover reserves category. Neftyanoe khozyaystvo – Oil Industry, No. 4, 2022, pp. 3843, DOI:10.24887/0028-2448-2022-4-38-43.

Sharma V., Nand S., Pramanik S., Chen C., Mishra M. Control of radial miscible viscous fingering. Journal of Fluid Mechanics, Vol. 884, A16, 2020, DOI:10.1017/jfm.2019.932.

Skauge A., Sorbie K., Ormehaug P.A., Skauge T. Experimental and numerical modeling studies of viscous unstable displacement. In: 15th European Symposium on Improved Oil Recovery, Paris, France, 2009, pp. 262-273, https://doi.org/10.3997/2214-4609.201404837.

Thompson J.M.T. Instabilities and catastrophes in science and engineering. Edition**,** 99. Wiley. 1982, 226 p.

Udy J., Hansen B., Maddux S., Petersen D., Heilner S. et al. Review of field development optimization of waterflooding, EOR, and well placement focusing on history matching and optimization algorithms. Processes, Vol. *5*(3), 2017, p. 34, https://doi.org/10.3390/PR5030034.

Wang D., Niu D., Li H.A. Predicting waterflooding performance in low-permeability reservoirs with linear dynamical systems. SPE Journal, Vol. 22(5), 2017, pp. 1596-1608, https://doi.org/10.2118/185960-pa.

Shakhverdiev A.H., Mandrik I.E. Influence of technological features of hardly recoverable hydrocarbons reserves output on an oil-recovery ratio. Neftyanoe khozyaystvo - Oil Industry, No. 5, 2007, pp. 76-79.

Shakhverdiev Ah.K., Shestopalov Y.V. Qualitative analysis of quadratic polynomial dynamical systems associated with the modeling and monitoring of oil fields. Lobachevskii journal of mathematics, Vol. 40. No. 10, 2019, pp. 1695-1710, https://doi.org/10.1134/S1995080219100226 (in Russian).

Shakhverdiev A.Kh., Denisov A.V., Tumanova V.D. New optimization criteria of waterflood patterns preventing premature water breakthrough in the context of water-oil displacement front instability. 7th Scientific Exploration Conference, Tyumen 2021: Natural Resources Management as a Cross-Functional Process, Vol. 1, 2021, pp. 1-5, https://doi.org/10.3997/2214-4609.202150063.

Shakhverdiev A.Kh., Shestopalov Y.V., Mandrik I.E., Arefiev S.V. Alternative concept of monitoring and optimization water flooding of oil reservoirs in the conditions of instability of the displacement front. Neftyanoe Khozyaystvo - Oil Industry, No. 12, 2019, pp. 118-123, https://doi.org/10.24887/0028-2448-2019-12-118-123.

Shakhverdiev A.Kh., Panahov G.M., Abbasov E.M., Jiang R., Bakhtiyarov S. High efficiency EOR and IOR technology on in-situ CO2 generation. Neftyanoe khozyaystvo - Oil Industry, No. 5, 2014, pp. 90-95.

Sharma V., Nand S., Pramanik S., Chen C., Mishra M. Control of radial miscible viscous fingering. Journal of Fluid Mechanics, Vol. 884, A16, 2020, DOI:10.1017/jfm.2019.932.

Skauge A., Sorbie K., Ormehaug P.A., Skauge T. Experimental and numerical modeling studies of viscous unstable displacement. In: 15th European Symposium on Improved Oil Recovery, Paris, France, 2009, pp. 262-273, https://doi.org/10.3997/2214-4609.201404837.

Thompson J.M.T. Instabilities and catastrophes in science and engineering. Edition**,** 99. Wiley. 1982, 226 p.

Udy J., Hansen B., Maddux S., Petersen D., Heilner S. et al. Review of field development optimization of waterflooding, EOR, and well placement focusing on history matching and optimization algorithms. Processes, Vol. *5*(3), 2017, p. 34, https://doi.org/10.3390/PR5030034.

Wang D., Niu D., Li H.A. Predicting waterflooding performance in low-permeability reservoirs with linear dynamical systems. SPE Journal, Vol. *22*(5), 2017, pp. 1596-1608, https://doi.org/10.2118/185960-pa.

Мандрик И.Э., Панахов Г.М., Шахвердиев А.Х. Научно-методические и технологические основы оптимизации процесса повышения нефтеотдачи пластов. Нефтяное хозяйство. Москва, 2010, 284 с.

Мирзаджанзаде А.К., Шахвердиев А.Х. Динамические процессы в нефтегазодобыче. Наука. Москва, 1997.

Чарный И.А. Подземная гидрогазодинамика. Гостоптехиздат. Москва, 1963, 397 с.

Шахвердиев А.Х. Системная оптимизация процесса разработки нефтяных месторождений Недра. Москва, 2004, 452 с.

Шахвердиев А.Х. Некоторые концептуальные аспекты системной оптимизации разработки нефтяных месторождений. Нефтяное хозяйство, No. 2, 2017, с. 58-63.

Шахвердиев А.Х., Арефьев С.В. Концепция мониторинга и оптимизации процесса заводнения нефтяных пластов при неустойчивости фронта вытеснения. Нефтяное хозяйство, No. 11, 2021, с. 104-109.

Шахвердиев А.К., Шестопалов Я.В. Качественный анализ квадратичных полиномиальных динамических систем, связанных с моделированием и мониторингом нефтяных месторождений. Lobachevskii journal of mathematics, Т. 40, No. 10, 2019, с. 1695-1710, https://doi.org/10.1134/S1995080219100226.

ОПТИМИЗАЦИЯ ЗАВОДНЕНИЯ ПЛАСТОВ С НЕУСТОЙЧИВЫМ ФРОНТОМ ВЫТЕСНЕНИЯ

Шахвердиев А.Х.[1], Шестопалов Я.В.[2], Мандрик И.Е.[3], Арефьев С.В.[4]

[1]Российский государственный геологоразведочный университет
117997, Москва, ул. Миклухо-Маклая, д.23
[2]Академия технологии и окружающей среды, Университет Эвле,
SE-801 76 Швеция
[3]ПАО ЛУКОИЛ, Россия
101000, Москва, Сретенский бульвар,11
[4]ООО «ЛУКОЙЛ-Западная Сибирь», Россия

Резюме. Нестационарное заводнение нефтенасыщенных пластов давно и прочно занимает место основного вторичного метода добычи нефти и поддержания пластового давления при разработке большинства нефтяных залежей. Закачка воды в пласт создает отложенную проблему – неизбежное, часто катастрофическое обводнение нефтедобывающих скважин, спровоцированное резким и необратимым изменением водонасыщенности. Созданная Бакли и Леверетом теория фильтрации

двухфазных потоков не учитывает потерю устойчивости фронта вытеснения, что провоцирует резкое изменение и утроенные значения водонасыщенности. Поэтому в свое время был предложен математически упрощенный подход – многократно дифференцируемая аппроксимация, исключающая "скачок" водонасыщенности. Такое упрощенное решение привело к хорошо известным негативным последствиям практики заводнения, которые специалисты называют "вязкостной неустойчивостью Фронта вытеснения", "пальцеобразным вытеснением". По результатам исследований предлагается полная качественная теория подобных квадратичных полиномиальных динамических систем, включающая исчерпывающий анализ всех их сингулярных точек и особенностей решения. Свойства решений изучались на фазовых плоскостях самих параметров и времени. Показано, что полиномиальные дискриминанты представляют собой управляющие параметры, определяющие существенные свойства решений. Предложена классификация решений в зависимости от знаков дискриминантов и от семейства, к которому принадлежит решение. В данной работе впервые представлен новый подход к формулированию решающих правил, позволяющих своевременно обнаружить и предотвратить последствия потери устойчивости фронта вытеснения и целенаправленно управлять системой заводнения путем остановки, форсирования, ограничения режимов работы, назначения ремонтных режимов добывающих и нагнетательных скважин. Появляется возможность оперативно решать важные краткосрочные практические задачи, минуя традиционные трудоемкие некорректные детерминированные задачи и сложные методы решения, мобилизуя нагнетаемую воду и управляя дебитом жидкости, точнее воды и нефти на основе дискриминантного критерия.

Ключевые слова: *заводнение, неустойчивость фронта вытеснения, оптимизация, «пальцеобразование», теория катастроф, фазовая плоскость*

QEYRİ-SABİT SIXIŞDIRMA CƏBHƏSİ İLƏ SU LAYLARIN SUVURMANIN OPTİMALLAŞDIRILMASI

Şahverdiyev A.X.[1], Şestopalov Y.V.[2], Mandrik I.E.[3], Arefev S.V.[4]
[1]Rusiya Dövlət Geoloji Kəşfiyyat Universiteti, Rusiya
117997, Moskva, Mikluxo-Maklay küç., 23
[2]Texnologiya və Ətraf Mühit Akademiyası, Evle Universiteti,
SE-801 76 İsveç
[3]PJSC "Lukoil", Rusiya
101000, Moskva, Sretensky Bulvarı, 11
[4]«LUKOIL-Qərbi Sibir» MMC, Rusiya

Xülasə. Neft yataqlarının işlənmə zamanı hasilatını və lay təzyiqini sabit saxlaması üçün neftlə doymuş laylara qeyri-stasionar suvurma texnologiyası çoxdan əsas ikinci üsul kimi qəbul olunur. Laya suyun vurulması su ilə doyma əmsalın kəskin və geri dönməz dəyişməsi səbəbindən quyuların qaçılmaz və katastrofik sulaşması təxirə salınmış bir problem yaradır. Buckley və Leverett tərəfindən yaradılan iki fazalı axınların filtrasiya nəzəriyyəsi, suyun doymasının kəskin dəyişməsinə və üçqat dəyərinə səbəb olan sıxışdırma cəbhəsinin sabitliyinin itirilməsini nəzərə almır. Buna görə, bir vaxtlar riyazi cəhətdən sadələşdirilmiş bir yanaşma təklif edildi – Su doymasının "sıçrayışını" istisna edən dəfələrlə fərqlənən yaxınlaşma. Belə bir sadələşdirilmiş həll, mütəxəssislərin "sıxışdırma cəbhəsinin viskoz qeyri-sabitliyi", "barmaq şəklində sıxışdırma" adlandırdığı suvurma təcrübəsinin mənfi nəticələrinə səbəb oldu. İşdə ilk dəfə sıxışdırma cəbhəsinin dayanıqlığının itirilməsinin nəticələrini vaxtında aşkar etməyə və qarşısını almağa və iş rejimlərini məhdudlaşdırmaqla, sürətləndirməklə, məhdudlaşdırmaqla, hasilat və vurucu quyularının təmir rejimlərini təyin edilməklə, suvurma sistemini məqsədyönlü şəkildə idarə etməyə imkan verən həlledici qaydaların formalaşdırılmasına yeni bir yanaşma təqdim edilir. Ənənəvi vaxt aparan korrekt olmayan deterministik məsələləri və mürəkkəb həll üsulları keçərək, vurulan suyu səfərbər edərək və diskriminant meyarı əsasında mayenin, daha doğrusu su və neftin axın sürətini idarə edərək vacib qısamüddətli praktik problemləri tez bir zamanda həll edilməsi mümkün olur.

Açar sözlər*: suvurma, sıxışdırma cəbhəsinin qeyri-sabitliyi, optimallaşdırma, "barmaq şəklində sıxışdırma", fəlakət nəzəriyyəsi, faza müstəvisi*

ANAS Transactions Earth Sciences 2 / 2023

http://www.journalesgia.com

ИССЛЕДОВАНИЕ ПОВЕРХНОСТНОЙ ТЕМПЕРАТУРЫ КАСПИЙСКОГО МОРЯ ПО ДАННЫМ РЕАНАЛИЗОВ MERRA-2 ЗА ПЕРИОД 1980-2021 гг.

Сафаров С.Г.[1], Исмайылов В.Г.[2], Сафаров Э.С.[1]

[1]Министерство науки и образования Азербайджанской Республики,
Институт географии имени акад. Г. Алиева, Азербайджан
AZ1070, г. Баку, просп. Г.Джавида, 115: safarov53@mail.ru
[2]Бакинский Государственный Университет, Азербайджан
AZ1148, Баку, ул.З. Халилов 23: vusalhakimoglu@gmail.com

STUDY OF THE SURFACE TEMPERATURE OF THE CASPIAN SEA ACCORDING TO MERRA-2 REANALYSIS DATA FOR THE PERIOD 1980-2021

Safarov S.H.[1], Ismayilov V.G.[2], Safarov E.S.[1]
[1]Ministry of Science and Education of the Republic of Azerbaijan, Institute of Geography named after acad. G. Aliyev, Azerbaijan
115, H.Javid ave., Baku, AZ1070: safarov53@mail.ru
[2]Baku State University, Azerbaijan
23, Akademik Zahid Xalilov str., Baku, AZ1148

Keywords: *Caspian Sea, climate change, sea surface temperature, linear trend, sea level changes*

Summary. According to the data collected from MERRA-2 reanalysis for 1980-2021, using different statistical methods, the changes of the sea surface temperature in the Northern, Middle and Southern Caspian Sea, the reasons of their occurrence were studied, and the corresponding linear trends were estimated. It was found out that the average annual surface temperature in the period 2001-2021 increased by 0.5ºC in the Northern Caspian, by 0.9ºC in the Middle Caspian and by 0.7ºC in the Southern Caspian compared with the period of 1980-2000. Different trends in surface temperature in different months and seasons have been revealed under the conditions of global warming and lowering of the level of the Caspian Sea in different parts of the water area. In 1980-2021 there is a significant negative trend in surface temperature in winter in the Northern Caspian Sea, but in other seasons, a positive trend is observed throughout the sea. All trends, except for autumn in the Northern Caspian Sea, were statistically significant at 0.05 level, and in most cases even at 0.01 level. Increase of contrasts between winter and spring surface temperatures in the Northern Caspian Sea against the background of sea level fall can extremely negatively affect the ecological state, including the biodiversity of the sea.

© 2023 Earth Science Division, Azerbaijan National Academy of Sciences. All rights reserved.

Введение

Как известно, Каспийское море является крупнейшим замкнутым водоемом в мире, и его уровень постоянно подвержен колебаниям. Согласно современным представлениям, изменения уровня моря напрямую связаны с его водным балансом. Водный баланс, в свою очередь, определяется количеством речных стоков и атмосферных осадков, выпадающих на поверхность моря, которые составляют его приходную часть, а также количеством испарения с поверхности, составляющим его выходную часть. Одним из основных факторов, влияющих на испарение с поверхности моря, является температура поверхности моря (ТПМ). В связи с этим изучение поверхностного температурного режима и его изменений в акватории Каспийского моря имеет большое научное и практическое значение.

Каспийское море по своим физико-географическим условиям и рельефу дна делится на три части: Северный, Средний и Южный Каспий (Гидрометеорология..., 1992). Кроме того, максимальная глубина Северного Каспия составляет 20 м, Среднего Каспия — 788 м, Южного Каспия — 1025 м (Водный баланс..., 2016).

До недавнего времени исследования ТПМ Каспийского моря проводились в основном по данным измерений береговых наблюдательных пунктов, которые не могут объективно характеризовать всю морскую акваторию, особенно дина-

мику поверхностной температуры в открытом море. С другой стороны, хотя измерения, полученные морскими экспедициями, организованными в отдельные периоды, и измерения, проведенные дрифтерами на ограниченных участках, лишь частично решают проблему, однако они не позволяют объективно определить пространственно-временные характеристики ТПМ (Məmmədov və b., 2012). Упразднение ряда наблюдательных пунктов после распада Советского Союза и отсутствие адекватного обмена гидрометеорологической информацией между прикаспийскими странами усугубляют данную проблему (Мамедов, 2007). В связи с этим возможность использования данных современных гидродинамических моделей и спутниковых наблюдений (Гинзбург и др., 2004; Ginzburg et al., 2005; Гинзбург и др., 2012; Костяной и др., 2014; Гинзбург и др., 2020; Гинзбург и др., 2021; Kazmin, 2021; Səfərov və b., 2022) с целью исследования поверхностной температуры Каспийского моря вызывает большой интерес. Одним из основных преимуществ такого подхода является то, что в отличие от контактных данных, здесь можно оценить ТПМ по всей акватории, особенно в открытом море, при текущем уровне разрешения.

Использованные материалы и методы исследования

В работе были использованы среднемесячные данные ТПМ MERRA-2 (The Modern-Era Retrospective analysis for Research and Applications) за период 1980-2021 гг., включенный в интернет-портал GIOVANNI (https://giovanni.gsfc.nasa.gov/giovanni/). Для определения статистических характеристик поверхностной температуры в открытом море и влияния на них климатических изменений и других факторов проведено осреднение данных реанализа по акваториям Каспийского моря отдельно в пределах Северного, Среднего и Южного Каспия. Для более удобного расчета температурных характеристик морской поверхности, как и (Гинзбург и др., 2004; Гинзбург и др., 2021) в качестве границы между Северным и Средним Каспием использовалась широта 44°30′ с. ш. В качестве границы между Средним и Южным Каспием применялась общепринятая широта 40°15' с. ш.

Отметим, что хотя данные реанализов MERRA-2 охватывают относительно больший период (1980-2022 гг.), из-за небольшого их пространственного разрешения (0.5^0 x 0.625^0 или 40-50 км) они не очень удобны для изучения особенностей распределения поверхностной температуры по акваториям моря. Однако относительно длинные временные ряды позволяют изучать вариации поверхностной температуры в разных районах морской акватории. Для определения характеристик изменений ТПМ во времени статистические ряды были разделены на два равных периода (1980-2000 и 2001-2021 гг.), и для каждого из них были рассчитаны среднегодовые, среднесезонные и среднемесячные значения ТПМ, проведено их сравнение и проверена статистическая значимость выявленных изменений по критериям Стьюдента. Кроме того, для определения тенденций изменений ТПМ были построены соответствующие линейные тренды и проверена их статистическая значимость по следующему неравенству:

$$R/\sigma_R \geq s, \qquad (1)$$

где R – коэффициент корреляции, σ_R – случайная среднеквадратичная погрешность, s – критическое значение критерия Стьюдента (Рождественский, Лобанова, 2010; Сикан, 2007).

Случайная среднеквадратическая ошибка рассчитывается по следующей формуле:

$$\sigma_R = (1 - R^2)/\sqrt{(n-1)}, \qquad (2)$$

где n — количество членов временного ряда. При 5%-ном уровне значимости n=40 s=2.02.

Указанные процедуры проводились также для отдельных месяцев и сезонов.

Полученные результаты и их обсуждение

На основе данных реанализов MERRA-2 были проанализированы месячные данные за период 1980-2021 гг. с целью более детального изучения пространственно-временных изменений поверхностной температуры Северного, Среднего и Южного Каспия. В табл. 1 представлены изменения температуры поверхности всех трех частей Каспийского моря во втором полупериоде по сравнению с таковым первым.

Как видно из табл. 1, в период 2001-2021 гг. по сравнению с периодом 1980-2000 гг. среднегодовое значение ТПМ Северного Каспия увеличилось на 0.5ºС Наибольшее повышение температуры на 1.8ºС и 1.9ºС было зафиксировано в апреле и мае соответственно, а в январе и декабре отмечено резкое понижение температуры соответственно на 1.2ºС и 1.9ºС. Как уже было указано выше, статистическую значимость температурных аномалий оценивали при 5% уровне значимости по критериям Стьюдента. Поскольку степень свободы здесь связана с количеством лет в рассматриваемом временном ряду (40-2=38), по специальной

таблице (Иманов, 2011; Шуленин, 2012) можно определить, что соответствующее критическое значение критерия Стьюдента равно 2.024. Как видно из табл. 1, за исключением февраля, октября и ноября, в остальные месяцы происходили статистически значимые изменения в температурном режиме поверхностных вод Северного Каспия.

Как известно, Средний Каспий занимает большую площадь моря, чем Северный Каспий (Гидрометеорология…, 1992). Как видно из табл. 1, среднегодовое значение ТПМ за период 2001-2021 гг. увеличилось на 0.9ºС по сравнению с периодом 1980-2000 гг. Наибольшее повышение было зафиксировано в августе и сентябре на 1.4 и 1.6ºС соответственно, а наименьшее – в апреле на 0.1ºС. Как видно из таблицы, статистически значимые повышения ТПМ Среднего Каспия происходили во все месяцы, за исключением апреля.

Южный Каспий отличается тем, что он глубже Северного и Среднего Каспия. Как видно из табл. 1, среднегодовые значения ТПМ в Южном Каспии наибольшие, что в основном связано с географическими условиями его расположения. Среднегодовая температура водной поверхности в районе увеличивается с севера на юг (Гидрометеорология...,1992). Как видно из табл. 1, за период 2001-2021 гг. среднегодовая температура поверхности моря увеличилась на 0.7ºС по сравнению с периодом 1980-2000 гг. Наибольшее повышение температуры происходило в июле и августе на 1.1 и 1.3°С соответственно, а наименьшее – в апреле на 0.1°С. За исключением января, апреля, ноября и декабря, в остальные месяцы повышения ТРМ Южного Каспия оказались статистически значимыми (табл.1).

Сравнительный анализ режима ТПМ для разных районов Каспийского моря в отдельные сезоны года позволяет глубже понять процессы, происходящие в гидрологии моря. Хотя данный вопрос детально изучен для прибрежных районов моря по данным контактных наблюдений (Щербак, 1940; Зульфугаров, 1966; Пармузина, 1971; Потайчук, 1978; Гидрометеорология…, 1992; Дьяконов, Ибраев, 2003; Мамедов, 2007; Аллахвердиев, 2016), для районов открытого моря он исследован недостаточно подробно из-за малочисленности или отсутствия наблюдательных пунктов.

Таблица 1

Распределение средней поверхностной температуры моря (ºС) по месяцам в периоды 1980-2000 и 2001-2021 гг., температурные аномалии и их статистическая значимость при 0.05

Периоды	Северный Каспий												
	Январь	Февраль	Март	Апрель	Май	Июнь	Июль	Август	Сентябрь	Октябрь	Ноябрь	Декабрь	Год
1980-2000	1.7	0.4	1.5	8.5	17.1	23.4	26.4	25.2	19.9	13.3	7.2	4.5	12.4
2001-2021	0.6	0.3	2.8	10.3	19.0	24.6	27.1	26.2	20.7	13.7	7.1	2.7	12.9
Аномалия	-1.2	-0.1	1.3	1.8	1.9	1.2	0.7	1.0	0.9	0.4	-0.1	-1.9	0.5
t-тест	-4.0	-0.5	2.9	3.4	5.2	3.0	2.7	3.0	3.1	1.0	-0.3	-4.7	3.6
Статистическая значимость	+	–	+	+	+	+	+	+	+	–	–	+	+
Периоды	Средний Каспий												
1980-2000	7.4	6.6	6.7	9.0	13.6	19.9	24.1	24.8	21.9	17.5	12.7	9.2	14.5
2001-2021	8.1	7.2	7.4	9.1	14.7	21.1	25.1	26.2	23.5	18.7	13.7	9.9	15.4
Аномалия	0.7	0.7	0.7	0.1	1.2	1.2	1.0	1.4	1.6	1.2	1.0	0.7	0.9
t-тест	4.0	3.7	3.5	0.3	4.5	3.1	3.3	3.6	6.2	3.8	3.2	2.9	6.7
Статистическая значимость	+	+	+	–	+	+	+	+	+	+	+	+	+
Периоды	Южный Каспий												
1980-2000	12.2	10.7	10.5	12.8	17.1	22.0	25.0	26.4	24.7	21.5	17.9	14.6	17.9
2001-2021	12.5	11.3	11.2	13.0	17.9	23.0	26.1	27.7	25.7	22.2	18.3	14.8	18.6
Аномалия	0.4	0.6	0.7	0.1	0.8	1.0	1.1	1.3	1.0	0.7	0.5	0.2	0.7
t-тест	1.6	2.6	3.4	0.7	2.4	2.6	3.6	3.8	4.6	2.9	1.7	0.7	4.9
Статистическая значимость	–	+	+	–	+	+	+	+	+	+	–	–	+

Ниже показана динамика среднегодовой ТПМ во всех трех районах Каспийского моря (рис. 1). Как видно, динамика среднегодового повышения ТПМ наблюдается во всех трех частях Каспийского моря, но наибольшее повышение выявлено в Среднем Каспии, а наименьшее – в Северном Каспии. Более высокие ТПМ отмечаются в Южном Каспии (17.0÷19.7ºС), а самые низкие – в Северном (11.0÷13.7ºС). В Среднем Каспии ТПМ колеблется от 13.3 до 16.1ºС. Годы, в которые наблюдаются экстремумы, почти совпадают. Коэффициенты корреляции между ТПМ Северного Каспия и Среднего Каспия, а также Южного Каспия составляют 0.82 и 0.68 соответственно, а между Средним Каспием и Южным Каспием – 0.89.

Для изучения характера изменения ТПМ во времени в различных частях Каспийского моря были рассчитаны соответствующие тренды (табл. 2). Как видно из таблицы, наибольший рост среднегодовой ТПМ в рассматриваемый период отмечен в Среднем Каспии (0.392ºС/10 лет), наименьший – в Северном Каспии (0.202ºС/10 лет) и 0.299ºС/10 лет в Южном Каспии, значения которых близки к полученным в (Гинзбург и др., 2021).

Как уже было упомянуто выше, для определения статистической значимости линейных трендов использовалось неравенство $R/\sigma_R \geq s$. В табл. 3 приведены коэффициенты детерминации и расчетные значения R/σ_R для каждой части Каспийского моря и каждого сезона. Для 40-летнего временного ряда значение s равно 2.02 при уровне значимости 0.05 и 2.7 при уровне значимости 0.01 (Иманов, 2011). С учетом этого и на основании рис. 1 и табл. 3 можно отметить, что линейные тренды среднегодовой ТПМ для всей акватории Каспийского моря статистически значимы на уровне 0.01.

Динамика средней зимней ТПМ Северного, Среднего и Южного Каспия во времени представлена на рис. 2. В отличие от годовой ТПМ, в этом сезоне для разных районов Каспия наблюдалась разная динамика. Как видно из рис. 2, на фоне заметного повышения ТПМ в Среднем Каспии и умеренного ее повышения в Южном Каспии, в Северном Каспии наблюдалось резкое ее снижение. Более высокие температуры отмечаются в Южном Каспии (11.0÷14.0ºС), а самые низкие – в Северном Каспии (0.2÷3.7ºС). В Среднем Каспии температура поверхности колеблется в пределах 6.9÷9.3ºС.

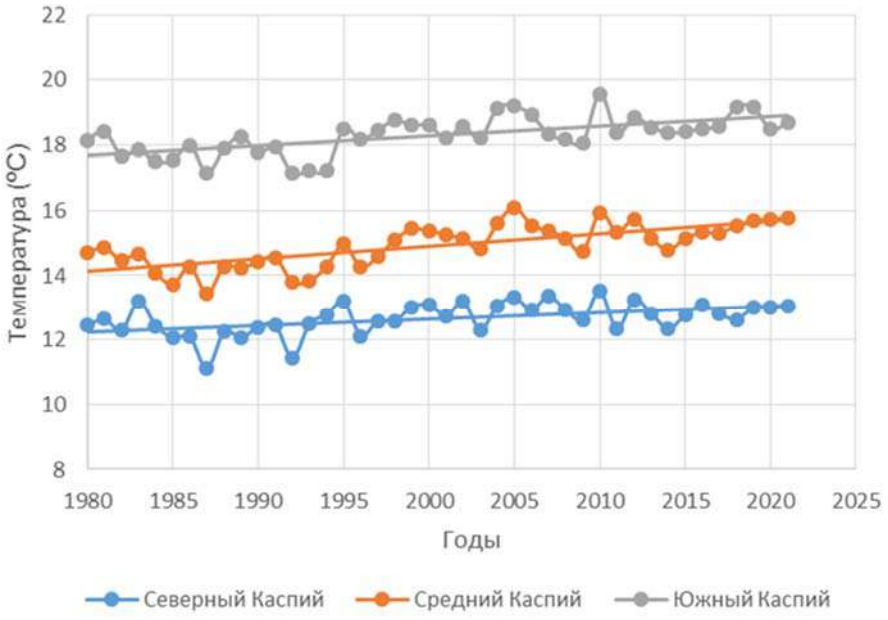


Рис. 1. Временной ход среднегодовой ТПМ в различных частях Каспийского моря

Таблица 2

Линейные тренды (ºС/10 лет) ТПМ Северного, Среднего и Южного Каспия для разных сезонов за 1980-2021 гг.

Акватории Каспия	Год	Зима	Весна	Лето	Осень
Северный	0.202	-0.475	0.743	0.465	0.076
Средний	0.392	0.279	0.263	0.544	0….481
Южный	0.299	0.153	0.277	0.517	0.256

Таблица 3

Коэффициенты детерминации (R^2) и отношения R/σ_R трендов ТРМ для разных сезонов года в акватории Каспийского моря за 1980-2021 гг.

Акватории Каспия	Год		Зима		Весна		Лето		Осень	
	R^2	R/σ_R	R^2	R/σ_R	R^2	R/σ_R	R^2	R/σ_R	R^2	R/σ_R
Северный	0.244	3.50	0.461	5.70	0.417	5.21	0.395	4.98	0.013	0.73
Средний	0.539	6.67	0.297	4.01	0.244	3.50	0.401	5.04	0.380	4.83
Южный	0.399	5.03	0.106	2.12	0.261	3.66	0.375	4.77	0.195	3.04

Хотя годы, в которые наблюдаются экстремумы, несколько перекрываются для Среднего и Южного Каспия, они существенно различаются для Северного Каспия. Об этом также свидетельствуют соответствующие значения коэффициентов корреляции. Так, коэффициент корреляции между ТРМ Северного и Среднего Каспия составляет -0.30, Северного и Южного Каспия – -0.38, а между Средним Каспием и Южным Каспием – 0.72.

В табл. 2 приведены значения линейных трендов средних зимних ТПМ, рассчитанные по рис. 2 для разных районов Каспийского моря. Как видно, в зимний период произошло резкое понижение ТПМ Северного Каспия с отрицательным трендом -0.475 ºС/10 лет. Как уже указывалось выше, в последние годы происходит резкое падение уровня моря (Сафаров и др., 2017; Chen et al., 2017; Arpe et al., 2020; Выручалкина и др., 2020). Температура водной поверхности Северного Каспия, мелеющей с понижением уровня моря, становится более чувствительной к температурным изменениям окружающего воздуха из-за ухудшения вертикального теплообмена (Потайчук, 1978). В дальнейшем, в связи с ожидаемым продолжением падения уровня моря, данная тенденция может усилиться. Как видно из табл. 2, тренды температуры в Среднем и Южном Каспии положительные и составляют 0.279 и 0.153ºС/10 лет соответственно. По табл. 3 можно отметить, что для Северного и Среднего Каспия тренды средней зимней ТРМ статистически значимы на уровне 0.01 и для Южного Каспия – на уровне 0.05.

Весной характер изменения средней ТПМ от года к году в различных частях Каспийского моря также отличается своеобразием (рис. 3). Как видно из рисунка, более высокие температуры наблюдаются в Южном Каспии и имеют возрастающую динамику, колеблются в пределах 12.0÷15.2ºС. Динамика изменения (повышения) температуры Среднего Каспия соответствует Южному Каспию и колеблется в пределах 8.5÷11.3ºС.

Как видно из рис. 3 и табл. 2, динамика повышения ТПМ Северного Каспия стала более резкой и изменялась в диапазоне 6.2÷11.9ºС. В результате этого в период после 2005 г. весенняя ТПМ Северного Каспия быстро повышалась и превышала температуру Среднего Каспия. Основная причина этого в том, что из-за мелководья Северного Каспия его поверхностные воды нагреваются быстрее. В последнее время в связи с понижением уровня моря влияние данного фактора становится все более острым.

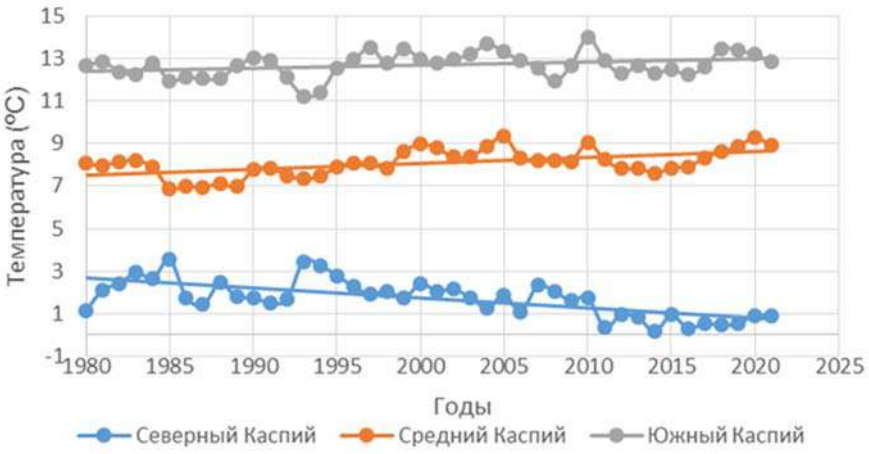


Рис. 2. Временной ход среднезимней ТПМ в различных частях Каспийского моря

Годы экстремальных температур в основном совпадают. Это также находит отражение в значениях коэффициентов взаимной корреляции. Так, коэффициенты корреляции между поверхностными температурами Северного Каспия и Среднего и Южного Каспия составили 0.86 и 0.83 соответственно, а между Средним Каспием и Южным Каспием – 0.84.

На основании рис. 3 рассчитаны линейные тренды ТПМ для каждой части Каспийского моря (табл. 2) и определено, что ее значение для Северного Каспия (0.743ºC/10 лет) значительно больше, чем для Среднего и Южного Каспия (0.263 и 0.267ºC/10 лет соответственно). Более резкое повышение температуры поверхности Северного Каспия связано с глобальным потеплением и резким падением уровня моря.

Как видно из табл. 3, линейные тренды ТПМ для всей акватории Каспийского моря в весенний период статистически значимы на уровне 0.01.

В летний сезон в рассматриваемых частях Каспийского моря характеристики изменений средней ТПМ от года к году отличаются своими особенностями и имеют возрастающую динамику (рис. 4). Как видно из рисунка, летом более высокие ТПМ наблюдаются не в Среднем и Южном Каспии, а в Северном Каспии и колеблются в пределах 23.9÷27.5ºC. Линейный тренд для Южного Каспия проходит примерно на 0.5ºC ниже, чем для Северного Каспия (рис. 4). Годы, в которые наблюдаются экстремумы, в основном совпадают для всех трех областей. Коэффициент корреляции между средними летними ТПМ Северного и Среднего Каспия, а также Северного и Южного Каспия составляет 0.93 и 0.87 соответственно. Между ТПМ Среднего и Южного Каспия также существует достаточно тесная связь (0.2).

Как видно из рис. 4 и табл. 2, летом во всех трех частях Каспийского моря наблюдаются значительные тренды ТПМ (0.465-0.544ºC/10 лет), которые статистически значимы на уровне 0.01.

Осенью характер распределения ТПМ по акватории в основном адекватен географическим широтам. Так, самая высокая температура зафиксирована в Южном Каспии, а самая низкая – в Северном (рис. 5).

Как видно из рис. 5 и табл. 2, средняя осенняя ТПМ Северного Каспия колеблется в пределах 12.1÷15.2ºC и практически не имеет заметного тренда. ТПМ Среднего Каспия колеблется в пределах 15.8÷19.8ºC, а линейный тренд соответствует значительному росту. ТПМ в Южном Каспии колеблется в пределах 19.6÷22.9ºC, а линейный тренд соответствует умеренному росту.

Коэффициент корреляции между средними осенними ТПМ Северного и Среднего Каспия, а также Севернего и Южного Каспия составляет 0.73 и 0.76 соответственно. Между ТПМ Среднего и Южного Каспия также существует достаточно тесная связь (0.93).

Как видно из рис. 5 и табл. 2, в Среднем Каспии наблюдается резкий (0.481ºC/10 лет), а в Южном Каспии значительный положительный (0.256ºC/10 лет) тренд ТПМ. В Северном Каспии заметного тренда ТПМ не наблюдается (0076ºC/10 лет). Как видно из табл. 3, в Среднем и Южном Каспии тренды средне-осенней ТПМ статистически значимы при уровне 0.01, а в Северном Каспии тренд не является статистически значимым даже при уровне 0.05.

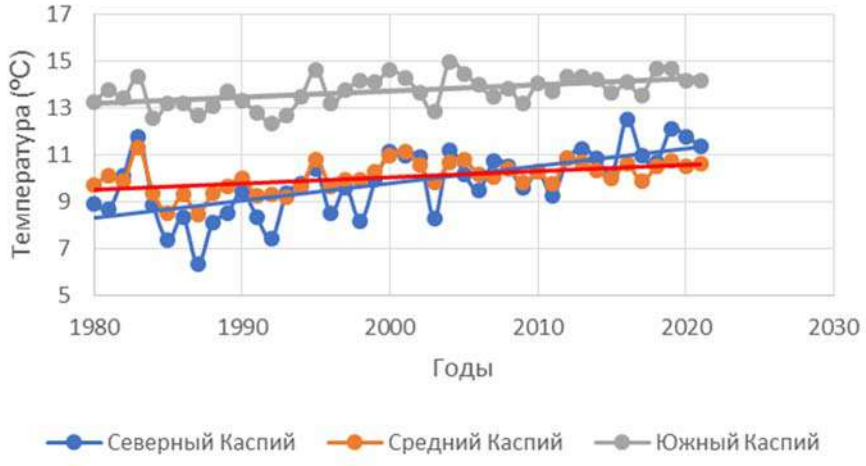


Рис. 3. Временной ход средневесенней ТПМ в различных частях Каспийского моря

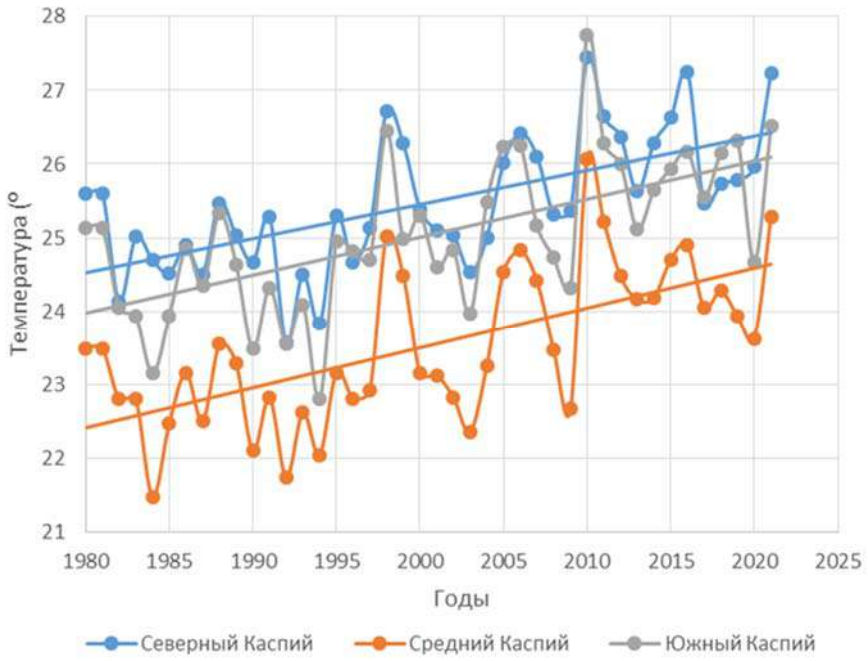


Рис. 4. Временной ход среднелетней ТПМ в различных частях Каспийского моря

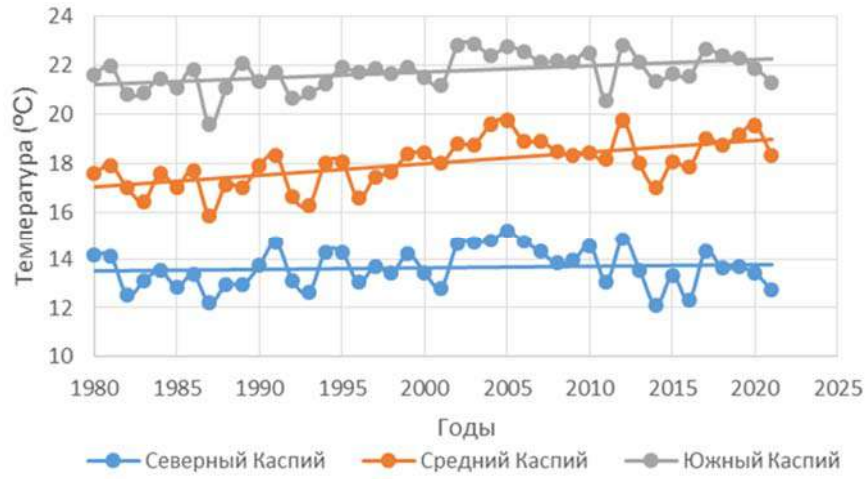


Рис. 5. Временной ход средней осенней ТПМ в различных частях Каспийского моря

Выводы

На основе анализа данных реанализа MERRA-2 по поверхностной температуре Каспийского моря за 1980-2021 гг. были получены следующие результаты:

1. В целом среднегодовая температура поверхности моря уменьшается с юга Каспийского моря на север. Однако весной и особенно в летние месяцы эта закономерность нарушается, так как температура поверхности Северного Каспия весной приближается к температуре Среднего Каспия и даже превосходит ее после 2005 г. Летом самые низкие сезонные температуры наблюдаются в Среднем Каспии, тогда как температура Северного Каспия почти равна температуре Южного Каспия.
2. На фоне глобального потепления и климатических изменений, наблюдается статистически значимые повышения среднегодовой температуры поверхности Северного, Среднего и Южного Каспия, так что в период 2001-2021 гг. по сравнению с периодом 1980-2000 гг. это увеличение составляет 0.4ºC, 0.9ºC и 0.7ºC соответственно.
3. Трендовый анализ показал, что во все сезоны температура поверхности моря в той или иной степени повышается, однако в зимний сезон температура поверхности моря в Северном Каспии имеет тенденцию к значительному снижению, что с большей вероятностью может быть объяснено его обмелением в результате падения уровня моря.

4. В летнем сезоне наибольшие значения температуры поверхности моря наблюдаются в Северном Каспии, что может быть объяснено его мелководьем и постепенным обмелением в связи с падением уровня моря.
5. В условиях глобального потепления и понижения уровня Каспийского моря в разных частях акватории выявлены разные тренды изменения температуры поверхности моря в разные месяцы и сезоны года. Так, в 2001-2021 гг. по сравнению с 1980-2000 гг. в декабре и январе месяцах средняя температура поверхности Северного Каспия снизилась на -1.9ºC и -1.2ºC соответственно, а в апреле и мае повысилась на 1.8ºC и 1.9ºC соответственно, что в основном связано с ускорением обмеления.

Таким образом, на фоне падения уровня моря увеличение контрастов между зимними и весенними поверхностными температурами в Северном Каспии может нарушить традиционные циркуляционные процессы и крайне отрицательно повлиять на экологическое состояние моря, в том числе на его биоразнообразие.

ЛИТЕРАТУРА

Аллахвердиев З.С. Воздействие климатических изменений на температуру поверхности воды западного Каспия (Южная территория Азербайджана). Гидрометеорология и экология. Алматы, вып.1, 2016, с. 41-48.

Водный баланс и колебания уровня Каспийского моря. Моделирование и прогноз. Научно-метод. пособие (под ред. Е.С.Нестерова). Триада-ЛТД. Москва. 2016, 378 с.

Выручалкина Т.Ю., Дианский Н.А., Фомин В.В. Влияние на эволюцию уровня Каспийского моря многолетних изменений режима ветра над его регионом в 1948-2017 гг. Водные ресурсы, No. 2 (47), 2020, с. 230-240.

Гидрометеорология и гидрохимия морей. Проект «Моря». Том VI. Каспийское море. Вып. 1. Гидрометеорологические условия (Под ред. Ф.С.Терзиева, А.Н.Косарева и А.А.Керимова). Гидрометеоиздат. Санкт-Петербург, 1992, 359 с.

Гинзбург А. И., Костяной А. Г., Шеремет Н. А. Динамика зоны апвеллинга у восточного побережья Каспия в сезонном цикле (май-сентябрь) по спутниковым среднемноголетним температурным данным (2003-2019). В: Современные проблемы дистанционного зондирования Земли из космоса. Том 17, No. 7, 2020, с. 215-226, DOI:10.21046/ 2070-7401-2020-17-7-215-226.

Гинзбург А.И., Костяной А. Г., Шеремет Н. А. Сезонная и межгодовая изменчивость температуры поверхности Каспийского моря. Океанология, Т. 44, No. 5, 2004, с. 645-659.

Гинзбург А.И., Костяной А.Г., Серых И.В., Лебедев С.А. Климатические изменения гидрометеорологических параметров Каспийского моря (1980-2020). В: Современные проблемы дистанционного зондирования Земли из космоса. Том 18, No. 5, 2021, с. 277-291, DOI:10.21046/2070-7401- 2021.18.5.277-291.

Гинзбург А.И., Костяной А.Г., Шеремет Н.А. Долговременная изменчивость температуры поверхности Каспийского моря. В: Современные проблемы дистанционного зондирования Земли из космоса. Том 9, No. 2, 2012, с. 262-269.

Дьяконов Г.С., Ибраев Р.А. Динамика вод Каспийского моря над Апшеронским порогом в 2003 году. Морской гидрофизический журнал, Т.35, No. 6, 2019, с. 633-645, https//doi.org/10.22449/0233-7584-2019-6-633-645.

Зулфугаров Т.Х. Об аномалии температуры воды в прибрежных водах западного побережья Среднего Каспия. Труды Азербайджанского Географического Общества. Т. 3, 1966, с. 162-167.

Костяной А.Г., Гинзбург А.И., Лебедев С.А., Шеремет Н.А. Южные моря России. Второй оценочный доклад Росгидромета об изменениях климата и их последствиях на территории Российской Федерации (ред. В.М. Катцов, С.М.Семенов). ИГКЭ Росгидромета и РАН. Москва, 2014, с. 644-683.

REFERENCES

Allahverdiev Z.S. Impact of climate change on water surface temperature in the western Caspian (southern territory of Azerbaijan). Hydrometeorology and ecology. Almaty, Vol. 1, 2016, pp. 41-48 (in Russian).

Arpe K., Molavi-Arabshahi M., Leroy S. Wind variability over the Caspian Sea, its impact on Caspian seawater level and link with ENSO. International Journal of Climatology, No. 14, 2020, pp. 6039-6054/ https://doi.org/10.1002/joc.6564.

Chen J.L., Pekker T., Wilson C.R., Tapley B.D., Kostianoy A.G., Cretaux J.-F., Safarov E.S. Longterm Caspian Sea level change. Geophysical Research Letters, Vol. 44, 2017, pp. 6993-7001, DOI: 10.1002/2017GL073958.

Dyakonov G.S., Ibraev R.A. Dynamics of the waters of the Caspian Sea over the Apsheron threshold in 2003. Marine Hydrophysical Journal, Vol. 35, No. 6, 2019, pp. 633-645, https://doi.org/10.22449/0233-7584-2019-6-633-645 (in Russian).

Ginzburg A.I., Kostianoy A.G., Sheremet N.A. Sea surface temperature variability. In: The Caspian Sea Envoroment. The Handbook of Environmental Chemistry. Springer-Verlag. Berlin Heldeiberg. Vol. 5 Part P, 2005, pp. 59-81, DOI: 10.1007/698 5 004.

Ginzburg A.I., Kostyanoy A.G., Serykh I.V., Lebedev S.A. Climatic changes in hydrometeorological parameters of the Caspian Sea (1980-2020). In: Modern problems of remote sensing of the Earth from space. Vol. 18, No. 5, 2021, pp. 277-291, DOI:10.21046/2070-7401-2021-18.5.277-291 (in Russian).

Ginzburg A.I., Kostyanoy A.G., Sheremet N.A. Dynamics of the upwelling zone near the eastern coast of the Caspian Sea in the seasonal cycle (May-September) according to satellite long-term average temperature data (2003–2019). In: Modern problems of remote sensing of the Earth from space. Vol. 17, No. 7, 2020, pp. 215-226, DOI:10.21046/2070-740-2020-17-7-215-226 (in Russian).

Ginzburg A.I., Kostyanoy A.G., Sheremet N.A. Long-term surface temperature variability of the Caspian Sea. In: Modern problems of remote sensing of the Earth from space. T.9, No. 2, 2012, pp. 262-269 (in Russian).

Ginzburg A.I., Kostyanoy A.G., Sheremet N.A. Seasonal and interannual variability of the surface temperature of the Caspian Sea. Oceanology, Vol. 44, No. 5, 2004, pp. 645-659 (in Russian).

Hydrometeorology and hydrochemistry of the seas. Sea project. Volume VI. Caspian Sea. Issue 1. Hydrometeorological conditions. Edited by F.S.Terzieva, A.N.Kosarev and A.A.Kerimov. Gidrometeoizdat. St. Petersburg, 1992, 359 p. (in Russian).

Imanov F.A. Statistical methods in hydrometeorology. Baku, 2011, 272 p. (in Azerbaijani).

Kostyanoy A.G., Ginzburg A.I., Lebedev S.A., Sheremet N.A. South Seas of Russia. In: The second assessment report of Roshydromet on climate change and its consequences on the

Мамедов Р.М. Гидрометеорологическая изменчивость и экогеографические проблемы Каспийского моря. Элм. Баку, 2007, 453 с.

Пармузина Т.А. Некоторые особенности пространственно-временной изменчивости температуры поверхности Каспийского моря. Труды НИИАК, вып. 76, 1971, с. 74-89.

Потайчук С.И. Изменение температурного режима Северного Каспия при падении и повышении уровня моря. Труды ГОИН, Вып. 139, 1978, с. 65-71.

Рождественский А.В., Лобанова А.Г. Методические рекомендации по оценке однородности гидрологических характеристик и определению их расчетных значений по неоднородным данным. Нестор-История. С-Пб., 2010, 162 с.

Сафаров Э.С., Родриго Абарка Дел-Рио, Сафаров С.Г., Мамедов Р.М., Крето Ж-Ф. Явление Эль-ниньо и колебание уровня Каспийского моря. Гидрометеорология и Экология, No. 1, 2017, с. 7-14.

Сикан А.В. Методы статистической обработки гидрометеорологической информации. РГГМУ. С-Пб., 2007, 279 с.

Шуленин В.П. Математическая статистика. Ч. 1. Параметрическая статистика: учебник. Изд-во НТЛ. Томск, 2012, 540 с.

Щербак С.Я. Температура воды на поверхности в средней и южной частях Каспийского моря. В: Труды по комплексному изучению Каспийского моря. Изд-во АН СССР. Москва-Ленинград, 1940, с. 66-69.

Arpe K., Molavi-Arabshahi M., Leroy S. Wind variability over the Caspian Sea, its impact on Caspian seawater level and link with ENSO. International Journal of Climatology, No. 14, 2020, pp. 6039-6054/ https://doi.org/10.1002/joc.6564.

Chen J.L., Pekker T., Wilson C.R., Tapley B.D., Kostianoy A.G., Cretaux J.-F., Safarov E.S. Longterm Caspian Sea level change. Geophysical Research Letters, Vol. 44, 2017, pp. 6993-7001, DOI: 10.1002/2017GL073958.

Ginzburg A.I., Kostianoy A.G., Sheremet N.A. Sea surface temperature variability. In: The Caspian Sea Envoroment. The Handbook of Environmental Chemistry. Springer-Verlag. Berlin Heldeiberg. Vol. 5 Part P, 2005, pp. 59-81, DOI: 10.1007/698 5 004.

Kazmin A.S. Multidecadal variability of the hydrometeorological parameters in the Caspian Sea. Estuarine, Coastal and Shelf Science, Vol. 250, 2021, 107150, https://doi.org/ 10.1016/ j.ecss.2020.107150.

İmanov F.A. Hidrometeorologiyada statistik metodlar. Bakı, 2011, 272 s.

Məmmədov R.M., Səfərov E.S., Səfərov S.H. Xəzər dənizində səth suları temperaturunun drifterlər vasitəsilə tədqiqi. AMEA Xəbərləri. Yer elmləri seriyası, No. 1, 2012, s. 55-59.

Səfərov S.H., Əhlimanova İ.V., İsmayılov V.Y. Qizilağac körfəzi akvatoriyasinda su səthinin temperaturunun reanaliz məlumatlari əsasinda tədqiqi. "Müasir təbiət və iqtisad elmlərinin aktual problemləri" mövzusunda Beynəlxalq elmi konfrans (Ümummilli Lider Heydər Əliyevin anadan olmasının 99-ci ildönümünə həsr olunub), 3-cü cild, Gəncə ş., 2022, s. 87-88.

territory of the Russian Federation(Ed. V.M.Kattsov, S.M.Semenov), IGKE of Roshydromet and RAS, Moscow, 2014, pp. 644-683 (in Russian).

Kazmin A.S. Multidecadal variability of the hydrometeorological parameters in the Caspian Sea. Estuarine, Coastal and Shelf Science, Vol. 250, 2021, 107150, https://doi.org/ 10.1016/ j.ecss.2020.107150.

Mamedov R.M. Hydrometeorological variability and ecogeographic problems of the Caspian Sea. Elm. Baku, 2007, 453 p. (in Russian).

Mammadov R.M., Safarov E.S., Safarov S.H. Study of the surface temperature regime in the Caspian Sea using drifters. ANAS Proceedings. The Sciences of Earth, No. 1, 2012, pp. 55-59 (in Azerbaijani).

Parmuzina T.A. Some features of space-time variability surface temperature of the Caspian Sea. Proceedings of NIIAK, No.76, 1971, pp. 74-89 (in Russian).

Potaichuk S.I. Changes in the temperature regime of the Northern Caspian during the fall and rise of the sea level. Proceedings of the State Oceanographic Institute, No. 139, 1978, pp. 65-71 (in Russian).

Rozhdestvensky A.V., Lobanova A.G. Guidelines for evaluating homogeneity hydrological characteristics and determination of their calculated values from heterogeneous data. Nestor-Istoriya. St. Petersburg, 2010, 162 p. (in Russian).

Safarov E.S., Rodrigo Abarca Del-Rio, Safarov S.H., Mamedov R.M., Creto J-F. The phenomenon of El Niño and fluctuations in the level of the Caspian Sea. Hydrometeorology and Ecology, No. 1, 2017, pp. 7-14 (in Russian).

Safarov S.H., Ahlimanova I.V., Ismayilov V.Y. Research of water surface temperature in the water area of Kyzilagac Bay based on reanalysis data. International scientific conference on "Current problems of modern natural and economic sciences" (dedicated to the 99th anniversary of the birth of National Leader Heydar Aliyev), Ganja city, Vol. 3, 2022, pp. 87-88 (in Azerbaijani).

Shcherbak S.Ya. Surface water temperature in the middle and southern parts of the Caspian Sea. Proceedings on the integrated study of the Caspian Sea. Publishing House of the Academy of Sciences of the USSR. Moscow-Leningrad, 1940, pp. 66-69 (in Russian).

Shulenin V.P. Mathematical statistics. Part 1. Parametric statistics: textbook. NTL Publishing House. Tomsk, 2012, 540 p. (in Russian).

Sikan A.V. Methods of statistical processing of hydrometeorological information. RGGMU. St. Petersburg, 2007, 279 p. (in Russian).

Vyruchalkina T.Yu., Diansky N.A., Fomin V.V. Effect on the evolution of the Caspian Sea level of long-term changes in the wind regime over its region in 1948–2017. Water resources, No. 2 (47), 2020, pp. 230-240 (in Russian).

Water balance and fluctuations in the level of the Caspian Sea. Modeling and forecast: educational and methodical manual edited by E.S.Nesterov. Triada ltd. Moscow, 2016, 378 p. (in Russian).

Zulfugarov T.Kh. On the anomaly of water temperature in the coastal waters of the western coast of the Middle Caspian. Proceedings of the Azerbaijan Geographical Society, Vol. 3, 1966, pp. 162-167 (in Russian).

ИССЛЕДОВАНИЕ ПОВЕРХНОСТНОЙ ТЕМПЕРАТУРЫ КАСПИЙСКОГО МОРЯ ПО ДАННЫМ РЕАНАЛИЗОВ MERRA-2 ЗА ПЕРИОД 1980-2021 гг.

Сафаров С.Г[1]., Исмайылов В.Г[2]., Сафаров Э.С.[1]
[1]Министерство науки и образования Азербайджанской Республики,
Институт географии имени акад. Г. Алиева, Азербайджан
AZ1070, г. Баку, просп. Г.Джавида, 115: safarov53@mail.ru
[2]Бакинский Государственный Университет, Азербайджан
AZ 1148, Баку, ул.З. Халилов 23: vusalhakimoglu@gmail.com

Резюме. В статье по данным реанализа MERRA-2 за 1980-2021 гг. с применением различных статистических методов изучены изменения поверхностной температуры Северного, Среднего и Южного Каспия и их причины, а также оценены соответствующие линейные тренды. Установлено, что среднегодовая поверхностная температура за период 2001-2021 гг. увеличилась на 0.5ºC в Северном Каспии, на 0.9ºC в Среднем Каспии и на 0.7ºC в Южном Каспии по сравнению с периодом 1980-2000 гг. В условиях глобального потепления и понижения уровня Каспийского моря в разных частях акватории выявлены разные тренды изменения температуры поверхности в разные месяцы и сезоны года. Так, во втором периоде по сравнению с первым, средняя температура поверхности Северного Каспия снизилась соответственно на -1.9ºC и -1.2ºC в декабре и январе и на 1.8ºC и 1.9ºC повысилась в апреле и мае, что в основном связано с ускорением обмеления. Хотя в Среднем и Южном Каспии повышение поверхностной температуры регистрируется во все месяцы, более значительное повышение происходит в более теплые периоды года. В 1980-2021 гг. зимой в Северном Каспии отмечен значительный отрицательный тренд поверхностной температуры, однако в остальные сезоны по всей акватории моря наблюдается положительный тренд. Все тренды, за исключением осеннего в Северном Каспии, оказались статистически значимыми на уровне 0.05, а в большинстве случаев даже на уровне 0.01. Увеличение контрастов между зимними и весенними поверхностными температурами в Северном Каспии на фоне падения уровня моря может крайне отрицательно повлиять на экологическое состояние, в том числе на биоразнообразие моря.

Ключевые слова: *Каспийское море, изменения климата, температура поверхности моря, линейный тренд, изменения уровня моря*

MERRA-2 REANALİZ MƏLUMATLARINA ƏSASƏN 1980-2021 DÖVRÜ ÜÇÜN XƏZƏR DƏNİZİNİN SƏTH TEMPERATURUNUN TƏDQİQİ

Səfərov S.H.[1], İsmayılov V.H.[2], Səfərov E.S.[1]
[1] Azərbaycan Reshublikası Elm və Təhsil Nazirliyiç akademik G.Əliyev adına Coğrafiya İnstitutu, Azərbaycan
AZ1070, Bakı, H.Cavid prosp., 115: safarov53@mail.ru
[2]Bakı Dövlət Universiteti, Azərbaycan
Akademik Zahid Xəlilov küçəsi, 23, Bakı, AZ1148

Xülasə. Məqalədə 1980-2021-ci illər MERRA-2 reanaliz məlumatlarına əsasən və müxtəlif statistik metodların tətbiqi ilə Şimali, Orta və Cənubi Xəzərin səth temperaturunda baş verən dəyişikliklər və onları yaradan səbəblər tədqiq edilmiş, həmçinin müvafiq xətti trendlər statistik üsullarla qiymətləndirilmişdir. Müəyyən edilmişdir ki, 1980-2000 dövrünə nisbətən 2001-2021 dövründə orta illik səth temperaturu Şimali Xəzərdə 0.5 ºC, Orta Xəzərdə 0.9 ºC, Cənubi Xəzərdə isə 0.7 ºC artmışdır. Qlobal istiləşmə və Xəzər dənizi səviyyəsinin azalması şəraitində akvatoriyanın müxtəlif hissələrində səth temperaturunun ilin müxtəlif ay və fəsilləri üzrə fərqli dəyişmə tendensiyaları aşkara çıxarılmışdır. Belə ki, 2-ci dövrdə 1-ci dövrə nisbətən Şimali Xəzərdə orta səth temperaturu dekabr və yanvar aylarında müvafiq olaraq -1.9 ºC və -1.2 ºC aşağı düşmüş, aprel və may aylarında isə müvafiq olaraq 1.8 ºC və 1.9 ºC artmışdır ki, bu da dayazlaşmanın sürətlənməsi ilə əlaqədardır. Orta və Cənubi Xəzər üzrə bütün aylarda səth temperaturunun artımı qeydə alınsa da, daha böyük artımlar ilin daha isti dövrlərini əhatə edir. 1980-2021-ci illərdə qışda Şimali Xəzərin səth temperaturunda əhəmiyyətli mənfi tendensiya qeyd edilsə də, digər mövsümlərdə bütün dəniz akvatoriyası üzrə müsbət tendensiya müşahidə olunur. Şimali Xəzərdə payız fəsli istisna olmaqla, bütün digər temperatur trendləri 0.05ºC, əksər hallarda isə hətta 0.01ºC səviyyəsində statistik əhəmiyyətli olmuşdur. Dəniz səviyyəsinin aşağı düşməsi fonunda Şimali Xəzərdə qış və yaz səth temperaturları arasındakı təzadların artması ekoloji vəziyyətə, o cümlədən dənizin biomüxtəlifliyinə son dərəcə mənfi təsir göstərə bilər.

Açar sözlər: *Xəzər dənizi, iqlim dəyişmələri, dənizin səth temperaturu, xətti trend, dəniz səviyyə dəyişmələri.*

ANAS Transactions Earth Sciences 2 / 2023

http://www.journalesgia.com

МНОГОУРОВНЕВАЯ ТЕХНИЧЕСКАЯ ДИАГНОСТИКА КАК ИНСТРУМЕНТ УПРАВЛЕНИЯ БЕЗОПАСНОСТЬЮ И НАДЁЖНОСТЬЮ ОБЪЕКТОВ НЕФТЕГАЗОВОЙ ОТРАСЛИ

Спасибов В.М., Земенков Ю.Д., Бастриков С.Н., Земенкова М.Ю., Чижевская Е.Л.

Тюменский индустриальный университет, Россия

625000, г.Тюмень, ул. Володарского, 38: spasibovvm@tyuiu.ru

MULTILEVEL TECHNICAL DIAGNOSTICS AS A TOOL FOR MANAGING THE SAFETY AND RELIABILITY OF OIL AND GAS FACILITIES

Spasibov V.M., Zemenkov Y.D., Bastrikov S.N., Zemenkova M.Y., Chizhevskaya E.L.

Industrial University of Tyumen, Russia

38, Volodarskiy str., Tyumen, 625000: spasibovvm@tyuiu.ru

Keywords: *multilevel diagnostics, reliability management, hazardous conditions, safety of process facilities*

Summary. The activity of industrial facilities of the fuel and energy complex is associated with ensuring the reliability, and safety of technological processes and technical diagnostics is one of the effective tools for solving this problem. Of particular importance in this case is the early prediction of an emergency situation for objects with a high accident price. At the same time, two aspects are important. Firstly, it is impossible to miss the signal about the beginning of the development of abnormal operation of the equipment, which inevitably leads to an accident; secondly, it is necessary to clearly filter out false signals, since they can lead to an unmotivated shutdown of the equipment and economic losses. The way out of this situation is possible in the integration of various methods, so that various hindrances, fundamental for one method, have a weak effect on the results given by another method.

The paper considers three diagnostic methods: brittle strain-sensitive coatings, acoustic emission and generation of aerosol particles. The research presented in the paper is aimed at studying the method of early diagnosis of dangerous conditions of objects by combining the methods discussed above. The paper presents the results of experiments in assessing the loading of test samples before plastic deformation and destruction are achieved, which allow us to conclude that a multi-level diagnostic method is possible for early warning of the occurrence of a pre-emergency condition of the object.

© 2023 Earth Science Division, Azerbaijan National Academy of Sciences. All rights reserved.

1. Актуальность

Осуществление деятельности предприятий в современных условиях сопряжено с большим количеством факторов риска, среди которых важную роль играют угрозы безопасности и надежности функционирования хозяйствующих субъектов. Еще в начале XXI века промышленно развитые страны, в первую очередь Россия и США, в качестве одного из основных элементов государственной политики в области национальной безопасности выдвинули задачу защиты критически важных объектов от угроз и чрезвычайных ситуаций техногенного, природного характера, а также от террористических действий. Большинство предприятий нефтегазового комплекса – это сложно построенные технологические объекты, деятельность которых связана с повышенным риском, поэтому они относятся к категории опасных производственных объектов (ОПО). Более того объекты нефтегазовой отрасли относятся к потенциально опасным и критически важным для национальной безопасности объектам, одним из действенных инструментов эффективного управления которыми является формирование стратегии совершенствования технологий мониторинга безопасности и надёжности с учетом требований действующих директивных документов федерального и отраслевого уровня (Земенкова, 2018; Zemenkova et al.,2020, 2021). Обеспечение соблюдения требований федерального законодательства, международных соглашений, отраслевых стандартов и норм, ре-

гламентирующих деятельность в области промышленной безопасности, является обязанностью как нефтегазовых компаний, так и контролирующих органов, общественных организаций. Несмотря на повышенное внимание компаний вопросы создания информационной базы данных, упреждающего мониторинга надежности, безопасности, экологичности промышленных объектов, действующих в режиме реального времени, остаются открытыми и актуальными.

По материалам документа «Основы промышленной политики РФ в области промышленной безопасности (ПБ) до 2025 года и дальнейшую перспективу» (Указ Президента №198) в РФ зарегистрировано более 170 тыс. опасных производственных объектов, причем 60-70% оборудования отработало нормативные сроки службы, а социально-экономический ущерб от аварий может оцениваться в 600-700 млрд. рублей (Zemenkova et al., 2021). Объективно раннее предсказание аварийной ситуации имеет большое значение, особенно для объектов с высокой ценой последствий аварии. Это связано с тем, что по сигналам ранней диагностики становится возможным остановить процесс развития аварийной ситуации до перехода её в необратимую фазу, когда уже приходится разбираться с последствиями аварии – человеческими жертвами и огромными экономическими потерями. В этой деятельности крайне важны два аспекта. Во-первых, никак нельзя пропустить сигнал о начале развития нештатной ситуации в работе оборудования, неминуемо приводящей к аварии; во-вторых, необходимо чётко отфильтровывать ложные сигналы, так как они могут привести к немотивированной остановке оборудования и экономическим потерям.

Для решения задачи диагностирования и раннего предупреждения о возникновении предаварийного состояния объекта исследования применяют различные средства технической диагностики и неразрушающего контроля (ТД и НК): локальные, интегральные и расчётные. К локальным средствам относят тензометрический, визуальный, ультразвуковой, магнитный, радиационный и вихревой контроль (Клюев, 2003). Они, как правило, могут дать точечную информацию о напряжённо-деформированном состоянии конструкции на месте их установки (тензорезисторы, ультразвуковые преобразователи и радиационные устройства) или зарегистрировать факт начала разрушения конструкции (системы видеонаблюдения). К интегральным средствам диагностирования относятся акустико-эмиссионный метод, термоэмиссионный, рентгенографический, а также метод фотоупругих и хрупких покрытий (Kobayashi, 1987; Махутов и др., 2011). Другим направлением НК можно считать метод счётной концентрации аэрозолей в контролируемом пространстве (Райст, 1987), активно развиваемый в настоящее время для диагностики состояния технически сложных и опасных систем. Принцип регистрации отдельных микрочастиц представляет возможности обнаружения аварийных ситуаций различной природы. Это связано с тем, что практически любое значительное изменение режима работы систем или нарушение хода технологических процессов сопровождается резким увеличением выбросов микрочастиц в сопредельном пространстве. В процессе испытания и эксплуатации диагностируемых объектов эти методы позволяют получать интегральную картину напряжённо-деформированного состояния в зоне исследования, своевременно обнаруживать развивающиеся напряжения, определять пространственные координаты разрушения, устанавливать их характер и степень опасности.

Применение существующих методов НК для диагностирования объектов не является достаточной мерой, которая обеспечивает предупреждение и предотвращение разрушений. Целесообразно проводить мониторинг, сочетая различные методы диагностики, что обусловлено необходимостью, во-первых, учета факторов, влияющих на повреждаемость конструкций, а во-вторых, повышения вероятности выявления потенциально опасных и сложно идентифицируемых дефектов с применением других методов контроля. Комплексное использование методов диагностики, наряду с повышением вероятности обнаружения мест повреждения объектов, позволит более достоверно определять напряжённо-деформированное состояние элементов конструкций, контролировать усадки, регистрировать смещения и нарастание деформаций в несущих элементах конструкции, оценивать их текущее состояние и выделять зоны, наиболее подверженные опасности разрушения.

При одновременном применении различных методов важно учитывать, чтобы различные помехи, принципиальные для одного метода, оказывали слабое влияние на результаты, получаемые с использованием другого. Такой подход в совокупности с адекватной обработкой результатов позволит выдавать надёжные данные в начале аварийного развития процесса. Например, для нефтегазовой отрасли – области, где цена аварии действительно очень высока, в целях предотвращения разрыва магистрального трубопровода высокого давления предпочтительным является иметь методы диагностики, основанные на разных физических принципах. Речь идёт о методах,

перспективной целью которых является определение времени безопасной работы оборудования при обнаружении сигнала о начале аварийного процесса. Это даёт возможность при наличии модели развития аварийной ситуации принять обоснованное решение – немедленно останавливать работу либо без серьёзной опасности продолжать работу оборудования до следующего планового ремонта. Такой подход сулит существенные экономические выгоды, но требует создания моделей аварии и методов ранней диагностики комплексного вида.

Работа направлена на исследование способа многоуровневой диагностики штатных и опасных состояний технических объектов, включающего совместное применение трёх методов диагностики: акустическая эмиссия, генерация аэрозольных частиц и хрупкие тензочувствительные покрытия. Известна высокая чувствительность первых двух методов к механическим напряжениям металлов. Для ещё большего повышения чувствительности к напряжениям используется хрупкое покрытие основного металла, в котором трещины появляются значительно раньше, чем в собственно металле. Появление трещин сопровождается акустической эмиссией и генерацией аэрозольных частиц. Таким образом, применяется три различных метода ранней диагностики в реальном времени. Результаты исследований первого этапа их совместного применения продемонстрированы в данной статье.

2. Методы исследования

Экспериментальные исследования, с целью оценки возможности реализации способа многоуровневой диагностики состояний технических объектов, осуществлялись посредством нагружения двух образцов (№3 и №4) с хрупким тензочувствительным покрытием и двух образцов (№1 и №2) без покрытия до уровня достижения пластической деформации и разрушения опытных образцов, регистрации сигналов акустической эмиссии (АЭ) и концентрации аэрозольных частиц. Исследования проводились на экспериментальной базе Федерального государственного бюджетного учреждения «Институт машиноведения им. А.А.Благонравова Российской академии наук». В качестве образцов использовались плоские пластины толщиной 2 мм из высокопрочного алюминиевого сплава В95. Согласно справочным данным (Серенсен и др., 1975) сплав В95 имеет следующие механические характеристики: σ_B=520 МПа, σ_{02}=440 МПа, E=0.7.10-5 МПа. На рис.1 приведены основные размеры испытуемого образца, а также показаны места установки оксидного тензоиндикатора и широкополосных преобразователей акустической эмиссии (ПАЭ) G 200, используемых для регистрации сигналов акустической эмиссии в процессе нагружения образцов.

Следует отметить, что ПАЭ устанавливались на противоположной относительно оксидного тензоиндикатора стороне образца. На самом же тензоиндикаторе в средней его части герметично крепилась приёмная камера, позволяющая регистрировать выбросы микрочастиц в процессе образования трещин в оксидной плёнке тензоиндикатора с применением лазерного аэрозольного счетчика Lighthouse Handheld 3106. В качестве хрупких покрытий использовались оксидные тензоиндикаторы, разработанные ИМАШ и предназначенные для проведения исследований в области упругих и упругопластических деформаций (от 400 до 4000 мкм/м) при температурах от -200 до +200^{0}C в различных средах (вода, масло, жидкий азот) в течение длительного времени эксплуатации (не менее 5 лет). Хрупкий оксидный тензоиндикатор (Пригоровский, Панских, 1978; Пригоровский, 1983) представляет собой тонкую алюминиевую фольгу, подвергнутую электрохимическому анодированию для получения оксидной пленки Al_2O_3 (толщиной 10–40 мкм) и наклеенную на исследуемый элемент конструкции.

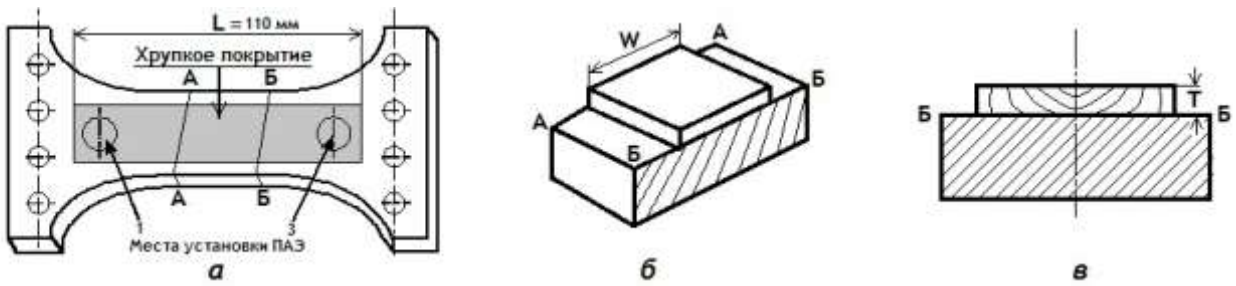


Рис. 1. Схема расположения ПАЭ на испытательном образце (*а*);
сечение образца и хрупкого покрытия (*б*); схема образования и распространения трещины в хрупком покрытии (*в*)

При возникновении в подложке алюминиевой фольги деформаций ε_1, превышающих величину пороговой деформации ε_o (для образца №3 – 1000 мкм/м и 1500 мкм/м для образца №4), в оксидной пленке тензоиндикатора образуются картины трещин, отражающие поле наибольших деформаций на поверхности конструкции. Используя характеристики тензочувствительности тензоиндикаторов (ε_o, σ_o) и график изменения численности трещин в оксидной пленке (Ψ) от уровня деформаций в подложке, представляется возможным произвести оценку значений наибольших деформаций (напряжений) на поверхности исследуемой конструкции в области распространения трещин с погрешностью не большей 20%.

Нагружение образцов при испытаниях производилось на электрогидравлической установке MTS, позволяющей создавать усилие до 50 т, и проводить испытания как в ручном, так и автоматическом режиме нагружения с заданной скоростью приложения нагрузки. При этом диаграмма нагружения может быть построена в координатах нагрузка – время, либо нагрузка – удлинение.

С целью настройки применяемой аппаратуры, определения уровня нагрузок, требуемых для пластического деформирования и разрушения объектов исследования, отработки оптимальных режимов нагружения были проведены тестовые испытания образцов (№1 и №2) без тензопокрытий.

Образец устанавливался в захваты верхней и нижней траверсы испытательного стенда, после чего к нему через слой смазки крепились широкополосные преобразователи акустической эмиссии G 200 (рис. 2).

При проведении экспериментов для исследования метода АЭ применялась многоканальная многопараметрическая акустико-эмиссионная система A-Line 32D и широкополосные акустико-эмиссионные преобразователи (ПАЭ) ***G-200*** с резонансной частотой 150 кГц. Предварительные усилители имели полосу пропускания 30-500 кГц, а коэффициент усиления 26 дБ. При испытаниях образцов использовались два ПАЭ, устанавливаемые на расстоянии 110 мм, как показано на рис.1. Скорость ультразвуковых волн при вычислении координат источников АЭ принималась равной 3000 м/с.

Перед проведением испытаний исследуемых образцов была выполнена калибровка ПАЭ и каналов аппаратуры АЭ. При калибровке использовались:

– имитатор АЭ – источник Су-Нильсена;

– электронный калибратор AECAL-2 (фирма PAC (США).



Рис. 2. Вид образца с тензопокрытием и преобразователями сигналов АЭ на стенде MTS

Используемая в процессе испытаний многоканальная многопараметрическая акустико-эмиссионная система, регистрируя и обрабатывая импульсы АЭ, формирует блок информации, характеризующий поступившее в канал событие:

- время регистрации сигнала – момент времени первого превышения порога дискриминации;
- время нарастания импульса – интервал между началом импульса и моментом, когда амплитуда достигнет максимальной величины;
- длительность импульса – интервал между началом импульса и моментом, когда амплитуда сигнала станет ниже порога дискриминации;
- количество выбросов импульсов – число пересечений установленного порогового уровня амплитуды внутри сигнала;
- амплитуду импульса – максимальное значение амплитуды сигнала;
- энергию импульса.

3. Результаты и обсуждение

Согласно принятому в Механике и Физике Разрушения положению «Акустическая эмиссия (АЭ) – испускание объектом контроля (испытаний) акустических волн» (Иванов и др., 2005), данное определение охватывает весьма широкий круг явлений. В данной работе с целью диагностики процессов разрушения оксидных тензоиндикаторов и подложки при испытаниях образцов на разрыв регистрировалась акустическая эмиссия материалов. Данный метод АЭ позволяет класси-

фицировать дефекты не по размерам, а по степени их влияния на прочность объекта. В такой классификации может оказаться, что большие по размерам дефекты попадут в класс неопасных, не требующих ремонта элементов конструкции.

Как при пластической деформации, так и при образовании и росте трещин, которые являются импульсными процессами, основным элементом сигнала АЭ является единичный импульс, образующийся за счёт разрыва атомной связи. Разрыв носит скачкообразный характер, он сопровождается релаксацией других атомных связей и излучением импульса упругих колебаний от места разрыва. Этот элементарный импульс АЭ, который можно описать в терминах квантовой механики, был назван фрактоном (Иванов и др., 2005). Энергия такого элементарного импульса составляет единицы эВ. При пластической деформации, являющейся процессом массового образования и движения дислокаций, генерируется последовательность импульсов, которая после прохождения акустико-электронного канала, включающего Источник АЭ → Контролируемый объект → Преобразователь АЭ → Система АЭ, трансформируется в акустический сигнал, представленный на рис. 3.

Регистрация сигналов АЭ представляет собой импульсный стохастический процесс, составляющий поток импульсов, которые можно принять раздельно, либо слившимися в непрерывный поток, как это видно из записи сигналов на рис. 3. В параметрах этого процесса и зависимостях от времени и нагрузки содержится информация о состоянии деформирования и разрушения диагностируемого объекта. При этом основными наиболее информативными параметрами и зависимостями процесса АЭ являются: зависимость суммы импульсов АЭ, активности АЭ, амплитуды импульсов АЭ, энергии АЭ от времени и нагрузки.

На рис. 4 показаны этапы нагружения и зависимости параметров АЭ при упругой и пластической деформации гладких образцов на растяжение.

Этапы от 0 деформации до Δl = 1мм соответствуют упругому участку деформирования. Сигналы АЭ, зарегистрированные на этом участке, возникают в результате релаксации напряжений на неоднородностях структуры образцов. Активная АЭ возникает при начале пластической деформации материала. Для реального объекта глобальная пластическая деформация не допускается. Поэтому необходим индикатор, свидетельствующий, что деформации не достигли критического уровня. Таким индикатором и служит хрупкое тензопокрытие с величиной пороговой деформации значительно меньшей предела текучести материала диагностируемой конструкции.

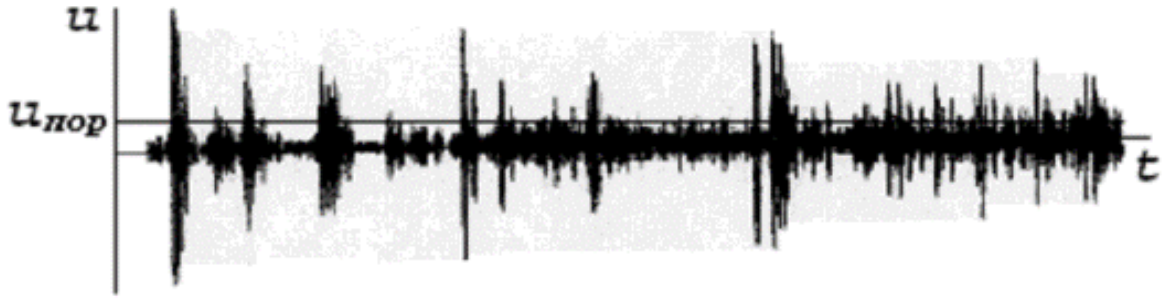


Рис. 3. Запись процесса АЭ, полученная при натурных испытаниях

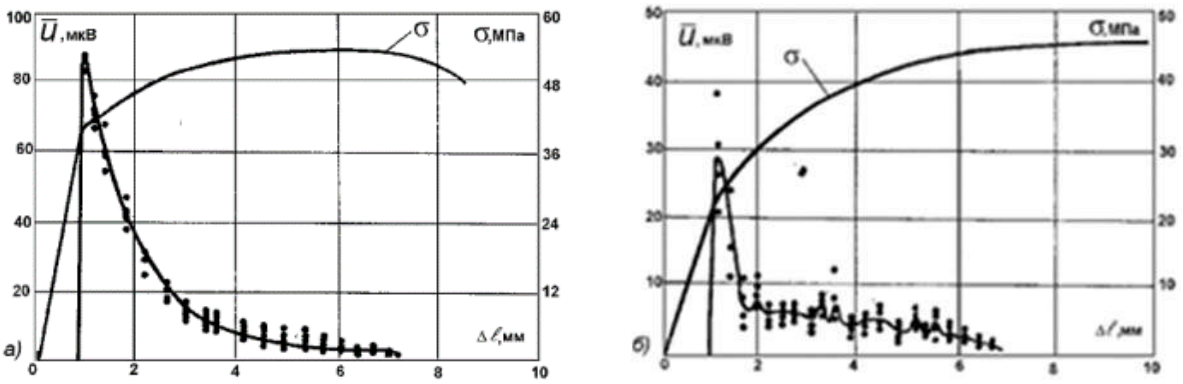


Рис. 4. Зависимости среднеквадратического значения АЭ ū и механического напряжения σ от удлинения Δl при растяжении гладких образцов из стали 10ГН2МФА (*а*) и стали 10 (*б*)

Результаты выполненных исследований по диагностике процесса разрушения оксидных тензоиндикаторов и материала подложки при испытаниях образцов №1-4 на разрыв приведены на рис. 5-8. При этом на всех графиках параметров акустической эмиссии отражено изменение уровня растягивающего усилия на образце.

Диагностика процесса разрушения образца №1 при испытании на разрыв. На рис. 5 приведены графики изменения ***суммы импульсов АЭ*** (***N***) и уровня нагрузки (***P***) от времени (τ).

Активность АЭ пропорциональна нагрузке, она возрастает при приближении к области пластической деформации и уменьшается после начала пластической деформации (рис. 5***а***, 5***б***).

Амплитуда сигналов АЭ (рис. 5***в***) максимальна при уровне нагрузки, соответствующей началу пластической деформации материала, и достигает 75 дБ. ***Энергия*** АЭ сигналов при этом составляет 105 дБ (рис. 5***г***). Затем ***амплитуда*** и ***энергия*** сигналов АЭ заметно падает и составляет перед разрушением образца 55 и 90 дБ соответственно.

Диагностика процесса разрушения образца №2 при испытании на разрыв. На рис. 6 приведены графики изменения ***суммы импульсов АЭ*** (***N***) и уровня нагрузки (*P*) от времени (τ).

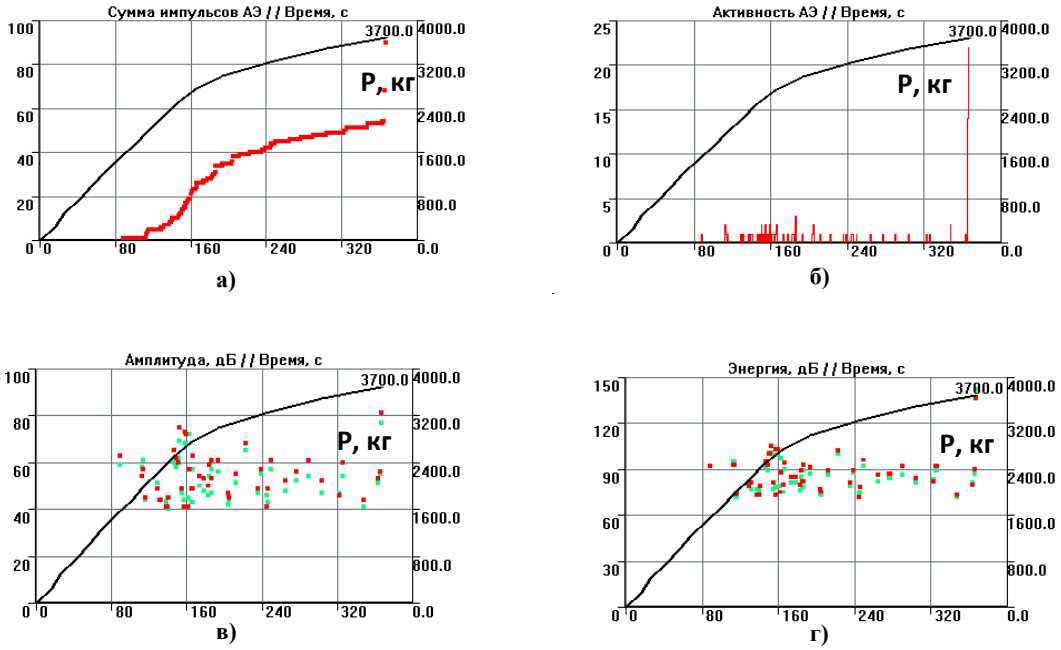


Рис. 5. Параметры сигналов АЭ, регистрируемые при испытании образца №1

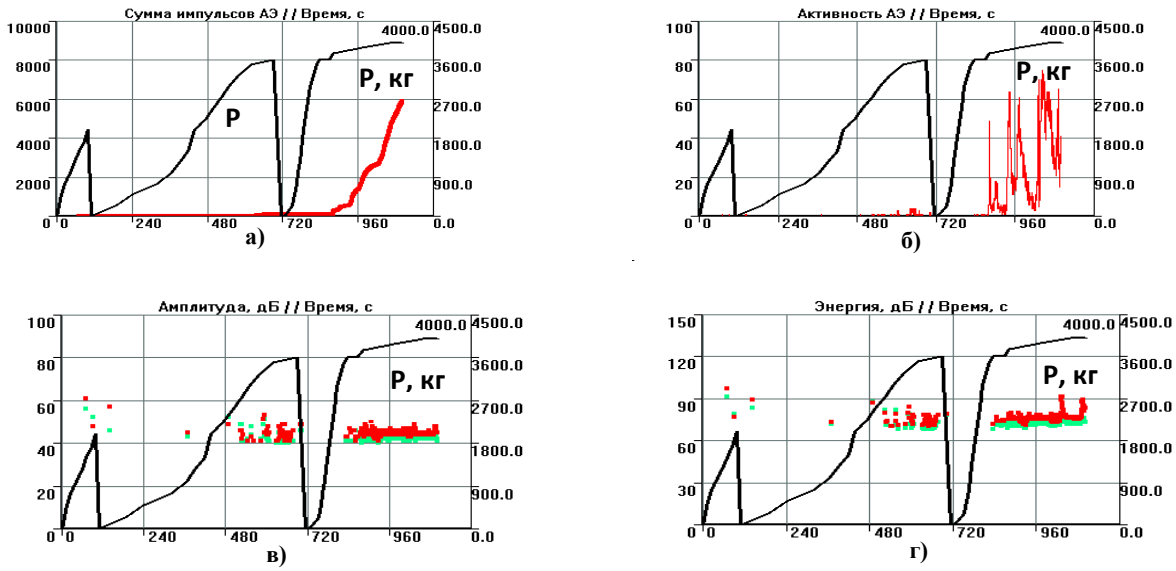


Рис. 6. Параметры сигналов АЭ, регистрируемые при испытании образца № 2

Активность АЭ (рис. 6***а*** и 6***б***) возрастает в начале области пластической деформации при ***P***=27 кН. Затем ***активность*** АЭ резко возрастает при нагружении свыше ***P***=36 кН. ***Амплитуда*** единичных АЭ сигналов (рис. 6***в***) максимальна в области упругой деформации и достигает 60 дБ. ***Энергия*** АЭ сигналов – 95 дБ (рис. 6***г***). С ростом ***активности амплитуда*** и ***энергия*** сигналов АЭ заметно падает до 52 и 80 дБ соответственно. При повторном нагружении и перед разрушением ***амплитуда*** сигналов АЭ не превышает 50 дБ, энергия – 90 дБ.

Диагностика процесса разрушения образца №3 (с тензопокрытием) при испытании на разрыв. На рис. 7 приведены графики изменения ***суммы импульсов АЭ*** (***N***) и уровня нагрузки (***P***) от времени (τ).

Активная регистрация сигналов АЭ (рис. 7***а*** и 7***б***) начиналась при ***P***=5.8 кН (в области упругих деформаций) и продолжается до 25.0 кН. Дальнейшее увеличение нагрузки сопровождалось новым ростом активности АЭ, что наблюдалось на всех циклах нагружения образца. Наибольшая ***активность*** АЭ имела место при повышении нагрузки от 40 до 42.5 кН. При выдержке на этом уровне ***активность*** сигналов АЭ заметно уменьшилась, а на этапе разгрузки образца не наблюдалась. АЭ вновь была зарегистрирована после подъема нагрузки до 42.50 кН и резко возросла по истечении 60 секундной выдержки при 42.5 кН, что свидетельствовало о высоком уровне пластических деформаций в зоне разрушения образца, когда её рост происходил без увеличения нагрузки. На этапе разгрузки образца активность АЭ упала до нуля. В следующем цикле нагружения ***активность*** АЭ наблюдалась уже при малых значениях нагрузки и постоянно возрастала вплоть до момента разрушения.

Амплитуда сигналов АЭ достигает максимума уже на первых циклах испытания при повышении нагрузки от 15 до 30 кН (рис. 7***в***) и составляет 90-95 дБ, а максимальная ***энергия*** достигает 130 дБ (рис. 7***г***). В последующих циклах, несмотря на повышение нагрузки и ***активности*** АЭ, ***амплитуда*** и ***энергия*** АЭ сигналов заметно падает (до 50 и 80 дБ соответственно). Усредненные значения ***амплитуды*** и ***энергии*** сигналов АЭ в дальнейшем заметно падают, несмотря на рост нагрузки. В момент разрушения ***амплитуда*** и ***энергия*** сигналов АЭ составляют 50 и 90 дБ соответственно.

Диагностика процесса разрушения образца №4 (с тензопокрытием) при испытании на разрыв. На рис. 8 приведены графики изменения суммы импульсов АЭ (***N***) и уровня нагрузки (***P***) от времени (τ).

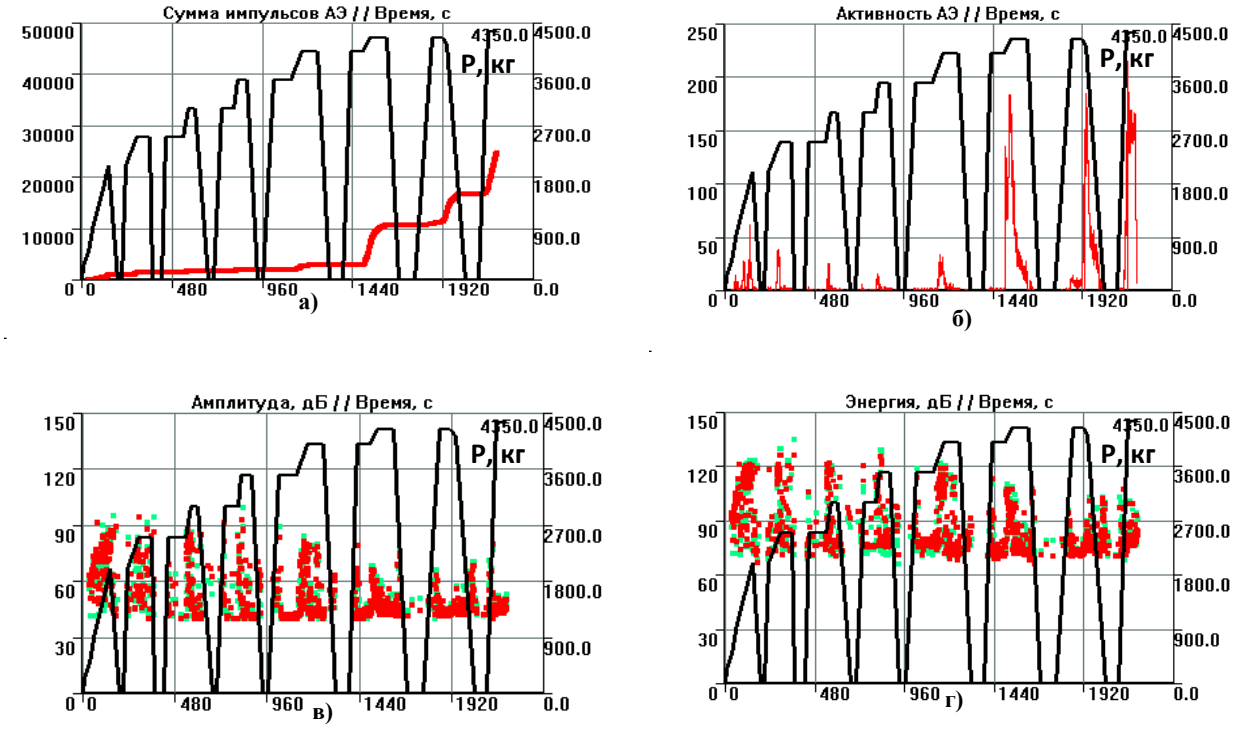


Рис. 7. Параметры сигналов АЭ, регистрируемые при испытании образца №3

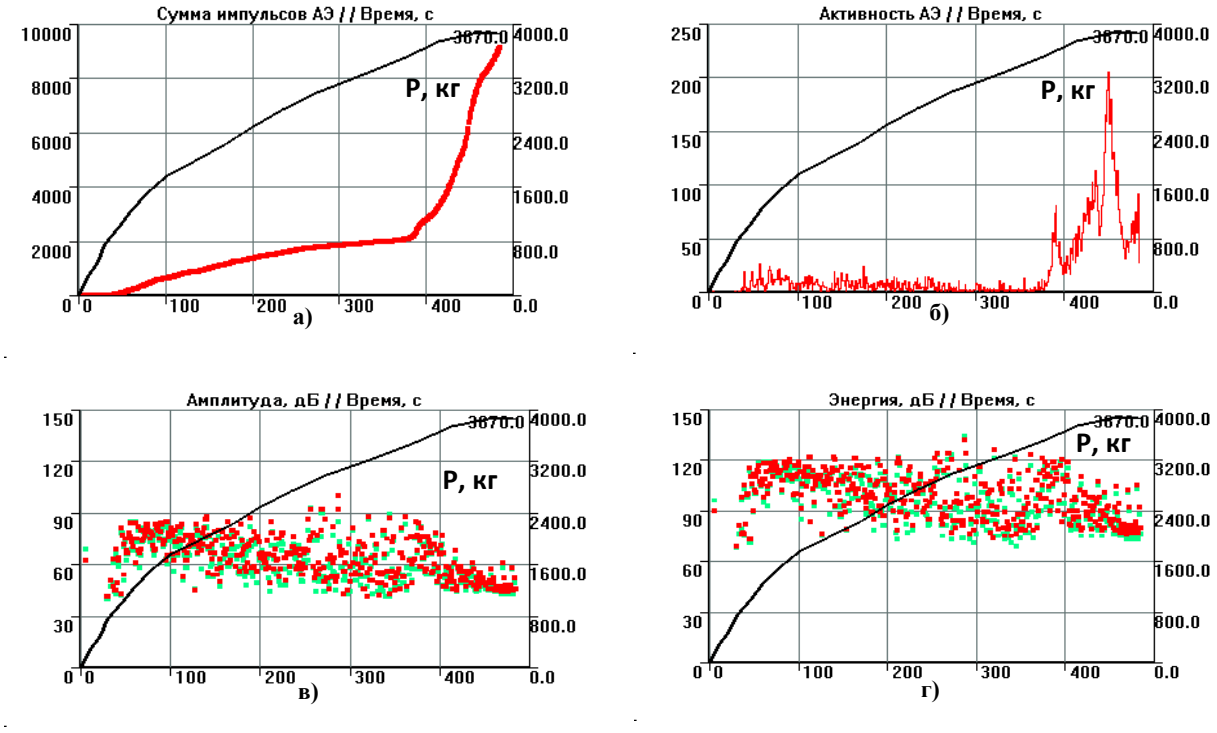


Рис. 8. Параметры сигналов АЭ, регистрируемые при испытании образца №4

Активность сигналов АЭ (рис. 8***а***, 8***б***) заметна уже в начале области упругой деформации при ***P***=7.5 кН и постепенно возрастает с ростом нагрузки до уровня ***P***=34.5 кН, соответствующей началу перехода материала образца в область пластической деформации. Затем ***активность*** сигналов АЭ резко повышается и достигает своего максимума при ***P***=38.25 кН, после чего активность АЭ заметно снижается и вновь возрастает лишь перед разрушением образца.

Амплитуда сигналов АЭ достигает 90 дБ уже в начале нагружения и повышается до 95 дБ при *P*= 34.50 кН (рис. 8***в***). При этом ***энергия*** сигналов АЭ достигает 125 дБ (рис. 8***г***). С ростом ***активности*** сигналов АЭ ***амплитуда*** и ***энергия*** сигналов заметно падает до 60 и 105 дБ соответственно. Перед разрушением образца ***амплитуда*** АЭ сигналов не превышает 60 дБ, а энергия – 90 дБ.

Сравнительный анализ результатов диагностики образцов №2 и №4. Так как диаграммы нагружения этих образцов были близки, то представляется интересным сопоставить результаты акустико-эмиссионной диагностики образца №2 (без тензоиндикатора) и образца №4 (с тензоиндикатором).

Активность АЭ. Образец №4 – ***активность*** АЭ наблюдается уже при нагрузке 8 кН и постепенно возрастает до уровня, соответствующего области пластической деформации. Затем резко возрастает в начальный момент структурной перестройки, потом падает и вновь возрастает перед разрушением образца (рис. 8***б***).

Образец №2 – ***активность*** АЭ резко возрастает в области пластической деформации и растет вплоть до разрушения (рис. 6***б***).

Общее число зарегистрированных сигналов АЭ в образце №4 оказалось в полтора раза большим, чем в образце № 2 (рис. 8***а*** и 6***а***).

Вывод: ***Активность*** АЭ в образце №4 в области упругих деформаций вызвана образованием трещин в тензоиндикаторе. В области пластической деформаций ***активность*** АЭ вызвана структурной перестройкой материала подложки и его разрушением.

Амплитуда АЭ сигналов

Образец №4 – максимальная ***амплитуда*** до 85 дБ наблюдается в области упругих деформаций, затем снижение уровня до 55 дБ перед разрушением образца (рис. 8***в***).

Образец №2 – максимальная ***амплитуда*** до 50 дБ в начале области пластической деформации, затем снижение до 45 дБ перед разрушением образца (рис. 6***в***).

Вывод: сигналы АЭ с большой ***амплитудой*** в образце №4 вызваны образованием трещин в тензопокрытии, сигналы АЭ с малой ***амплитудой*** вызваны структурной перестройкой и разрушением материала подложки.

Энергия сигналов АЭ

Образец №4 – максимальная энергия до 125 дБ наблюдается в области упругой и малых упруго-пластических деформаций, затем снижение до 100 дБ перед разрушением образца (рис. 8***г***).

Образец №2 – максимальная *энергия* до 90 дБ в начале области пластической деформации, затем снижение до 75 дБ перед разрушением образца (рис. 6*г*).

Вывод: сигналы АЭ с большой ***энергией*** в образце №4 вызваны образованием трещин в тензопокрытии, сигналы АЭ с малой ***энергией*** в области пластических деформаций вызваны структурной перестройкой и разрушением материала подложки.

4. Заключение

1. Акустико-эмиссионная диагностика состояния оксидных тензоиндикаторов и материала подложки, проведенная при испытаниях образцов на разрыв, показала высокую эффективность предложенного метода неразрушающего контроля. Экспериментально полученные основные параметры сигналов АЭ в процессе разрушения оксидных тензоиндикаторов и материала подложки могут быть использованы в системах многоуровневой диагностики и раннего предупреждения о возникновении и развитии опасных состояний в контролируемых объектах.

2. Совместное использование оксидных тензоиндикаторов и акустико-эмиссионной системы A-Line 32D позволило с высокой степенью надежности контролировать весь процесс нагружения образцов, начиная от упругих деформаций порядка 0.05% и до значительных пластических деформаций 5-7%, при которых происходило их разрушение. При этом по уровню ***активности*** сигналов АЭ, их ***амплитуде*** и ***энергии*** можно контролировать динамику изменения напряженного состояния, возникновение зон пластических деформаций, их рост, предельное состояние образцов перед разрушением.

3. Сигналы АЭ, вызываемые образованием трещин в тензоиндикаторах и возникающие при структурных изменениях и разрушении материала подложки, достаточно хорошо различаются по таким параметрам, как ***амплитуда***, ***энергия*** и ***активность*** АЭ.

4. Разрабатываемый многоуровневый метод комплексной диагностики, наряду с повышением вероятности обнаружения мест накопления повреждений, позволяет с высокой степенью надежности контролировать нагруженность диагностируемого объекта, сигнализируя о возникновении потенциальных угроз (по скорости и уровню роста деформаций) задолго до возникновения необратимых структурных изменений в материале конструкции.

5. Использование многоуровневого метода комплексной диагностики позволит обеспечить решение важнейшей задачи управления современным предприятием – обеспечения устойчивого, безопасного и надежного функционирования за счет раннего предупреждения и предотвращения аварийных ситуаций и ущербов, в том числе в условиях опасных производственных объектов.

Авторы благодарят за поддержку данного исследования национальный проект «Наука и университеты» Министерства науки и высшего образования Российской Федерации (FEWN-2021-0012).

ЛИТЕРАТУРА

Земенкова М.Ю. Методологическое обеспечение экспертных систем мониторинга показателей надежности объектов трубопроводного транспорта углеводородов. ТИУ. Тюмень, 2018, 411 с.

Иванов В.И., Власов И.Э. Метод акустической эмиссии. В книге: Неразрушающий контроль: Справочник. Том 7. Книга 1. Машиностроение. Москва, 2005, 340 с.

Махутов Н.А., Шемякин В.В., Ушаков Б.Н., Петерсен Т.Б., Васильев И.Е. Применение акустической эмиссии для контроля за процессом образования трещин в хрупких оксидных тензоиндикаторах. Заводская лаборатория. Диагностика материалов, Том 77, No. 6, 2011, с.41-44.

Клюев В.В. (под ред.). Неразрушающий контроль и диагностика. Справочник 2–е изд. Машиностроение. Москва, 2003, 656 с.

Пригоровский Н.И. Методы и средства определения полей деформаций и напряжений. Машиностроение. Москва, 1983, 248 с.

Пригоровский Н.И., Панских В.К. Метод хрупких тензочувствительных покрытий. Наука. Москва, 1978, 183 с.

Райст П. Аэрозоли. Введение в теорию. Мир. Москва, 1987, 278 с.

Серенсен С.В., Когаев В.П., Шнейдерович Р.М. Несущая способность и расчеты деталей машин на прочность. Машиностроение. Москва, 1975, 488 с.

REFERENCES

Ivanov V.I., Vlasov I.E. Acoustic emission method. In the book: Non-destructive testing: A Reference book. Vol. 7. Book 1. Mechanical engineering. Moscow, 2005, 340 p. (in Russian).

Kobayashi A.S. Handbook on experimental mechanics. Prentice-Hall. Society for Experimental Mechanics, Inc. New Jercey, 1987, 1002 p., https://doi.org/10.1111/j.1747-1567.1989.tb01038.x.

Makhutov N.A., Shemyakin V.V., Ushakov B.N., Petersen T.B., Vasiliev I.E. The use of acoustic emission to control the process of crack formation in brittle oxide strain gauges. Factory laboratory. Diagnostics of materials, Vol. 77, No. 6, 2011, pp. 41-44 (in Russian).

Klyuev V.V. (ed.). Non-destructive testing and diagnostics. Handbook. 2nd ed. Mechanical Engineering. Moscow, 2003, 656 p. (in Russian).

Prigorovsky N.I. Methods and means of determining fields of deformations and stresses. Mechanical engineering. Moscow, 1983, 248 p. (in Russian).

Prigorovsky N.I., Panskikh V.K. The method of brittle strain-sensitive coatings. Nauka. Moscow, 1978, 183 p. (in Russian).

Raist P. Aerosols. Introduction to theory. Mir. Moscow, 1987, 278 p. (in Russian).

Serensen S.V., Kogaev V.P., Shneiderovich R.M. Load-bearing capacity and calculations of machine parts for strength. Me-

Kobayashi A.S. Handbook on experimental mechanics. Prentice-Hall. Society for Experimental Mechanics, Inc. New Jercey, 1987, 1002 p., https://doi.org/10.1111/j.1747-1567.1989.tb01038.x.

Zemenkova M.Y., Gladenko A.A., Zemenkov Y.D. Innovative intelligent technologies for predictive reliability and risk management in oil and gas transport and storage systems. AIP Conference Proceedings. Omsk, Vol. 2285, 2020, pp. 050012, https://doi.org/10.1063/5.0029598.

Zemenkova M.Yu., Gladenko A.A., Zemenkov Yu.D., Chizhevskaya E.L., Polyanskaya O.I. Timely intellectual control of safety and reliability of operation of power-mechanical equipment during transportation of oil and petroleum products. AIP Conference Proceedings, Omsk, Vol. 2412, 2021, pp. 060020, https://doi.org/10.1063/5.0075848.

chanical engineering. Moscow, 1975, 488 p. (in Russian).

Zemenkova M. Yu. Methodological support of expert monitoring systems for reliability indicators of hydrocarbon pipeline transport facilities. TIU. Tyumen, 2018, 411 p. (in Russian).

Zemenkova M.Y., Gladenko A.A., Zemenkov Y.D. Innovative intelligent technologies for predictive reliability and risk management in oil and gas transport and storage systems. AIP Conference Proceedings. Omsk, Vol. 2285, 2020, pp. 050012, https://doi.org/10.1063/5.0029598.

Zemenkova M.Yu., Gladenko A.A., Zemenkov Yu.D., Chizhevskaya E.L., Polyanskaya O.I. Timely intellectual control of safety and reliability of operation of power-mechanical equipment during transportation of oil and petroleum products. AIP Conference Proceedings, Omsk, Vol. 2412, 2021, pp. 060020, https://doi.org/10.1063/5.0075848.

МНОГОУРОВНЕВАЯ ТЕХНИЧЕСКАЯ ДИАГНОСТИКА КАК ИНСТРУМЕНТ УПРАВЛЕНИЯ БЕЗОПАСНОСТЬЮ И НАДЁЖНОСТЬЮ ОБЪЕКТОВ НЕФТЕГАЗОВОЙ ОТРАСЛИ

Спасибов В.М., Земенков Ю.Д., Бастриков С.Н., Земенкова М.Ю., Чижевская Е.Л.
Тюменский индустриальный университет, Россия
625000, г.Тюмень, ул. Володарского, 38: spasibovvm@tyuiu.ru

Резюме. Деятельность промышленных объектов топливно-энергетического комплекса сопряжена с обеспечением надежности и безопасности осуществления технологических процессов, и техническая диагностика является одним из действенных инструментов решения этой задачи. Особо важное значение при этом имеет раннее предсказание аварийной ситуации для объектов с большой ценой аварии. Это связано с тем, что по сигналам ранней диагностики оказывается возможным прекратить процесс развития аварийной ситуации до перехода её в необратимую фазу, когда уже придётся разбираться с последствиями аварии – человеческими жертвами и огромными экономическими потерями. При этом важны два аспекта. Во-первых, нельзя пропустить сигнал о начале развития нештатной работы оборудования, неминуемо приводящей к аварии; во-вторых, необходимо чётко отфильтровывать ложные сигналы, так как они могут привести к немотивированной остановке оборудования и к экономическим потерям. Выход из этой ситуации возможен в комплексировании различных методов с тем, чтобы различные помехи, принципиальные для одного метода, оказывали слабое влияние на результаты, даваемые другим методом. В работе рассмотрены три метода диагностики: хрупкие тензочувствительные покрытия, акустическая эмиссия и генерация аэрозольных частиц. Для ещё большего повышения чувствительности к механическим напряжениям основного металла используется хрупкое покрытие основного металла, в котором трещины появляются значительно раньше, чем в собственно металле. Появление трещин сопровождается акустической эмиссией и генерацией аэрозольных частиц. Исследования, представленные в работе, направлены на изучение способа ранней диагностики опасных состояний объектов, посредством совмещения рассмотренных выше методов. В статье представлены результаты экспериментов при оценке нагружения испытательных образцов до достижения пластической деформации и разрушения, позволяющие сделать вывод о возможности способа многоуровневой диагностики осуществления раннего предупреждения о возникновении предаварийного состояния объекта.

Ключевые слова: *многоуровневая диагностика, управление надежностью, опасные состояния, безопасность технологических объектов*

NEFT-QAZ SAHƏSİ OBYEKTLƏRİNİN TƏHLÜKƏSİZLİYİ VƏ ETİBARLILIĞININ İDARƏEDİLMƏSİ VASİTƏSİ KİMİ ÇOXSƏVİYYƏLİ TEXNİKİ DİAQNOSTİKA

Spasibov V.M., Zemenkov Yu.D., Bastrikov S.N., Zemenkova M.Yu., Çijevskaya E.L.
Tümen Sənaye Universiteti, Rusiya
625000, Tümen şəhəri, Volodarski küçəsi, 38: spasibovvm@tyuiu.ru

Xülasə. Yanacaq-energetika kompleksinin sənaye istehsalı obyektlərinin fəaliyyəti texnoloji proseslərin həyata keçirilməsinin etibarlılığının və təhlükəsizliyinin təmin edilməsi ilə bağlıdır. Qəza dərəcəsinin yüksək olduğu obyektlər üçün qəza vəziyyətinin əvvəllər proqnozlaşdırılması xüsusi əhəmiyyətə malikdir. Bu onunla əlaqədardır ki, erkən diaqnostika siqnallarına görə qəzanın nəticələri – insan qurbanları və böyük iqtisadi itkilər ilə məşğul olmaq məcburiyyətində qaldıqdan əvvəl qəza vəziyyətinin inkişaf prosesini dayandırmaq mümkündür. Bu baxımdan diaqnostika fövqəladə halların qarşısını almaq və istehsalın stabil fəaliyyətini təmin etmək üçün qeyd edilən mühüm problemin həllində və istehsal obyektinin vəziyyətinin idarə edilməsində ən təsirli vasitələrdən biridir. Aparılan tədqiqat üç diaqnostik metodun: akustik emissiya, aerozol hissəciklərinin əmələ gəlməsi və kövrək gərginliyə həssas örtüklərin birləşməsini nəzərdə tutan texniki obyektlərin müntəzəm və təhlükəli vəziyyətlərinin çoxsəviyyəli diaqnostikası metodunun öyrənilməsinə yönəlib. Bu metodların əsas metalın mexaniki gərginliyinə qarşı yüksək həssaslığı məlumdur. Gərginliyə qarşı həssaslığı daha da artırmaq üçün əsas metalın kövrək örtüyündən istifadə olunur,burada metalın özündən əvvəl onun çatları meydana çıxır.Çatların yaranması akustik emissiya və aerozol hissəciklərinin generasiyası ilə müşayiət olunur. Məqalədə plastik deformasiyaya və dağıntıya çatana qədər sınaq nümunələrinin artmasının qiymətləndirilməsində bu üsulların birgə istifadəsi ilə bağlı təcrübələrin nəticələri təqdim olunur və bu, çoxsəviyyəli diaqnostika metodunun obyektin fövqəladə haldan əvvəl vəziyyətin baş verməsi barədə xəbərdarlığı qabaqcadan həyata keçirmək üçün mümkün olduğu qənaətinə gəlməyə imkan verir.

Açar sözlər: *çoxsəviyyəli diaqnostika, etibarlılığın idarə edilməsi, təhlükəli vəziyyətlər, texnoloji obyektlərin təhlükəsizliyi*

ANAS Transactions Earth Sciences 2 / 2023

http://www.journalesgia.com

MÜNDƏRİCAT

Boqoyavlenskiy V.İ., Boqoyavlenskiy İ.V., Nikonov R.A. – Arktikada və dünyanın digər regionlarında (quru və akvatoriyalarda) təbii və texnogen fəlakətli tullantılar və qaz partlayışları 3-13

Əhədov B., Çin Ş. – 2018 M_W = 7.5 Palu, Indoneziya zəlzələsinin Coulomb stress dəyişikliklərinin təsiri 14-25

Salmanov A.M., Qaragözov E.Ş., Əhmədov E.H. – Karbohidrogen yataqlarında su hövzəsinin hidrodinamik aktivlik modeli (Cənubi Xəzər çökəkliyinin timsalında) 26-35

Xutorskoy M.D. – Çökmə hövzələrin kəşfiyyatında termik tomoqrafiyanın tətbiqi 36-50

Babayev T.H., Aliyev Y.N., Muradi I.B., Aliyev M.M. – Zəlzələlərin dinamik xüsusiyyətlərinin məlumatlarına əsasən Şəmkir su anbarının ərazisinin seysmik təhlili 51-63

Şahverdiyev A.X., Şestopalov Y.V., Mandrik İ.E., Arefev S.V. – Qeyri-sabit sıxışdırma cəbhəsi ilə su layların suvurmanın optimallaşdırılması 64-78

Səfərov S.H., İsmayılov V.H., Səfərov E.S. – MERRA-2 reanaliz məlumatlarına əsasən 1980-2021 dövrü üçün Xəzər dənizinin səth temperaturunun tədqiqi 79-88

Spasibov V.M., Zemenkov Yu.D., Bastrikov S.N., Zemenkova M.Yu., Çijevskaya E.L. – Neft-qaz sahəsi obyektlərinin təhlükəsizliyi və etibarlılığının idarəedilməsi vasitəsi kimi çoxsəviyyəli texniki diaqnostika 89-98

CONTENTS

Bogoyavlensky V.I., Bogoyavlensky I.V., Nikonov R.A. – Natural and technogenic catastrophic blowouts and gas explosions in the Arctic and other regions (onshore and offshore) 3-13

Ahadov B., **Jin Sh.** – The impact of Coulomb stress changes of the 2018 M_W 7.5 Palu Earthquake, Indonesia 14-25

Salmanov A.M., Garagozov E.Sh., Ahmadov E.H. – Aquifer activity model in hydrocarbon fields (South Caspian Basin as a case study)..... 26-35

Khutorskoy M.D. – Thermal tomography application for prospecting in the sedimentary basins..... 36-50

Babayev T.H., Aliyev Y.N., Muradi I.B., Aliyev M.M. – Seismic analysis of the Shamkir reservoir area through insights into the dynamics of the earthquake characteristics 51-63

Shakhverdiev A.Kh., Shestopalov Y.V., Mandrik I.E., Arefyev S.V. – Optimization of reservoir waterflooding with unstable displacement front 64-78

Safarov S.H., Ismayilov V.G., Safarov E.S. – Study of the surface temperature of the Caspian Sea according to MERRA-2 reanalysis data for the period 1980-2021 79-88

Spasibov V.M., Zemenkov Y.D., Bastrikov S.N., Zemenkova M.Y., Chizhevskaya E.L. – Multi-level technical diagnostics as a tool for managing the safety and reliability of oil and gas facilities.....89-98

ОГЛАВЛЕНИЕ

Богоявленский В.И., Богоявленский И.В., Никонов Р.А. – Природные и техногенные катастрофические выбросы и взрывы газа в Арктике и других регионах мира (суша и акватории) 3-13

Ахадов Б., Чин Ш. – Влияние изменений кулоновского напряжения при землетрясении силой M_W =7.5 в Палу, Индонезия в 2018 г. 14-25

Салманов А.М., Гарагезов Э.Ш., Ахмедов Э.Г. – Моделирование гидродинамической активности бассейна на углеводородных месторождениях (на примере Южно-Каспийской впадины) 26-35

Хуторской М.Д. – Применение термической томографии для разведки в осадочных бассейнах 36-50

Бабаев Т.Х., Алиев Я.Н., Муради И.Б., Алиев М.М. – Сейсмический анализ территории Шамкирского водохранилища по данным динамических характеристик землетрясений..... 51-63

Шахвердиев А.Х., Шестопалов Я.В., Мандрик И.Е., Арефьев С.В. – Оптимизация заводнения пластов с неустойчивым фронтом вытеснения 64-78

Сафаров С.Г., Исмайылов В.Г., Сафаров Э.С. – Исследование поверхностной температуры Каспийского моря по данным реанализов MERRA-2 за период 1980-2021 гг. 79-88

Спасибов В.М., Земенков Ю.Д., Бастриков С.Н., Земенкова М.Ю., Чижевская Е.Л. – Многоуровневая техническая диагностика как инструмент управления безопасностью и надёжностью объектов нефтегазовой отрасли 89-98